



FEDERAL UNIVERSITY OF SANTA CATARINA
TECHNOLOGY CENTER
POSTGRADUATE PROGRAM IN AUTOMATION AND SYSTEMS ENGINEERING

Marduck Montoya Henao

Bifurcation analysis of non-smooth dynamical systems with multiple boundaries

Florianópolis
2023

Marduck Montoya Henao

Bifurcation analysis of non-smooth dynamical systems with multiple boundaries

Thesis submitted to the Postgraduate Program
in Automation and Systems Engineering of the
Federal University of Santa Catarina, as part of the
requirements for obtaining the degree of Doctor in
Automation and Systems Engineering.

Advisor: Prof. Daniel Juan Pagano, Dr.

Co-advisor: Prof. Rony Cristiano, Dr.

Florianópolis
2023

Ficha de identificação da obra elaborada pelo autor,
através do Programa de Geração Automática da Biblioteca Universitária da UFSC.

Montoya Henao, Marduck

Bifurcation analysis of non-smooth dynamical systems
with multiple boundaries / Marduck Montoya Henao ;
orientador, Daniel Juan Pagano, coorientador, Rony
Cristiano, 2023.

164 p.

Tese (doutorado) - Universidade Federal de Santa
Catarina, Centro Tecnológico, Programa de Pós-Graduação em
Engenharia de Automação e Sistemas, Florianópolis, 2023.

Inclui referências.

1. Engenharia de Automação e Sistemas. 2. Discontinuous
piecewise smooth systems. 3. sliding mode control. 4.
multiple switching boundaries. I. Pagano, Daniel Juan .
II. Cristiano, Rony. III. Universidade Federal de Santa
Catarina. Programa de Pós-Graduação em Engenharia de
Automação e Sistemas. IV. Título.

Marduck Montoya Henao

Bifurcation analysis of non-smooth dynamical systems with multiple boundaries

This doctoral thesis was evaluated and approved by an examination committee composed of the following members:

Prof. Durval Tonon , Dr.
Federal University of Goiás - UFG

Prof. Hector Bessa Silveira, Dr.
Federal University of Santa Catarina - UFSC

Prof. Marcelo De Lellis Costa de Oliveira, Dr.
Federal University of Santa Catarina- UFSC

We certify that this is the original and final format of the course conclusion work that was considered approved for obtaining the Doctor in Automation and Systems Engineering degree.

Prof. Julio E. Normey Rico, Dr.
Postgraduate Program Coordinator

Prof. Daniel Juan Pagano, Dr.
Advisor

Florianópolis, 2023.

*“One of the basic rules of the universe is that nothing is perfect.
Perfection simply doesn't exist.....
Without imperfection, neither you nor I would exist”.*

Stephen Hawking.

Acknowledgement

I would like to thank the following people, without whom I would not have been able to complete this stage of my life, and without whom I would not have made it through my doctorate!

Thanks to my parents, Octavio and Sandra; and my sisters, Dayana and Caren for all the unconditional support you have shown me through this very intense academic doctor degree.

I also would like to say special thank you to professors Daniel Juan Pagano Dr. and Rony Cristiano Dr., who were my advisor and co-advisor, respectively. For their enthusiasm for the project, their wise guidance, their support, encouragement and patience. I just couldn't have done it without you.

To the professors of the examining board of my doctoral thesis: Durval Tonon Dr., Hector Bessa Silveira Dr. and Marcelo de Lellis Costa de Oliveira Dr. For the comments and suggestions that helped to improve this thesis.

To my best friend Cindy for your support and sincere words that have always encouraged me and given me joy during difficult times in my life, being such a lovely and unconditional friend. I am so glad we are friends.

To my boyfriend Raul for caring and for being my biggest encourager, the person I can always count on. I could never achieve success without your support.

To all those who somehow contributed or cheered for me to achieve this goal and who for some reason were not mentioned here, my sincere thanks.

To the postgraduate Program in Automation and Systems Engineering at the Federal University of Santa Catarina (UFSC) for the opportunity to do the doctorate, to its professors who were part of my academic growth, and to CAPES for financial support during the doctorate.

Abstract

The aim of this thesis is to study the dynamics of discontinuous piecewise-smooth systems (DPWS) that exhibit more than one switching boundary, i.e. multiple discontinuity boundaries. In particular, 2D/3D-DPWS systems with two discontinuity boundaries that are usually given by line/planes are studied. More precisely, we aim to investigate the different scenarios that can appear in the phase portraits of DPWS systems when a real parameter generates a disturbance of the system being able to manifest qualitative changes in the dynamics of these systems. This class of dynamical phenomena leads to the study of bifurcations in DPWS systems and can reveal classic bifurcations such as saddle-node, Hopf, Pitchfork, etc., and discontinuity induced bifurcations (DIBs) that are unique to piecewise smooth systems. Within this former group of bifurcations are the boundary equilibrium bifurcations (BEBs) and the “sliding bifurcations” characterized by having a sliding segment at the discontinuity boundary. A classical geometric approach is adopted to study this class of dynamical systems and for the sliding dynamics that may occur on the discontinuity boundary, the Filippov convection method is used. In this sense, this work presents a qualitative and geometrical analysis of the bifurcations and their unfolding, in particular, of codimension 1 and 2 that involve natural equilibria, boundary equilibria, pseudo-equilibria, limit cycles and surfaces. We present original contributions which are obtained from the study of DPWS systems theory applied in three different case studies in power electronics and in a prey-predator Lotka-Volterra system modeled by two predators competing for one prey and including harvesting actions. The first application considers a capacitors voltage balancing system in a modular multilevel converter (MMC) using a sliding mode control law (SMC). The second application is for a bidirectional dc-dc buck converter feeding a nonlinear load of constant power-type (CPL). This system is composed of two buck converters connected in a cascade structure, the first being a buck converter controlled by a SMC and the second converter modeled by a CPL defined by a piecewise function. The third application consists of the study of the global dynamics of a Lotka-Volterra system described by two species of predators competing for prey with human action of harvesting the species of predators. The fourth application is on the analysis of the nonlinear dynamics of a DC-DC buck converter controlled by a sliding mode control (SMC) law connected in parallel to two power converters where one of them is a boost converter and the other is a buck converter, both modeled by CPL piecewise functions. In addition, we present numerical simulations for a better understanding of the dynamics of the systems in question and to verify the theoretical results obtained.

Keywords: Discontinuous piecewise smooth systems, multiple switching boundaries, sliding mode control, discontinuity induced bifurcations, buck power converter, constant power load, DC distributed power system, stability analysis, two predator-one prey system, global stability.

Resumo

O objetivo desta tese é estudar a dinâmica de sistemas descontínuos suaves por partes (DPWS) que exibem mais de um limite de comutação, ou seja, limites de múltiplas descontinuidades. Em particular, são estudados sistemas 2D/3D-DPWS com dois contornos de descontinuidade que normalmente são dados por hipersuperfícies (planos). Mais precisamente, pretendemos investigar os diferentes cenários que podem aparecer nos retratos de fase de sistemas DPWS quando um parâmetro real gera uma perturbação do sistema podendo manifestar mudanças qualitativas na dinâmica desses sistemas. Essa classe de fenômenos dinâmicos leva ao estudo de bifurcações em sistemas DPWS e pode revelar bifurcações clássicas como sela-nó, Hopf, forquilha etc. e bifurcações induzidas por descontinuidade (DIBs) que são exclusivas de sistemas suaves por partes. Dentro deste antigo grupo de bifurcações estão as bifurcações de equilíbrio de contorno (BEBs) e as “bifurcações deslizantes” caracterizadas por ter um segmento deslizante no limite da descontinuidade. Uma abordagem geométrica clássica é adotada para estudar esta classe de sistemas dinâmicos e para a dinâmica de deslizamento que podem ocorrer no limite da descontinuidade, a convecção de Filippov é usado. Nesse sentido, este trabalho apresenta uma análise qualitativa e geométrica das bifurcações e seus desdobramentos, em particular, das codimensões 1 e 2 que envolvem equilíbrios naturais, equilíbrios de contorno, pseudo-equilíbrios, ciclos limite e superfícies invariantes. Apresentamos contribuições originais que são obtidas a partir do estudo da teoria de sistemas DPWS aplicada em três diferentes estudos de caso em eletrônica de potência e um sistema presa-predador Lotka-Volterra modelado por dois predadores competindo por uma presa e incluindo ações de colheita. A primeira aplicação considera um sistema de balanceamento de tensão de capacitores em um conversor modular multinível (MMC) usando uma lei de controle de modo deslizante (SMC). A segunda aplicação é para um conversor buck CC-CC bidirecional alimentando uma carga não linear do tipo potência constante (CPL). Este sistema é composto por dois conversores buck conectados em uma estrutura em cascata, sendo o primeiro um conversor buck controlado por um SMC e o segundo conversor modelado por um CPL definido por uma função por partes. A terceira aplicação consiste no estudo da dinâmica global de um sistema Lotka-Volterra descrito por duas espécies de predadores competindo por presas com a ação humana de colher as espécies de predadores. A quarta aplicação é sobre a análise da dinâmica não linear de um conversor DC-DC buck controlado por uma lei de controle de modo deslizante (SMC) conectado em paralelo a dois conversores de potência onde um deles é um conversor boost e o outro é um conversor buck, ambos modelados por uma função CPL por partes. Além disso, apresentamos simulações numéricas para um melhor entendimento da dinâmica dos sistemas em questão e para verificar os resultados teóricos obtidos.

Palavras-chave: Sistemas contínuos suaves por partes, sistemas descontínuos suaves por partes, múltiplas fronteiras de descontinuidade, controle por modo deslizante, bifurcações induzidas por descontinuidade, conversor buck, carga de potência constante, sistema de energia distribuída CC, análise de estabilidade, sistema de dois predadores e uma presa, estabilidade global.

Resumo Expandido

Introdução

A teoria dos Sistemas Dinâmicos é fruto de um longo período de desenvolvimento científico, e determinar sua origem não é simples. No entanto, pode-se identificar o início dessa teoria no século XVI, na teoria da mecânica celeste de Johannes Kepler e na formalização da mecânica clássica de Isaac Newton. Aleksander Lyapunov e Henri Poincaré, matemáticos russos e franceses, respectivamente, são considerados os fundadores da teoria moderna dos sistemas dinâmicos. Eles introduziram vários conceitos de análise qualitativa de equações diferenciais, como estabilidade da solução, comportamento assintótico, entre outros. Normalmente tais sistemas dinâmicos são não lineares ou mesmo descontínuos e dependem de parâmetros. Consequentemente, o estudo do comportamento qualitativo de suas soluções é uma tarefa difícil e desafiadora. Um método bastante eficaz para lidar com sistemas dinâmicos é a teoria de bifurcações, segundo a qual o problema original é uma perturbação de um problema solucionável, e estamos interessados em mudanças qualitativas de propriedades de soluções para pequenas variações de parâmetros. Atualmente, a teoria da bifurcação está bem desenvolvida e os métodos aplicados por essas teorias são bastante amplos, incluindo ferramentas analíticas funcionais e também simulações numéricas.

Dentro desta abrangente área, o estudo de *sistemas dinâmicos suaves por partes* (PWS, por suas siglas em inglês), ou sistemas dinâmicos não suaves é relativamente recente e tem grande relevância na pesquisa científica atual. Os trabalhos pioneiros de Andronov (1971) sobre bifurcações em sistemas dinâmicos não suaves e de Filippov (1988) sobre movimento deslizante estabelecem as bases para o desenvolvimento desta linha de pesquisa. Os sistemas PWS são frequentemente considerados em sistemas físicos e aplicações de engenharia para descrever fenômenos envolvendo fricção, colisão, sistemas intermitentemente restritos ou processos com componentes de comutação. As bifurcações em sistemas PWS têm sido objeto de estudo em diversos trabalhos de pesquisa até hoje, pois ainda não há um entendimento completo das bifurcações locais e globais desses sistemas.

Em sistemas dinâmicos PWS pode-se, em geral, distinguir entre dois tipos de bifurcações. O primeiro tipo é semelhante às bifurcações que conhecemos para sistemas dinâmicos suaves. Estes incluem bifurcações locais, que podem ser analisadas inteiramente através de mudanças nas propriedades de estabilidade local de equilíbrios, órbitas periódicas ou outros conjuntos invariantes como cruzamentos de parâmetros através

de limiares críticos (nó de sela, bifurcações de Hopf, etc); e bifurcações globais, que geralmente ocorrem quando conjuntos invariantes maiores do sistema 'colidem' uns com os outros, ou com equilíbrios do sistema. Eles não podem ser detectados puramente por uma análise de estabilidade dos equilíbrios (bifurcações homoclínicas, bifurcações heteroclínicas de equilíbrios e órbitas periódicas, etc). O segundo tipo de bifurcações referido como bifurcações border-collision está relacionado com situações em que a trajetória começa a cruzar uma das chamadas superfícies de comutação ou superfícies de descontinuidade, ou seja, superfícies que dividem o espaço de fase em domínios de diferentes dinâmicas. Dentro de cada um desses domínios, o sistema é suave, mas as equações de movimento mudam abruptamente de um domínio para o outro. Este tipo de bifurcação, que normalmente envolve saltos abruptos nos autovalores da órbita, não pode ocorrer em sistemas dinâmicos suaves.

Assim esta tese é dedicada ao estudo da dinâmica de sistemas descontínuos suaves por partes (DPWS) que exibem mais de um limite de comutação, ou seja, limites de múltiplas descontinuidades com aplicações em sistemas de controle não lineares em diferentes áreas da ciência e engenharia, como biologia e eletrônica de potência. Em particular, são estudados sistemas 2D/3D-DPWS com duas fronteiras de descontinuidade que normalmente são dados por superfícies planas. Nesse sentido, este trabalho apresenta uma análise qualitativa e geométrica das bifurcações e seus desdobramentos, em particular, das codimensões 1 e 2 que envolvem equilíbrios naturais, equilíbrios de contorno, pseudo-equilíbrios, ciclos limite e superfícies invariantes. Apresentamos contribuições originais que são obtidas a partir do estudo da teoria de sistemas DPWS aplicada em três diferentes estudos de caso em eletrônica de potência e um sistema presa-predador Lotka-Volterra modelado por dois predadores competindo por uma presa e incluindo ações de colheita. Além disso, apresentamos simulações para realizar cálculos de continuação numérica usando pacotes computacionais como o XPP-AUTO e assim obter uma melhor compreensão da dinâmica dos sistemas em questão e verificar os resultados teóricos obtidos.

Objetivos

O principal objetivo desta tese é o estudo de sistemas dinâmicos suaves por partes (PWS) com aplicações em sistemas de controle não lineares em diferentes áreas da ciência e engenharia, em particular:

- Estudar a dinâmica e a estabilidade de um sistema de n capacitores conectados em série a uma fonte de tensão e controlados por uma lei de controle por modo deslizante com múltiplas fronteiras de descontinuidade usando as ferramentas da teoria de sistemas PWS.
- Analisar a dinâmica local e global de um circuito eletrônico de potência alimentando uma carga de potência constante e controlado por uma lei de controle por modo deslizante que é modelado como um sistema 3D-DPWS com dois limites de comutação transversais.
- Analisar a dinâmica local e global de um sistema de dois predadores e uma presa

sob ações de colheita que são introduzidas por meio de duas ações de controle de comutação definidas nas espécies dos predadores; e determinar as condições nos parâmetros do sistema para que o equilíbrio de coexistência dos predadores seja globalmente estável.

- Fornecer simulações numéricas dos sistemas estudados para ter uma melhor compreensão do comportamento dinâmico dos mesmos e verificar os resultados teóricos obtidos.

Metodologia

Através de uma revisão bibliográfica, observamos que: é um problema complicado analisar todos os casos possíveis para lidar com sistemas DPWS com n fronteiras, pois não existe uma teoria geral. Esta classe de sistemas é estudada caso a caso utilizando ferramentas de geometria de campos vetoriais. Sabemos que a teoria estabelecida por Filippov tem como pressuposto fundamental uma superfície regular entre duas regiões lisas, mas muitos fenômenos de grande relevância requerem modelos onde ocorram dois ou mais fronteiras de descontinuidade que não sejam necessariamente superfícies planas, onde pode haver uma interseção entre eles e/ou podem ocorrer mudanças em sua dinâmica. Na última década, três principais metodologias surgiram para o estudo desses sistemas. Uma das metodologias foi apresentada por *Jeffrey (2014)* e propõe uma extensão da dinâmica de Filippov para pontos onde a variedade chaveada Σ se auto-intersecta através do chamado “canopy”. Outra metodologia foi apresentada por *Diece et al. (2009)*, que propõe uma construção similar onde ocorre a não unicidade dos vetores deslizantes. Aqui, foi mostrado que, ao impor certas hipóteses de atratividade na variedade de comutação Σ , muitas conclusões podem ser provadas sobre o comportamento da dinâmica. No entanto, impor condições sobre Σ é restritivo. Finalmente, *Buzzi et al. (2012)* propõem uma extensão da dinâmica de Filippov para pontos onde a auto-intersecção através da aplicação de uma explosão adequada e o uso da Teoria da Perturbação Singular Geométrica (Teoria-GSP) para estudar os sistemas lento-rápidos resultantes. Embora distante de uma generalização direta da convenção de Filippov, esta metodologia também é uma abordagem natural com vantagens sobre as anteriores, uma vez que a não unicidade do campo deslizante é prevista e gerenciada naturalmente. Ainda mais, nenhuma suposição sobre Σ ou os campos vetoriais subjacentes $f^{(i)}$ são necessários aqui. No entanto, todas estas metodologias carecem de uma apresentação e justificação clara para a dinâmica induzida nos pontos onde ocorre uma auto-intersecção de Σ . Motivados no estudo de esta classe de sistemas, por meio do estudo de casos, dedicamos esta tese ao estudo de bifurcações locais e globais para sistemas dinâmicos PWS com no máximo dois limites de comutação também chamados de superfícies de descontinuidade as quais vão ser normalmente superfícies planas, onde o método dado por Filippov (convenção de Filippov) será aplicado para analisar a descontinuidade dos sistemas dinâmicos suaves por partes (DPWS) com aplicações em sistemas de controle não lineares em diferentes áreas da ciência e engenharia, como biologia e eletrônica de potência.

Resultados e Considerações Finais

Como resultado de nossa pesquisa, propomos e estudamos três aplicações dos sistemas DPWS, e como resultado de ela obtivemos três artigos publicados.

A primeira aplicação considera um sistema de balanceamento de tensão de capacitores em um conversor modular multinível (MMC) usando uma lei de controle de modo deslizante (SMC) deu origem a nossa primeira publicação: Rony Cristiano, Daniel J. Pagano and Marduck M. Henao. Multiple boundaries sliding mode control applied to capacitor voltage-balancing systems *Commun Nonlinear Sci Numer Simulat.*, 91 (2020), doi:10.1016/j.cnsns.2020.105430.


A segunda aplicação é para um conversor buck CC-CC bidirecional alimentando uma carga não linear do tipo potência constante (CPL). Este sistema é composto por dois conversores buck conectados em uma estrutura em cascata, sendo o primeiro um conversor buck controlado por um SMC e o segundo conversor modelado por um CPL definido por uma função por partes deu origem a nossa segunda publicação: Marduck M. Henao, Rony Cristiano, Daniel J. Pagano. Bifurcation analysis of 3D-PWS systems with two transversal switching boundaries: A case study in power electronics, *Physica D Nonlinear Phenomena*, 442 (2022), doi: 10.1016/j.physd.2022.133505.

A terceira aplicação consiste no estudo da dinâmica global de um sistema Lotka-Volterra descrito por duas espécies de predadores competindo por presas com a ação humana de colher as espécies de predadores deu origem a nossa terceira publicação: Rony Cristiano, Marduck M. Henao, Daniel J. Pagano. Global stability of a Lotka-Volterra piecewise-smooth system with harvesting actions and two predators competing for one prey, *Journal of Mathematical Analysis and Applications*, 522 (2023), doi: 10.1016/j.jmaa.2023.126998.

Cabe mencionar que para o estudo de cada problema de aplicação apresentados neste trabalho, foram feitos cálculos de continuação numérica usando pacotes computacionais para assim ter uma melhor compreensão da dinâmica dos sistemas estudados e também validar os resultados teóricos obtidos.

Palavras-chave: Sistemas contínuos suaves por partes, sistemas descontínuos suaves por partes, múltiplas fronteiras de descontinuidade, controle por modo deslizante, bifurcações induzidas por descontinuidade, conversor buck, carga de potência constante, sistema de energia distribuída CC, análise de estabilidade, sistema de dois predadores e uma presa, estabilidade global.

List of Figures

1.1	Piecewise-smooth vector field.	28
1.2	Tangent points: (a) visible and (b) invisible of a plane Filippov system. The solid region (dotted) of the boundary Σ represents the sliding region (crossing).	31
1.3	Geometric definition of the sliding vector field.	31
1.4	Some modes on Σ . In (a) is shown the attractive sliding motion that occurs in the set Σ_{as} , where $L_{\mathbf{F}_2}h(\mathbf{x}) < 0$ and $L_{\mathbf{F}_1}h(\mathbf{x}) > 0$. In (b) the crossing mode is shown, where a trajectory crosses Σ at a point of Σ_c^- (restricted to $L_{\mathbf{F}_2}h(\mathbf{x}) < 0$ and $L_{\mathbf{F}_1}h(\mathbf{x}) < 0$), passing from R_2 to R_1 . In (c)-(d) are shown the behavior of the system's orbits close to a tangency point at 0, associated to vector field \mathbf{F}_2 , being of the invisible fold type in (c), since $L_{\mathbf{F}_2}h(0) = 0$ and $L_{\mathbf{F}_2}^2h(0) < 0$, and of the visible fold type in (d), since $L_{\mathbf{F}_2}h(0) = 0$ and $L_{\mathbf{F}_2}^2h(0) > 0$	32
1.5	State space configuration in \mathbb{R}^3 with $\Sigma_1 \cup \Sigma_2$ attracting in finite time all nearby trajectories. The vector fields \mathbf{F}_i point to the switching boundaries Σ_1 and Σ_2 in all regions. Then, sliding vector fields can be defined in Σ_1 , Σ_2 and $\Sigma_1 \cap \Sigma_2$, being denoted by $F_{s_1}^\pm$, $F_{s_2}^\pm$ and F_s , respectively.	34
1.6	Limit Cycle Trajectories.	37
1.7	Homoclinic bifurcation for a saddle equilibrium creating a stable limit cycle. In figure (a) there is a stable periodic orbit; in figure (b) the periodic orbit approaches the homoclinic orbit; and in figure (c), the homoclinic orbit is broken and there is no periodic orbit.	38
1.8	Heteroclinic bifurcation for two saddles equilibrium creating a stable limit cycle. In figure (a) there is an unstable equilibrium coexists with two saddles; in figure (b) the heteroclinic orbits connecting the saddles, forming a heteroclinic cycle; and in figure (c) there is a stable limit cycle that disappears through heteroclinic bifurcation.	38
1.9	Grazing-sliding bifurcation in 2D.	41
2.1	MMC with pre-charge circuit. L_a stands for the equivalent arm inductance; L_f is the output ac inductance; V_{dc} is the dc voltage source; R_l stands for the equivalent circuit resistance; R_b and S_b are the balancing resistance and control switch, respectively; S_1 and S_2 are the submodule switches; C_i is the submodule capacitor; APS is the auxiliary power supply; K_1 , K_2 and K_{ac} denote pre-charge and operating circuit switches. Adapted from [7].	43
2.2	Equivalent circuit for one leg with two arms of the MMC circuit shown in Figure 2.1. Note that N is an even number and the symbol  denotes a constant power source (P_i/v_{C_i}).	45

2.3	State space of system (2.3.1)-(2.3.4): $D = \Sigma_1 \cup \Sigma_2 \cup D_1 \cup D_2 \cup D_3 \cup D_4$.	49
2.4	A geometric illustration of vector fields of the system (2.3.5)-(2.3.7) assuming $b_1 = b_2 = 0$ and (2.3.8).	51
2.5	Simulations of the system (2.3.5)-(2.3.7) assuming $c_1 = 2$, $c_2 = 1$, $b_1 = b_2 = 0$, $a = 1$ and input references $\mu_1 = 0.3$ and $\mu_2 = 0.5$. A hysteresis band of 0.005 is considered.	54
2.6	Local stability analysis at (μ_1, μ_2) .	56
2.7	Domain of operation for the system (2.3.5)-(2.3.7). To ensure local stability at the desired operating point (μ_1, μ_2) , we must choose values of μ_1 and μ_2 within the set Ω , represented by the painted areas.	57
2.8	Existence and stability of equilibria of the vector field \mathbf{F}_{+-} . (a) Graphics of (2.3.14). (b) Bifurcation diagram in the (x_2, c) -plane. (c) $Det(J(1, 0))$ (eq. (2.3.15)) and $Tr(J(1, 0))$ (eq. (2.3.16)) in the (x_2, b) -plane.	60
2.9	Phase portraits of system (2.3.5)-(2.3.7) assuming $a = 1$, $b_1 = b_2 = 0.01$, $c_1 = c_2 = 1/2$ in (a)-(b) and $c_1 = c_2 = 3$ in (c).	61
2.10	Phase portraits of \mathbf{F}_{s1} restricted to Σ_1^{as} . In (a) we use $r = 1$, $b = 1/16$, $c = 3$ and $\mu = 1/4$; in (b), $r = 1$, $b = 1/16$, $c = 3/2$ and $\mu = 1/4$.	65
2.11	Phase portrait of system (2.4.1)-(2.4.3) assuming $b = 1/16$, $c = 3$, $r = 1$ and $\mu = 1/4$. Gray vectors indicate sliding motion.	67
2.12	Response time of system (2.2.4)-(2.2.5) with initial conditions at $v_{C_i}(0) = 2V$ for $i = 1, 2, \dots, 10$. A hysteresis band of 0.1V is applied.	68
3.1	Block diagram of a simplified dc electrical distribution system (dc microgrid) with cascaded interconnected converters architecture and two dc buses (Bus1 and Bus2)..	71
3.2	a) Cascaded power converters block diagram. b) Experimental CPL curve corresponding to the PC2 plus load ($P_{in} = P_0 = 2.4W$, $V_{th} = 6v$).	71
3.3	The converter at the load point behaves as a constant power load for the feeder buck converter, see [51].	73
3.4	Basic topology of a Buck converter connected to a CPL load and under a sliding mode and washout filter control strategy. The control function is defined as $u = \frac{1}{2}(1 - \text{sign}[H(i_L, v_C, z_F)])$. The filtered inductor current given by $i_F = i_L - z_F$ expresses the difference between the inductor current i_L and the filtered signal z_F .	74
3.5	Switching boundaries defined in (3.2.9).	77
3.6	Sliding (gray region) and crossing regions (white region) in the (y, x) -plane for parameters $\omega = 1$, $b = 0.2$, $k = 2$, $y_{th} = 0.1$, $y_r = 0.5$ and $d = 0.3$.	78
3.7	Equilibria of system (3.2.11) when varying the value of bifurcation parameter d for $w = 1$, $b = 0.2$, $k = 2$, $y_{th} = 0.1$, showing the collision between regular and pseudo-equilibrium points on the (y, x) -plane. Figures (a) to (e) $y_r = 0.5$ and figure (f) $y_r = 0.25$.	82
3.8	Bifurcation set in (y_r, d) -plane showing the main local and global bifurcations curves. a) (y_r, d) -plane assuming $b = 0.2$, $k = 0.1$ and $\omega = 1$. b) (y_r, d) -plane assuming $b = \sqrt{1/3}$, $k = 0.5$, $\omega = 1$.	86

3.9	Bifurcation diagrams of system (3.2.11) considering d as the bifurcation parameter for $b = 0.2$, $k = 0.1$, $\omega = 1$, $y_{th} = 0.1$ and $y_r = 0.25$. Black curves stand for the limit cycle, red line denotes the pseudo-equilibria, blue and green line represent the equilibrium \bar{x}_4^+ and the equilibrium \bar{x}_4^- , respectively; the violet line stands for the equilibrium \bar{x}_3 . Dashed curve indicates the unstable equilibrium/limit cycle and the solid line indicates the stable equilibrium/limit cycle, and dotted curves mean the virtual equilibrium.	90
3.10	Bifurcation diagrams of system (3.2.11) considering d as the bifurcation parameter for $b = 0.2$, $k = 0.1$, $\omega = 1$, $y_{th} = 0.1$ and $y_r = 0.5$. Black curves stand for the limit cycle, red line denotes the pseudo-equilibria, blue and green line represent the equilibrium \bar{x}_4^+ and the equilibrium \bar{x}_4^- , respectively; the violet line stands for the equilibrium \bar{x}_3 . Dashed curve indicates the unstable equilibrium/limit cycle and the solid line indicates the stable equilibrium/limit cycle; and dotted curves mean the virtual equilibrium.	91
3.11	Bifurcation diagrams of system (3.2.11) considering d as the bifurcation parameter for $b = 0.2$, $k = 0.1$, $\omega = 1$, $y_{th} = 0.1$ and $y_r = 0.75$. Black curves stand for the limit cycle, red line denotes the pseudo-equilibria, blue and green line represent the equilibrium \bar{x}_4^+ and the equilibrium \bar{x}_4^- , respectively; the violet line stands for the equilibrium \bar{x}_3 . Dashed curve indicates the unstable equilibrium/limit cycle and the solid line indicates the stable equilibrium/limit cycle; and dotted curves mean the virtual equilibrium.	92
3.12	Bifurcation diagrams of system (3.2.11) considering d as the bifurcation parameter for $b = 0.2$, $k = 0.1$, $\omega = 1$, $y_{th} = 0.1$ and $y_r = 0.93$. Black curves stand for the limit cycle, red line denotes the pseudo-equilibria, blue and green line represent the equilibrium \bar{x}_4^+ and the equilibrium \bar{x}_4^- , respectively; the violet line stands for the equilibrium \bar{x}_3 . Dashed curve indicates the unstable equilibrium/limit cycle and the solid line indicates the stable equilibrium/limit cycle; and dotted curves mean the virtual equilibrium.	93
3.13	Bifurcation diagrams of system (3.2.11) considering d as the bifurcation parameter for $b = 0.2$, $k = 0.1$, $\omega = 1$, $y_{th} = 0.1$ and $y_r = 0.99$. Black curves stand for the limit cycle, red line denotes the pseudo-equilibria, blue and green line represent the equilibrium \bar{x}_4^+ and the equilibrium \bar{x}_4^- , respectively; the violet line stands for the equilibrium \bar{x}_3 . Dashed curve indicates the unstable equilibrium/limit cycle and the solid line indicates the stable equilibrium/limit cycle; and dotted curves mean the virtual equilibrium.	94

3.14	Bifurcation diagrams of system (3.2.11) considering d as the bifurcation parameter for $b = \sqrt{\frac{1}{3}}$, $k = 0.5$, $\omega = 1$, $y_{th} = 0.1$ and $y_r = 0.937$. Black curves stand for the limit cycle, red line denotes the pseudo-equilibria, blue and green line represent the equilibrium $\bar{\mathbf{x}}_4^+$ and the equilibrium $\bar{\mathbf{x}}_4^-$, respectively; the violet line stands for the equilibrium $\bar{\mathbf{x}}_3$. Dashed curve indicates the unstable equilibrium/limit cycle and the solid line indicates the stable equilibrium/limit cycle; and dotted curves mean the virtual equilibrium.	95
3.15	Simulation results of system (3.2.11) with parameters $b = 0.2$, $\omega = 1$, $k = 0.1$ and $y_r = 0.93$ showing the stable limit cycle in blue color and the unstable limit cycle in black color; the points of focus equilibrium, pseudo-node and boundary equilibrium are represent by green, red and black dots, respectively.	97
3.16	Simulation results of system (3.2.11) with parameters $b = \sqrt{1/3}$, $\omega = 1$, $k = 0.5$, $y_r = 0.937$ and $d = 0.305$ showing the Grazing-sliding bifurcation (see violet cycle) and the Homoclinic connection bifurcation (see maroon cycle).	98
4.1	Phase portraits of the vector field \mathbf{F}_{ij} in \mathcal{D} from the choice of (μ_1^i, μ_2^j) , assuming $\mu_1^i \neq \mu_2^j$, $\mu_1^i < 1/\beta$, $\mu_2^j < 1/\beta$ and $\alpha = 1$. The green, blue and red dot represent the equilibrium points \mathbf{e} , \mathbf{e}_2^j and \mathbf{e}_1^i , respectively	105
4.2	Configuration on $\Sigma = \Sigma_1 \cup \Sigma_2$ assuming $y_r > 1 - \beta\mu_1^-$, $z_r > 1 - \beta\mu_2^-$, $\mu_1^- < \mu_2^-$, $\mu_1^+ > \mu_2^+$, where $\mathbf{q}_{20}^+ = (\mu_2^+, y_r, z_r) \in T_2^+ \cap \Sigma_1$ and $\mathbf{q}_{20}^- = (\mu_2^-, y_r, z_r) \in T_2^- \cap \Sigma_1$ are fold points of the sliding vector field in Σ_1^{as} with its switching boundary $\Sigma_1 \cap \Sigma_2$	108
4.3	Sliding dynamics in Σ_1 . In (a) is shown a set of bifurcations in the (y_r, z_r) -plane of parameters assuming $\mu_2^\pm \in (\mu_1^-, \mu_1^+)$ and $\mu_1^+ < 1/\beta$, where the red and blue lines indicate the Persistence BPEB involving the boundary pseudo-equilibrium $\mathbf{p} = \mathbf{p}_{12}^+$ and $\mathbf{p} = \mathbf{p}_{12}^-$, respectively. For points (y_r, z_r) in the regions 1, 2 or 3, one of the pseudo-equilibria involved becomes real, and all of them, real and virtual, are located in Σ_1^{as} , being that \mathbf{p}_{12}^+ (resp. \mathbf{p}_{12}^-) have positive coordinates if on the left of the horizontal dashed line in red (resp. blue) color. In (b) there are shown some phase portraits of the sliding dynamics restricted to $S_1 = T_1^- \cup \Sigma_1^{as} \cup T_1^+ \subset \Sigma_1$, taking (y_r, z_r) in the regions 1 (left), 2 (center) and 3 (right) of the bifurcations set. The green dot represents the \mathbf{p}_{11} point, the red dots represent the \mathbf{p}_{12}^\pm points and the blue dot represents the \mathbf{p} point. They are virtual when represented by a small circle with an empty interior. The black dots represent the pseudo-folds \mathbf{q}_{20}^+ and \mathbf{q}_{20}^- . Consider $z^* = 1 - \beta\mu_2^-$	112
4.4	Figure (a) shows a phase portrait of the system with parameters $\mu_1^+ = 0.8$, $\mu_1^- = 0.1$, $\mu_2^+ = 0.7$, $\mu_2^- = 0.2$, $\beta = 1$, $\alpha = 1$, $y_r = z_r = 0.325$ for various initial conditions of the prey and predators populations. The green dot represents the point \mathbf{p}_{11} and the blue dot represents the pseudo-equilibrium point \mathbf{p} . Figures (b)-(d) exhibit the population dynamics for one prey and two predators over time for distinct initial conditions.	117

4.5	Figure (a) shows a phase portrait of the system with parameters $\mu_1^+ = 0.8$, $\mu_1^- = 0.1$, $\mu_2^+ = 0.7$, $\mu_2^- = 0.2$, $\beta = 1$, $\alpha = 1$, $y_r = 0.2$ and $z_r = 0.3$ ($y_r < z_r$) for various initial conditions of the prey and predators populations. The green dot represents the point \mathbf{p}_{11} and the blue dot represents the pseudo-equilibrium point \mathbf{p} . Figures (b)-(d) exhibit the population dynamics for one prey and two predators over time for distinct initial conditions. . . .	118
5.1	Block diagram of the studied DC microgrid. Simplified system diagram assuming that the loads are represented by CPLs and the PV source by a CPS. V_{in} is the battery voltage and DBC stands for the bidirectional power converter controlling the DC bus voltage.	122
5.2	Basic topology of a dc-dc buck converter controlled by a sliding mode and washout filter control strategy, connected to two converters in parallel. The control function is defined as $u = \frac{1}{2}(1 - \text{sign}[H(i_L, v_C, z_F)])$. The filtered inductor current given by $i_F = i_L - z_F$ expresses the difference between the inductor current i_L and the filtered signal z_F	123
5.3	Show the switching boundaries defined in (5.2.8). Figure (a) shows the switching boundaries when $y_{th1} = y_{th2}$, defined by $\Sigma_{\{2,3\}}$. Figure (b) shows the switching boundaries when $y_{th1} \neq y_{th2}$	127
5.4	Simulation results of system (5.3.1) with parameters $b = 0.006742$, $k = 0.6742$, $d_2 = d_3 = 0.02575$, $y_{th1} = 0.0416667$, $y_{th2} = 0.0833333$ and $y_r = 0.5$ showing the unstable limit cycle in black color; the point of pseudo equilibrium is represented by red.	132
5.5	Bifurcation set in (k, d_1) -plane showing the main local bifurcations assuming $b = 0.006742$, $k = 0.6742$, $d_2 = d_3 = 0.02575$, $y_{th1} = 0.0416667$, $y_{th2} = 0.0833333$, $\omega = 0.461288$ and $y_r = 0.5$	132

List of Tables

2.1	Normalization.	47
3.1	Normalized variables, parameters and time	75
3.2	Classification of Equilibria and Pseudo-equilibria according to figure 3.8(a). 87	
3.3	Number and stability of coexisting limit cycles from the bifurcation set of Figure 3.8(a).	95
3.4	Number and stability of coexisting limit cycles from the bifurcation set of Figure 3.8(b).	96
5.1	Normalized variable, parameters and time.	125

Nomenclature

- APS* Auxiliary power supply
- BEB_{NF}* Boundary equilibrium bifurcations nonsmooth fold
- BEB_P* Boundary equilibrium bifurcations persistence
- BEBs* Boundary equilibrium bifurcations
- BFB* Boundary Focus Bifurcation
- BPEB* Boundary pseudo-equilibrium bifurcation
- CPL* Constant power load
- CPWS* Continuous piecewise-smooth systems
- DC* Direct current
- DIBs* Discontinuity-induced bifurcations
- DPSs* Distributed power systems
- DPWS* Discontinuous piecewise smooth systems
- DSN* Discontinuous saddle-node
- GS* Grazing-sliding bifurcations
- GSP* Geometrical Singular Perturbation Theory
- H_{sub}* Subcritical Hopf bifurcation
- HC* Homoclinic bifurcation
- HVDC* High Voltage Direct Current
- IGBT* Insulated-gate bipolar transistors
- LC* Limit Cycle
- LCB* Limit Cycle Bifurcations
- MMC* Multilevel modular converter
- MPPT* Maximum power point tracking

ODEs Ordinary differential equations

PWS Piecewise smooth system

SM Submodules

SMC Sliding mode control law

SNe Saddle-node bifurcation

SNPO Saddle-node bifurcation of periodic orbits

Contents

Index	xviii
Introduction	17
1 Preliminaries and background materials	23
1.1 Smooth dynamical systems	23
1.2 Piecewise-smooth control system	26
1.2.1 A single switching boundary	29
1.2.2 Two switching boundaries	34
1.3 Bifurcations of piecewise-smooth dynamical systems	36
1.3.1 Boundary equilibrium bifurcations	39
1.3.2 Discontinuous saddle-node bifurcation	40
1.3.3 Grazing-sliding bifurcation	40
2 Multiple boundaries sliding mode control applied to capacitor voltage-balancing systems	42
2.1 Introduction	42
2.2 Model description and main result	45
2.3 Qualitative analysis of the planar case with two-boundaries	48
2.3.1 Case Study for $b_1 = b_2 = 0$ ($P_i = 0$)	49
2.3.2 Case Study for $b_1 > 0$ and $b_2 > 0$ ($P_i > 0$)	55
2.4 Study of the sliding dynamics in \mathbb{R}^3 with two-boundaries	62
2.5 Simulation results	67
2.6 Conclusion	68
3 Bifurcation analysis of 3D-PWS systems with two transversal switching boundaries: a case study in power electronics	70
3.1 Introduction	70
3.2 The buck converter feeding a nonlinear load of CPL-type	73
3.2.1 Normalized model	75
3.2.2 Regular equilibria and stability	78
3.2.3 Sliding vector field and pseudo-equilibria	80
3.2.4 Two local DIBs of equilibrium collision with borders	81
3.3 Boundary equilibrium bifurcations	83
3.4 Two-parameter bifurcation analysis	85
3.4.1 Limit cycle bifurcations	87
3.5 Conclusion	98

4	Global stability of a Lotka-Volterra piecewise-smooth system with harvesting actions and two predators competing for one prey	100
4.1	Introduction	100
4.2	A two-predator one-prey system under harvesting actions	102
4.2.1	Dynamics of vector field \mathbf{F}_{ij}	103
4.2.2	Configuration on $\Sigma = \Sigma_1 \cup \Sigma_2$	105
4.3	Sliding vector fields and pseudo-equilibria	108
4.3.1	Sliding dynamics on Σ_1 and bifurcations	108
4.3.2	Sliding dynamics on Σ_2 and bifurcations	113
4.4	Conditions of global stability for the coexistence of predators	116
4.4.1	Simulation results	117
4.4.2	Harvesting control	118
4.5	Conclusion	119
5	Nonlinear analysis of DC power converters connected in parallel	120
5.1	Introduction	120
5.2	Model description	121
5.3	Case study for $y_{th1} = y_{th2}$	126
5.3.1	Regular equilibria and stability	128
5.3.2	Sliding vector field and pseudo-equilibria	130
5.3.3	Boundary equilibrium bifurcation	131
5.4	Case study for $y_{th1} < y_{th2}$	132
5.4.1	Regular equilibria and stability	134
5.4.2	Sliding vector field and pseudo-equilibria	139
5.5	Case study for $y_{th1} > y_{th2}$	139
5.5.1	Regular equilibria and stability	141
5.5.2	Sliding vector field and pseudo-equilibria	143
5.6	Conclusion	144
6	Final Remarks	145
	References	148

Introduction

Motivation and goals

Dynamical Systems theory is the result of a long time of scientific development, and determining its origin is not simple. However, one can identify the beginnings of this theory in the 16th century, in the celestial mechanics theory by Johannes Kepler, and in the formalization of classical mechanics by Isaac Newton. Aleksander Lyapunov and Henri Poincaré, Russian and French mathematicians respectively, are considered founders of the modern theory of dynamical systems. They introduced several concepts of qualitative analysis of differential equations, such as solution stability, asymptotic behavior, among others. Usually such dynamical systems are nonlinear or even discontinuous and depend on parameters. Consequently, the study of the qualitative behavior of their solutions is a difficult and challenging task. A rather effective method for handling dynamical systems is the bifurcation theory, whereby the original problem is a perturbation of a solvable problem, and we are interested in qualitative changes of properties of solutions for small parameter variations. Currently, bifurcation theory is well developed and the methods applied by these theories are quite broad, including functional analytical tools and numerical simulations as well; see e.g. [49, 50, 55, 57, 54, 56]

Within this comprehensive area, the study of *piecewise-smooth dynamical systems* (**PWS**, for short), or non-smooth dynamical systems is relatively recent and it has great relevance in current scientific research. The pioneering works of Andronov [54] on bifurcations in non-smooth dynamical systems, and Filippov [1] on sliding motion, lay the foundations for the development of this line of research. **PWS** systems are often considered in physical systems and engineering applications to describe phenomena involving friction, collision, intermittently constrained systems, or processes with switching components, see [8].

Bifurcations in **PWS** systems have been the object of study in several works by many researchers until nowadays because there is not yet a complete understanding of local and global bifurcations for these systems.

In **PWS** dynamical systems one can in general distinguish between two types of bifurcations. The first type is similar to the bifurcations we know for smooth dynamical systems. These include local bifurcations, which can be analyzed entirely through changes in the local stability properties of equilibria, periodic orbits or other invariant sets as parameter crossings through critical thresholds (saddle-node, Hopf bifurcations, etc); and global bifurcations, which often occur when larger invariant sets of the system 'collide' with each other, or with equilibria of the system. They cannot be detected purely by a stability analysis of the equilibria (Homoclinic bifurcations, Heteroclinic Bifurcation of equilibria and periodic orbits, etc). The second type of bifurcations referred to as

border-collision bifurcations is connected with situations where the trajectory starts to intersect one of the so-called switching surfaces or discontinuity surfaces, i.e., surfaces that divide the phase space into domains of different dynamics. Within each such domain, the system is smooth, but the equations of motion change abruptly from one domain to the next. This type of bifurcation, which typically involves abrupt jumps in the eigenvalues of the orbit, cannot occur in smooth dynamical systems.

It is a cumbersome problem to analyze all the possible cases to deal with **DPWS** systems with n boundaries since we do not have a general theory. This class of systems is studied on a case-by-case basis using vector field geometry tools. We know that the theory established by Filippov has as its fundamental assumption a regular surface between two smooth regions, but many highly relevant phenomena require models where two or more discontinuity boundaries occur that are not necessarily plane surfaces, where there can be an intersection between them and changes in its dynamics may occur, see [8, 9, 13, 18, 97, 100]. In the last decade, three main methodologies have emerged for the study of these systems. One of the methodologies was presented by *Jeffrey* and proposes an extension of the Filippov dynamics to points where the switching manifold Σ self-intersects through the so-called “canopy”, a convex-like ruled surface, for more details see [18]. The next one, presented by *Diece et al.*, which is older than the previous methodology, proposes a similar construction where the nonuniqueness of sliding vectors happens. Here, however, it was shown that by imposing certain attractivity hypotheses on the switching manifold Σ , many conclusions can be proved on the behavior of the dynamics. However, imposing conditions on Σ is a fundamental and restrictive hypothesis here, for more details see [9]. Finally, *Buzzi et al.* propose an extension of the Filippov dynamics to points where Σ self-intersects through the application of a proper blow-up and the use of Geometrical Singular Perturbation Theory (GSP-Theory for short) to study the resulting slow-fast systems. Although distant from a direct generalization of Filippov’s convention, this methodology is also a natural approach with advantages over the previous ones, since, the non-uniqueness of the sliding field is predicted and it is managed naturally. Even more, no assumptions neither on Σ or the underlying vector fields $f^{(i)}$ are required here. However, the works lack a clear presentation and justification for the dynamics induced over points where Σ self-intersects, for more details see [97].

This thesis is dedicated to the study of local and global bifurcations for **PWS** dynamical systems with at most two switching boundaries also called discontinuous surface (normally plane surfaces), where the method given by Filippov (Filippov’s convention) will be applied to analyze the *discontinuous piecewise-smooth dynamical systems* (**DPWS** systems, for short).

The **PWS** systems are described as a set of ordinary differential equations of the form

$$\dot{\mathbf{x}} = f^{(i)}(\mathbf{x}), \quad \mathbf{x} \in R_i \subset \mathbb{R}^n, \quad (1)$$

where $f^{(i)} : R_i \rightarrow \mathbb{R}^n$ and R_i ($i = 1, 2, 3, \dots, m$) are open regions separated by switching boundaries Σ_{ij} of $(n - 1)$ -dimension and $f^{(i)}$ and Σ_{ij} are supposed to be smooth. The union of all Σ_{ij} and all regions R_i covers the entire state space of (1).

The nonsmoothness of the system occurs on the switching boundaries Σ_{ij} . Moreover, **PWS** systems are classified depending on the type of non-smoothness; see [8],

- Continuous piecewise-smooth systems (**CPWS** systems) if the vector field (1) is

continuous but it is not differentiable at some points, i.e.,

$$f^{(i)}(\mathbf{x}) = f^{(j)}(\mathbf{x}) \quad \text{with} \quad f_x^{(i)}(\mathbf{x}) \neq f_x^{(j)}(\mathbf{x}), \quad \text{for some} \quad \mathbf{x} \in \Sigma_{ij}.$$

CPWS systems do not have sliding motion.

- Discontinuous piecewise-smooth systems (**DPWS** systems) if

$$f^{(i)}(\mathbf{x}) \neq f^{(j)}(\mathbf{x}) \quad \text{for some} \quad \mathbf{x} \in \Sigma_{ij}.$$

In **DPWS** systems there can be sliding motion in a region of Σ_{ij} fulfilling certain conditions. Such systems are also known in the literature as Filippov systems and are described by a set of first-order differential equations with a discontinuous right-hand side. Also, it is possible to construct an appropriate vector field to describe this sliding motion, called sliding vector field (see [1]).

PWS systems exhibit the classical bifurcations (saddle-node, transcritical, Hopf, homoclinic, etc.) of smooth systems (see [19, 50]) and also unconventional bifurcations, unique to non-smooth systems, known as *discontinuity-induced bifurcations* (DIBs), see [43]. Bifurcations that determine changes in the number and nature of the equilibria and of the limit cycles of the system of study are of particular importance to this work. The topological changes from real to virtual equilibrium points (or vice versa), due to changes in some system parameters, can lead to boundary equilibrium bifurcations (BEB); see [23, 19, 20, 24, 25]. Besides the classical bifurcations, the DIBs, such as sliding bifurcations of limit cycles that occur when a limit cycle develops an intersection (tangential or transversal) with a sliding region as Grazing-sliding bifurcations (GS); see [19, 26, 37, 27, 38, 39, 28] are dealt with in this thesis; and discontinuous saddle-node (DSN, [22]).

An important feature of **PWS** systems is the presence of different types of equilibrium points such as regular equilibrium, boundary equilibrium and the so-called pseudo-equilibrium. In particular, the latter is the equilibrium at the switching boundary where the sliding vector field becomes stationary, and can be achieved in finite time by trajectories initiated outside of the boundary. In *Sliding* mode control (SMC) processes [14], the desired operating point is a stable pseudo-equilibrium of the system that belongs to an attractive region into the switching boundary where the sliding occurs. The output of the pseudo-equilibrium of this attractive sliding region, induced by the variation of a system parameter, is usually associated with typical bifurcations of **DPWS** systems such as the boundary equilibrium bifurcations (BEBs) which will be studied in detail in this thesis.

General Purpose

The main objective of this thesis is the study of piecewise smooth (**PWS**) dynamical systems with applications in non-linear control systems in different areas of science and engineering such as biology and power electronics. In particular, we are interested in **PWS** systems with two and three dimensions, and in the qualitative analysis of these systems, paying special attention to the constant solutions on the switching boundaries associated with the resulting sliding vector field equilibrium, as well as the characterization and classification of bifurcations induced by the switching boundaries by numerical and analytical methods.

Specific Objectives

- Study the dynamics and the stability of a system of n capacitors connected in a serial arrangement to a voltage source and controlled by a switching control law with multiple boundaries by using the tools of the **PWS** systems theory.
- Analyze the local and global dynamics of a power electronic circuit feeding a constant power load and controlled by a sliding mode control law which is modeled as a 3D **DPWS** system with two transversal switching boundaries.
- Analyze the local and global dynamics of a two-predator one-prey system under harvesting actions that it is introduced by means of two switching control actions defined on the predator species and determine the conditions on the system parameters so that the coexistence equilibrium (which is the reference pseudo-equilibrium of the system) of the predators is globally stable.
- Provide numerical simulations of the studied systems to better understand the dynamic behavior of such systems, and to check the theoretical results obtained.

Outline

This document is organized as follows:

Chapter 1 presents the elementary definitions related to the **DPWS** systems as well as the tools to analyze the dynamic behavior of these systems. Also, we describe briefly discontinuous-induced bifurcations (DIB) such as boundary equilibrium bifurcation (BEB), discontinuous saddle-node (DSN) and Grazing-sliding bifurcation.

Chapter 2 we study an application of the capacitor voltage-balancing system found in modular multilevel converters (MMC) and we show an important result on local stability of the model with n submodules (SM). Moreover, we describe the global dynamics of systems with two SMs, modeled by **2D-DPWS** and **3D-DPWS** systems with two transversal switching boundaries. Also, we analyze and characterize the sliding vector field at the intersection of two transversal switching boundaries. Finally, to validate the theoretical analysis, we provide the results of numerical simulations on a MMC with 10 SMs. This chapter originated from the published paper: Rony Cristiano, Daniel J. Pagano and Marduck M. Henao. Multiple boundaries sliding mode control applied to capacitor voltage-balancing systems *Commun Nonlinear Sci Numer Simulat.*, 91 (2020), doi:10.1016/j.cnsns.2020.105430.

Chapter 3 we analyse a dc-dc bidirectional buck composed of two buck converters connected in a cascade structure being the first buck converter controlled by a sliding mode control (SMC) law and the second converter modeled by a piecewise constant power load (CPL). In particular, we analyze a piecewise smooth dynamical system in \mathbb{R}^3 with two transversal switching boundaries where the sliding motion occurs only at the SMC-boundary. Furthermore, the local and global phenomena associated with bifurcations induced by two transversal switching boundaries are shown (DIB, BEB, DSN, GS). Also, we present numerical results on the bifurcation and study the vanishing (or birth) of limit cycles. This chapter originates from the published paper: Marduck

M. Henao, Rony Cristiano, Daniel J. Pagano. Bifurcation analysis of 3D-PWS systems with two transversal switching boundaries: A case study in power electronics, *Physica D Nonlinear Phenomena*, 442 (2022), doi: 10.1016/j.physd.2022.133505.

Chapter 4 consists of an investigation of the global dynamics of a three-dimensional Lotka-Volterra system described by two predator species competing for one prey and with human harvesting action on the predator species. The harvesting action is introduced by means of two switching control actions defined on the predator species. We prove that there is a global stable equilibrium point where the three species can coexist due to the proposed harvesting action. This chapter originates from the published paper: Rony Cristiano, Marduck M. Henao, Daniel J. Pagano. Global stability of a Lotka-Volterra piecewise-smooth system with harvesting actions and two predators competing for one prey, *Journal of Mathematical Analysis and Applications*, 522 (2023), doi: 10.1016/j.jmaa.2023.126998.

Chapter 5 we analyse the nonlinear dynamics of a DC-DC buck converter controlled by a sliding mode control law connected to two power converters where one of them is a boost converter and the other is a buck converter, both modeled by a CPL piecewise function. The main focus is to study the stability analysis method of this type of model and its pseudo equilibrium point, which is the operating point. The results obtained in this chapter will be published in another scientific journal.

Chapter 6 presents the final remarks of this thesis.

List of publications

As a result of the work developed during the doctorate, we obtained three articles published in recognized journals and works presented at national and international scientific events.

- Published:

- 1 Rony Cristiano, Daniel J. Pagano, Marduck M. Henao, “Multiple boundaries sliding mode control applied to capacitor voltage-balancing systems”, manuscript accepted for publication in *Communications in Nonlinear Science and Numerical Simulation (CNSNS)*, 91 (2020), doi:10.1016/j.cnsns.2020.105430.
- 2 Marduck M. Henao, Rony Cristiano, Daniel J. Pagano, “Bifurcation analysis of 3D-PWS systems with two transversal switching boundaries: A case study in power electronics”, manuscript accepted for publication in *Physica D Nonlinear Phenomena*, 442 (2022), doi: 10.1016/j.physd.2022.133505.
- 3 Rony Cristiano, Marduck M. Henao, Daniel J. Pagano, “Global stability of a Lotka-Volterra piecewise-smooth system with harvesting actions and two predators competing for one prey”, manuscript accepted for publication in *Journal of Mathematical Analysis and Applications*, 522 (2023), doi: 10.1016/j.jmaa.2023.126998.

- Works of scientific events:

- 4 XXIX IME Week and IME/UFG Research and Postgraduate Seminar (Virtual Edition) on October 5 to 8, 2021, presenting a talk entitled *Local and global bifurcations in 3D-PWS systems with two transversal switching boundaries: a case study in power electronics*. Goiânia-GO.
- 5 Second Virtual Workshop on Dynamical Systems on November 10 to 12, 2021, presenting a talk entitled *Dynamic behaviors of a Lotka-Volterra piecewise-smooth system with two predators competing for one prey and harvesting actions*. Ribeirão Preto-SP.
- 6 XI workshop on Dynamical Systems on November 07 to 10, 2022, presenting a poster entitled *Complex Dynamics in DC-DC power converters connected in parallel*. Ribeirão Preto-SP, FFCLRP-USP.

Chapter 1

Preliminaries and background materials

In this chapter, we present a brief outline of the mathematical structure and notations that we will use throughout this work. We start with a brief introduction to the qualitative theory for smooth dynamical systems, including a quick review of classical bifurcations for these systems (saddle node, transcritical, Hopf, etc.), highlighting that they also make sense for nonsmooth systems. Then we present the definitions and notations regarding **DPWS** dynamical systems, as well as the tools for the analysis of these systems. In particular, we are interested in two and three-dimensional **DPWS** systems with two switching boundaries.

1.1 Smooth dynamical systems

We begin with a formal definition of a dynamical system and recall elements of the concept from the theory of smooth dynamical systems that can also be applied to non-smooth systems. In general terms, dynamic systems are systems whose states evolve over time. Knowing the current state of the system and the laws that govern its evolution, the behavior of such a system can be predicted to some extent, provided the laws do not change over time. Therefore, a dynamical system can be defined through three components: a state space, a non-empty set representing the space of time, and a law of evolution of the state in time.

Let $X \subset \mathbb{R}^n$ be the state space. We can define an operator ϕ in \mathbf{x} that evolves previously known elements x_0 through a “time” t to a state \mathbf{x}_t :

$$\begin{aligned}\phi^t : X &\rightarrow X \\ x &\mapsto \phi^t(\mathbf{x}) = \mathbf{x}_t.\end{aligned}$$

The time t assumes values in a set of indices \mathcal{T} , which is usually discrete (\mathbb{Z}) or continuous (\mathbb{R}). The operator ϕ^t is called “the evolution operator” and defines a dynamic system when it is equipped with a *semi-group* structure, see [8].

Definition 1.1.1. *A state space X , a time set \mathcal{T} and the evolution operator ϕ^t define a dynamical system if*

- (i) $\phi^0(\mathbf{x}) = \mathbf{x}$, for all $\mathbf{x} \in X$,

(ii) $\phi^{t+s}(\mathbf{x}) = \phi^t(\phi^s(\mathbf{x}))$, for all $\mathbf{x} \in X$ and $t, s \in \mathcal{T}$.

The above definition is quite general and encompasses the two major strands of dynamic systems theory, namely, continuous-time and discrete-time dynamical systems. We will consider here only systems of the first type, that is, when \mathcal{T} is an interval $I \subset \mathbb{R}$, [8].

Consider a system of *ordinary differential equations* (ODEs)

$$\dot{\mathbf{x}} = F(\mathbf{x}), \quad \mathbf{x} \in \mathcal{D} \subset \mathbb{R}^n, \quad (1.1.1)$$

where \mathcal{D} is a domain and $F : \mathcal{D} \subset \mathbb{R}^n \rightarrow \mathbb{R}^n$ is a vector field sufficiently smooth.

If we define $X = \mathcal{D}$, $\mathcal{T} = I \subset \mathbb{R}$ and $\phi^t(\mathbf{x}) = \varphi(\mathbf{x}, t)$, where $\varphi(\mathbf{x}, t)$ is the *flow* that takes the initial condition \mathbf{x} to its solution at time t :

$$\frac{\partial}{\partial t} \varphi(\mathbf{x}, t) = F(\varphi(\mathbf{x}, t)), \quad \varphi(\mathbf{x}, 0) = \mathbf{x},$$

then $\{X, \mathcal{T}, \phi^t\}$ defines a *continuous dynamical system*.

We say that a dynamical system is smooth of index r , or of class \mathbf{C}^r , if the first r derivatives of φ with respect to \mathbf{x} exist and are continuous at every point $\mathbf{x} \in X$. Thus, if we suppose that the vector field F in (1.1.1) is of class \mathbf{C}^{r-1} for some $r \geq 2$, then the *flow* $\varphi(\mathbf{x}, t)$ is of a smoother index and therefore the dynamical system $\{D, I, \varphi\}$ is \mathbf{C}^r .

Definition 1.1.2. *The subset $\mathcal{O}(\mathbf{x}_0) = \{\mathbf{x} \in D : \mathbf{x} = \varphi(\mathbf{x}_0, t), t \in I\}$ is called orbit or trajectory through the point \mathbf{x}_0 . The phase portrait of the dynamical system is the partitioning of the state space into orbits.*

Definition 1.1.3. *A point $\mathbf{x} \in D \subset \mathbb{R}^n$ is said to be an equilibrium point of (1.1.1) if $F(\mathbf{x}) = 0$.*

Definition 1.1.4. *A cycle (or a closed orbit) is a periodic orbit, that is, an orbit γ not reduced to a point such that each point $\mathbf{x} \in \gamma$ satisfies $\varphi(\mathbf{x}, t + t_0) = \varphi(\mathbf{x}, t)$ for some $t_0 > 0$.*

Definition 1.1.5. *A closed orbit γ in a neighborhood in which there are no other cycles is called a limit cycle.*

Usually, it is important that the dynamics of the system behave in a stable manner, that is, the final state of the dynamics does not change due to small changes in the initial conditions.

Definition 1.1.6. *An equilibrium point x_0 of (1.1.1) is (Lyapunov) stable if for all neighborhood $U_1 \subset \mathcal{D}$ of x_0 there is a neighborhood $U_2 \subset U_1$ of \mathbf{x}_0 such that every solution $\varphi(\mathbf{x}_0, t)$ of (1.1.1) with $\varphi(\mathbf{x}_0, 0) \in U_2$ is defined and in U_1 for all $t \geq 0$.*

Definition 1.1.7. *An equilibrium \mathbf{x}_0 of (1.1.1) is said to be asymptotically stable (in the sense of Lyapunov) if*

(i) *it is stable;*

(ii) $\lim_{t \rightarrow \infty} \varphi(\mathbf{x}, t) = \mathbf{x}_0$, *para todo \mathbf{x} in some neighborhood of \mathbf{x}_0 .*

We will say that an equilibrium is unstable if it is not stable according to Definition 1.1.6.

One of the goals of the dynamical system theory is to qualitatively classify dynamics. Roughly speaking, structurally stable systems are those in which all “close” systems have qualitatively “equivalent” dynamics. The notion of proximity and equivalence is formalized below, following [8].

We will denote by $\Omega^r = \Omega^r(\mathcal{D})$ the space of the vector fields of class \mathbf{C}^r in \mathcal{D} , with $r \geq 1$. Consider \mathbf{C}^r a topology of Ω^r , whose basic neighborhood of radius ϵ of a field $F_0 \in \Omega^r$ is defined as

$$\mathcal{B}(F_0, \epsilon) = \{F \in \Omega^r; \|F - F_0\|_r < \epsilon\},$$

where

$$\|F\|_r := \sup_{\mathbf{x} \in \mathcal{D}} \{\|F\|, \|DF\|, \dots, \|D^r F\|\}.$$

Remark 1.1.8. $\|\cdot\|_{\text{sup}}$ denotes the norm of vectors (and matrices) called the supremum norm

$$\|\mathbf{x}\|_{\text{sup}} = \sup \left(\sqrt{\sum_{i=1}^n x_i^2} \right) \quad \text{and} \quad \|A\|_{\text{sup}} = \sup \left(\sqrt{\sum_{i,j=1}^n a_{ij}^2} \right),$$

where $\mathbf{x} = (x_1, \dots, x_n)$ and $A = (a_{ij})_n$.

Now consider two dynamical systems

$$\dot{\mathbf{x}} = F(\mathbf{x}), \quad \mathbf{x} \in \mathcal{D} \subset \mathbb{R}^n, \quad (1.1.2)$$

$$\dot{\mathbf{x}} = G(\mathbf{x}), \quad \mathbf{x} \in \mathcal{D} \subset \mathbb{R}^n, \quad (1.1.3)$$

where F and G are smooth vector fields in \mathcal{D} .

We say that the systems (1.1.2) and (1.1.3) are ϵ -proximals in \mathcal{D} if $\|F - G\|_r < \epsilon$ for some $\epsilon > 0$, or equivalently, if it exists some basic neighborhood \mathcal{B}_ϵ of Ω^r that contains $F, G \in \Omega^r$.

Definition 1.1.9. *Perturbation of parameter of the system (1.1.2) generates another system given by*

$$\dot{\mathbf{x}} = F(\mathbf{x}) + \mu G(\mathbf{x}) \quad \mathbf{x} \in \mathcal{D} \subset \mathbb{R}^n, \quad \mu \in \mathbb{R}, \quad (1.1.4)$$

where G is smooth field in \mathcal{D} and $\mu \in \mathbb{R}$ is the parameter.

Notice that, if $\mu = 0$ in (1.1.4), we recover (1.1.2). Thus, (1.1.4) can be rewritten as follows

$$\dot{\mathbf{x}} = G(\mathbf{x}, \mu) \quad \mathbf{x} \in \mathcal{D} \subset \mathbb{R}^n, \quad \mu \in \mathbb{R},$$

with $G(\mathbf{x}, 0) = F(\mathbf{x})$. A perturbation (1.1.4) has a maximum size ϵ if (1.1.4) is ϵ -proximal to system (1.1.2).

Definition 1.1.10. *Two dynamical systems $\dot{\mathbf{x}} = F(\mathbf{x})$ and $\dot{\mathbf{x}} = G(\mathbf{x})$ are topologically equivalent if there exists a homeomorphism $h : \mathbb{R}^n \rightarrow \mathbb{R}^n$ that carries the orbits of the first system onto orbits of the second one, preserving the orientation of the trajectories in time.*

Definition 1.1.11. A system is structurally stable if there is an $\epsilon > 0$ such that all perturbations of maximum size ϵ to the vector field F are topologically equivalent to G .

There is also the concept of smooth system conjugations, where the travel time of a trajectory is conserved by homeomorphism, see [8].

Definition 1.1.12. The systems $\dot{\mathbf{x}} = F(\mathbf{x})$ and $\dot{\mathbf{x}} = G(\mathbf{x})$ are topologically conjugates if it exists a homeomorphism $h : \mathbb{R}^n \rightarrow \mathbb{R}^n$ such that,

$$\varphi(\mathbf{x}, t) = h^{-1}(\psi(h(\mathbf{x}), t))$$

where $\varphi(\mathbf{x}, t)$ and $\psi(h(\mathbf{y}), t)$ are the flow generated by fields F and G , respectively.

Consider again a smooth dynamical system that depends on parameters, that is,

$$\dot{\mathbf{x}} = F(\mathbf{x}, \mu) \quad \mathbf{x} \in \mathcal{D} \subset \mathbb{R}^n, \quad \mu \in \mathbb{R}^p.$$

When considering a perturbation of the system under the action of the parameters, its phase portraits may vary. Thus, there are two possibilities: either the system remains topologically equivalent to the original or its topology changes. Next, we define a bifurcation in terms of the loss of structural stability when a parameter acts as a perturbation of the system (some types of smooth system bifurcations have been studied and classified; for more details see [49, 57, 54, 56]).

Definition 1.1.13. A bifurcation occurs at a parameter bifurcation $\mu = \mu_0$ if the dynamic system is not structurally stable.

- An unfolding of a bifurcation is a simplified system that for μ close to μ_0 it contains all possible structurally stable phase portraits that arise under small perturbations of the system at the bifurcation point.
- The codimension of a bifurcation is the dimension of parameter space required to unfold the bifurcation.
- A bifurcation diagram is a graphic representation that helps to understand how the phase portrait of the system varies with the parameter.

For more details see [8].

1.2 Piecewise-smooth control system

In this section, we present definitions, notations, and elementary concepts regarding **DPWS** systems as well as the tools for the analysis of the dynamic behaviour of such systems, and properties related to boundary equilibrium bifurcations (BEBs). In particular, we are interested in **DPWS** systems with multiple switching boundaries.

Since our interest is to study the piecewise-smooth control systems we consider a control system of the form

$$\dot{\mathbf{x}} = f(\mathbf{x}) + g(\mathbf{x})u, \tag{1.2.1}$$

where $\mathbf{x} = (x_1, x_2, \dots, x_n) \in \mathbb{R}^n$ is the state vector, $n \geq 2$, the dot "·" indicates derivatives with respect to t and the functions $f : \mathbb{R}^n \rightarrow \mathbb{R}^n$ and $g : \mathbb{R}^n \rightarrow \mathbb{R}^{n \times m}$ such that $g(\mathbf{x}) \neq 0$,

are smooth and the control signal $u = (u_1, u_2, \dots, u_m)$ is supposed to be a discontinuous function, which gives the discontinuity of the dynamical system (1.2.1). We assume that u_1, u_2, \dots, u_m are piecewise constant functions, defined by

$$u_k = \begin{cases} u_k^+, & \text{if } h_k(\mathbf{x}) > 0, \\ u_k^-, & \text{if } h_k(\mathbf{x}) < 0, \end{cases} \quad (1.2.2)$$

for $k = 1, 2, \dots, m$ and $u_k^+ \neq u_k^-$, where each function $h_k : \mathbb{R}^n \rightarrow \mathbb{R}$ fulfill $\nabla h_k(\mathbf{x}) \neq 0$, for all $\mathbf{x} \in \mathbb{R}^n$, where $\nabla h_k(\mathbf{x})$ represent the gradient of h_k . Thus, system (1.2.1) presents m switching boundaries of $(n - 1)$ -dimension, being defined by

$$\Sigma_k = \{\mathbf{x} \in \mathbb{R}^n : h_k(\mathbf{x}) = 0\}.$$

In addition, we assume that the gradient vectors $\{\nabla h_k\}_{k=1}^m$ are linearly independent and $\bigcap_{k=1}^m \Sigma_k$ is not empty.

System (1.2.1) endowed with the control law (1.2.2) constitutes a DPWS system of form

$$\dot{\mathbf{x}} = \mathbf{F}_i(\mathbf{x}), \quad \mathbf{x} \in R_i \subset \mathbb{R}^n, \quad (1.2.3)$$

where R_i , $i = 1, 2, \dots, 2^m$, are open regions separated by m switching boundaries Σ_k of $(n - 1)$ -dimension, transversely intersecting at a same point. The union of all boundaries Σ_k and all regions R_i covers the entire state space \mathcal{D} of (1.2.3), i.e.,

$$\left(\bigcup_{j=1}^{m-1} \Sigma_j\right) \cup \left(\bigcup_{i=1}^{2^m} R_i\right) = \mathcal{D}.$$

The non-smoothness occurs at one of the switching boundaries Σ_k and, if Σ_{ij} is the boundary that separates R_i from R_j , then $\mathbf{F}_i(\mathbf{x}) \neq \mathbf{F}_j(\mathbf{x})$ for some $\mathbf{x} \in \Sigma_{ij}$, see [8].

Remark 1.2.1. *It is worth to mention that (1.2.3) does not specify how the dynamics of the system evolve within the switching boundary. This basically depends on the dynamics of each vector field f_i near the border. One possibility is that the piecewise-smooth system crosses transversely Σ_{ij} , as in Figure 1.1; in this case, without loss of generality, we can establish that Σ_{ij} belongs to a single region \bar{R}_i . However, there may be a case where the dynamics of the DPWS system are confined to a switching boundary after contact with it (sliding motion). The region on Σ_{ij} where the sliding motion occurs is known as the sliding region. There are two approaches to studying the dynamics of this kind of system in the sliding region: Utkin's control method [14] and Filippov's Convex Method [1] (Utkin's method is an extension of Filippov's Method).*

Definition 1.2.2. *Two piecewise-smooth systems with switching boundaries Σ_k and $\tilde{\Sigma}_k$ are topologically equivalent by parts if:*

- 1.) *They are topologically equivalent, that is, there is a homeomorphism $h : \mathbb{R}^n \rightarrow \mathbb{R}^n$ that carries the orbits of the first system into the orbits of the second, preserving the orientation of the trajectories, so that $\phi(\mathbf{x}, t) = h^{-1}(\tilde{\phi}(h(\mathbf{x}), s))$, where the application $t \rightarrow s(t)$ is continuous and inverse.*
- 2.) *The homeomorphism h preserves each of the switching boundaries, that is, $h(\Sigma_k) = \tilde{\Sigma}_k$.*

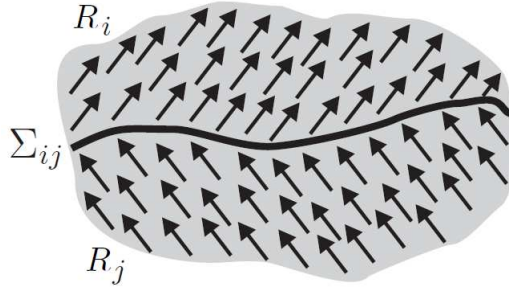


Figure 1.1: Piecewise-smooth vector field.

The sliding dynamics of system (1.2.3) occurs on $\Sigma = \bigcup_{k=1}^m \Sigma_k$ and exists when Σ attracts close trajectories in finite time, so that trajectories become restricted to Σ following a sliding motion. Associated to the sliding dynamics there is a vector field, known as *sliding vector field*. Following [1], we consider that a sliding vector field is any vector field given by

$$\mathbf{F}_s(\mathbf{x}) = \sum_{i=1}^{2^m} \lambda_i(\mathbf{x}) \mathbf{F}_i(\mathbf{x}),$$

such that $\mathbf{x} \in \Sigma$, $\lambda_i(\mathbf{x}) \geq 0$ and $\sum_{i=1}^{2^m} \lambda_i(\mathbf{x}) = 1$. The functions $\lambda_1(\mathbf{x}), \lambda_2(\mathbf{x}), \dots$, are selected in such a way that \mathbf{F}_s is tangent to Σ at \mathbf{x} , that is, λ_i must satisfy the constraint $\nabla h_k(\mathbf{x})^T \cdot \mathbf{F}_s(\mathbf{x}) = 0$, i.e.,

$$\sum_{i=1}^{2^m} \lambda_i(\mathbf{x}) \nabla h_k(\mathbf{x})^T \cdot \mathbf{F}_i(\mathbf{x}) = 0, \quad \text{for } k = 1, 2, \dots, m.$$

From the constraint above it is generally not possible to obtain $\lambda_i(\mathbf{x})$'s functions uniquely, which can lead to many sliding vectors at \mathbf{x} , see [18]. This ambiguity problem does not appear when the sliding motion occurs at a single switching boundary, as shown in Subsection 1.2.1. The method used in this case is well known in the literature and appears in many works, see for instance [19, 20]. On the other hand, when the sliding motion occurs at the intersection of two or more switching boundaries, there is still no widespread general method that determines a single sliding vector field, being able to describe the dynamic characteristics of this sliding motion. Some recent works deal with the problem of sliding vector ambiguity and present proposals on how to define a sliding vector field at the intersection of switching boundaries, see for instance [10, 18].

However, for **DPWS** systems derived from the control system given in (1.2.1)-(1.2.2), it is possible to obtain a single solution for the sliding vector at the intersection of switching boundaries. To see this, just use the *equivalent control method*, see [14, 15] and Subsection 1.2.2. Then, we define $h^T(\mathbf{x}) = [h_1(\mathbf{x}) \ h_2(\mathbf{x}) \ \dots \ h_m(\mathbf{x})]$, $L_g h(\mathbf{x}) = h_x(\mathbf{x}) \cdot g(\mathbf{x})$ and $L_f h(\mathbf{x}) = h_x(\mathbf{x}) \cdot f(\mathbf{x})$, where $h_x(\mathbf{x})$ is a $m \times n$ matrix whose rows are the gradients of the functions h_k . In addition, we assume that $L_g h(\mathbf{x})$ is nonsingular for all \mathbf{x} . The equivalent control $u_{eq}(\mathbf{x})$ is solution of

$$\frac{d}{dt} h(\mathbf{x}) = L_f h(\mathbf{x}) + L_g h(\mathbf{x}) \cdot u_{eq}(\mathbf{x}) = 0,$$

i.e.,

$$u_{eq}(\mathbf{x}) = -(L_g h(\mathbf{x}))^{-1} \cdot L_f h(\mathbf{x}). \quad (1.2.4)$$

Introducing the equivalent control in the equations of system (1.2.1), we obtain the sliding vector field

$$\mathbf{F}_s(\mathbf{x}) = f(\mathbf{x}) - g(\mathbf{x}) \cdot (L_g h(\mathbf{x}))^{-1} \cdot L_f h(\mathbf{x}), \quad (1.2.5)$$

restricted to the intersection of the switching boundaries $\Sigma_1, \Sigma_2, \dots$, given by $h(\mathbf{x}) = 0$.

By the above assumptions, if $m \geq n$ then the switching boundaries intersect transversely at a single point of \mathbb{R}^n , say \mathbf{x} , and the sliding vector field on it is null, i.e., $\mathbf{F}_s(\mathbf{x}) = 0$. In this case, \mathbf{x} is a pseudo-equilibrium point of the switching system.

Definition 1.2.3. *Consider the dynamical system (1.2.3) and let $x \in \mathbb{R}^n$. We say that:*

- (i) \mathbf{x} is a **regular equilibrium** point associated to the vector field \mathbf{F}_i if $\mathbf{F}_i(\mathbf{x}) = 0$ and $\mathbf{x} \in \bigcup_{i=1}^{2^m} R_i$. It is real (admissible) whenever $\mathbf{x} \in R_i$, or virtual in the other case.
- (ii) \mathbf{x} is a **boundary equilibrium** point associated to the vector field \mathbf{F}_i if $\mathbf{F}_i(\mathbf{x}) = 0$ and $\mathbf{x} \in \overline{R_i}$ (implies $\mathbf{x} \in \Sigma_k$ for some k).
- (iii) Some other stationary point that is not equilibrium in any of the vector fields \mathbf{F}_i , may appear over one of the switching boundaries $\Sigma_1, \Sigma_2, \dots$, including at the intersection of two or more boundaries. Such a point is called **pseudo-equilibrium**. In addition, if \mathbf{x} is a pseudo-equilibrium then it is an equilibrium of the sliding dynamics induced by vector fields $\mathbf{F}_1, \mathbf{F}_2, \dots$, in the neighborhood of \mathbf{x} .

It is a difficult problem to analyze all possible cases for dealing with **DPWS** systems with n boundaries, as we do not have a general theory. This class of systems is studied case by case. It might not be surprising that simulating a set of equations across a discontinuity results in some irregular or unpredictable behavior. In the intersection of discontinuity surfaces the dynamic of the system evolves approximately along a discontinuity surface, the dynamics find an attractor that approximates, but the attractor can be sensitive to parameters of the vector field or the switching method, undergoing numerous bifurcations that affect the speed of the sliding motion. The problem of motion along the intersection of discontinuity surfaces was left open in Filippov's influential work [1] and has recently been taken up from a variety of perspectives based on practical considerations of how to model dynamics around discontinuities, see e.g. [11, 12, 9, 18, 13, 100] or on more theoretical considerations such as equivalence classes and stability, see e.g. [98, 99] and references therein. Next, we will show theoretical tools for qualitative analysis of **DPWS** systems in \mathbb{R}^n with one or two discontinuity boundaries (plane surfaces).

1.2.1 A single switching boundary

We consider $m = 1$ in system (1.2.3), and $\Sigma = \{x \in \mathbb{R}^n : h(x) = 0\}$ for some $h : \mathbb{R}^n \rightarrow \mathbb{R}$, as being a switching boundary splitting the state space into two open regions

$$R_1 = \{x \in \mathbb{R}^n : h(x) < 0\} \text{ and } R_2 = \{x \in \mathbb{R}^n : h(x) > 0\}$$

such that $\mathbb{R}^n = R_1 \cup R_2 \cup \Sigma$. Therefore, the general system (1.2.3) becomes a **DPWS** dynamical system of the form:

$$\dot{\mathbf{x}} = \begin{cases} \mathbf{F}_1(\mathbf{x}), & \text{if } \mathbf{x} \in R_1, \\ \mathbf{F}_2(\mathbf{x}), & \text{if } \mathbf{x} \in R_2, \end{cases} \quad (1.2.6)$$

Remark 1.2.4. *The contact type of the orbits of a vector field \mathbf{F} with a switching boundary Σ defined by $h(\mathbf{x}) = 0$, are provided by the directional Lie derivatives: $L_{\mathbf{F}}h = \nabla h^T \cdot \mathbf{F}$ (or $L_{\mathbf{F}}h = \langle \nabla h, \mathbf{F} \rangle$). The higher order Lie derivatives are given by $L_{\mathbf{F}}^q h = \nabla L_{\mathbf{F}}^{q-1} h^T \cdot \mathbf{F}$ (or $L_{\mathbf{F}}^q h = \langle \nabla L_{\mathbf{F}}^{q-1} h, \mathbf{F} \rangle$).*

The switching boundary Σ can be partitioned into regions with different dynamical behaviours: (i) **crossing** regions (Σ_c^\pm), where one vector field is pointing to Σ and the other is pointing out of the boundary; (ii) **attractive sliding** region (Σ_{as}), where the vector fields \mathbf{F}_1 and \mathbf{F}_2 point towards Σ from both sides; (iii) **repulsive sliding** region (Σ_{rs}), where both \mathbf{F}_1 and \mathbf{F}_2 are pointing out of Σ from either sides. Points in such regions are qualified accordingly. Thus, we can explicitly determine the sliding and crossing regions as follows:

$$\Sigma_{as} = \{\mathbf{x} \in \Sigma : L_{\mathbf{F}_2}h(\mathbf{x}) < 0 < L_{\mathbf{F}_1}h(\mathbf{x})\}, \quad (1.2.7)$$

$$\Sigma_{rs} = \{\mathbf{x} \in \Sigma : L_{\mathbf{F}_1}h(\mathbf{x}) < 0 < L_{\mathbf{F}_2}h(\mathbf{x})\}, \quad (1.2.8)$$

$$\Sigma_c^- = \{\mathbf{x} \in \Sigma : L_{\mathbf{F}_1}h(\mathbf{x}) < 0 \text{ and } L_{\mathbf{F}_2}h(\mathbf{x}) < 0\}, \quad (1.2.9)$$

$$\Sigma_c^+ = \{\mathbf{x} \in \Sigma : L_{\mathbf{F}_1}h(\mathbf{x}) > 0 \text{ and } L_{\mathbf{F}_2}h(\mathbf{x}) > 0\}. \quad (1.2.10)$$

These regions are separated by lines formed by tangency points of the vector fields $\mathbf{F}_{1,2}$ with Σ , satisfying the tangency condition $L_{\mathbf{F}_{1,2}}h(\mathbf{x}) = 0$ and $h(\mathbf{x}) = 0$. Then, we define two sets of tangential singularities:

$$T_+ = \{\mathbf{x} \in \Sigma : L_{\mathbf{F}_2}h(\mathbf{x}) = 0\}$$

and

$$T_- = \{\mathbf{x} \in \Sigma : L_{\mathbf{F}_1}h(\mathbf{x}) = 0\};$$

one for each vector field involved. Note that these tangency points are assumed to be smooth curves contained in Σ , that is, to T_+ (resp. T_-) as the **tangency line** of \mathbf{F}_2 (resp. \mathbf{F}_1). Points where both vector fields $\mathbf{F}_{1,2}$ are tangent to Σ , that is, $\mathbf{x} \in T_+ \cap T_-$ are called **double tangency points** which are classified generically as two-fold singularities. The following provides the definition of tangential singularities; see [1, 19].

Definition 1.2.5. (i) $\hat{\mathbf{x}} \in \Sigma$ is a fold point of \mathbf{F}_1 if $\hat{\mathbf{x}} \in T_+$, $L_{\mathbf{F}_1}h(\hat{\mathbf{x}}) = 0$ and $L_{\mathbf{F}_1}^2h(\hat{\mathbf{x}}) \neq 0$ (the contact of \mathbf{F}_1 with Σ is quadratic). Moreover, we say that this fold point is **visible** (resp. **invisible**) if $L_{\mathbf{F}_1}^2h(\hat{\mathbf{x}}) < 0$ (resp. $L_{\mathbf{F}_1}^2h(\hat{\mathbf{x}}) > 0$), i.e., the orbit of $\dot{\mathbf{x}} = \mathbf{F}_1(\mathbf{x})$ starting at $\hat{\mathbf{x}}$, belongs to R_1 (resp. R_2) for all sufficiently small $|t| \neq 0$. See Figure 1.2(a)-(b), respectively.

(ii) $\hat{\mathbf{x}} \in \Sigma$ is a fold point of \mathbf{F}_2 if $\hat{\mathbf{x}} \in T_-$, $L_{\mathbf{F}_2}h(\hat{\mathbf{x}}) = 0$ and $L_{\mathbf{F}_2}^2h(\hat{\mathbf{x}}) \neq 0$. Moreover, we say that this fold point is **visible** (resp. **invisible**) if $L_{\mathbf{F}_2}^2h(\hat{\mathbf{x}}) > 0$ (resp. $L_{\mathbf{F}_2}^2h(\hat{\mathbf{x}}) < 0$), i.e., the orbit of $\dot{\mathbf{x}} = \mathbf{F}_2(\mathbf{x})$ starting at $\hat{\mathbf{x}}$, belongs to R_2 (resp. R_1) for all sufficiently small $|t| \neq 0$. See Figure 1.2(a)-(b), respectively.

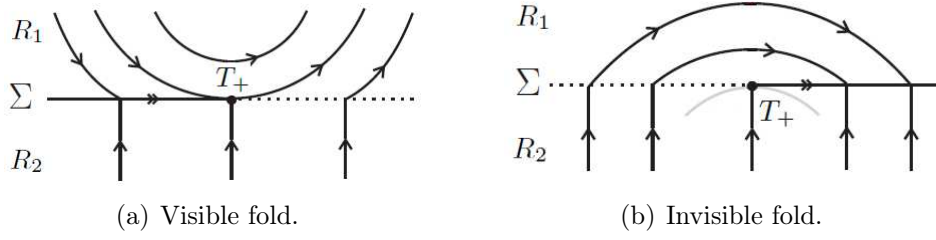


Figure 1.2: Tangent points: (a) visible and (b) invisible of a plane Filippov system. The solid region (dotted) of the boundary Σ represents the sliding region (crossing).

- Definition 1.2.6.** (i) $\mathbf{x}_c \in \Sigma$ is a cusp point of \mathbf{F}_1 if $\mathbf{x}_c \in T_-$, $L_{\mathbf{F}_1}^2 h(\mathbf{x}_c) = 0$, $L_{\mathbf{F}_1}^3 h(\mathbf{x}_c) \neq 0$ and the set $\{\nabla h(\mathbf{x}_c), \nabla L_{\mathbf{F}_1} h(\mathbf{x}_c), \nabla L_{\mathbf{F}_1}^2 h(\mathbf{x}_c)\}$ is linearly independent.
- (ii) $\mathbf{x}_c \in \Sigma$ is a cusp point of \mathbf{F}_2 if $\mathbf{x}_c \in T_+$, $L_{\mathbf{F}_2}^2 h(\mathbf{x}_c) = 0$, $L_{\mathbf{F}_2}^3 h(\mathbf{x}_c) \neq 0$ and the set $\{\nabla h(\mathbf{x}_c), \nabla L_{\mathbf{F}_2} h(\mathbf{x}_c), \nabla L_{\mathbf{F}_2}^2 h(\mathbf{x}_c)\}$ is linearly independent.

The orbits of system (1.2.6) can be constructed by concatenating standard solutions in $R_{1,2}$ and sliding solutions on Σ following the Filippov convex method [1]. Once the sliding mode has been achieved introduced by the discontinuous vector field (1.2.6), the states are forced to follow a trajectory over the surface. This dynamic is restricted to the sliding set $\Sigma_{as} \cup \Sigma_{rs}$, and described by the sliding vector field

$$\mathbf{F}_s(\mathbf{x}) = (1 - \lambda)\mathbf{F}_1(\mathbf{x}) + \lambda\mathbf{F}_2(\mathbf{x}), \quad \text{with } \lambda = \frac{L_{\mathbf{F}_1} h(\mathbf{x})}{L_{\mathbf{F}_1} h(\mathbf{x}) - L_{\mathbf{F}_2} h(\mathbf{x})}, \quad (1.2.11)$$

or more concretely,

$$\mathbf{F}_s(\mathbf{x}) = \frac{L_{\mathbf{F}_2} h(\mathbf{x})\mathbf{F}_1(\mathbf{x}) - L_{\mathbf{F}_1} h(\mathbf{x})\mathbf{F}_2(\mathbf{x})}{L_{\mathbf{F}_2} h(\mathbf{x}) - L_{\mathbf{F}_1} h(\mathbf{x})}, \quad (1.2.12)$$

provided that the above denominator does not vanish. Therefore, $\lambda \in (0, 1)$ for all $\mathbf{x} \in \Sigma_{as} \cup \Sigma_{rs}$. While $\lambda = 0$ implies that $L_{\mathbf{F}_1} h(\mathbf{x}) = 0$, i.e., \mathbf{x} is a tangency point of the vector field \mathbf{F}_1 with the boundary Σ and $\mathbf{F}_s(\mathbf{x}) = \mathbf{F}_1(\mathbf{x})$ (\mathbf{x} becomes a boundary equilibrium if $\mathbf{F}_1(\mathbf{x}) = 0$); and $\lambda = 1$ implies that $L_{\mathbf{F}_2} h(\mathbf{x}) = 0$, i.e., \mathbf{x} is a tangency point of the vector field \mathbf{F}_2 with the boundary Σ and $\mathbf{F}_s(\mathbf{x}) = \mathbf{F}_2(\mathbf{x})$ (\mathbf{x} becomes a boundary equilibrium if $\mathbf{F}_2(\mathbf{x}) = 0$). Naturally, $\lambda \in (-\infty, 0) \cup (1, \infty)$ for all $\mathbf{x} \in \Sigma_c^+ \cup \Sigma_c^-$.

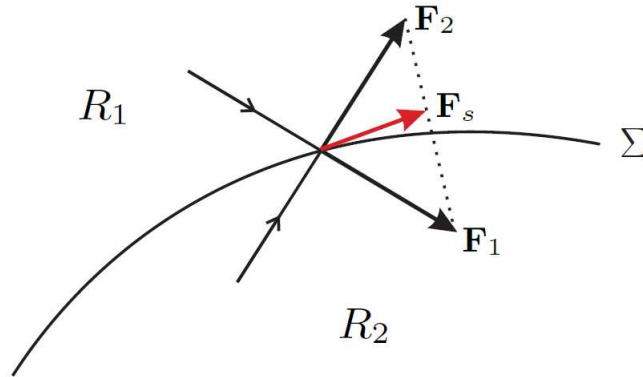


Figure 1.3: Geometric definition of the sliding vector field.

The sliding vector field \mathbf{F}_s can be rewritten in terms of the f and g functions from the control system given in (1.2.1). For this, we use the general sliding vector field given in (1.2.5), obtained from Utkin's equivalent control method [14], and so

$$\mathbf{F}_s(\mathbf{x}) = \mathbf{F}_1(\mathbf{x}) + \mathbf{F}_2(\mathbf{x})u_{eq}(\mathbf{x}),$$

where

$$u_{eq}(\mathbf{x}) = -\frac{L_{\mathbf{F}_1}h(\mathbf{x})}{L_{\mathbf{F}_2}h(\mathbf{x})}.$$

Note that the transversality condition $L_{\mathbf{F}_2}h(\mathbf{x}) \neq 0$ is a necessary condition for the existence of u_{eq} . Moreover, the attractive sliding condition at $\mathbf{x} \in \Sigma$ becomes

$$L_{\mathbf{F}_2}h(\mathbf{x})u^- < L_{\mathbf{F}_1}h(\mathbf{x}) < L_{\mathbf{F}_2}h(\mathbf{x})u^+.$$

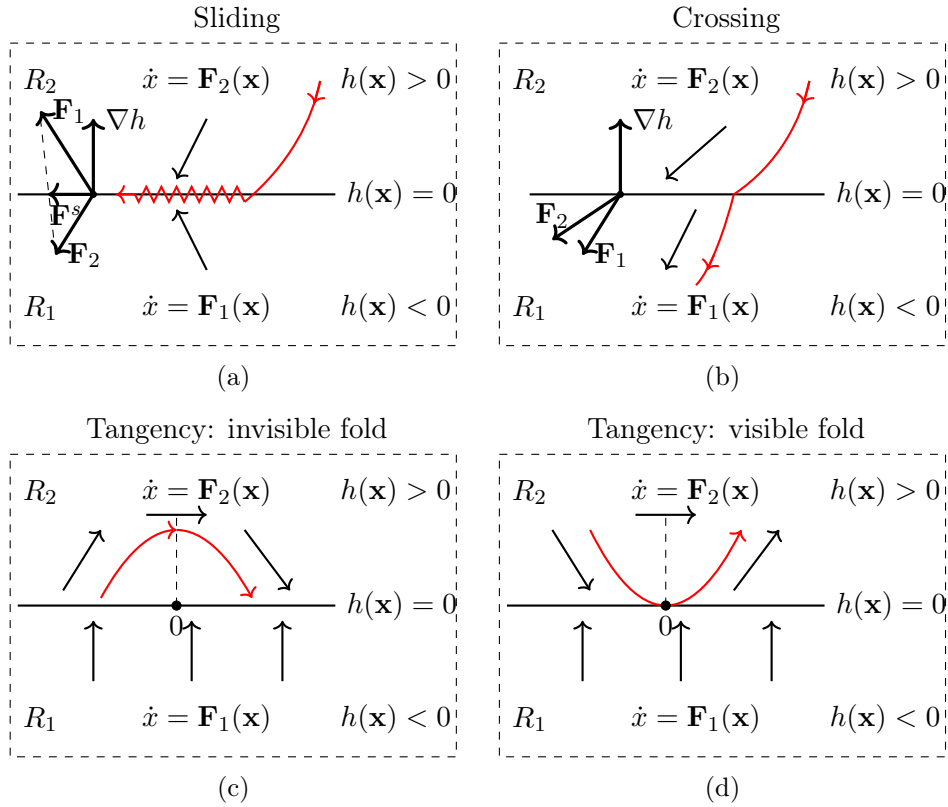


Figure 1.4: Some modes on Σ . In (a) is shown the attractive sliding motion that occurs in the set Σ_{as} , where $L_{\mathbf{F}_2}h(\mathbf{x}) < 0$ and $L_{\mathbf{F}_1}h(\mathbf{x}) > 0$. In (b) the crossing mode is shown, where a trajectory crosses Σ at a point of Σ_c^- (restricted to $L_{\mathbf{F}_2}h(\mathbf{x}) < 0$ and $L_{\mathbf{F}_1}h(\mathbf{x}) < 0$), passing from R_2 to R_1 . In (c)-(d) are shown the behavior of the system's orbits close to a tangency point at 0, associated to vector field \mathbf{F}_2 , being of the invisible fold type in (c), since $L_{\mathbf{F}_2}h(0) = 0$ and $L_{\mathbf{F}_2}^2h(0) < 0$, and of the visible fold type in (d), since $L_{\mathbf{F}_2}h(0) = 0$ and $L_{\mathbf{F}_2}^2h(0) > 0$.

The orbits of system (1.2.6) can be constructed by concatenating *standard* solutions in $R_1 \cup R_2$, and *sliding* solutions on Σ following the sliding system $\dot{\mathbf{x}} = \mathbf{F}_s(\mathbf{x})$; see [19, 21, 20].

The forward orbit of (1.2.6) that crosses Σ , goes from R_1 to R_2 through $x_0 \in \Sigma_c^+$ and goes from R_2 to R_1 through $x_0 \in \Sigma_c^-$ (see Figure 1.4(b)). The forward orbit of (1.2.6) that intersects Σ at a point $x_0 \in \Sigma_{as}$, continues from this point x_0 on a contained sliding motion in Σ (see Figure 1.4(a)). The forward orbits of (1.2.6) through $x_0 \in R_1 \cup R_2$ never reach the repulsive sliding region Σ_{rs} . But if $x_0 \in \Sigma_{rs}$, we can assume that there is a sliding motion starting at x_0 that follows the orbit of \mathbf{F}_s .

Sliding regions are delimited by tangency points. In addition, the sliding vector field \mathbf{F}_s is transversal to the set of tangency singularities at any fold point of this set, such that each invisible fold point is an entry point for attractive sliding dynamics and each visible fold point is an exit point from attractive sliding dynamics. The trajectory that leaves the attractive sliding region by a visible fold point of \mathbf{F}_1 (resp. \mathbf{F}_2), enters the R_1 (resp. R_2) region, see [21, 20]. Next, we refine the definition of natural equilibrium and pseudo-equilibrium point given in *Definition 1.2.3(iii)* for the vector field (1.2.6).

Definition 1.2.7. *The points $\tilde{\mathbf{x}} \in \Sigma$ are called **pseudo-equilibrium point** of the Filippov system (1.2.6) if $\tilde{\mathbf{x}} \in \Sigma_{as} \cup \Sigma_{rs}$ and it is an equilibrium for the sliding vector field \mathbf{F}_s , i.e.,*

$$\mathbf{F}_s(\tilde{\mathbf{x}}) = \mathbf{0} \quad \text{and} \quad h(\tilde{\mathbf{x}}) = 0.$$

For instance, suppose that \mathbf{F}_2 and \mathbf{F}_1 are transversal to Σ and anti-collinear at a certain point of this surface, that is, there exist $\lambda_1, \lambda_2 > 0$, such that

$$\lambda_1 \mathbf{F}_2 + \lambda_2 \mathbf{F}_1 = \mathbf{0}.$$

The point is necessarily in Σ_{as} , since then $L_{\mathbf{F}_{1,2}(\mathbf{x})}h(\mathbf{x})$ are non-zero and with different sign. In fact, it is immediate to conclude that at such point one has $\mathbf{F}_s = \mathbf{0}$, being a pseudo-equilibrium for (1.2.1). Reciprocally, if \mathbf{x} is a point of Σ_s with $\mathbf{F}_s(\mathbf{x}) = \mathbf{0}$ and it is not tangency point, both vector fields are anti-collinear at point. Sliding regions are delimited by points where the vector fields $\mathbf{F}_{1,2}$ are tangent to Σ . We recall that the discontinuous system (1.2.1) inherits the equilibrium vector field (1.2.12), and that they can be admissible (real) or non admissible (virtual) equilibria depending on its position with respect to the switching boundary.

Definition 1.2.8. *A point $\bar{\mathbf{x}} \in \mathbb{R}^n$ is a natural equilibrium of (1.2.6) if it is an equilibrium of the vector field \mathbf{F}_1 or \mathbf{F}_2 . Moreover, we say that $\bar{\mathbf{x}} \in \mathbb{R}^n$ is real (admissible) if*

$$\mathbf{F}_1(\bar{\mathbf{x}}) = \mathbf{0} \quad \text{and} \quad h(\bar{\mathbf{x}}) < 0,$$

or

$$\mathbf{F}_2(\bar{\mathbf{x}}) = \mathbf{0} \quad \text{and} \quad h(\bar{\mathbf{x}}) > 0.$$

Whenever $\mathbf{F}_2(\bar{\mathbf{x}}) = \mathbf{0}$ or $\mathbf{F}_1(\bar{\mathbf{x}}) = \mathbf{0}$ and $h(\bar{\mathbf{x}}) = 0$, the point $\bar{\mathbf{x}}$ is called **boundary equilibrium** of system (1.2.6). Thus, a boundary equilibrium point is at the boundary of the sliding set Σ_{as} ; and so from [19] it can also be considered a pseudo-equilibrium point. Therefore, some interaction between the equilibria of the two involved vector fields and the pseudo-equilibria of the sliding vector field appears whenever, by moving parameters, a real equilibrium point collides with Σ . We say then that the system undergoes a *boundary equilibrium bifurcation* of codimension-two (**BEB** for short).

1.2.2 Two switching boundaries

We consider in system (1.2.3) that $m = 2$ and there are two switching boundaries that intersect transversely, defined by

$$\begin{aligned}\Sigma_1 &= \{\mathbf{x} \in \mathbb{R}^n : h_1(\mathbf{x}) = 0\}, \\ \Sigma_2 &= \{\mathbf{x} \in \mathbb{R}^n : h_2(\mathbf{x}) = 0\}.\end{aligned}$$

In this case we have four open regions, given by

$$\begin{aligned}R_1 &= \{\mathbf{x} \in \mathbb{R}^n : h_1(\mathbf{x}) > 0 \text{ and } h_2(\mathbf{x}) > 0\}, \\ R_2 &= \{\mathbf{x} \in \mathbb{R}^n : h_1(\mathbf{x}) < 0 \text{ and } h_2(\mathbf{x}) > 0\}, \\ R_3 &= \{\mathbf{x} \in \mathbb{R}^n : h_1(\mathbf{x}) < 0 \text{ and } h_2(\mathbf{x}) < 0\}, \\ R_4 &= \{\mathbf{x} \in \mathbb{R}^n : h_1(\mathbf{x}) > 0 \text{ and } h_2(\mathbf{x}) < 0\};\end{aligned}$$

as Figure 1.5 shows.

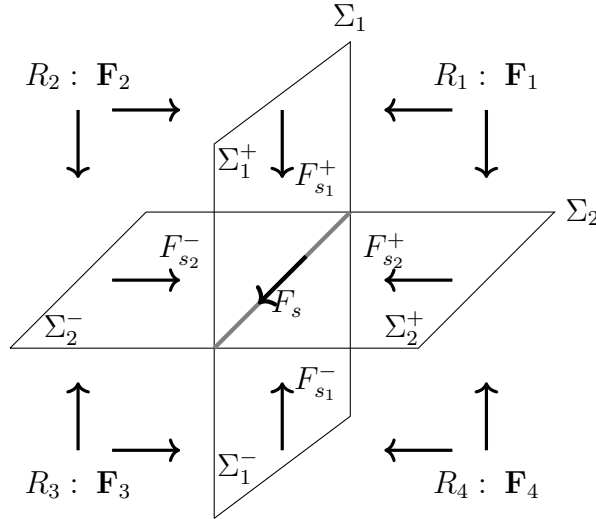


Figure 1.5: State space configuration in \mathbb{R}^3 with $\Sigma_1 \cup \Sigma_2$ attracting in finite time all nearby trajectories. The vector fields \mathbf{F}_i point to the switching boundaries Σ_1 and Σ_2 in all regions. Then, sliding vector fields can be defined in Σ_1 , Σ_2 and $\Sigma_1 \cap \Sigma_2$, being denoted by $F_{s_1}^\pm$, $F_{s_2}^\pm$ and F_s , respectively.

The Σ_1 boundary is divided into two parts, one for $h_2(\mathbf{x}) > 0$ and the other for $h_2(\mathbf{x}) < 0$, denoted by Σ_1^+ and Σ_1^- , respectively. In each part we can find sliding, crossing and tangency sets, as well as points of boundary equilibrium and of pseudo-equilibrium. Such elements are obtained and classified using the results and tools for the case with a single switching boundary, presented in the previous subsection. In addition, the sliding dynamics in Σ_1^+ (resp. Σ_1^-) can be analyzed using the sliding vector field defined in (1.2.11). The same applies to the Σ_2 boundary.

The interesting thing when it comes to systems with two switching boundaries is what happens at the intersection of these boundaries. Of course, in $\Sigma_1 \cap \Sigma_2$ we can also find singularities as the pseudo-equilibria, boundary equilibria, tangencies, besides sliding and

crossing sets. But for this, we must take into account the four vector fields, \mathbf{F}_1 , \mathbf{F}_2 , \mathbf{F}_3 and \mathbf{F}_4 , around this intersection.

We assume that there is a subset Σ_s of $\Sigma_1 \cap \Sigma_2$, such that

$$L_{\mathbf{F}_1} h_1(\mathbf{x}) < 0, \quad L_{\mathbf{F}_1} h_2(\mathbf{x}) < 0, \quad (1.2.13)$$

$$L_{\mathbf{F}_2} h_1(\mathbf{x}) > 0, \quad L_{\mathbf{F}_2} h_2(\mathbf{x}) < 0, \quad (1.2.14)$$

$$L_{\mathbf{F}_3} h_1(\mathbf{x}) > 0, \quad L_{\mathbf{F}_3} h_2(\mathbf{x}) > 0, \quad (1.2.15)$$

$$L_{\mathbf{F}_4} h_1(\mathbf{x}) < 0, \quad L_{\mathbf{F}_4} h_2(\mathbf{x}) > 0, \quad (1.2.16)$$

for all \mathbf{x} in that subset. In this case, both the switching boundaries Σ_1 and Σ_2 present sets of attractive sliding in a neighborhood of $\Sigma_1 \cap \Sigma_2$. In Σ_1 the sliding vector field, denoted by \mathbf{F}_{s_1} , is a piecewise smooth vector field of form

$$\mathbf{F}_{s_1}(\mathbf{x}) = \begin{cases} \mathbf{F}_{s_1}^+(\mathbf{x}), & \text{if } h_2(\mathbf{x}) > 0, \\ \mathbf{F}_{s_1}^-(\mathbf{x}), & \text{if } h_2(\mathbf{x}) < 0, \end{cases}$$

with $\mathbf{F}_{s_1}^\pm$ calculated from (1.2.11), getting

$$\mathbf{F}_{s_1}^+(\mathbf{x}) = \frac{L_{\mathbf{F}_2} h_1(\mathbf{x}) \cdot \mathbf{F}_1(\mathbf{x}) - L_{\mathbf{F}_1} h_1(\mathbf{x}) \cdot \mathbf{F}_2(\mathbf{x})}{L_{\mathbf{F}_2} h_1(\mathbf{x}) - L_{\mathbf{F}_1} h_1(\mathbf{x})},$$

for $h_2(\mathbf{x}) > 0$ and

$$\mathbf{F}_{s_1}^- = \frac{L_{\mathbf{F}_3} h_1(\mathbf{x}) \cdot \mathbf{F}_4(\mathbf{x}) - L_{\mathbf{F}_4} h_1(\mathbf{x}) \cdot \mathbf{F}_3(\mathbf{x})}{L_{\mathbf{F}_3} h_1(\mathbf{x}) - L_{\mathbf{F}_4} h_1(\mathbf{x})},$$

for $h_2(\mathbf{x}) < 0$.

In Σ_2 the sliding vector field, denoted by \mathbf{F}_{s_2} , is a piecewise smooth vector field of form

$$\mathbf{F}_{s_2}(\mathbf{x}) = \begin{cases} \mathbf{F}_{s_2}^+(\mathbf{x}), & \text{if } h_1(\mathbf{x}) > 0, \\ \mathbf{F}_{s_2}^-(\mathbf{x}), & \text{if } h_1(\mathbf{x}) < 0, \end{cases}$$

with $\mathbf{F}_{s_2}^\pm$ calculated from (1.2.11), getting

$$\mathbf{F}_{s_2}^+ = \frac{L_{\mathbf{F}_4} h_2(\mathbf{x}) \cdot \mathbf{F}_1(\mathbf{x}) - L_{\mathbf{F}_1} h_2(\mathbf{x}) \cdot \mathbf{F}_4(\mathbf{x})}{L_{\mathbf{F}_4} h_2(\mathbf{x}) - L_{\mathbf{F}_1} h_2(\mathbf{x})},$$

for $h_1(\mathbf{x}) > 0$ and

$$\mathbf{F}_{s_2}^- = \frac{L_{\mathbf{F}_3} h_2(\mathbf{x}) \cdot \mathbf{F}_2(\mathbf{x}) - L_{\mathbf{F}_2} h_2(\mathbf{x}) \cdot \mathbf{F}_3(\mathbf{x})}{L_{\mathbf{F}_3} h_2(\mathbf{x}) - L_{\mathbf{F}_2} h_2(\mathbf{x})},$$

for $h_1(\mathbf{x}) < 0$.

Note that $\Sigma_1 \cap \Sigma_2 = \Sigma_0$ is the switching boundary for both the vector fields \mathbf{F}_{s_1} , restricted to Σ_1 , and \mathbf{F}_{s_2} restricted to Σ_2 . The assumed conditions (1.2.13)-(1.2.16) ensure that $\Sigma_s \subset \Sigma_0$ is attractive in finite time, that is, for any $\mathbf{x} \in \Sigma_s$ we have

$$\begin{aligned} L_{\mathbf{F}_{s_1}^+} h_2(\mathbf{x}) &< 0, & L_{\mathbf{F}_{s_1}^-} h_2(\mathbf{x}) &> 0, \\ L_{\mathbf{F}_{s_2}^+} h_1(\mathbf{x}) &< 0, & L_{\mathbf{F}_{s_2}^-} h_1(\mathbf{x}) &> 0. \end{aligned}$$

We assume that the sliding vector field, denoted by \mathbf{F}_s and restricted to Σ_s , is given by

$$\mathbf{F}_s(\mathbf{x}) = \lambda_1 \mathbf{F}_1(\mathbf{x}) + \lambda_2 \mathbf{F}_2(\mathbf{x}) + \lambda_3 \mathbf{F}_3(\mathbf{x}) + \lambda_4 \mathbf{F}_4(\mathbf{x}), \quad (1.2.17)$$

where λ_i 's are smooth functions of \mathbf{x} , such that $\lambda_i \geq 0$ and $\lambda_1 + \lambda_2 + \lambda_3 + \lambda_4 = 1$. The λ_i 's functions must be chosen in order to fulfill the equations $L_{\mathbf{F}_s} h_1(\mathbf{x}) = 0$ and $L_{\mathbf{F}_s} h_2(\mathbf{x}) = 0$. For systems like (1.2.1)-(1.2.2), if we define $\mathbf{F}_1(\mathbf{x}) = f(\mathbf{x}) + g(\mathbf{x})u^{++}$, $\mathbf{F}_2(\mathbf{x}) = f(\mathbf{x}) + g(\mathbf{x})u^{-+}$, $\mathbf{F}_3(\mathbf{x}) = f(\mathbf{x}) + g(\mathbf{x})u^{--}$ and $\mathbf{F}_4(\mathbf{x}) = f(\mathbf{x}) + g(\mathbf{x})u^{+-}$, where

$$u^{++} = \begin{bmatrix} u_1^+ \\ u_2^+ \end{bmatrix}, \quad u^{-+} = \begin{bmatrix} u_1^- \\ u_2^+ \end{bmatrix}, \quad u^{--} = \begin{bmatrix} u_1^- \\ u_2^- \end{bmatrix}, \quad u^{+-} = \begin{bmatrix} u_1^+ \\ u_2^- \end{bmatrix},$$

then (1.2.17) is reduced to $\mathbf{F}_s(\mathbf{x}) = f(\mathbf{x}) + g(\mathbf{x})u_{eq}$ after taking

$$\lambda_1 u^{++} + \lambda_2 u^{-+} + \lambda_3 u^{--} + \lambda_4 u^{+-} = u_{eq}.$$

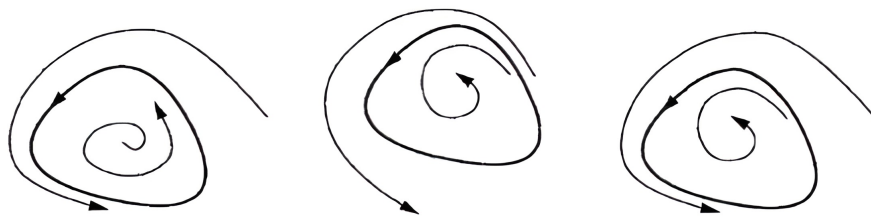
The u_{eq} vector, so-called equivalent control (see [15]), is obtained in a unique way from formula (1.2.4), leading to a well-defined and smooth sliding vector field at the intersection of Σ_1 and Σ_2 , which is, consequently, calculated by the formula given in (1.2.5).

1.3 Bifurcations of piecewise-smooth dynamical systems

In this section, we describe the basic concepts of smooth (or non-smooth) systems bifurcations, for which it is necessary to talk a little about *limit cycles*.

A *limit cycle* is an isolated and closed trajectory that can appear in the phase portrait of nonlinear systems. An isolated periodic orbit means the absence of other infinitesimally close closed trajectories. In this sense, neighboring trajectories close to a limit cycle must either approach or move away from it. If the trajectories that start in a neighborhood tend to the limit cycle, then we say that the *limit cycle is stable*, see Figure 1.6(a); otherwise, in which the trajectories move away from the limit cycle, we say that there is an *unstable limit cycle*, see Figure 1.6(b). If for certain neighborhoods the trajectories converge to the limit cycle and for other neighborhoods, the trajectories move away from the limit cycle, we say that the limit cycle is semi-stable, see Figure 1.6(c). The study of limit cycles has been used to model the behavior of a large number of dynamical systems in the real world, as the dynamics of a system can be characterized by its critical points and position of the variant manifolds. This generated a great deal of research interest in mathematicians, physicists and engineers. Although there is a lot of work on the existence and number of limit cycles in DPWS systems, this is still an open problem, even if we consider the discontinuity manifold as a straight line or plane surface. In general, finding limit cycles in a system is an arduous task and almost impossible in some cases. However, there are qualitative and numerical methods to find them.

The most important kind of limit cycle is the stable limit cycle, where nearby curves spiral toward the limit cycle on both sides. Periodic processes in nature can often be represented as stable limit cycles, so great interest is attached to finding such trajectories if they exist. Unfortunately, surprisingly little is known about how to do this, or how to



(a) Stable limit cycle. (b) Unstable limit cycle. (c) Semi-stable limit cycle.

Figure 1.6: Limit Cycle Trajectories.

show that a system has no limit cycles. There is active research on this subject today, for example, the Poincare-Bendixson Theorem, Bendixson's Criterion, Levinson-Smith Theorem, for more details see [101, 102, 50].

In this sense, it is necessary to describe what is meant by bifurcations in non-smooth systems. Consider a general invariant set of a piecewise-smooth system. Bifurcations that involve invariant sets contained in a single region R_i for all parameter values of interest can be studied using the bifurcation theory for smooth systems. The topological changes in the phase portrait of the system can be confined to arbitrarily small neighborhoods of the bifurcation fixed points by moving the bifurcation parameter close to such bifurcation point (hence "local").

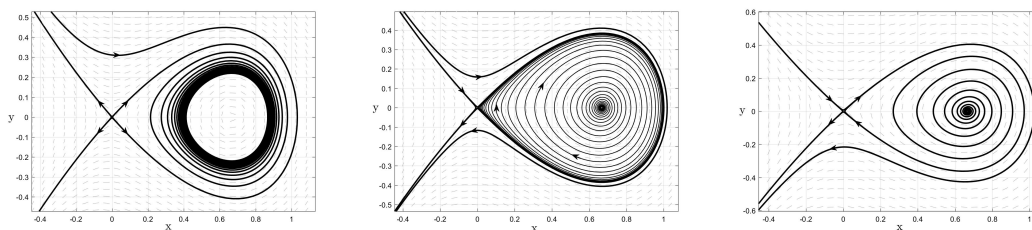
Local bifurcations can be analyzed entirely through changes in the local stability properties of equilibria, periodic orbits, or other invariant sets as parameters cross through critical thresholds, as for example:

- *saddle-node bifurcation* which is common to both smooth and non-smooth dynamical systems. It is a local bifurcation where two equilibria collide and annihilate each other; see [50, 49].
- *Hopf bifurcation* is a critical point where the stability of the system switches and a periodic solution arises. More concretely, it is a local bifurcation where a fixed point of the dynamical system loses its stability (as a pair of complex conjugate eigenvalues-of the linearization around the fixed point-crosses the complex plane imaginary axis). Under reasonably generic assumptions about the dynamical system, a small-amplitude limit cycle branches from the (critical) Hopf bifurcation point. This limit cycle is stable if the *first Lyapunov coefficient is negative*, in this case, we say that the bifurcation is a *supercritical Hopf bifurcation*. Otherwise, it is unstable and the bifurcation is a *subcritical Hopf bifurcation*; see [49].

Hopf and saddle-node bifurcations occur only in smooth systems, but appear in nonsmooth systems when they occur in regions defined by smooth vector fields.

Global bifurcations typically occur because 'larger' invariant sets, such as periodic orbits, collide with equilibria. This causes changes in the topology of the trajectories in the phase space which cannot be confined to a small neighborhood, as is the case with local bifurcations. Some examples of global bifurcations are:

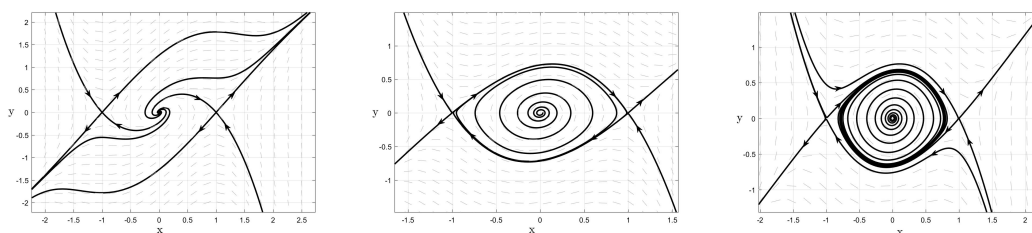
- *Homoclinic bifurcation* is where a limit cycle collides with a saddle point, see Figure 1.7. The variant above is one type of homoclinic bifurcation. Still, there is another type of homoclinic bifurcation in which the homoclinic orbit "traps" the other ends of the unstable and stable manifolds of the saddle. Higher codimension bifurcations can occur in three or more dimensions, producing complicated, possibly chaotic dynamics, see [8, 49].



(a) Periodic orbit. (b) Homoclinic orbit. (c) Homoclinic orbit is broken.

Figure 1.7: Homoclinic bifurcation for a saddle equilibrium creating a stable limit cycle. In figure (a) there is a stable periodic orbit; in figure (b) the periodic orbit approaches the homoclinic orbit; and in figure (c), the homoclinic orbit is broken and there is no periodic orbit.

- *Heteroclinic bifurcation* is when a limit cycle collides with two or more saddle points (see Figure 1.8). A heteroclinic orbit is an invariant set in the phase space of a dynamical system. If a heteroclinic orbit is asymptotically stable, approaching trajectories spend longer and longer periods of time in a neighbourhood of successive equilibria. In general, the heteroclinic connections of dynamic systems are of high codimension, that is, they will not persist if the parameters are varied.



(a) Unstable equilibrium and two saddles coexisting. (b) Heteroclinic orbit. (c) Limit cycle before heteroclinic bifurcation.

Figure 1.8: Heteroclinic bifurcation for two saddles equilibrium creating a stable limit cycle. In figure (a) there is an unstable equilibrium coexists with two saddles; in figure (b) the heteroclinic orbits connecting the saddles, forming a heteroclinic cycle; and in figure (c) there is a stable limit cycle that disappears through heteroclinic bifurcation.

Global bifurcations can also involve more complicated sets such as causing the sudden appearance or disappearance of a chaotic attractor in a boundary crisis bifurcation, see [8].

The classical bifurcations (saddle-node bifurcation, Hopf bifurcation, etc) also occurs in **DPWS** systems. However, there exists other bifurcations that are exclusive of the piecewise-smooth systems, such as those that normally involve interactions of an invariant set with a discontinuity boundary, known in the literature as *discontinuity-induced bifurcations* (DIBs); see [8, 64]. These bifurcations occur when an invariant set (equilibrium point, limit cycle, etc) crosses or touches tangentially the switching boundary Σ in state space. The topological changes from real to virtual equilibrium points (or vice versa), due to changes in some system parameters, can lead to a BEB; see [19, 20, 23, 24, 25]. There are other DIBs, such as *sliding bifurcations of limit cycles* that occur when a limit cycle develops an intersection (tangential or transversal) with a sliding region; see [59], *Grazing-sliding bifurcations* (GS) that occurs when a limit cycle intersects tangentially a switching boundary; see, [19, 26, 27, 28, 37, 38, 39], and *discontinuous saddle-node* (DSN) bifurcation that occurs when the equilibria in different vector fields collide, defined as a non-smooth analog of the saddle-node bifurcation; see [22].

1.3.1 Boundary equilibrium bifurcations

The *boundary equilibrium bifurcations* (BEB) have been the object of study of many works in the last few years and they have been identified in mathematical models of a wide variety of physical systems. For two-dimensional **DPWS** systems, there is a complete classification of the BEBs and their unfolding, see [1, 24, 25, 59, 63]. For three-dimensional **DPWS** systems, the BEBs have a greater complexity of phenomena, with many possible geometric combinations. We still do not find a classification in the literature that is similar to the two-dimensional systems for the three-dimensional ones, although there are recent studies focused on the study of phenomena linked to BEBs as, for example, [23, 26, 20].

Definition 1.3.1. *The DPWS system (1.2.6) undergoes a **boundary equilibrium bifurcation** on the parameter $\mu = \mu^*$ ($\mu \in \mathbb{R}$) in relation to vector fields \mathbf{F}_i ($i = 1, 2$), if there is a point \mathbf{x}^* such that:*

$$(i) \mathbf{F}_i(\mathbf{x}^*, \mu^*) = 0, \text{ but } \mathbf{F}_j(\mathbf{x}^*, \mu^*) \neq 0;$$

$$(ii) h(\mathbf{x}^*, \mu^*) = 0;$$

$$(iii) \nabla_x \mathbf{F}_i(\mathbf{x}^*, \mu^*) \text{ is invertible (equivalently, } \text{Det}[\nabla_x \mathbf{F}_i(\mathbf{x}^*, \mu^*)] \neq 0);$$

$$(iv) \nabla_\mu h(\mathbf{x}^*, \mu^*) - \nabla_x h(\mathbf{x}^*, \mu^*) [\nabla_x \mathbf{F}_i^{-1} \nabla_\mu \mathbf{F}_i] (\mathbf{x}^*, \mu^*) \neq 0.$$

where $\nabla_x = (\frac{\partial}{\partial x_1}, \frac{\partial}{\partial x_2}, \dots, \frac{\partial}{\partial x_n})$ and $\nabla_\mu = (\frac{\partial}{\partial \mu_1}, \frac{\partial}{\partial \mu_2}, \dots, \frac{\partial}{\partial \mu_n})$.

Remark 1.3.2. *Items (i)-(ii) say just that \mathbf{x}^* is a boundary equilibrium at parameter $\mu = \mu^*$. After the analysis of just the linear part of the system, we have that with the Implicit Function theorem¹ we can conclude the validity of the results for the complete non-linear system, as indicated by the item (iii). item (iv) means that the branches of the*

¹See, [8, Theorem 2.4]

equilibria of the vector fields \mathbf{F}_1 and \mathbf{F}_2 cross Σ transversely at the bifurcation point of the boundary equilibrium (\mathbf{x}^*, μ^*) .

A BEB is classified according to two possible scenarios, that take into account only the positions of the equilibria involved in relation to the boundaries of their respective vector fields:

- (i) **Persistence scenario** occurs when a natural equilibrium turns into a pseudo-equilibrium. In this case, if the natural equilibrium is real (resp. virtual), then the pseudo-equilibrium is virtual (resp. real).
- (ii) **Nonsmooth fold scenario** occurs when both a natural equilibrium and a pseudo-equilibrium collide and disappear. In this case, if the natural equilibrium is real (resp. virtual), then so is the pseudo-equilibrium.

To distinguish between the persistence and nonsmooth fold scenarios, we use the BEB-Theorem shown in [8] which is enunciated below.

Theorem 1.3.3. *Let $D \subset \mathbb{R}^n$ be the region containing the origin, the Filippov system*

$$\dot{\mathbf{x}} = \begin{cases} \mathbf{F}_1(\mathbf{x}, \mu), & \text{if } h(\mathbf{x}, \mu) > 0, \\ \mathbf{F}_2(\mathbf{x}, \mu), & \text{if } h(\mathbf{x}, \mu) < 0, \end{cases} \quad (1.3.1)$$

where $\mathbf{x} \in \mathbb{R}^n$, $\mu \in \mathbb{R}$, $\mathbf{F}_1, \mathbf{F}_2 : \mathbb{R}^{n+1} \rightarrow \mathbb{R}^n$ and $h : \mathbb{R}^{n+1} \rightarrow \mathbb{R}$ are smooth functions in D , and Σ is a switching boundary. Suppose that (1.3.1) undergoes a boundary equilibrium bifurcation at $(\mathbf{x}^*, \mu^*) = (0, 0)$ in relation to \mathbf{F}_1 . So, assuming

$$C^T N_1^{-1} E \neq 0,$$

where $N_1 = \nabla_x \mathbf{F}_1(0, 0)$, $C^T = \nabla_x h(0, 0)$, $E = \mathbf{F}_2 - \mathbf{F}_1$, we have :

- (i) *The persistence scenario occurs if $C^T N_1^{-1} E < 0$.*
- (ii) *The nonsmooth fold scenario occurs if $C^T N_1^{-1} E > 0$.*

1.3.2 Discontinuous saddle-node bifurcation

A *Discontinuous saddle-node bifurcation* is a codimension-one situation defined as by a nonsmooth analog of the saddle-node bifurcation. This type of bifurcation is a nonsmooth fold, that is, two equilibria coexist and collide and annihilate at the discontinuous bifurcation. It is worth mentioning that this bifurcation occurs in the **CPWS** systems; see [22].

1.3.3 Grazing-sliding bifurcation

Another important case of DIB caused by the interaction of a trajectory with the boundary of a sliding region is the *grazing-sliding bifurcations*(GS) that occurs when a limit cycle entirely contained in some region R_i collides with the switching boundary Σ , generating a sliding cycle. The dynamics associated can be simple or extremely complicated and appear under a continuous small change in initial conditions, see [8].

Figure 1.9 (below) shows that as we vary parameter $\mu \in \mathbb{R}$ in a **2D-DPWS** system, two generic cases can appear depending on the stability of the tangent cycle L at $\mu = 0$. In Case 1 (Fig. 1.9(a)), the L cycle is stable and, for $\mu < 0$, there is a stable limit cycle $L_\mu \subset R_1$. This cycle becomes a sliding cycle for $\mu > 0$. In Case 2 (Fig. 1.9(b)), the L cycle is unstable and, for $\mu < 0$ there are two limit cycles: an unstable $L_\mu^u \subset R_1$ cycle and a stable L_μ sliding cycle. In this case, when $\mu > 0$ there is no cycle, see [19].

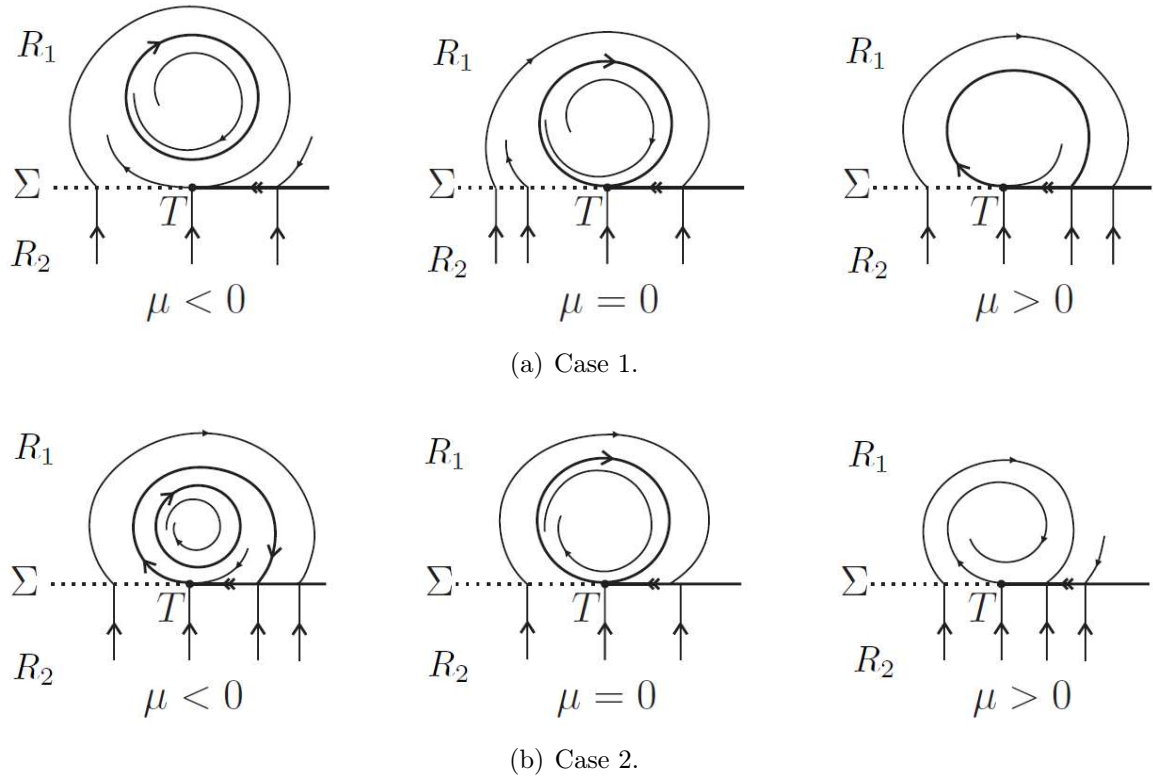


Figure 1.9: Grazing-sliding bifurcation in 2D.

Chapter 2

Multiple boundaries sliding mode control applied to capacitor voltage-balancing systems

In this chapter, we are interested in studying the stability of an active voltage balancing strategy for pre-charging MMCs (Modular Multilevel Converters), since the voltage balancing of the floating capacitors in the submodules of the MMC during its pre-charging operating stage is a key issue insomuch as it is a critical task for the correct operation of these converters. The adopted voltage-balancing strategy consists in adding a resistance to each submodule of the MMC by means of a controlled switch. These switches are being controlled by a sliding mode control algorithm with multiple boundaries (discontinuity surfaces of high co-dimension). These systems are essentially discontinuous piecewise smooth dynamical systems (Filippov systems) commanded by electronic switches. In this chapter, the local stability of the voltage balanced system is analytically proven for an arbitrary number of sub-modules. In addition, a detailed analysis of the global dynamics of this system with two sub-modules and two switching boundaries sliding mode control is presented. Moreover, simulation results obtained on an MMC with 10 submodules are shown to validate the theoretical analysis.

2.1 Introduction

A very interesting problem in power electronics is to equalize the voltage of an arbitrary number of floating capacitors connected in series or parallel arrangements to a voltage source. This problem so called *capacitor voltage-balancing* is well known to power electronics engineers and its solution has motivated different balancing strategies. These systems are in essence dynamic switching systems (Filippov systems [1]) commanded by electronic switches, typically MOSFET for low power applications and insulated-gate bipolar transistors (IGBT) for medium power systems.

Capacitor voltage-balancing systems are commonly used in different circuit applications in power electronics, see for instance [2]. A particular application of the capacitor voltage-balancing techniques is found in modular multilevel converters (MMC) during its pre-charge operating stage [3, 4]. A typical three-phase MMC, first proposed by Lesnicar and Marquardt in 2003 [5], is shown in Figure 2.1. Nowadays, it is one of the main

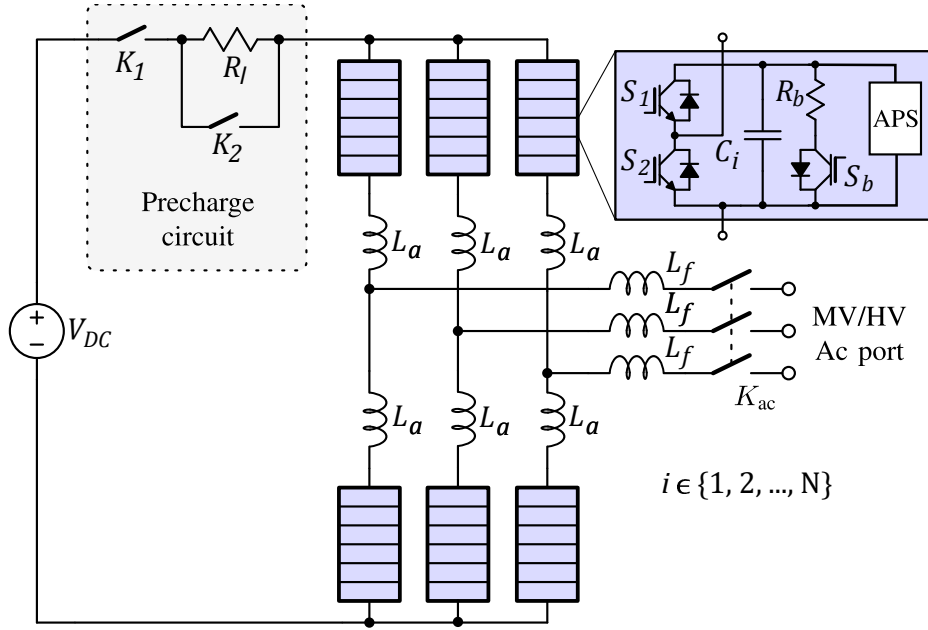


Figure 2.1: MMC with pre-charge circuit. L_a stands for the equivalent arm inductance; L_f is the output ac inductance; V_{dc} is the dc voltage source; R_l stands for the equivalent circuit resistance; R_b and S_b are the balancing resistance and control switch, respectively; S_1 and S_2 are the submodule switches; C_i is the submodule capacitor; APS is the auxiliary power supply; K_1 , K_2 and K_{ac} denote pre-charge and operating circuit switches. Adapted from [7].

modular converter topologies used in High Voltage Direct Current (HVDC) and is also widely used in other applications including medium voltage drives and renewable energy sources integration. The MMC is composed of fundamental units called submodules (SM). A set of serially connected submodules is called an arm, and two arms, one superior and one inferior compose one phase leg of the MMC. A detailed state-space model of the three-phase MMC can be found in [6]. The topology used within the SMs can vary, being the most common the half-bridge and full-bridge converters, connected to a capacitor. Summing up the output voltages of several SMs it is possible to have different levels of voltage in each phase [7].

In practical MMCs, each SM local signal electronics circuits are self-powered by means of a local auxiliary power supply (APS) fed from the SM DC-link [7]. However, the cascade of hundreds of SMs also brings a major challenge to the system's capacitor voltage balancing during the pre-charge stage where this configuration might not lead to balanced or stable SM voltages. The connection of the converter to the grid can only be performed after pre-charging all capacitors to minimum voltage levels, which prevents inrush currents. In this sense, the balancing of the MMC's capacitor voltages during its pre-charge stage is critical for the correct operation of these converters [7]. The capacitor voltage balancing of the MMC can be classified into two different methods (i) a passive balancing strategy that consists in adding a balancing fixed resistance in parallel to each one of the SMs; (ii) an active balancing strategy implemented by controlled switches that connect/disconnect the balancing resistance for each SM.

A passive balancing strategy considering the switch S_b closed in Figure 2.1 and varying

the balancing resistance R_b is studied in depth in [7]. In this chapter, an active balancing strategy that consists in adding a balancing resistance in parallel to each one of the SMs being controlled by a switch S_b is analysed from the point of view of the discontinuous piecewise smooth dynamical systems (**DPWS** systems, for short) theory [8].

In **DPWS** systems, when a discontinuous flow through a switching boundary points inwards, so that it cannot escape, it induces a single flow within the boundary, so called sliding mode regime. When several of these switching boundaries intersect (discontinuity surfaces of high co-dimension), a method to analyse this type of systems is to seek a flow within the intersection, but some difficulties can arise. The widely adopted Filippov method [1] to define the sliding vector field is, in general, ambiguous. For instance, when sliding takes place on a surface of co-dimension 2, that is, the intersection of two co-dimension 1 surfaces, even if the surface attracts nearby dynamics, an ambiguity may arise to solve the problem. The ambiguity involved in this situation can be solved by different practical approaches: (i) globally smoothing out the vector field, see for instance, previous works on **DPWS** with two or more switching boundaries, Dieci et al. [9, 10] ; (ii) blending technique, that is essentially an interpolation of the vector fields in the neighborhood of the discontinuity boundaries, see [11], [12]; (iii) to impose further constraints on the class of Filippov vector fields, in order to regularize the problem on the co-dimension 2 surface [13].

For **DPWS** systems derived from control systems like (1.2.1)-(1.2.2), Utkin's equivalent control method [14, 15] provides a single sliding vector field at the intersection of the m switching boundaries. When the system is linear with respect to the control variable, the Filippov and Utkin methods return the same sliding vector field over a switching boundary between two vector fields, but may differ if this relationship is non-linear, see [16]. The same occurs when the sliding motion is restricted to the intersection of m switching boundaries. However, Utkin's method for determining the sliding vector field at the intersection of the m switching boundaries of control systems such as (1.2.1)-(1.2.2) is simpler to apply than Filippov's method, which can show up to m possible ways to obtain the same sliding vector field.

The main contributions of this chapter is to study the dynamics and the stability of a system of n capacitors connected in a serial arrangement to a voltage source and controlled by a switching control law with multiple boundaries. Our case is to solve the problem of capacitor voltage balance during pre-charge operation of multilevel modular converters, as it is an interesting problem, less addressed in the literature. Moreover, we use standard tools for **DPWS** systems and we have numerical simulations of the studied systems, which verify the analytical results.

This chapter is organized as follows. Section 2.1 presents a brief introduction to the problem of capacitor voltage-balancing. Section 2.2 is dedicated to modeling and introducing the main result obtained on local stability of the model with n submodules; see Theorem 2.2.1. A brief description of other results obtained in the following sections is also provided. A qualitative analysis of the case in \mathbb{R}^2 corresponding to two SM planar systems is studied in Section 2.3. In Section 2.4 we analyze the case in \mathbb{R}^3 with two switching boundaries, taking into account the dynamics of the equivalent inductor. Simulation results are shown in Section 2.5. Finally, Section 2.6 presents the main conclusions.

Previous results on **DPWS** systems are necessary for the development of this work. Chapter 1 reviews the main aspects of these systems, relevant to our objectives.

2.2 Model description and main result

Only one leg with two arms of the MMC circuit shown in Figure 2.1 is reduced to an equivalent circuit that operates during pre-charge operation, as shown in Figure 2.2, to analyze the voltage balancing mechanism of the active capacitor. The equivalent circuit is obtained when K_1 is closed, K_2 is open, K_{ac} is open, all the IGBTs are blocked and the APSs are turned on. The control switches S_b are employed to switch-on/switch-off the balancing resistances R_b in such a way to control the SM voltages.

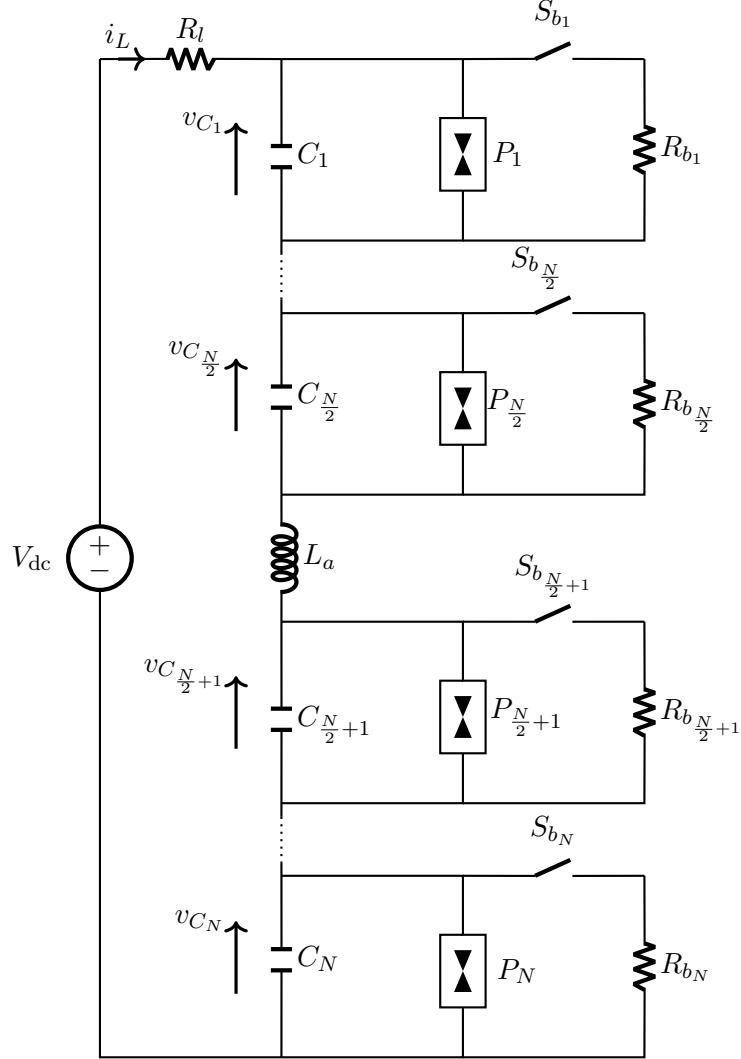


Figure 2.2: Equivalent circuit for one leg with two arms of the MMC circuit shown in Figure 2.1. Note that N is an even number and the symbol $\blacktriangleleft\blacktriangleright$ denotes a constant power source (P_i/v_{C_i}).

The dynamics of the circuit shown in Figure 2.2 can be expressed by equations

$$\begin{aligned} C_i \frac{dv_{C_i}}{dt} &= i_L - \frac{P_i}{v_{C_i}} - \frac{v_{C_i}}{R_{b_i}} u_i \\ L_a \frac{di_L}{dt} &= V_{dc} - i_L R_l - \sum_{k=1}^N v_{C_k} \end{aligned} \quad (2.2.1)$$

for $i = 1, 2, 3, \dots, N$, where N (even number) stands for the number of SMs of the MMC. If we can assume that the second equation of (2.2.1) has fast-scale dynamics and it is everywhere stable, so we have the approximation

$$0 = V_{\text{dc}} - i_L R_l - \sum_{k=1}^N v_{C_k} \quad (2.2.2)$$

for very small L_a value ($L_a > 0$) and we can solve this equation for i_L to get

$$i_L = \frac{1}{R_l} \left(V_{\text{dc}} - \sum_{k=1}^N v_{C_k} \right), \quad (2.2.3)$$

then a standard singular perturbation analysis shows that (2.2.1), by substituting (2.2.3) in first equation of (2.2.1), can be reduced to

$$C_i \frac{dv_{C_i}}{dt} = \frac{1}{R_l} \left(V_{\text{dc}} - \sum_{k=1}^N v_{C_k} \right) - \frac{P_i}{v_{C_i}} - \frac{v_{C_i} u_i}{R_{b_i}} \quad (2.2.4)$$

for $i = 1, 2, 3, \dots, N$.

In system (2.2.4) the state variables are the voltage capacitors $v_{C_i} = v_{C_i}(t)$, such that $v_{C_i} \in (0, V_{\text{dc}}]$, the parameters are $V_{\text{dc}} > 0$, $C_i > 0$, $P_i \geq 0$, $R_l > 0$, $R_{b_i} > 0$. The control variables are $u_i \in \{0, 1\}$, 0 for open switch (S_{b_i} in Figure 2.1) and 1 for closed switch. The control objectives are basically: (i) to stabilize the voltage of each capacitor at a desired value $V_{r_i} \in (0, V_{\text{dc}})$, where $V_{\text{dc}} > \sum_{k=1}^N V_{r_k}$; (ii) to ensure the robustness of the system to parameter variations, produced mainly by load and power demand changes (parameters P_i and R_{b_i}). We adopt a Sliding Mode Control (SMC) strategy that depends on the voltage capacitor error signal on each capacitor, given by

$$u_i = \frac{1}{2}(1 + \text{sign}[v_{C_i} - V_{r_i}]), \quad (2.2.5)$$

for $i = 1, 2, \dots, n$, where $v_{C_i} - V_{r_i} = 0$ stands for the switching boundaries. This leads us to deal with piecewise smooth systems that have n switching boundaries that intersect at the desired operating point since there are N independent control variables. Such class of switching control law is well-known as multiple boundaries SMC.

For the study carried out in this and the next section, we consider the system (2.2.4)-(2.2.5) in a normalized form given by

$$\frac{1}{a_i} \frac{dx_i}{d\tau} = 1 - \sum_{k=1}^n x_k - \frac{b_i}{x_i} - c_i x_i u_i, \quad (2.2.6)$$

with

$$u_i = \frac{1}{2}(1 + \text{sign}[x_i - \mu_i]), \quad (2.2.7)$$

and for $i = 1, 2, \dots, n$. System (2.2.6)-(2.2.7) is obtained by applying the standard change of variables (state and time, see Wang et al. [17]) and parameters, defined in Table 2.1, to the original system (2.2.4)-(2.2.5). So, the new state vector is $\mathbf{x} = (x_1, x_2, \dots, x_n) \in D \subset \mathbb{R}_+^n$ such that

$$D = \{0 < x_i \leq 1 \text{ for } i = 1, 2, \dots, n\},$$

and $\mathbf{x}_{\text{ref}} = (\mu_1, \mu_2, \dots, \mu_n)$ is the normalized voltage reference vector whose components meet the inequality $\mu_1 + \mu_2 + \dots + \mu_n \leq 1$. Switching boundaries are defined by

$$\Sigma_i = \{\mathbf{x} \in D : h_i(\mathbf{x}) = x_i - \mu_i = 0\}$$

for $i = 1, 2, \dots, n$. In this case, if $h_i(\mathbf{x}) > 0$ then $u_i = 1$ and if $h_i(\mathbf{x}) < 0$ then $u_i = 0$. Note that these sets are orthogonal to each other and $\Sigma_1 \cap \Sigma_2 \cap \dots \cap \Sigma_n = \{\mathbf{x}_{\text{ref}}\}$.

State and Time Variables	Parameters
$x_i = v_{C_i}/V_{dc}$	$\mu_i = V_{r_i}/V_{dc}$
	$a_i = C_N/C_i$
	$b_i = P_i R_l / V_{dc}^2$
$\tau = t/(R_l C_N)$	$c_i = R_l / R_{b_i}$

Table 2.1: Normalization.

In what follows, the local stability of the desired operation equilibrium point (balanced system) of the equivalent system shown in Figure 2.2 is analytically proven for an arbitrary number of submodules.

Theorem 2.2.1. *Point $(V_{r_1}, V_{r_2}, \dots, V_{r_N})$ is a local attractor for system (2.2.4)-(2.2.5) whenever*

$$\frac{V_{r_i}}{R_l} \left(V_{dc} - \sum_{k=1}^N V_{r_k} - \frac{R_l}{R_{b_i}} V_{r_i} \right) < P_i < \frac{V_{r_i}}{R_l} \left(V_{dc} - \sum_{k=1}^N V_{r_k} \right). \quad (2.2.8)$$

for $i = 1, 2, \dots, n$.

Proof. We use a special notation for Lie derivatives, namely

$$\dot{x}_i^+(\mathbf{x}) = \frac{dx_i}{d\tau}(u_i = 1) \quad \text{and} \quad \dot{x}_i^-(\mathbf{x}) = \frac{dx_i}{d\tau}(u_i = 0),$$

in order to simplify the analysis of the contact of the system's orbits with the switching boundaries Σ_i . From this, we can determine the sliding regions in Σ_i and conditions on the system parameters to ensure stability at the point \mathbf{x}_{ref} , which is the desired operating point.

Attractive sliding regions are given by

$$\Sigma_i^{as} = \{\mathbf{x} \in \Sigma_i : \dot{x}_i^+(\mathbf{x}) < 0 < \dot{x}_i^-(\mathbf{x})\},$$

where

$$\dot{x}_i^+(\mathbf{x}) = a_i \left(1 - \sum_{k=1}^n x_k - \frac{b_i}{x_i} - c_i x_i \right) \quad \text{and} \quad \dot{x}_i^-(\mathbf{x}) = a_i \left(1 - \sum_{k=1}^n x_k - \frac{b_i}{x_i} \right).$$

We have $\Sigma_1^{as} \cap \Sigma_2^{as} \cap \dots \cap \Sigma_n^{as} = \{\mathbf{x}_{\text{ref}}\}$ iff $\dot{x}_i^+(\mathbf{x}_{\text{ref}}) < 0 < \dot{x}_i^-(\mathbf{x}_{\text{ref}})$ for all i . This condition is obtained for the system parameters satisfying

$$\mu_i \left(1 - \sum_{k=1}^n \mu_k - c_i \mu_i \right) < b_i < \mu_i \left(1 - \sum_{k=1}^n \mu_k \right). \quad (2.2.9)$$

Condition (2.2.9) is rewritten as condition (2.2.8) of Theorem 2.2.1, applying the changes given in Table 2.1.

Assuming (2.2.9) in system (2.2.6)-(2.2.7), we can ensure that it exists a neighborhood V of \mathbf{x}_{ref} , including \mathbf{x}_{ref} , such that for any \mathbf{x} in V we get

$$\dot{x}_i^-(\mathbf{x}) > 0 \quad \text{if } x_i \leq \mu_i, \quad \text{and} \quad \dot{x}_i^+(\mathbf{x}) < 0 \quad \text{if } x_i \geq \mu_i,$$

for all i . Then \mathbf{x}_{ref} is a local attractor of system (2.2.6)-(2.2.7), which we call pseudo-equilibrium point. Furthermore, such a pseudo-equilibrium point is reached in finite time. \square

In this way the local stability of the desired operation point $(V_{r_1}, V_{r_2}, \dots, V_{r_n})$ of the equivalent system is analytically proven for an arbitrary number of submodules. Determining the attraction domain of this equilibrium point remains an interesting issue for future research.

2.3 Qualitative analysis of the planar case with two-boundaries

In this section we consider in system (2.2.6)-(2.2.7) that $n = 2$, and we get

$$\frac{1}{a} \frac{dx_1}{d\tau} = 1 - x_2 - (1 + c_1 u_1) x_1 - \frac{b_1}{x_1}, \quad (2.3.1)$$

$$\frac{dx_2}{d\tau} = 1 - x_1 - (1 + c_2 u_2) x_2 - \frac{b_2}{x_2}, \quad (2.3.2)$$

with $(x_1, x_2) \in D \subset \mathbb{R}^2$ and

$$u_1 = \frac{1}{2}(1 + \text{sign}[x_1 - \mu_1]), \quad (2.3.3)$$

$$u_2 = \frac{1}{2}(1 + \text{sign}[x_2 - \mu_2]). \quad (2.3.4)$$

Switching boundaries are defined by

$$\begin{aligned} \Sigma_1 &= \{(x_1, x_2) \in D : h_1(x_1, x_2) = x_1 - \mu_1 = 0\}, \\ \Sigma_2 &= \{(x_1, x_2) \in D : h_2(x_1, x_2) = x_2 - \mu_2 = 0\}, \end{aligned}$$

which are orthogonal at (μ_1, μ_2) . Then the state space is divided into four open regions, namely

$$\begin{aligned} D_1 &= \{(x_1, x_2) \in D : h_1(x_1, x_2) > 0 \text{ and } h_2(x_1, x_2) > 0\}, \\ D_2 &= \{(x_1, x_2) \in D : h_1(x_1, x_2) < 0 \text{ and } h_2(x_1, x_2) > 0\}, \\ D_3 &= \{(x_1, x_2) \in D : h_1(x_1, x_2) < 0 \text{ and } h_2(x_1, x_2) < 0\}, \\ D_4 &= \{(x_1, x_2) \in D : h_1(x_1, x_2) > 0 \text{ and } h_2(x_1, x_2) < 0\}. \end{aligned}$$

In each of these regions there is a distinct vector field acting, obtained from system (2.3.1)-(2.3.4) and defined as in Figure 2.3.

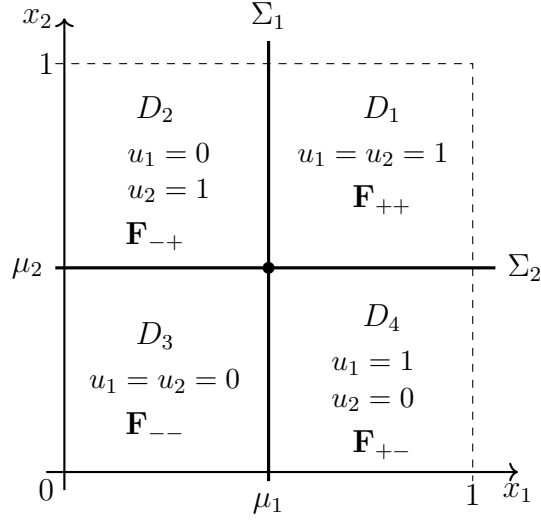


Figure 2.3: State space of system (2.3.1)-(2.3.4): $D = \Sigma_1 \cup \Sigma_2 \cup D_1 \cup D_2 \cup D_3 \cup D_4$.

System (2.3.1)-(2.3.4) is then represented as a 2D-DPWS system of the form

$$\begin{bmatrix} \frac{dx_1}{d\tau} \\ \frac{dx_2}{d\tau} \end{bmatrix} = \begin{cases} \mathbf{F}_{++}(x_1, x_2), & \text{if } (x_1, x_2) \in D_1 \\ \mathbf{F}_{-+}(x_1, x_2), & \text{if } (x_1, x_2) \in D_2 \\ \mathbf{F}_{--}(x_1, x_2), & \text{if } (x_1, x_2) \in D_3 \\ \mathbf{F}_{+-}(x_1, x_2), & \text{if } (x_1, x_2) \in D_4 \end{cases}, \quad (2.3.5)$$

composed by the vector fields

$$\mathbf{F}_{++}(x_1, x_2) = \begin{bmatrix} a \left(1 - (1 + c_1)x_1 - x_2 - \frac{b_1}{x_1} \right) \\ 1 - x_1 - (1 + c_2)x_2 - \frac{b_2}{x_2} \end{bmatrix}, \quad \mathbf{F}_{-+}(x_1, x_2) = \begin{bmatrix} a \left(1 - x_1 - x_2 - \frac{b_1}{x_1} \right) \\ 1 - x_1 - (1 + c_2)x_2 - \frac{b_2}{x_2} \end{bmatrix}, \quad (2.3.6)$$

$$\mathbf{F}_{--}(x_1, x_2) = \begin{bmatrix} a \left(1 - x_1 - x_2 - \frac{b_1}{x_1} \right) \\ 1 - x_1 - x_2 - \frac{b_2}{x_2} \end{bmatrix} \quad \text{and} \quad \mathbf{F}_{+-}(x_1, x_2) = \begin{bmatrix} a \left(1 - (1 + c_1)x_1 - x_2 - \frac{b_1}{x_1} \right) \\ 1 - x_1 - x_2 \end{bmatrix}, \quad (2.3.7)$$

for $u_1 = u_2 = 1$, $u_1 = 0$ and $u_2 = 1$, $u_1 = u_2 = 0$, $u_1 = 1$ and $u_2 = 0$, respectively. Vector fields must be appropriately extended to the switching boundaries using Filippov's theory.

2.3.1 Case Study for $b_1 = b_2 = 0$ ($P_i = 0$)

Sliding segments and tangential singularities

There is in Σ_1 an attractive sliding region given by the vertical line segment

$$\Sigma_1^{as} = \{x_1 = \mu_1, 1 - (1 + c_1)\mu_1 < x_2 < 1 - \mu_1\},$$

and obtained from the solution of the inequalities

$$\begin{aligned} L_{\mathbf{F}_{-+}} h_1(\mu_1, x_2) &= L_{\mathbf{F}_{--}} h_1(\mu_1, x_2) = a(1 - \mu_1 - x_2) > 0, \\ L_{\mathbf{F}_{++}} h_1(\mu_1, x_2) &= L_{\mathbf{F}_{+-}} h_1(\mu_1, x_2) = a(1 - (1 + c_1)\mu_1 - x_2) < 0. \end{aligned}$$

The same happens in Σ_2 , but given by the horizontal line segment

$$\Sigma_2^{as} = \{x_2 = \mu_2, 1 - (1 + c_2)\mu_2 < x_1 < 1 - \mu_2\},$$

which is obtained from the solution of the inequalities

$$L_{\mathbf{F}_{--}}h_2(x_1, \mu_2) = L_{\mathbf{F}_{+-}}h_2(x_1, \mu_2) = 1 - x_1 - \mu_2 > 0,$$

and

$$L_{\mathbf{F}_{-+}}h_2(x_1, \mu_2) = L_{\mathbf{F}_{++}}h_2(x_1, \mu_2) = 1 - x_1 - (1 + c_2)\mu_2 < 0.$$

According to the previous section, by constraint (2.2.9), $\Sigma_1^{as} \cap \Sigma_2^{as} = \{(\mu_1, \mu_2)\}$ occurs whenever the inequalities

$$1 - (1 + c_1)\mu_1 - \mu_2 < 0 < 1 - \mu_1 - \mu_2 \quad \text{and} \quad 1 - \mu_1 - (1 + c_2)\mu_2 < 0 < 1 - \mu_1 - \mu_2.$$

are satisfied. For this, the system parameters must satisfy the constraint:

$$\text{Max} \left[\frac{1 - \mu_1}{1 + c_2}; 1 - (1 + c_1)\mu_1 \right] < \mu_2 < 1 - \mu_1. \quad (2.3.8)$$

The ends of the sliding segment Σ_1^{as} are tangency points of the system orbits with Σ_1 , and such points have coordinates given by

$$T_1^- = (\mu_1, 1 - \mu_1) \quad \text{and} \quad T_1^+ = (\mu_1, 1 - (1 + c_1)\mu_1).$$

Similarly, the ends of the sliding segment Σ_2^{as} are tangency points of the system orbits with Σ_2 , and such points have coordinates given by

$$T_2^- = (1 - \mu_2, \mu_2) \quad \text{and} \quad T_2^+ = (1 - (1 + c_2)\mu_2, \mu_2).$$

Obviously, the sliding dynamics in Σ_1^{as} and Σ_2^{as} can be extended to its extremes. In this case we can consider the sliding dynamics in Σ_1 acting in all $\Sigma_1^{as} \cup T_1^- \cup T_1^+$, and in Σ_2 acting in all $\Sigma_2^{as} \cup T_2^- \cup T_2^+$.

We assume that the condition (2.3.8) is satisfied. Next, we identify which tangency points T_1^- , T_1^+ , T_2^- and T_2^+ are associated with the vector fields of (2.3.5). See Figure 2.4.

- (i) Vector field \mathbf{F}_{++} is transverse to the switching boundaries Σ_1 and Σ_2 , because $1 - (1 + c_2)\mu_2 < \mu_1 \leq x_1$ and $1 - (1 + c_1)\mu_1 < \mu_2 \leq x_2$, and therefore

$$\begin{aligned} L_{\mathbf{F}_{++}}h_1(\mu_1, x_2) &= a(1 - (1 + c_1)\mu_1 - x_2) < 0, \\ L_{\mathbf{F}_{++}}h_2(x_1, \mu_2) &= 1 - x_1 - (1 + c_2)\mu_2 < 0. \end{aligned}$$

- (ii) Vector field \mathbf{F}_{--} is transverse to the switching boundaries Σ_1 and Σ_2 , because $x_1 \leq \mu_1 < 1 - \mu_2$, $x_2 \leq \mu_2 < 1 - \mu_1$, and therefore

$$\begin{aligned} L_{\mathbf{F}_{--}}h_1(\mu_1, x_2) &= a(1 - \mu_1 - x_2) > 0, \\ L_{\mathbf{F}_{--}}h_2(x_1, \mu_2) &= 1 - x_1 - \mu_2 > 0. \end{aligned}$$

- (iii) Vector field \mathbf{F}_{-+} is tangent to Σ_1 at the point T_1^- and it is tangent to Σ_2 at T_2^+ . Both tangency points are classified as invisible fold, because

$$\begin{aligned} L_{\mathbf{F}_{-+}} h_1(T_1^-) &= 0, & L_{\mathbf{F}_{-+}}^2 h_1(T_1^-) &= ac_2(1 - \mu_1) > 0, \\ L_{\mathbf{F}_{-+}} h_2(T_2^+) &= 0, & L_{\mathbf{F}_{-+}}^2 h_2(T_2^+) &= -ac_2\mu_2 < 0. \end{aligned}$$

- (iv) Vector field \mathbf{F}_{+-} is tangent to Σ_1 at T_1^+ and it is tangent to Σ_2 at T_2^- . Both tangency points are classified as invisible fold, because

$$\begin{aligned} L_{\mathbf{F}_{+-}} h_1(T_1^+) &= 0, & L_{\mathbf{F}_{+-}}^2 h_1(T_1^+) &= -ac_1\mu_1 < 0, \\ L_{\mathbf{F}_{+-}} h_2(T_2^-) &= 0, & L_{\mathbf{F}_{+-}}^2 h_2(T_2^-) &= ac_1(1 - \mu_2) > 0. \end{aligned}$$

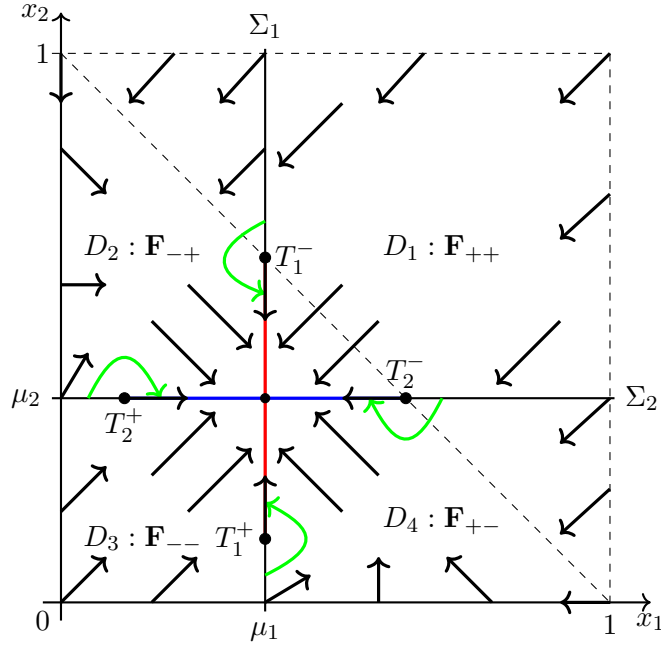


Figure 2.4: A geometric illustration of vector fields of the system (2.3.5)-(2.3.7) assuming $b_1 = b_2 = 0$ and (2.3.8).

Regular equilibria and stability

Below we describe the equilibria of the vector fields \mathbf{F}_{++} , \mathbf{F}_{-+} , \mathbf{F}_{--} and \mathbf{F}_{+-} .

- (i) Vector field \mathbf{F}_{--} has no equilibrium point. But there is an invariant line of equation $x_2 = 1 - x_1$. Note that $\frac{dx_1}{d\tau} > 0$ and $\frac{dx_2}{d\tau} > 0$ for $x_2 < 1 - x_1$, whereas $\frac{dx_1}{d\tau} < 0$ and $\frac{dx_2}{d\tau} < 0$ for $x_2 > 1 - x_1$. Therefore, this invariant line is attracting. Following (2.3.8) we take $\mu_2 < 1 - \mu_1$ and, thus, such a line does not cut the region D_3 .
- (ii) Vector field \mathbf{F}_{-+} has an equilibrium point at $(1, 0)$. As $(1, 0) \notin D_2$, it is a virtual equilibrium.

(iii) Vector field \mathbf{F}_{+-} has an equilibrium point at $(0, 1)$. As $(0, 1) \notin D_4$, it is a virtual equilibrium.

(iv) Vector field \mathbf{F}_{++} has an equilibrium point at (\bar{x}_1, \bar{x}_2) , where

$$\bar{x}_1 = \frac{1}{1 + c_1 + \frac{c_1}{c_2}} \quad \text{and} \quad \bar{x}_2 = \frac{1}{1 + c_2 + \frac{c_2}{c_1}}.$$

Note that $\bar{x}_1 < 1$ and $\bar{x}_2 < 1$. Moreover, $1 - \bar{x}_1 - \bar{x}_2 = \frac{c_1 c_2}{c_1 + c_2 + c_1 c_2} > 0$, then (\bar{x}_1, \bar{x}_2) is located in the region below the straight line $x_2 = 1 - x_1$. This equilibrium is virtual if $\mu_1 > \bar{x}_1$ (since $h_1(\bar{x}_1, \bar{x}_2) = \bar{x}_1 - \mu_1 < 0$) or if $\mu_2 > \bar{x}_2$ (since $h_2(\bar{x}_1, \bar{x}_2) = \bar{x}_2 - \mu_2 < 0$). In the case $\mu_1 < \bar{x}_1$ and $\mu_2 < \bar{x}_2$ this equilibrium becomes real. However, the condition (2.3.8) does not allow the existence of a real equilibrium.

Both regular equilibria are classified as asymptotically stable node, since

$$\begin{aligned} \text{Det}[A] &= a(c_1 u_1(1 + c_2 u_2) + c_2 u_2) > 0, \\ \text{Tr}[A] &= -1 - a(1 + c_1 u_1) - c_2 u_2 < 0, \\ \Delta &= \text{Tr}[A]^2 - 4\text{Det}[A] = 4a + (-1 + a(1 + c_1 u_1) - c_2 u_2)^2 > 0, \end{aligned}$$

where A is the Jacobian matrix of system (2.3.1)-(2.3.2) with $b_1 = b_2 = 0$ and for u_1 and u_2 not simultaneously null. So the eigenvalues of A are real negative and distinct.

Sliding dynamics and pseudo-equilibria

Sliding motion occurs on segment lines defined by $T_1^+ \cup \Sigma_1^{as} \cup T_1^-$ and $T_2^+ \cup \Sigma_2^{as} \cup T_2^-$. Tangency points T_1^\pm and T_2^\pm are of the invisible fold type whenever the condition (2.3.8) is satisfied. Then, if an orbit system touches Σ_1 (or Σ_2) at a point of Σ_1^{as} (or Σ_2^{as}) for some time $\tau = \tau_0 > 0$, it remains in Σ_1^{as} (or Σ_2^{as}) for all $\tau > \tau_0$, sliding to a stable equilibrium. We will show below that this stable equilibrium is unique and appears at the point $(\mu_1, \mu_2) \in \Sigma_1^{as} \cap \Sigma_2^{as}$, which is called pseudo-equilibrium of system (2.3.5)-(2.3.7).

The sliding vector field defined in Σ_1 is given by

$$\mathbf{F}_{s1}(\mu_1, x_2) = \begin{bmatrix} 0 \\ 1 - \mu_1 - (1 + c_2 u_2)x_2 \end{bmatrix}$$

and, therefore, the sliding dynamics in Σ_1 is described by the piecewise linear one-dimensional system

$$\frac{dx_2}{d\tau} = \begin{cases} f_+(x_2) = 1 - \mu_1 - (1 + c_2) x_2 & \text{if } x_2 > \mu_2, \\ f_-(x_2) = 1 - \mu_1 - x_2 & \text{if } x_2 < \mu_2. \end{cases} \quad (2.3.9)$$

Point $x_2 = \mu_2$ is a single stable pseudo-equilibrium of (2.3.9) only for (μ_1, μ_2) satisfying the condition (2.3.8), because only then we get $f_+(x_2) < 0$ for all $x_2 > \mu_2$ and $f_-(x_2) > 0$ for all $x_2 < \mu_2$. In this case, point $x_2 = \mu_2$ is reached in finite time for any initial condition in $\Sigma_1^{as} \cup T_1^+ \cup T_1^-$.

The sliding vector field defined in Σ_2 is given by

$$\mathbf{F}_{s2}(x_1, \mu_2) = a \begin{bmatrix} 1 - (1 + c_1 u_1)x_1 - \mu_2 \\ 0 \end{bmatrix}$$

and, therefore, the sliding dynamics in Σ_2 is described by the piecewise linear one-dimensional system

$$\frac{dx_1}{d\tau} = \begin{cases} g_+(x_1) = a(1 - (1 + c_1)x_1 - \mu_2) & \text{if } x_1 > \mu_1, \\ g_-(x_1) = a(1 - x_1 - \mu_2) & \text{if } x_1 < \mu_1. \end{cases} \quad (2.3.10)$$

Point $x_1 = \mu_1$ is a single stable pseudo-equilibrium of (2.3.9) only for (μ_1, μ_2) satisfying the condition (2.3.8), because only then we get $g_+(x_1) < 0$ for all $x_1 > \mu_1$ and $g_-(x_1) > 0$ for all $x_1 < \mu_1$. In this case, point $x_1 = \mu_1$ is reached in finite time for any initial condition in $\Sigma_2^{as} \cup T_2^+ \cup T_2^-$.

Therefore, (μ_1, μ_2) is the only pseudo-equilibrium of system (2.3.5)-(2.3.7) for $b_1 = b_2 = 0$, and it is globally stable in $T_1^+ \cup \Sigma_1^{as} \cup T_1^- \cup T_2^+ \cup \Sigma_2^{as} \cup T_2^-$ whenever the condition (2.3.8) is satisfied.

Global analysis and simulations

We assume system (2.3.5)-(2.3.7) under the condition (2.3.8) and with $b_1 = b_2 = 0$. We include to the state space D the coordinate axes x_1 and x_2 , being redefined as

$$\bar{D} = \{(x_1, x_2) \in \mathbb{R}^2 : 0 \leq x_1 \leq 1 \text{ and } 0 \leq x_2 \leq 1\}.$$

For any initial condition in \bar{D} the system trajectory remains in $\text{Int}[\bar{D}]$ for all $\tau > 0$. In fact, since the vector fields of system (2.3.5)-(2.3.7) point into square \bar{D} everywhere on its sides, except at the vertices $(1, 0)$ and $(0, 1)$ where the acting vector field is tangent; see Figure 2.4. This is verified by analysing the signal of the vector components

$$\begin{aligned} \mathbf{F}_{++}(1, x_2) &= \begin{bmatrix} -a(c_1 + x_2) \\ -(1 + c_2)x_2 \end{bmatrix}, & \mathbf{F}_{++}(x_1, 1) &= \begin{bmatrix} -a(1 + c_1)x_1 \\ -x_1 - c_2 \end{bmatrix}, \\ \mathbf{F}_{-+}(0, x_2) &= \begin{bmatrix} a(1 - x_2) \\ 1 - (1 + c_2)x_2 \end{bmatrix}, & \mathbf{F}_{-+}(x_1, 1) &= \begin{bmatrix} -ax_1 \\ -x_1 - c_2 \end{bmatrix}, \\ \mathbf{F}_{--}(0, x_2) &= \begin{bmatrix} a(1 - x_2) \\ 1 - x_2 \end{bmatrix}, & \mathbf{F}_{--}(x_1, 0) &= \begin{bmatrix} a(1 - x_1) \\ 1 - x_1 \end{bmatrix}, \\ \mathbf{F}_{+-}(x_1, 0) &= \begin{bmatrix} a(1 - (1 + c_1)x_1) \\ 1 - x_1 \end{bmatrix}, & \mathbf{F}_{+-}(1, x_2) &= \begin{bmatrix} -a(c_1 + x_2) \\ -x_2 \end{bmatrix}. \end{aligned}$$

Figure 2.4 illustrates, based on the results obtained so far, how the vector fields of the system (2.3.5)-(2.3.7) are organized in \bar{D} . Such an illustration helps us understand how the trajectories of system (2.3.5)-(2.3.7) evolve inside \bar{D} . For any initial condition \mathbf{x}_0 in the region D_1 the system trajectory intersects the switching boundary: (i) Σ_1 ; or (ii) Σ_2 , at a crossing or sliding point \mathbf{x}_1 ; and (iii) there is a particular initial condition that leads directly to the pseudo-equilibrium point (μ_1, μ_2) . If \mathbf{x}_1 is a crossing point the trajectory goes to region (i) D_2 or (ii) D_4 . If \mathbf{x}_1 is a sliding point then the trajectory starts to slide on (i) Σ_1 or (ii) Σ_2 , towards the point (μ_1, μ_2) ; or (iii) remains at (μ_1, μ_2) . The same is true for initial conditions in D_3 . For any initial condition in the region D_2 the system trajectory intersects the switching boundary Σ_1 , or Σ_2 , at a sliding point and then slides on Σ_1 , or Σ_2 , towards the point (μ_1, μ_2) . Also, there is a particular initial condition that leads directly to (μ_1, μ_2) . The same is true for initial conditions in D_4 .

Note that the tangency points, which mark the ends of the sliding segments, are of the invisible fold type. Therefore, any trajectory that goes into sliding motion no longer comes out (except for a brief moment after a sudden small change in the reference values μ_i). In addition, all sliding trajectories tend to the point (μ_1, μ_2) , and in finite time since this point is not a regular equilibrium of system (2.3.5)-(2.3.7) nor sliding systems (2.3.9) and (2.3.10).

Based on the study carried out in this subsection, we enunciate the following Lemma, whose proof is obtained directly from the previous results presented.

Lemma 2.3.1. *Assume in system (2.3.5)-(2.3.7) that $b_1 = b_2 = 0$ and that (2.3.8) is satisfied. Then the point (μ_1, μ_2) is the global attractor of this system, being achieved in finite time.*

Example 1. *Figure 2.5 shows simulation results of the system (2.3.5)-(2.3.7) for some initial conditions in \bar{D} . In (a) we visualize the system phase portrait and in (b) the time response of each state variable. The constraint given in (2.3.8), which ensures global stability for the pseudo-equilibrium (μ_1, μ_2) , is geometrically represented by the region within the triangle in Figure 2.5(a), with the sides defined by the blue dashed lines. The region inside this triangle we call the Operating Region in (x_1, x_2) -plane and (μ_1, μ_2) is a global attractor only when located in that. Obviously, the global stability is preserved if (μ_1, μ_2) is exactly on one side of this triangle. However, this is a critical situation, since a disturbance in system parameter values may cause the system to operate at a different point than the desired one (μ_1, μ_2) . Therefore, we discard this situation and we consider the operating region only inside the triangle shown. In Figure 2.5(b), time solutions of (2.3.5)-(2.3.7) are represented in different colors for different initial conditions. We observed in these simulations that the sliding trajectories have a small oscillation around the operating point (μ_1, μ_2) . This is due to the introduction of a small hysteresis band, required for the implementation of the sliding mode controller.*

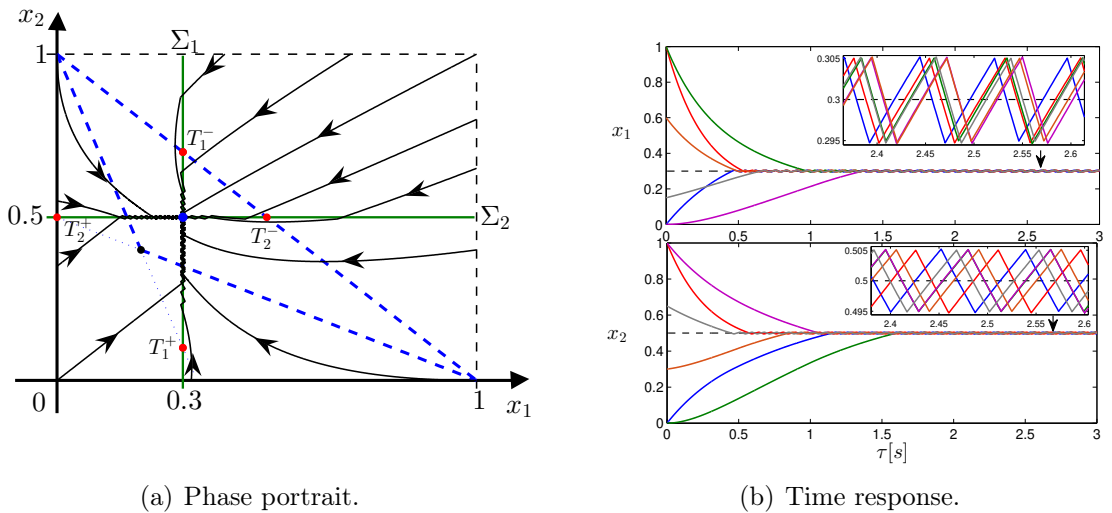


Figure 2.5: Simulations of the system (2.3.5)-(2.3.7) assuming $c_1 = 2$, $c_2 = 1$, $b_1 = b_2 = 0$, $a = 1$ and input references $\mu_1 = 0.3$ and $\mu_2 = 0.5$. A hysteresis band of 0.005 is considered.

2.3.2 Case Study for $b_1 > 0$ and $b_2 > 0$ ($P_i > 0$)

The sliding segments $\Sigma_1^{as} \subset \Sigma_1$ and $\Sigma_2^{as} \subset \Sigma_2$ are determined by imposing the sliding motion conditions on the system (2.3.5)-(2.3.7), that is,

$$\begin{aligned} L_{\mathbf{F}_{-+}} h_1(\mu_1, x_2) &= L_{\mathbf{F}_{--}} h_1(\mu_1, x_2) = a \left(1 - \mu_1 - \frac{b_1}{\mu_1} - x_2 \right) > 0, \\ L_{\mathbf{F}_{++}} h_1(\mu_1, x_2) &= L_{\mathbf{F}_{+-}} h_1(\mu_1, x_2) = a \left(1 - (1 + c_1)\mu_1 - \frac{b_1}{\mu_1} - x_2 \right) < 0, \end{aligned}$$

and

$$\begin{aligned} L_{\mathbf{F}_{--}} h_2(x_1, \mu_2) &= L_{\mathbf{F}_{+-}} h_2(x_1, \mu_2) = 1 - x_1 - \mu_2 - \frac{b_2}{\mu_2} > 0, \\ L_{\mathbf{F}_{-+}} h_2(x_1, \mu_2) &= L_{\mathbf{F}_{++}} h_2(x_1, \mu_2) = 1 - x_1 - (1 + c_2)\mu_2 - \frac{b_2}{\mu_2} < 0. \end{aligned}$$

This way we get the sliding segments

$$\begin{aligned} \Sigma_1^{as} &= \left\{ x_1 = \mu_1, 1 - (1 + c_1)\mu_1 - \frac{b_1}{\mu_1} < x_2 < 1 - \mu_1 - \frac{b_1}{\mu_1} \right\}, \\ \Sigma_2^{as} &= \left\{ x_2 = \mu_2, 1 - (1 + c_2)\mu_2 - \frac{b_2}{\mu_2} < x_1 < 1 - \mu_2 - \frac{b_2}{\mu_2} \right\}. \end{aligned}$$

Therefore, $\Sigma_1^{as} \cap \Sigma_2^{as} = \{(\mu_1, \mu_2)\}$ occurs only if the system parameters fulfil

$$\mu_1 (1 - (1 + c_1)\mu_1 - \mu_2) < b_1 < \mu_1 (1 - \mu_1 - \mu_2), \quad (2.3.11)$$

$$\mu_2 (1 - (1 + c_2)\mu_2 - \mu_1) < b_2 < \mu_2 (1 - \mu_1 - \mu_2). \quad (2.3.12)$$

Remember that $1 - \mu_1 - \mu_2 > 0$. According to Theorem 2.2.1, conditions (2.3.11) and (2.3.12) ensure local stability of the pseudo-equilibrium point (μ_1, μ_2) . In fact, since there is $\varepsilon_1 > 0$ such that for any $(x_1, \mu_2) \in \Sigma_2^{as}$ with $|x_1 - \mu_1| < \varepsilon_1$ we get

$$\begin{aligned} \frac{1}{a} \frac{dx_1}{d\tau}(x_1, \mu_2)|_{u_1=0} &= 1 - \mu_2 - x_1 - \frac{b_1}{x_1} > 0, \\ \frac{1}{a} \frac{dx_1}{d\tau}(x_1, \mu_2)|_{u_1=1} &= 1 - \mu_2 - (1 + c_1)x_1 - \frac{b_1}{x_1} < 0. \end{aligned}$$

Similarly, there is $\varepsilon_2 > 0$ such that for any $(\mu_1, x_2) \in \Sigma_1^{as}$ with $|x_2 - \mu_2| < \varepsilon_2$ we get

$$\begin{aligned} \frac{dx_2}{d\tau}(\mu_1, x_2)|_{u_2=0} &= 1 - \mu_1 - x_2 - \frac{b_2}{x_2} > 0, \\ \frac{dx_2}{d\tau}(\mu_1, x_2)|_{u_2=1} &= 1 - \mu_1 - (1 + c_2)x_2 - \frac{b_2}{x_2} < 0. \end{aligned}$$

Figure 2.6 illustrates how vector fields are directed in the neighborhood of the point (μ_1, μ_2) . Note that the sliding vector fields \mathbf{F}_{s1}^- and \mathbf{F}_{s1}^+ , as well as \mathbf{F}_{s2}^- and \mathbf{F}_{s2}^+ , are anti collinear at (μ_1, μ_2) . Moreover, (μ_1, μ_2) is not a regular equilibrium point of any of the vector fields involved. Then, this pseudo-equilibrium point is reached in finite time.

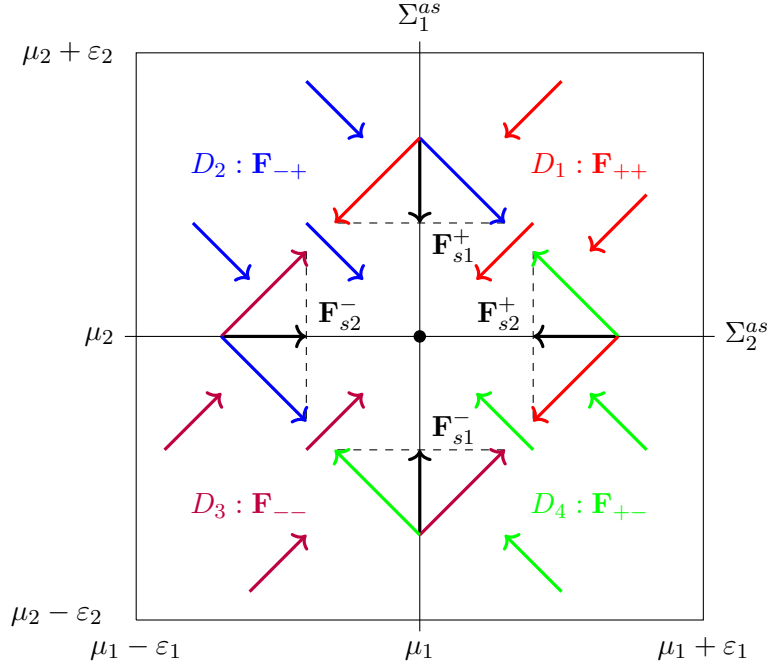


Figure 2.6: Local stability analysis at (μ_1, μ_2) .

Now, we consider in system (2.3.5)-(2.3.7) that $a = 1$, $b_1 = b_2 = b$ and $c_1 = c_2 = c$. Then, the local stability condition at (μ_1, μ_2) , given in (2.3.11)-(2.3.12), is rewritten as

$$\text{Max}[\mu_1(p - c\mu_1), \mu_2(p - c\mu_2)] < b < \text{Min}[\mu_1 p, \mu_2 p]. \quad (2.3.13)$$

where $p = p(\mu_1, \mu_2) = 1 - \mu_1 - \mu_2$. The maximum interval for the variation of b is $]0, 1/8[$ and occurs for $(\mu_1, \mu_2) = (1/4, 1/4)$ and $c \geq 2$.

The domain of operation Ω is a subset of D such that for any $(\mu_1, \mu_2) \in \Omega$ the constraint (2.3.13) is satisfied. Thus, $\Omega = \Omega_1 \cap \Omega_2$ with

$$\Omega_1 = \left\{ (x_1, x_2) \in D : 0 < 1 - x_1 - x_2 - \frac{b}{x_1} < cx_1 \right\},$$

$$\Omega_2 = \left\{ (x_1, x_2) \in D : 0 < 1 - x_1 - x_2 - \frac{b}{x_2} < cx_2 \right\}.$$

For any $b \in]0, 1/8[$ we have that Ω is not empty.

The set Ω determines in the (x_1, x_2) -plane two disjunct regions or a single region, as shown in Figures 2.7(a)-(b) and 2.7(c) by the painted areas. The first scenario occurs if $b \leq \frac{1}{4(2+c)}$, and the second if $b > \frac{1}{4(2+c)}$. The change from the first scenario to the second occurs simultaneously with the disappearance of the equilibria of the vector field \mathbf{F}_{++} . Such equilibria appear at the intersection points of the red curves shown in Figure 2.7, represented by the numbers 3, 4, 5 and 7. Intersection points of the green curves indicate the equilibria of the vector field \mathbf{F}_{--} , represented by the numbers 1 and 10. While the points of intersection between a red and a green curve indicate the equilibria of the vector fields \mathbf{F}_{-+} (represented by the numbers 2 and 8) and \mathbf{F}_{+-} (represented by the numbers 6 and 9).

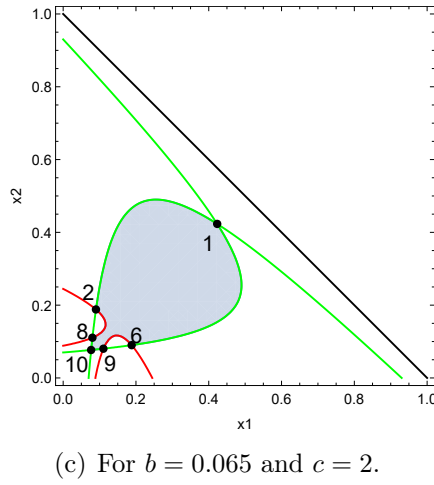
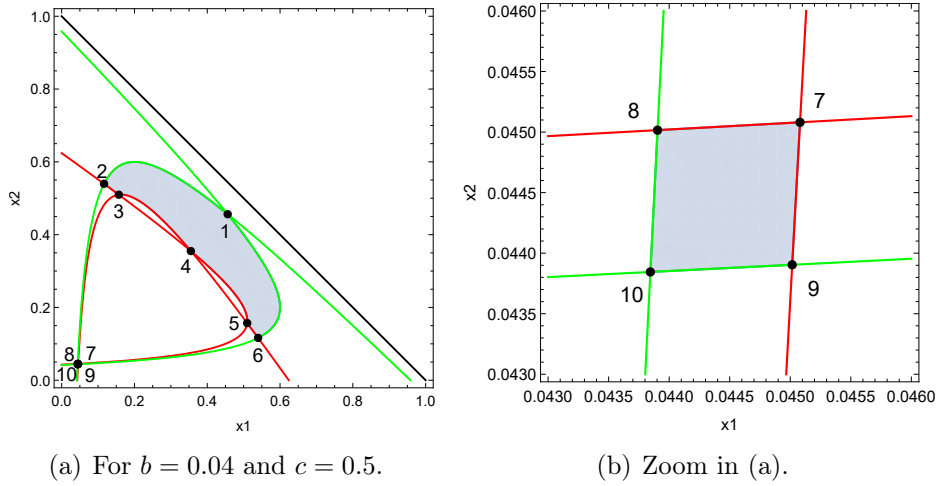


Figure 2.7: Domain of operation for the system (2.3.5)-(2.3.7). To ensure local stability at the desired operating point (μ_1, μ_2) , we must choose values of μ_1 and μ_2 within the set Ω , represented by the painted areas.

Naturally, for a given value of b such that $0 < b < 1/8$, the domain of operation Ω has maximum area when there are only the two equilibria of the vector field \mathbf{F}_{--} . This occurs for $c \geq c^*(b)$, with c^* defined above in the item (iv), which is part of the following analysis on the existence and stability of the regular equilibria of system (2.3.5)-(2.3.7). For the study of the equilibrium stability we use the Jacobian matrix given by

$$J(u_1, u_2) = \begin{pmatrix} -1 - cu_1 + \frac{b}{x_1^2} & -1 \\ -1 & -1 - cu_2 + \frac{b}{x_2^2} \end{pmatrix}.$$

This matrix is symmetric and thus its eigenvalues are real. Therefore, the equilibrium in analysis will be a saddle if $\text{Det}[J(u_1, u_2)] < 0$, but if $\text{Det}[J(u_1, u_2)] > 0$ and $\text{Tr}[J(u_1, u_2)] < 0$ (resp. $\text{Tr}[J(u_1, u_2)] > 0$) it will be a stable (resp. unstable) node. The following statements hold:

- (i) Vector field \mathbf{F}_{--} ($u_1 = u_2 = 0$) has two equilibrium points, given by $\hat{\mathbf{x}}^\pm = (\hat{x}^\pm, \hat{x}^\pm)$ with

$$\hat{x}^\pm = \frac{1}{4} \left(1 \pm \sqrt{1 - 8b} \right),$$

whenever $b < 1/8$.

If the condition of local stability at the pseudo-equilibrium (μ_1, μ_2) is satisfied, that is, the inequalities in (2.3.13) are true, then the regular equilibria $\widehat{\mathbf{x}}^\pm$ are defined because $b < \text{Min}[\mu_1 p, \mu_2 p] < 1/8$. Moreover, under such stability condition we have $\widehat{\mathbf{x}}^-$ real and $\widehat{\mathbf{x}}^+$ virtual. In order to prove this we can assume, without loss of generality, that $\mu_1 \leq \mu_2$. Then, we reduce both inequalities $h_2(\widehat{\mathbf{x}}^-) = \widehat{x}^- - \mu_2 \leq h_1(\widehat{\mathbf{x}}^-) = \widehat{x}^- - \mu_1 < 0$ and $h_1(\widehat{\mathbf{x}}^+) = \widehat{x}^+ - \mu_1 > 0$ to form $b < \mu_1(1 - 2\mu_1)$, which is true since $\mu_1(1 - \mu_1 - \mu_2) \leq \mu_1(1 - 2\mu_1)$ whenever $\mu_1 \leq \mu_2$.

To determine the stability of $\widehat{\mathbf{x}}^\pm$ we consider

$$\text{Det}[J(0, 0)] \Big|_{x_1=x_2} = \frac{b(b - 2x_2^2)}{x_2^4} \quad \text{and} \quad \text{Tr}[J(0, 0)] \Big|_{x_1=x_2} = \frac{2(b - x_2^2)}{x_2^2}.$$

Taking $x_2 = \widehat{x}^-$ we obtain $(\widehat{x}^-)^2 < b/2 < b$. Then $\widehat{\mathbf{x}}^-$ is an unstable node. And for $x_2 = \widehat{x}^+$ we obtain $(\widehat{x}^+)^2 > b/2$. Then $\widehat{\mathbf{x}}^+$ is a saddle. Evidently, for $b = 1/8$ a saddle-node bifurcation occurs.

- (ii) Vector field \mathbf{F}_{++} ($u_1 = u_2 = 1$) has a maximum of four equilibria, namely $\bar{\mathbf{x}}_\alpha^\pm = (\alpha^\pm, \alpha^\pm)$ and $\bar{\mathbf{x}}_\beta^\pm = \left(\beta^\pm, \frac{b}{c\beta^\pm}\right)$ with

$$\alpha^\pm = \frac{1 \pm \sqrt{1 - 4(2+c)b}}{2(2+c)} \quad \text{and} \quad \beta^\pm = \frac{c \pm \sqrt{c(c - 4b(1+c)^2)}}{2c(1+c)},$$

being $\bar{\mathbf{x}}_\alpha^\pm$ defined for $b \leq \frac{1}{4(2+c)}$ and $\bar{\mathbf{x}}_\beta^\pm$ defined for $b \leq \frac{c}{4(1+c)^2}$. If the condition of local stability at (μ_1, μ_2) is satisfied, then these equilibria are real whenever $\alpha^- > \text{Max}[\mu_1, \mu_2]$ or virtual otherwise.

To determine the stability of $\bar{\mathbf{x}}_\alpha^\pm$ we consider

$$\begin{aligned} \text{Det}[J(1, 1)] \Big|_{x_1=x_2} &= \frac{c(2+c)}{x_2^4} \left(x_2^2 - \frac{b}{c}\right) \left(x_2^2 - \frac{b}{2+c}\right), \\ \text{Tr}[J(1, 1)] \Big|_{x_1=x_2} &= -\frac{2(1+c)}{x_2^2} \left(x_2^2 - \frac{b}{1+c}\right). \end{aligned}$$

Taking $x_2 = \alpha^-$ we obtain $(\alpha^-)^2 < \frac{b}{2+c} < \frac{b}{1+c} < \frac{b}{c}$ whenever $b < \frac{1}{4(2+c)}$. Then $\bar{\mathbf{x}}_\alpha^-$ is an unstable node. Taking $x_2 = \alpha^+$ we obtain $(\alpha^+)^2 > \frac{b}{c} > \frac{b}{1+c} > \frac{b}{2+c}$ whenever $b < \frac{c}{4(1+c)^2}$. But, if $\frac{c}{4(1+c)^2} < b < \frac{c}{4(1+c)}$ we obtain $\frac{b}{c} > (\alpha^+)^2 > \frac{b}{2+c}$. Then $\bar{\mathbf{x}}_\alpha^+$ is a stable node for $b < \frac{c}{4(1+c)^2}$ and a saddle for $\frac{c}{4(1+c)^2} < b < \frac{1}{4(2+c)}$.

Regarding $\bar{\mathbf{x}}_\beta^\pm$ we obtain

$$\text{Det}[J(1, 1)] \Big|_{x_2=\frac{b}{cx_1}} = -\frac{(1+c)(b - cx_1^2)^2}{bx_1^2} < 0,$$

for both $x_1 = \beta^+$ and $x_1 = \beta^-$, whenever $b < \frac{c}{4(1+c)^2}$. Then $\bar{\mathbf{x}}_\beta^+$ and $\bar{\mathbf{x}}_\beta^-$ are saddle.

A pitchfork bifurcation occurs for $b = \frac{c}{4(1+c)^2}$. In fact, just note that $\bar{\mathbf{x}}_\alpha^+$ (stable node) and $\bar{\mathbf{x}}_\beta^+$ (saddle) coexist for $b < \frac{c}{4(1+c)^2}$; both collide for $b = \frac{c}{4(1+c)^2}$; and

\bar{x}_β^\pm disappear and \bar{x}_α^+ (saddle) remains. Moreover, \bar{x}_α^+ and (saddle) \bar{x}_α^- (unstable node) coexist for $b < \frac{1}{4(2+c)}$; collide for $b = \frac{1}{4(2+c)}$; and disappear $b > \frac{1}{4(2+c)}$. Then a saddle-node bifurcation occurs for $b = \frac{1}{4(2+c)}$.

(iii) Equilibria of the vector field \mathbf{F}_{+-} ($u_1 = 1, u_2 = 0$) fulfill the equations

$$\begin{aligned} 1 - (1+c)x_1 - x_2 - \frac{b}{x_1} &= 0, \\ 1 - x_1 - x_2 - \frac{b}{x_2} &= 0. \end{aligned}$$

Isolating x_1 in the second equation and replacing it in the first, and then isolating the parameter c , we obtain

$$c(x_2) = \frac{b(1 - 2x_2 - b/x_2)}{(1 - x_2 - b/x_2)^2 x_2}, \quad (2.3.14)$$

defined for $x_2 \in [\hat{x}^-, \hat{x}^+]$. From the graph of (2.3.14) on the (x_2, c) -plane, we can identify the number of equilibria of \mathbf{F}_{+-} . Graphs of this function are plotted in Figure 2.8(a) for some values of parameter b , showing that for each c in the image set there are always two possible values for x_2 . So \mathbf{F}_{+-} has a maximum of two equilibria.

Graph of (2.3.14) is illustrated in the Figure 2.8(b), where we highlight its zeros at \hat{x}^- and \hat{x}^+ , and the maximum point at (\hat{x}^*, c^*) . Note that $0 < \hat{x}^- < 1/4 < \hat{x}^+ < 1/2$ for $0 < b < 1/8$. Therefore, assuming $0 < b < 1/8$, there are two equilibrium points for $c \in]0, c^*[$, they collide for $c = c^*$ and disappear for $c > c^*$, with $c^* = c(x^*)$ and

$$x^* = \frac{1}{12} \left(-\sqrt[3]{3\sqrt{-72b + 2\sqrt{3}\sqrt{108b(4b-1) + 7} + 9}} + \frac{3^{2/3}}{\sqrt[3]{-72b + 2\sqrt{3}\sqrt{108b(4b-1) + 7} + 9}} + 3 \right).$$

In fact, since the derived function

$$c'(x_2) = \frac{b(b - x_2(x_2(4x_2 - 3) + 1))}{((1 - x_2 - b/x_2)x_2)^3}$$

has only one real zero, that occurs at $x_2 = x^*$.

Equilibrium point associated to the left branch of the graph of (2.3.14) shown in Figure 2.8(b) (solid line) is an unstable node, while the equilibrium point associated to the right branch (dashed line) is a saddle. At the maximum value $c = c^*$ a saddle-node bifurcation occurs. To prove these statements we use

$$\text{Det}[J(1, 0)] \Big|_{(x_1, c) = (1 - x_2 - b/x_2, c(x_2))} = c'(x_2) (1 - x_2 - b/x_2), \quad (2.3.15)$$

$$\text{Tr}[J(1, 0)] \Big|_{(x_1, c) = (1 - x_2 - b/x_2, c(x_2))} = -2 + \frac{b(b^2 - 2bx_2 + (1 + 3b)x_2^2 - 3x_2^3 + 4x_2^4)}{x_2^4(1 - x_2 - b/x_2)^2}, \quad (2.3.16)$$

where $1 - x_2 - b/x_2 > 0$ for all (x_2, b) such that $x_2 \in [\hat{x}^-, \hat{x}^+]$ and $b \in]0, 1/8[$. Figure 2.8(c) helps us to classify the types of equilibria involved. Note that $\text{Det}[J(1, 0)] = 0$

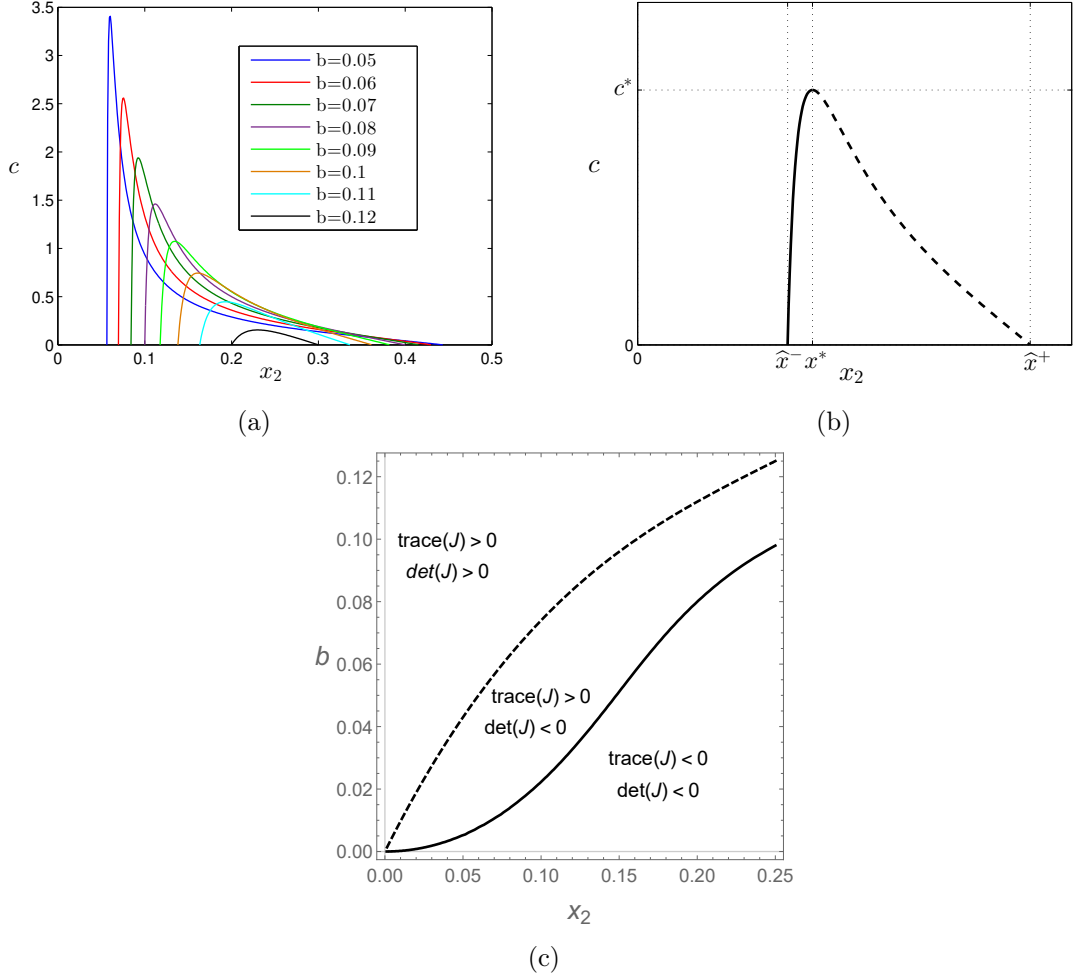


Figure 2.8: Existence and stability of equilibria of the vector field \mathbf{F}_{+-} . (a) Graphics of (2.3.14). (b) Bifurcation diagram in the (x_2, c) -plane. (c) $\text{Det}(J(1, 0))$ (eq. (2.3.15)) and $\text{Tr}(J(1, 0))$ (eq. (2.3.16)) in the (x_2, b) -plane.

(dashed line) iff $c'(x_2) = 0$, that occurs at $x_2 = x^*(b)$ for all $b \in]0, 1/8[$. We have $\text{Det}[J(1, 0)] < 0$ for all $x_2 > x^*$, while $\text{Det}[J(1, 0)] > 0$ and $\text{Tr}[J(1, 0)] > 0$ for all $x_2 < x^*$.

We denote by $\tilde{\mathbf{x}}^+ = (\tilde{x}_1^+, \tilde{x}_2^+)$ the saddle equilibrium and by $\tilde{\mathbf{x}}^- = (\tilde{x}_1^-, \tilde{x}_2^-)$ the unstable node equilibrium. If $\tilde{x}_1^+ > \mu_1$ and $\tilde{x}_2^+ < \mu_2$ then $\tilde{\mathbf{x}}^+$ is real. If $\tilde{x}_1^+ < \mu_1$ or $\tilde{x}_2^+ > \mu_2$ then $\tilde{\mathbf{x}}^+$ is virtual. If $\tilde{x}_1^- > \mu_1$ and $\tilde{x}_2^- < \mu_2$ then $\tilde{\mathbf{x}}^-$ is real. If $\tilde{x}_1^- < \mu_1$ or $\tilde{x}_2^- > \mu_2$ then $\tilde{\mathbf{x}}^-$ is virtual. If $\tilde{x}_1^- > \mu_1$ and $\tilde{x}_2^+ < \mu_2$ then both $\tilde{\mathbf{x}}^-$ and $\tilde{\mathbf{x}}^+$ are real. If $\tilde{x}_1^+ < \mu_1$ or $\tilde{x}_2^- > \mu_2$ then both $\tilde{\mathbf{x}}^-$ and $\tilde{\mathbf{x}}^+$ are virtual. All of these scenarios are possible even when restricted to the condition of local stability at (μ_1, μ_2) given in (2.3.13).

(iv) Vector field \mathbf{F}_{-+} ($u_1 = 0, u_2 = 1$) has the same equilibria as the vector field \mathbf{F}_{+-} ,

but with coordinates exchanged since

$$\mathbf{F}_{-+}(x_1, x_2) = \begin{bmatrix} 0 & 1 \\ 1 & 0 \end{bmatrix} \mathbf{F}_{+-}(x_2, x_1).$$

We assume (2.3.13) hold and $\alpha^-(c, b) < \text{Max}[\mu_1, \mu_2]$ (equilibria of \mathbf{F}_{++} are virtual). The basin of attraction Ψ for the pseudo-equilibrium (μ_1, μ_2) is a subset of D such that for any initial condition $(x_1(0), x_2(0)) = (x_{10}, x_{20}) \in \Psi$ the trajectory of system (2.3.5)-(2.3.7) tends to (μ_1, μ_2) . In particular, the reach time is finite since (μ_1, μ_2) is not an equilibrium of any of the vector fields involved, including sliding vector fields. Set Ψ is represented in Figure 2.9 by the region in the (x_1, x_2) -plane bounded by the purple lines.

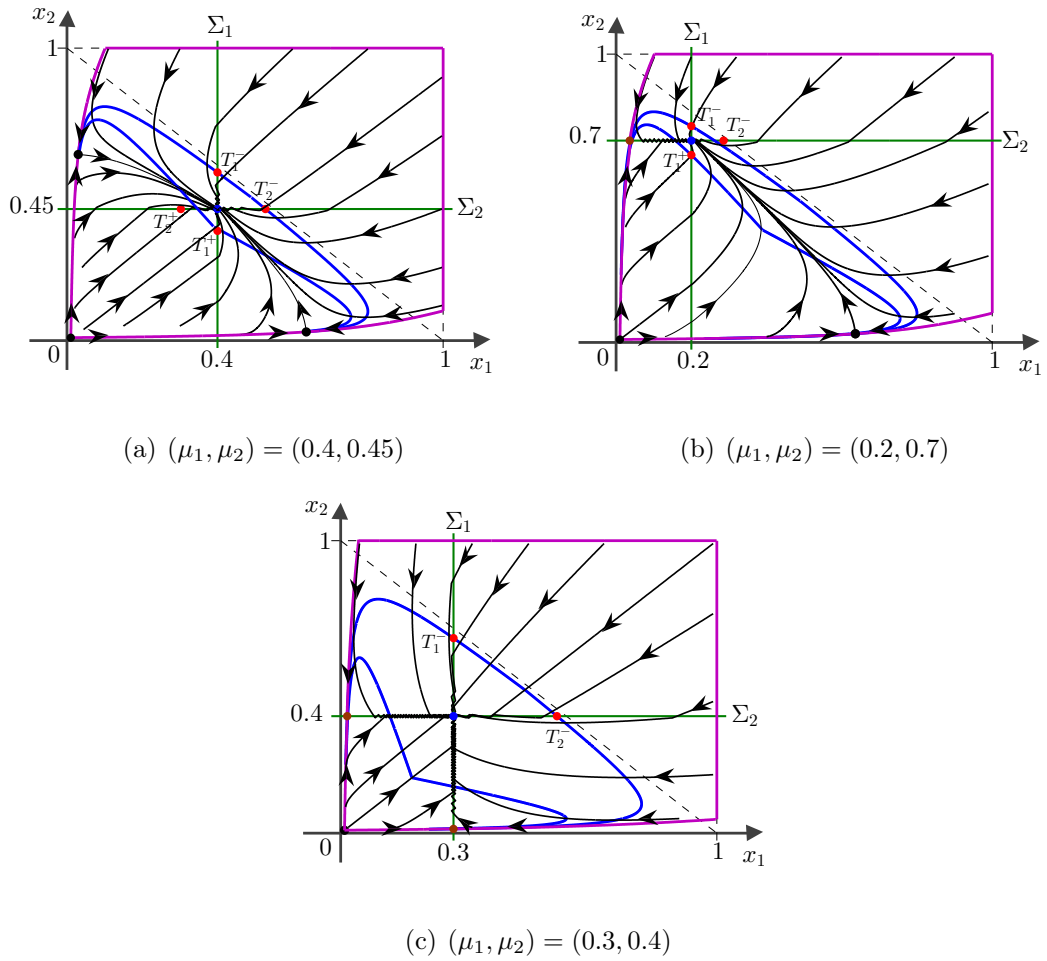


Figure 2.9: Phase portraits of system (2.3.5)-(2.3.7) assuming $a = 1$, $b_1 = b_2 = 0.01$, $c_1 = c_2 = 1/2$ in (a)-(b) and $c_1 = c_2 = 3$ in (c).

The upper limits for the x_1 and x_2 coordinates defined by Ψ are the same as for D , occurring at $x_1 = 1$ and $x_2 = 1$. Inferiorly, the x_1 and x_2 coordinates are bounded by two curve segments formed from system orbits (see Figure 2.9), and the following may occur:

- (a) If \mathbf{F}_{-+} (resp. \mathbf{F}_{+-}) has no equilibria or its equilibria are virtual, then the lower limit for the x_1 (resp. x_2) coordinate is given by a curve segment formed by the

union between the piece of orbit of \mathbf{F}_{-+} (resp. \mathbf{F}_{+-}) with extremes in $(x_1^*, 1)$ (resp. $(1, x_2^*)$) and (x_1^{**}, μ_2) (resp. (μ_1, x_2^{**})), the latter being an equilibrium point of the sliding vector field defined in Σ_2 (resp. Σ_1), the backward orbit of \mathbf{F}_{--} starting at (x_1^{**}, μ_2) (resp. (μ_1, x_2^{**})) and the equilibrium point $\hat{\mathbf{x}}^-$ of \mathbf{F}_{--} . See Figure 2.9(c).

- (b) Based on the assumptions made at the beginning of this paragraph, the vector field \mathbf{F}_{-+} (resp. \mathbf{F}_{+-}) can present a real saddle equilibrium. In this case, the curve segment is formed by the union between the saddle point, the trajectories belonging to the stable manifold of the saddle, the backward orbit of \mathbf{F}_{--} starting at (x_1^{***}, μ_2) (resp. (μ_1, x_2^{***})), this being the point of intersection of the stable manifold of the saddle with the switching boundary Σ_2 (resp. Σ_1), and the equilibrium point $\hat{\mathbf{x}}^-$ of \mathbf{F}_{--} . See Figure 2.9(a).

2.4 Study of the sliding dynamics in \mathbb{R}^3 with two-boundaries

In this section we consider the system (2.2.1) in \mathbb{R}^3 with two switching boundaries, taking into account the dynamics of the equivalent inductor. Moreover, we consider $C_1 = C_2$, $R_1 = R_2$, $P_1 = P_2$ and $V_{r_1} = V_{r_2}$. We will analyze the sliding dynamics of this system, with special attention to the sliding vector field at the intersection of the switching boundaries Σ_1 and Σ_2 , located at $V_{C_1} = V_{r_1}$ and $V_{C_2} = V_{r_2}$, respectively. For this, we take the equations of (2.2.1) in a normalized form, using the coordinates and parameters given in Table 2.1, redefining the state variables as $x_1 = x$ and $x_2 = y$, and we include the state variable $z = \frac{L}{RC_n V_{dc}} i_L$ and the parameter $r = \frac{R^2 C_n}{L}$. The normalized parameters are assumed as $a = 1$, $b_1 = b_2 = b$, $c_1 = c_2 = c$ and $\mu_1 = \mu_2 = \mu$, for $0 < \mu < 1/2$.

Next, we write the normalized system as a **3D-DPWS** system, namely

$$\frac{d}{d\tau} \begin{bmatrix} x \\ y \\ z \end{bmatrix} = \begin{cases} \mathbf{F}_{++}(x, y, z), & \text{if } (x, y, z) \in \mathbb{D}_1 \\ \mathbf{F}_{-+}(x, y, z), & \text{if } (x, y, z) \in \mathbb{D}_2 \\ \mathbf{F}_{--}(x, y, z), & \text{if } (x, y, z) \in \mathbb{D}_3 \\ \mathbf{F}_{+-}(x, y, z), & \text{if } (x, y, z) \in \mathbb{D}_4 \end{cases}, \quad (2.4.1)$$

composed by the vector fields

$$\mathbf{F}_{++}(x, y, z) = \begin{bmatrix} rz - cx - \frac{b}{x} \\ rz - cy - \frac{b}{y} \\ 1 - x - y - rz \end{bmatrix}, \quad \mathbf{F}_{-+}(x, y, z) = \begin{bmatrix} rz - \frac{b}{x} \\ rz - cy - \frac{b}{y} \\ 1 - x - y - rz \end{bmatrix}, \quad (2.4.2)$$

$$\mathbf{F}_{--}(x, y, z) = \begin{bmatrix} rz - \frac{b}{x} \\ rz - \frac{b}{y} \\ 1 - x - y - rz \end{bmatrix} \quad \text{and} \quad \mathbf{F}_{+-}(x, y, z) = \begin{bmatrix} rz - cx - \frac{b}{x} \\ rz - \frac{b}{y} \\ 1 - x - y - rz \end{bmatrix}, \quad (2.4.3)$$

being $\mathbb{D} = \{\mathbf{x} = (x, y, z) \in \mathbb{R}^3 : 0 < x, y \leq 1, z \geq 0\}$ the normalized state space. Then, $\mathbb{D} = \Sigma_1 \cup \Sigma_2 \cup \mathbb{D}_1 \cup \mathbb{D}_2 \cup \mathbb{D}_3 \cup \mathbb{D}_4$, where

$$\begin{aligned} \Sigma_1 &= \{\mathbf{x} \in \mathbb{D} : h_1(\mathbf{x}) = x - \mu\}, \\ \Sigma_2 &= \{\mathbf{x} \in \mathbb{D} : h_2(\mathbf{x}) = y - \mu\}, \end{aligned}$$

and

$$\begin{aligned}\mathbb{D}_1 &= \{\mathbf{x} \in \mathbb{D} : h_1(\mathbf{x}) > 0 \text{ and } h_2(\mathbf{x}) > 0\}, \\ \mathbb{D}_2 &= \{\mathbf{x} \in \mathbb{D} : h_1(\mathbf{x}) < 0 \text{ and } h_2(\mathbf{x}) > 0\}, \\ \mathbb{D}_3 &= \{\mathbf{x} \in \mathbb{D} : h_1(\mathbf{x}) < 0 \text{ and } h_2(\mathbf{x}) < 0\}, \\ \mathbb{D}_4 &= \{\mathbf{x} \in \mathbb{D} : h_1(\mathbf{x}) > 0 \text{ and } h_2(\mathbf{x}) < 0\}.\end{aligned}$$

System (2.4.1)-(2.4.3) presents sliding motion in $\Sigma_1 \cup \Sigma_2$, provided that the sliding conditions at Σ_1 and Σ_2 are satisfied, given by

$$\begin{aligned}L_{\mathbf{F}_{++}}h_1(\mu, y, z) &< 0 < L_{\mathbf{F}_{-+}}h_1(\mu, y, z), \\ L_{\mathbf{F}_{+-}}h_1(\mu, y, z) &< 0 < L_{\mathbf{F}_{--}}h_1(\mu, y, z),\end{aligned}$$

and

$$\begin{aligned}L_{\mathbf{F}_{++}}h_2(x, \mu, z) &< 0 < L_{\mathbf{F}_{+-}}h_2(x, \mu, z), \\ L_{\mathbf{F}_{-+}}h_2(x, \mu, z) &< 0 < L_{\mathbf{F}_{--}}h_2(x, \mu, z),\end{aligned}$$

respectively, with $L_{\mathbf{F}_{++}}h_1(\mu, y, z) = L_{\mathbf{F}_{++}}h_2(x, \mu, z) = L_{\mathbf{F}_{+-}}h_1(\mu, y, z) = L_{\mathbf{F}_{+-}}h_2(x, \mu, z) = rz - c\mu - \frac{b}{\mu}$ and $L_{\mathbf{F}_{--}}h_1(\mu, y, z) = L_{\mathbf{F}_{--}}h_2(x, \mu, z) = L_{\mathbf{F}_{-+}}h_1(\mu, y, z) = L_{\mathbf{F}_{-+}}h_2(x, \mu, z) = rz - \frac{b}{\mu}$. So, there are two attractive sliding regions, namely

$$\begin{aligned}\Sigma_1^{as} &= \left\{ \mathbf{x} \in \Sigma_1 : \frac{b}{\mu} < rz < \frac{b}{\mu} + c\mu \right\}, \\ \Sigma_2^{as} &= \left\{ \mathbf{x} \in \Sigma_2 : \frac{b}{\mu} < rz < \frac{b}{\mu} + c\mu \right\}.\end{aligned}$$

In Σ_1^{as} the sliding vector field, denoted by \mathbf{F}_{s1} , is piecewise smooth and has two vector fields which are calculated by formula

$$\mathbf{F}_{s1}^j = \frac{L_{\mathbf{F}_{-j}}h_1 \cdot \mathbf{F}_{+j} - L_{\mathbf{F}_{+j}}h_1 \cdot \mathbf{F}_{-j}}{L_{\mathbf{F}_{-j}}h_1 - L_{\mathbf{F}_{+j}}h_1},$$

for $j = +$ if $y > \mu$ and for $j = -$ if $y < \mu$. In this way, for $x = \mu$ we obtain

$$\mathbf{F}_{s1}(\mu, y, z) = \begin{cases} \mathbf{F}_{s1}^+(\mu, y, z), & \text{if } y > \mu \\ \mathbf{F}_{s1}^-(\mu, y, z), & \text{if } y < \mu \end{cases},$$

where

$$\mathbf{F}_{s1}^+(\mu, y, z) = \begin{bmatrix} 0 \\ rz - \frac{b}{y} - cy \\ 1 - \mu - y - rz \end{bmatrix} \quad \text{and} \quad \mathbf{F}_{s1}^-(\mu, y, z) = \begin{bmatrix} 0 \\ rz - \frac{b}{y} \\ 1 - \mu - y - rz \end{bmatrix}.$$

Vector fields \mathbf{F}_{s1}^+ and \mathbf{F}_{s1}^- can have two equilibrium points each. For the study of the stability of these equilibria, we can consider the vector fields

$$\mathbf{f}_{s1}^+(y, z) = \begin{bmatrix} rz - \frac{b}{y} - cy \\ 1 - \mu - y - rz \end{bmatrix} \quad \text{and} \quad \mathbf{f}_{s1}^-(y, z) = \begin{bmatrix} rz - \frac{b}{y} \\ 1 - \mu - y - rz \end{bmatrix},$$

composed of the last two components of \mathbf{F}_{s1}^+ and \mathbf{F}_{s1}^- , respectively. The following statements describe the characteristics of local dynamics of \mathbf{F}_{s1}^+ and \mathbf{F}_{s1}^- .

(i) Vector field \mathbf{F}_{s1}^+ has two equilibria, given by $\mathbf{q}_{1,2}^+ = (\mu, \tilde{y}_{1,2}^+, (1 - \mu - \tilde{y}_{1,2}^+)/r)$ with

$$\tilde{y}_{1,2}^+ = \sqrt{\frac{\nu_{sn}^+}{1+c}} \left(1 \pm \sqrt{1 - \frac{b}{\nu_{sn}^+}} \right), \quad \nu_{sn}^+ = \frac{(1-\mu)^2}{4(1+c)},$$

provided that $b < \nu_{sn}^+$. We have $\tilde{y}_2^+ \geq \sqrt{\frac{\nu_{sn}^+}{1+c}} \geq \tilde{y}_1^+$, being $\tilde{y}_2^+ = \tilde{y}_1^+$ iff $b = \nu_{sn}^+$. From a simple analysis of the sign of the determinant and trace of the Jacobian matrix of \mathbf{f}_{s1}^+ , given by

$$J_{s1}^+(\mathbf{q}_{1,2}^+) = \begin{bmatrix} 2(1+c) \left(\sqrt{\frac{\nu_{sn}^+}{1+c}} - \tilde{y}_{1,2}^+ \right) + \tilde{y}_{1,2}^+ & r\tilde{y}_{1,2}^+ \\ -\tilde{y}_{1,2}^+ & -r\tilde{y}_{1,2}^+ \end{bmatrix}$$

and

$$\begin{aligned} \text{Det} [J_{s1}^+(\mathbf{q}_{1,2}^+)] &= 2r(1+c) \left(\tilde{y}_{1,2}^+ - \sqrt{\frac{\nu_{sn}^+}{1+c}} \right) \tilde{y}_{1,2}^+, \\ \text{Tr} [J_{s1}^+(\mathbf{q}_{1,2}^+)] &= -2(1+c) \left(\tilde{y}_{1,2}^+ - \sqrt{\frac{\nu_{sn}^+}{1+c}} \right) - (r-1)\tilde{y}_{1,2}^+, \end{aligned}$$

we can conclude that if $b < \nu_{sn}^+$ then:

- \mathbf{q}_1^+ is a saddle equilibrium;
- \mathbf{q}_2^+ is a stable equilibrium whenever $r > 1 - \frac{2(1+c)}{\tilde{y}_2^+} \left(\tilde{y}_2^+ - \sqrt{\frac{\nu_{sn}^+}{1+c}} \right)$.

(ii) Vector field \mathbf{F}_{s1}^- has two equilibria, namely $\mathbf{q}_{1,2}^- = (\mu, \tilde{y}_{1,2}^-, (1 - \mu - \tilde{y}_{1,2}^-)/r)$ with

$$\tilde{y}_{1,2}^- = \sqrt{\nu_{sn}^-} \left(1 \pm \sqrt{1 - \frac{b}{\nu_{sn}^-}} \right), \quad \nu_{sn}^- = \frac{(1-\mu)^2}{4},$$

provided that $b < \nu_{sn}^-$. We have $\tilde{y}_2^- \geq \sqrt{\nu_{sn}^-} \geq \tilde{y}_1^-$, being $\tilde{y}_2^- = \tilde{y}_1^-$ iff $b = \nu_{sn}^-$. From a simple analysis of the sign of the determinant and trace of the Jacobian matrix of \mathbf{f}_{s1}^- , given by

$$J_{s1}^-(\mathbf{q}_{1,2}^-) = \begin{bmatrix} 2(\sqrt{\nu_{sn}^-} - \tilde{y}_{1,2}^-) + \tilde{y}_{1,2}^- & r\tilde{y}_{1,2}^- \\ -\tilde{y}_{1,2}^- & -r\tilde{y}_{1,2}^- \end{bmatrix}$$

and

$$\begin{aligned} \text{Det} [J_{s1}^-(\mathbf{q}_{1,2}^-)] &= 2r \left(\tilde{y}_{1,2}^- - \sqrt{\nu_{sn}^-} \right) \tilde{y}_{1,2}^-, \\ \text{Tr} [J_{s1}^-(\mathbf{q}_{1,2}^-)] &= -2 \left(\tilde{y}_{1,2}^- - \sqrt{\nu_{sn}^-} \right) - (r-1)\tilde{y}_{1,2}^-, \end{aligned}$$

we can conclude that if $b < \nu_{sn}^-$ then:

- \mathbf{q}_1^- is a saddle equilibrium;
- \mathbf{q}_2^- is a stable equilibrium whenever $r > 1 - \frac{2}{\tilde{y}_2^-} \left(\tilde{y}_2^- - \sqrt{\nu_{sn}^-} \right)$.

In the following example we show two main scenarios for the dynamics in Σ_1^{as} , taking into account that in practice r must be equal to or greater than 1. In addition, we consider the cases where the system parameters satisfy the condition

$$\mu(1 - (2 + c)\mu) < b < \mu(1 - 2\mu), \quad (2.4.4)$$

being that (2.4.4) is equivalent to the local stability condition established in Theorem 2.2.1 after the normalization of the variables and parameters given in Table 2.1 and the considerations on the normalized parameters assumed in this section.

Example 2. We assume that (2.4.4) is satisfied and $r \geq 1$. Figure 2.10 shows two main non-critical scenarios¹ for the dynamics in Σ_1^{as} . Such scenarios occur for $\mu \geq \frac{1}{3+2c}$. In fact, because we will have $\tilde{y}_1^+ < \tilde{y}_2^+ < \mu$ and $\tilde{y}_1^- < \mu < \tilde{y}_2^-$, with $\mathbf{q}_{1,2}^-$ existing, but \mathbf{q}_2^- always virtual, and $\mathbf{q}_{1,2}^+$ virtual when existing. The saddle equilibrium \mathbf{q}_1^- is real if $\tilde{y}_1^- > 1 - (1 + c)\mu - \frac{b}{\mu}$ (as in Fig. (a), red dot in Σ_1^{as-}) or virtual otherwise (as in Fig. (b)). Even when \mathbf{q}_1^- is virtual, it is a stable manifold cuts the Σ_1^{as-} region keeping it divided into two parts: one where the trajectories reach the switching boundary at $y = \mu$; and another where they do not (i.e. the trajectories). The green line at $y = \mu$ represents the switching boundary between the vector fields \mathbf{F}_{s1}^- and \mathbf{F}_{s1}^+ . This line is locally attractive and, in it, a sliding motion occurs and there is a stable equilibrium (blue dot). Naturally, the sliding dynamics in this line is governed by the third component of \mathbf{F}_{s1}^- and \mathbf{F}_{s1}^+ (which are the same) at $y = \mu$.

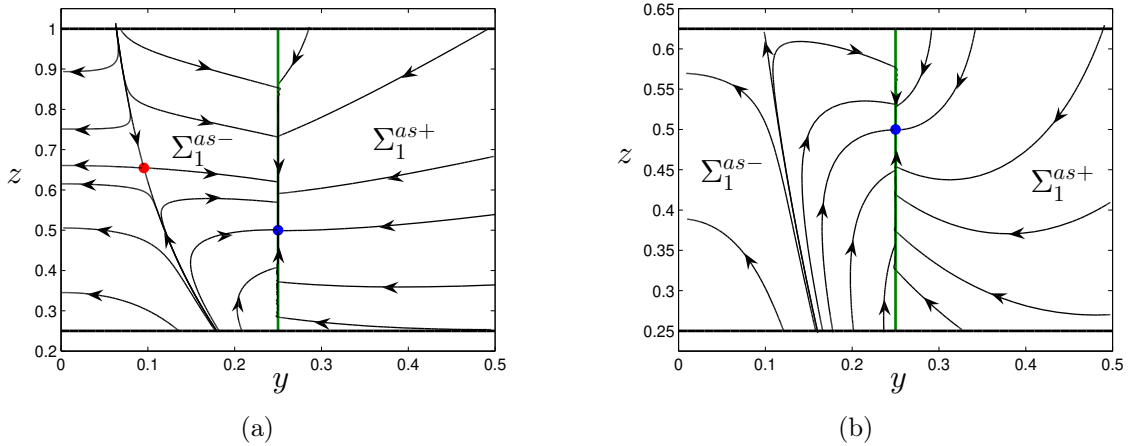


Figure 2.10: Phase portraits of \mathbf{F}_{s1} restricted to Σ_1^{as} . In (a) we use $r = 1$, $b = 1/16$, $c = 3$ and $\mu = 1/4$; in (b), $r = 1$, $b = 1/16$, $c = 3/2$ and $\mu = 1/4$.

In Σ_2^{as} the sliding vector field, denoted by \mathbf{F}_{s2} , also is piecewise smooth and has two vector fields which are calculated by formula

$$\mathbf{F}_{s2}^i = \frac{L_{\mathbf{F}_{i-}} h_2 \cdot \mathbf{F}_{i+} - L_{\mathbf{F}_{i+}} h_2 \cdot \mathbf{F}_{i-}}{L_{\mathbf{F}_{i-}} h_2 - L_{\mathbf{F}_{i+}} h_2},$$

¹They are not altered by slight variations in the parameters.

for $i = +$ if $x > \mu$ and for $i = -$ if $x < \mu$. Thus, we obtain

$$\mathbf{F}_{s_2}(x, \mu, z) = \begin{cases} \mathbf{F}_{s_2}^+(x, \mu, z), & \text{if } x > \mu \\ \mathbf{F}_{s_2}^-(x, \mu, z), & \text{if } x < \mu \end{cases},$$

where

$$\mathbf{F}_{s_2}^+(x, \mu, z) = \begin{bmatrix} rz - \frac{b}{x} - cx \\ 0 \\ 1 - \mu - x - rz \end{bmatrix} \quad \text{and} \quad \mathbf{F}_{s_2}^-(x, \mu, z) = \begin{bmatrix} rz - \frac{b}{x} \\ 0 \\ 1 - \mu - x - rz \end{bmatrix}.$$

Vector Fields $\mathbf{F}_{s_2}^+$ and $\mathbf{F}_{s_2}^-$ have the same dynamic behavior as the vector fields $\mathbf{F}_{s_1}^+$ and $\mathbf{F}_{s_1}^-$, respectively. Thus, the phase portraits shown in Figure 2.10 also occur in Σ_2^{as} , and for the same values of the parameters.

There is a line segment containing attractive sliding points, given by $\Sigma^{as} = \Sigma_1^{as} \cap \Sigma_2^{as}$, because

$$\begin{aligned} L_{\mathbf{F}_{s_1}^+} h_2(\mu, \mu, z) &< 0 < L_{\mathbf{F}_{s_1}^-} h_2(\mu, \mu, z), \\ L_{\mathbf{F}_{s_2}^+} h_1(\mu, \mu, z) &< 0 < L_{\mathbf{F}_{s_2}^-} h_1(\mu, \mu, z), \end{aligned}$$

where $L_{\mathbf{F}_{s_1}^+} h_2(\mu, \mu, z) = L_{\mathbf{F}_{s_2}^+} h_1(\mu, \mu, z) = rz - \frac{b}{\mu} - c\mu$ and $L_{\mathbf{F}_{s_1}^-} h_2(\mu, \mu, z) = L_{\mathbf{F}_{s_2}^-} h_1(\mu, \mu, z) = rz - \frac{b}{\mu}$. Then, we can determine a sliding vector field in Σ^{as} , by using the formula given in (1.2.5). Taking into account that

$$f(x, y, z) = \begin{bmatrix} rz - \frac{b}{x} \\ rz - \frac{b}{y} \\ 1 - x - y - rz \end{bmatrix} \quad \text{and} \quad g(x, y, z) = \begin{bmatrix} cx & 0 & 0 \\ 0 & cy & 0 \\ 0 & 0 & 0 \end{bmatrix},$$

from (1.2.5) we get

$$\mathbf{F}_s(\mu, \mu, z) = \begin{bmatrix} 0 \\ 0 \\ 1 - 2\mu - rz \end{bmatrix}.$$

From the statements above, we can conclude the following (remember that $0 < \mu < \frac{1}{2}$ and $r > 0$).

Proposition 2.4.1. *Sliding dynamics in Σ^{as} is described by $\frac{dz}{d\tau} = 1 - 2\mu - rz$, which has at $z = (1 - 2\mu)/r$ a stable equilibrium point.*

We then say that system (2.4.1)-(2.4.3) has a stable pseudo-equilibrium point at

$$\mathbf{p}(\mu) = (\mu, \mu, (1 - 2\mu)/r),$$

such that $\mathbf{p}(\mu) \in \Sigma^{as}$ whenever $L_{\mathbf{F}_{s_2}^+} h_1(\mathbf{p}(\mu)) < 0 < L_{\mathbf{F}_{s_2}^-} h_1(\mathbf{p}(\mu))$ and $L_{\mathbf{F}_{s_1}^+} h_2(\mathbf{p}(\mu)) < 0 < L_{\mathbf{F}_{s_1}^-} h_2(\mathbf{p}(\mu))$, i.e., whether the system parameters satisfy the condition (2.4.4).

Therefore, the condition (2.4.4) ensures local stability at \mathbf{p} . As we said before in this section, such a condition is equivalent to that established in Theorem 2.2.1. This reinforces the fact that in the stability analysis of system (2.2.1) we can disregard the dynamics imposed by the inductor, taking the reduced system (2.2.4), as done in the previous sections.

Example 3. We consider system (2.4.1)-(2.4.3) with $b = 1/16$, $c = 3$, $r = 1$ and $\mu = 1/4$. Figure 2.11 shows the system phase portrait for some initial conditions, along with the elements involved such as switching boundaries, tangency lines delimiting the sliding sets and equilibrium points. Such a choice for the values of the system parameters satisfies the local stability condition (2.4.4) of the pseudo-equilibrium \mathbf{p} (blue dot), which is a real stable equilibrium of the sliding vector field \mathbf{F}_s defined in Σ^{as} (green line segment with extremes in the red dots). In addition, there is a single real regular equilibrium point (green dot), which is a saddle equilibrium of the vector field \mathbf{F}_{--} . Two pseudo-saddles (black dots) also appear in the sliding regions (region between parallel black lines), one in $\Sigma_1^{as} \subset \Sigma_1$ being a real equilibrium of the sliding vector field \mathbf{F}_{s1}^- , and the other in $\Sigma_2^{as} \subset \Sigma_2$ being a real equilibrium of the sliding vector field \mathbf{F}_{s2}^- .

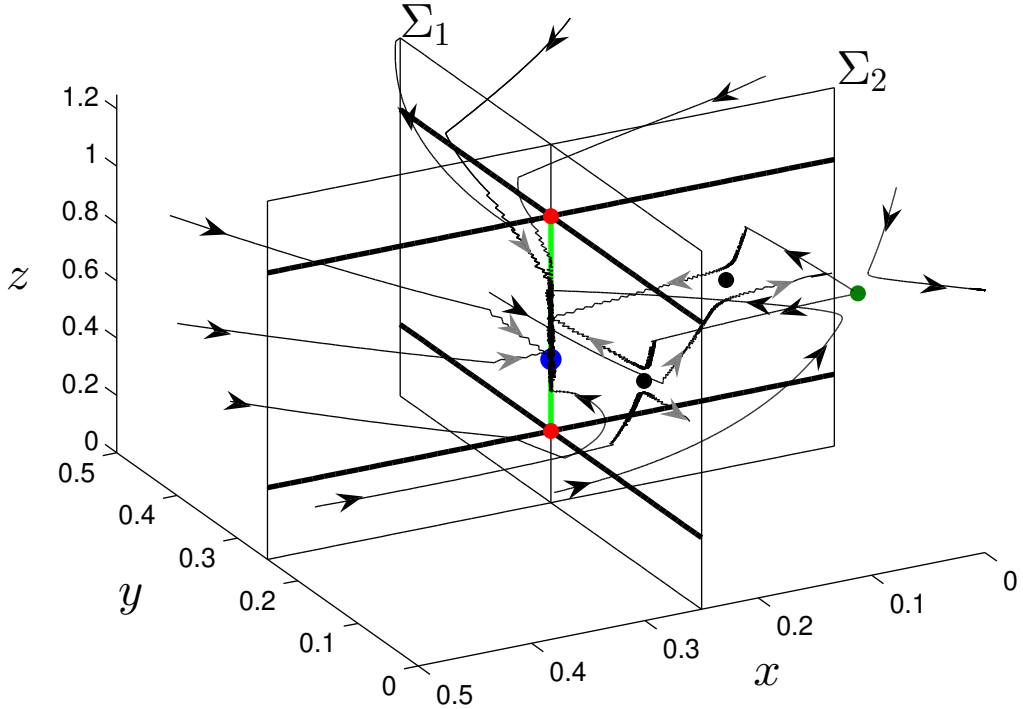


Figure 2.11: Phase portrait of system (2.4.1)-(2.4.3) assuming $b = 1/16$, $c = 3$, $r = 1$ and $\mu = 1/4$. Gray vectors indicate sliding motion.

2.5 Simulation results

We consider system (2.2.4)-(2.2.5) with $C_i = C$, $R_{b_i} = R_b$, $P_i = P$ and $V_{r_i} = V_r$ for all i . Then the local stability condition established in Theorem 2.2.1 becomes

$$\frac{V_r}{R_l} \left(V_{dc} - \left(n + \frac{R_l}{R_b} \right) V_r \right) < P < \frac{V_r}{R_l} (V_{dc} - nV_r).$$

We assume $n = 10$, $V_{dc} = 740$ V, $R_l = 100 \pm 5\%$ Ω , $C = 2.82 \pm 20\%$ mF, $P = 10.74$ W and $R_b = 375$ Ω , according to [7]. For these nominal values, the above constraint is satisfied if $70.5708V < V_r < 72.519V$ or $1.48099V < V_r < 1.48183V$. Naturally, the second option should be ruled out since the basin of attraction of the operating point is too small for this case, as there are unstable real equilibria very close to the operating point (as seen in subsection 2.3.2). Then we take the reference voltage as $V_r = 72$ V.

Figure 2.12 shows two simulation results. In (a) we consider an uncertainty of $\pm 5\%$ in the value of R_l , and in (b) an uncertainty of $\pm 20\%$ in the value of C . In both cases, we see that the system remains stable. Obviously, for such disturbances taken in these parameters, the choice of V_r still satisfies the stability condition of the operating point. Note that in (a) all equations in the system have the same parameter values, and so, all state variables have the same evolution over time, for the same initial condition in each state variable. But in (b), each equation has a different capacitance, and so, even with the same initial conditions for each state variable, the evolution over time of each state variable is different from one another.

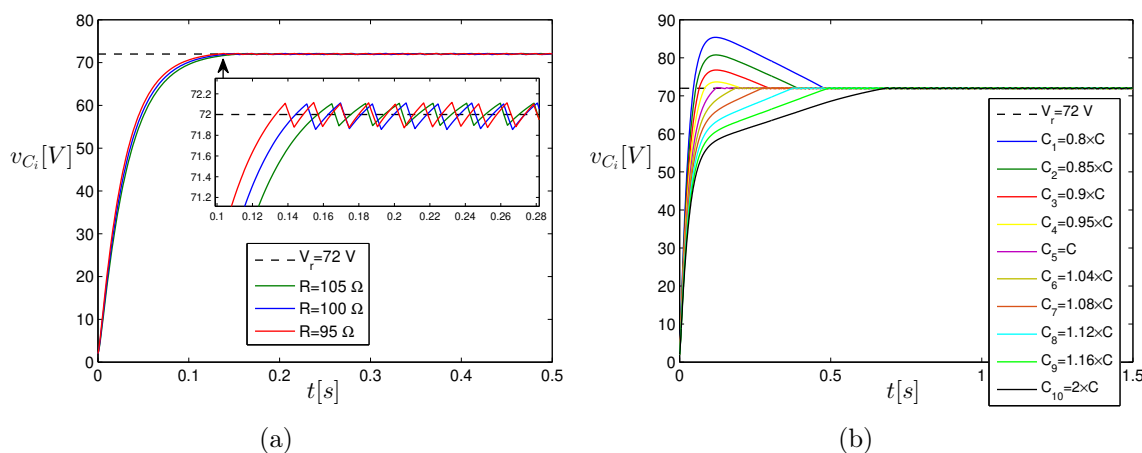


Figure 2.12: Response time of system (2.2.4)-(2.2.5) with initial conditions at $v_{C_i}(0) = 2$ V for $i = 1, 2, \dots, 10$. A hysteresis band of 0.1V is applied.

Remember that there is a real unstable equilibrium near the origin. Specifically, for these parameter values such equilibrium has coordinates $v_{C_i} = 1.48099$ V for all i . Therefore, to ensure that the operating point is reached, it is sufficient that we take equal initial conditions for each state variable, that is, $v_{C_1}(0) = v_{C_2}(0) = \dots = v_{C_{10}}(0) = v_C^0$, such that $1.48099V < v_C^0 < V_r = 72V$. Naturally, the closer to 1.48099V is the initial condition, the longer the system's response time to reach the operating point.

2.6 Conclusion

This chapter explored sliding mode control applied to capacitor voltage-balancing systems. In particular, a novel active capacitor voltage-balancing method for MMCs based on a sliding mode control with multiple switching boundaries (discontinuity surfaces of high co-dimension) was studied in depth. The main contribution of this chapter was

enunciated in Theorem 2.2.1 and its proof was developed in Section 2.2. In this Theorem, the local stability of the voltage balanced system is analytically proven for an arbitrary number of submodules. Furthermore, a detailed analysis of the global dynamics of this system with two submodules and two switching boundaries sliding mode control was presented, helping us to unravel the dynamical richness of this class of systems. The methodology developed in this chapter can be applied to other capacitor voltage-balancing systems found in power electronic circuits. As future research, a more detailed study should be carried out in a reduced circuit that considers all three legs of the MMC circuit and takes into account their dynamic interactions.

Chapter 3

Bifurcation analysis of 3D-PWS systems with two transversal switching boundaries: a case study in power electronics

In this chapter, we study piecewise smooth systems with two switching boundaries. A bifurcation approach is proposed in order to study local and global phenomena on a power electronic circuit feeding a piecewise constant power load and controlled by means of a sliding mode control law. This case study in power electronics allows us to characterize different switching dynamic phenomena and bifurcations like Boundary Equilibrium Bifurcations (BEB) and Limit Cycle Bifurcations (LCB) detected on the sliding and crossing regions. We present some novel results on the BEBs analysis in \mathbb{R}^3 and study various dynamic behaviors that are found in **DPWS** systems. In this sense, the analysis of a simple power electronic circuit allows to unveil a plethora of dynamic phenomena that are manifested in more complex **DPWS**. Furthermore, this case study in power electronics can be used, as a benchmark, to study in depth different dynamic phenomena that can lead to develop new techniques and methods to analyze this class of systems characterizing novel local and global bifurcations. Simulation results obtained on a controlled power buck converter feeding a constant power load are shown to validate the theoretical and numerical analysis.

3.1 Introduction

In typical direct current (for short, dc) electrical distribution systems, more known as dc microgrids, with a cascaded converters architecture (see Figure 3.1), loads connected to the bus by an electronic converter behave as a constant power drawn from the feeder, and can be modeled as a constant power load (for short, CPL); see [31, 29, 30]. Figure 3.2 shows a simplified view of two cascaded converters PC1 and PC2, also shown in Figure 3.1.

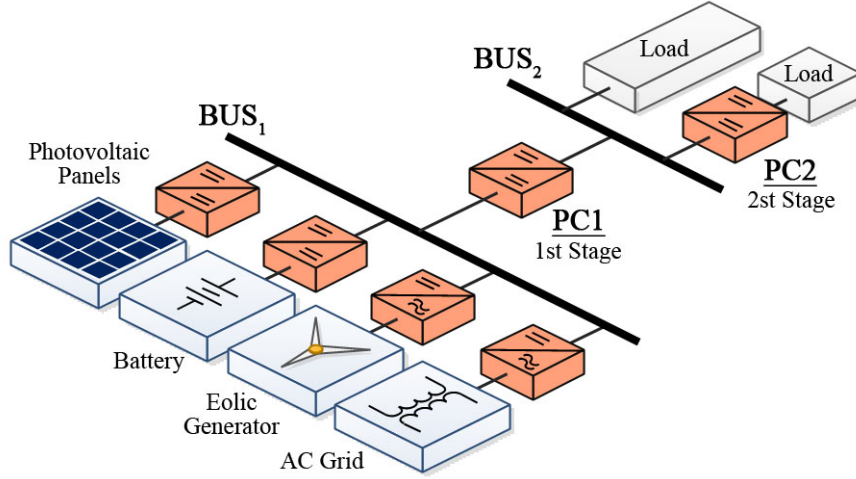


Figure 3.1: Block diagram of a simplified dc electrical distribution system (dc microgrid) with cascaded interconnected converters architecture and two dc buses (Bus1 and Bus2)..

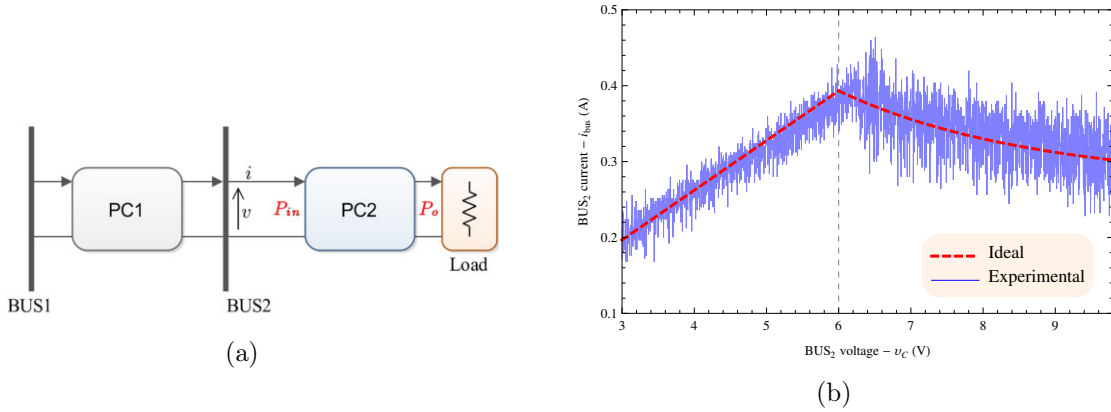


Figure 3.2: a) Cascaded power converters block diagram. b) Experimental CPL curve corresponding to the PC2 plus load ($P_{in} = P_o = 2.4W$, $V_{th} = 6v$).

Since the input and output power of PC2 (P_{in} and P_o) are constant, the static input voltage-current ($v_c - i$) function, $i_{bus} = f(v_c)$, is ideally a hyperbola given by $i = \frac{P_{in}}{v_c}$. The input resistance of PC2 has a negative impedance characteristic, where a voltage increment will cause a current decrease and vice versa. Therefore, the PC2 converter as seen by PC1 can be modeled as a CPL. Thus, assuming that the BUS1 voltage suffers small variations, the PC1 converter connected to the loads in BUS2 microgrid, see Figure 3.1, can be analyzed by the model depicted in Figure 3.2(a), composed by a first stage buck converter that feeds a CPL. This electronic circuit is composed of two buck converters connected in a cascade structure being the first buck converter controlled by a sliding mode control (for short SMC) law and the second converter modelled by a CPL, as shown in Figure 3.2(a).

In practice, function $i_{bus} = f(v_c)$ can be expressed as a power piecewise function for the buck converter case considered as a CPL. Figure 3.2(b) shows a CPL curve for a buck converter with resistive load obtained from an experimental circuit setup. This piecewise

function is continuous but not differentiable at $v_c = V_{th}$, being composed of two parts: (i) one linear function for $v_c \leq V_{th}$; and (ii) a hyperbolic function for $v_c > V_{th}$, where V_{th} stands for a voltage threshold, as will be seen in Section 3.2. This type of problem is well-known in power electronics literature but curiously is not treated in a rigorous mathematical form. An exception can be found in previous work on spacecraft power systems with CPL by David Hamill et al. [32, 33], and recent studies on applications in systems composed of interconnected power converters in an islanded dc microgrid by L. Benadero et al. [29].

The system under study can be considered as a piecewise smooth dynamical system in \mathbb{R}^3 (for short, **3D-DPWS** system) with two transversal switching boundaries defined by (i) the SMC law designed to control the voltage output of the first buck converter and (ii) the voltage threshold at $v_c = V_{th}$ due to the non-smooth characteristic of the CPL. It is noteworthy that the sliding motion occurs only at the SMC-boundary and the vector field that governs this motion, calculated following Filippov's convention, is continuous but not differentiable at the intersection with the CPL-boundary. In this sense, the study carried out in this work considers the theory of **CPWS** systems and Filippov systems (**DPWS**); see [1, 34].

DPWS dynamical system with two transversal switching boundaries has been approached by several researchers, see for instance [35, 36] (**CPWS**) and [10, 13, 42, 40, 18] (**DPWS**) where the sliding motion can occur at all switching boundaries involved, which is not our case study as mentioned in the previous paragraph.

The main goal of this chapter is to study local and global phenomena associated with bifurcations induced by the switching boundaries, as the Boundary Equilibrium Bifurcations (BEBs, [23, 19, 20, 24, 25]), the Grazing-Sliding (GS, [19, 26, 37, 27, 38, 39, 28]) and Discontinuous Saddle-Node (DSN, [22]), which are part of the group of Discontinuous Induced Bifurcations (DIBs, [41, 43]), and also the non-smooth limit cycles bifurcations, with or without sliding part (see [19, 44, 45, 46, 47, 48]). Classic bifurcations as the Hopf, Saddle-Node of equilibria, Saddle-Node of limit cycles, Homoclinic connection (see [50, 49]), are also found in the system under study. In the qualitative analysis carried out, we use standard tools for **DPWS** systems. Numerical continuation methods based on AUTO software are also employed to obtain bifurcation sets and bifurcation diagrams. The CPL equations used are class \mathcal{C}^0 functions, that is, continuous but with discontinuous derivatives. As a significant part of this chapter involves the bifurcation analysis of dynamic systems, \mathcal{C}^∞ models are more suitable for performing numerical continuation calculations using computational packages such as XPP-AUTO for which it is necessary to use the hyperbolic tangent functions to approximate \mathcal{C}^0 nonlinearities as \mathcal{C}^∞ , for instance

$$i(v_{bus}) = \frac{P_{dc}}{v_{bus}} \left[\frac{1}{2} + \frac{1}{2} \tanh \left(\frac{v_{bus} - V_{th}}{\epsilon} \right) \right] + \frac{v_{bus}}{R_{th}} \left[\frac{1}{2} - \frac{1}{2} \tanh \left(\frac{v_{bus} - V_{th}}{\epsilon} \right) \right],$$

where $R_{th} = \frac{V_{th}^2}{P_{dc}}$ with V_{th} being a reference signal for the converter output voltage modeled as CPL and ϵ is an adjustment parameter that must be small ($0 < \epsilon \ll 1$). Numerical simulations of the studied system are provided, which help us to better understand the dynamic behavior of this system, in addition to checking the results obtained.

This chapter is organized as follows. Section 3.1 presents a brief introduction to the electronic circuit composed of two buck converters connected in a cascade structure. The modeling of the dc-dc bidirectional buck converter by feeding a CPL is developed

in section 3.2 and we analyze the existence, local stability and bifurcations of regular equilibria, and pseudo-equilibria. In section 3.3 we study the boundary equilibrium bifurcations. Section 3.4 is dedicated to the study of limit cycle bifurcations by using numerical analysis. In addition, we present two bifurcation frameworks in two parameters (power load and control reference), considering two different case studies with the other system parameters taken fixed, where many equilibria and limit cycle bifurcations are predicted. Finally, in section 3.5 we present a brief conclusion.

Previous results on **DPWS** in chapter 1 are important for the development that follows.

3.2 The buck converter feeding a nonlinear load of CPL-type

In typical dc distribution systems with a cascaded converter architecture, loads connected to the bus by an electronic converter behave as constant power drawn from the feeder, and can be modelled as a load of CPL-type, see [31] and references therein. We will consider a **3D-PWS** system that models the voltage control process at the output of the dc-dc bidirectional buck converter by feeding a CPL, see Figure 3.3.

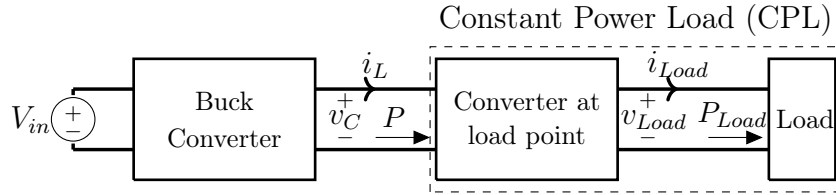


Figure 3.3: The converter at the load point behaves as a constant power load for the feeder buck converter, see [51].

The behavior of a dc-dc bidirectional buck converter controlled by a sliding mode control (SMC) law and the second converter modelled by a CPL piecewise function, can be studied using the circuit topology depicted in Figure 3.4, its model is given by

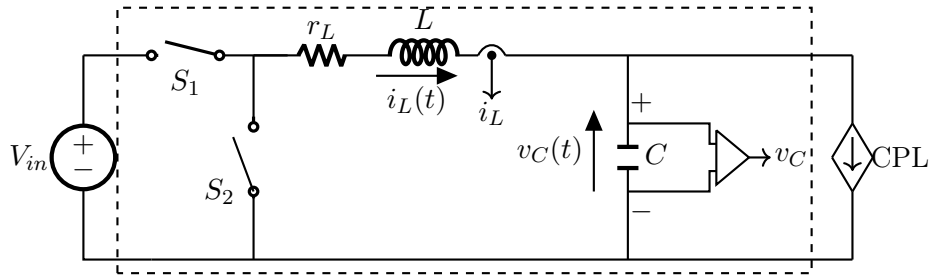
$$L \frac{di_L}{dt} = uV_{in} - r_L i_L - v_C, \quad (3.2.1)$$

$$C \frac{dv_C}{dt} = i_L - \xi(v_C), \quad (3.2.2)$$

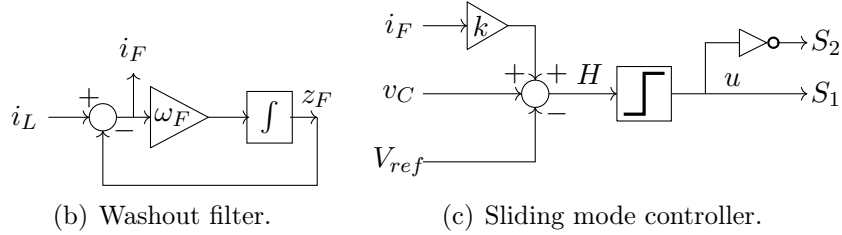
$$\frac{dz_F}{dt} = \omega_F (i_L - z_F), \quad (3.2.3)$$

where $\xi(v_C)$ is a CPL piecewise function defined by

$$\xi(v_C) = \begin{cases} \frac{P}{v_C}, & \text{if } v_C \geq V_{th}, \\ \frac{Pv_C}{V_{th}^2}, & \text{if } v_C < V_{th}, \end{cases} \quad (3.2.4)$$



(a) dc-dc bidirectional *buck* converter.



(b) Washout filter.

(c) Sliding mode controller.

Figure 3.4: Basic topology of a Buck converter connected to a CPL load and under a sliding mode and washout filter control strategy. The control function is defined as $u = \frac{1}{2}(1 - \text{sign}[H(i_L, v_C, z_F)])$. The filtered inductor current given by $i_F = i_L - z_F$ expresses the difference between the inductor current i_L and the filtered signal z_F .

where L , C , and r_L denote the inductance, the capacitance and the inductor resistance, respectively. $v_C > 0$ and $i_L \in (-i_{max}, i_{max})$, for some $i_{max} > 0$, are the instantaneous capacitor voltage and inductor current, respectively. The load parameter is denoted by $P \in \mathbb{R}$ and V_{th} is the voltage threshold. The filtered inductor current, denoted by variable z_F , is the output of the washout filter modelled by equation (3.2.3), where $\omega_F \leq 1/\sqrt{LC}$ is the cut-off filter frequency, which should be assigned to the natural frequency of the system (see [31, 52]).

The control law is defined as

$$u = \frac{1}{2}(1 - \text{sign}[H(i_L, v_C, z_F)]), \quad (3.2.5)$$

where $u = 0$ means that switch S_1 in Figure 3.4(a) is off and $u = 1$ means that it is on. Switches S_1 and S_2 are complementary. From this, the control surface is chosen as

$$H(i_L, v_C, z_F) = v_C - V_{ref} + K(i_L - z_F) = 0, \quad (3.2.6)$$

where $v_c \approx V_{ref} < V_{in}$ is the reference voltage (desired voltage value at the output) with V_{in} denoting the source voltage and $K > 0$ is the control parameter, which must be adjusted properly to ensure stability (at least local) of the desired operating point.

To obtain the desired voltage value V_{ref} at the output, a control strategy by sliding modes based on the use of a *washout* filter is implemented, as illustrated in Figure 3.4(b)-(c). The *washout* is a high-pass linear filter that washes out steady-state inputs while passing transient inputs (see [53]), and is chosen in order to reject load perturbations.

3.2.1 Normalized model

Looking for a simplified model with two planar switching surfaces, the equations (3.2.1)-(3.2.3) are normalized by applying the change of variables, time and parameters, given by Table 3.1. The switch position function is invariant with respect to normalization. In this way, we obtain a dimensionless dynamical system of the form

$$\begin{aligned} \dot{x} &= u - bx - y, \\ \dot{y} &= x - \xi(y), \\ \dot{z} &= (1 - kb)x + (\omega - k)y - \xi(y) - \omega z - \omega y_r + ku, \end{aligned} \quad (3.2.7)$$

where $\xi(y)$ is a normalized CPL piecewise function given by

$$\xi(y) = \begin{cases} \frac{d}{y} & \text{if } y \geq y_{th}, \\ \frac{dy}{y_{th}^2} & \text{if } y < y_{th}, \end{cases} \quad (3.2.8)$$

with $x \in (-x_{max}, x_{max})$ for some $x_{max} > 0$, $y > 0$ and $z \in \mathbb{R}$ are the normalized variables of inductor current, capacitor voltage and filter, respectively. The normalized parameters $d > 0$, $b > 0$, $\omega \in (0, 1]$, $k > 0$, $y_{th} > 0$ and $0 < y_r < 1$ correspond to the CPL, inductor resistance, filter cut-off frequency, control parameter, voltage threshold, and reference voltage, respectively (the dot “ \cdot ” indicates derivatives with respect to the normalized time τ).

Remark 3.2.1. *Throughout this chapter, we assume that $0 < y_{th} < y_r < 1$. Moreover, we will consider $0 < b < 1$ and $0 < k < 1/b$.*

State and Time Variables	Parameters
$i_L = V_{in} \sqrt{\frac{C}{L}} x$	$V_{ref} = y_r V_{in}$
$v_C = V_{in} y$	$P = V_{in}^2 \sqrt{\frac{C}{L}} d$
$z_F = i_L + \frac{v_C - V_{ref} - V_{in} z}{K}$	$K = k \sqrt{\frac{L}{C}}$
$t = \sqrt{CL} \tau$	$r_L = b \sqrt{\frac{L}{C}}$
	$\omega_F = \frac{\omega}{\sqrt{LC}}$

Table 3.1: Normalized variables, parameters and time

We denote $\mathbf{x} = (x, y, z) \in \mathcal{A}$, where

$$\mathcal{A} = \{\mathbf{x} \in \mathbb{R}^3 : x \in (-x_{max}, x_{max}), x_{max} > 0, y > 0 \text{ and } z \in \mathbb{R}\}.$$

Now for the normalized system (3.2.7), the control law can be rewritten as $u = \frac{1}{2}(1 + \text{sign}[z])$ and by redefining the planar switching surface as $h_1(\mathbf{x}) = z = 0$. In addition, there is another switching boundary, imposed by CPL loads and given by the planar

switching surface $h_2(\mathbf{x}) = y - y_{th} = 0$. In this way, the switching boundaries are defined by

$$\begin{aligned}\Sigma_1 &:= \{\mathbf{x} \in \mathcal{A} : h_1(\mathbf{x}) = z = 0\}, \\ \Sigma_2 &:= \{\mathbf{x} \in \mathcal{A} : h_2(\mathbf{x}) = y - y_{th} = 0\}.\end{aligned}\tag{3.2.9}$$

The system state space is divided into four different regions (see Figure 3.5), namely

$$\begin{aligned}D_1 &= \{\mathbf{x} \in \mathcal{A} : h_1(\mathbf{x}) > 0 \quad \text{and} \quad h_2(\mathbf{x}) > 0\}, \\ D_2 &= \{\mathbf{x} \in \mathcal{A} : h_1(\mathbf{x}) > 0 \quad \text{and} \quad h_2(\mathbf{x}) < 0\}, \\ D_3 &= \{\mathbf{x} \in \mathcal{A} : h_1(\mathbf{x}) < 0 \quad \text{and} \quad h_2(\mathbf{x}) < 0\}, \\ D_4 &= \{\mathbf{x} \in \mathcal{A} : h_1(\mathbf{x}) < 0 \quad \text{and} \quad h_2(\mathbf{x}) > 0\}.\end{aligned}\tag{3.2.10}$$

In each one of these regions there is a distinct vector field acting, obtained from system (3.2.7) and it is represented as a **3D-PWS** system of the form

$$\dot{\mathbf{x}} = \begin{cases} \mathbf{F}_1(\mathbf{x}) & \text{if } \mathbf{x} \in D_1, \\ \mathbf{F}_2(\mathbf{x}) & \text{if } \mathbf{x} \in D_2, \\ \mathbf{F}_3(\mathbf{x}) & \text{if } \mathbf{x} \in D_3, \\ \mathbf{F}_4(\mathbf{x}) & \text{if } \mathbf{x} \in D_4, \end{cases}\tag{3.2.11}$$

composed of the vector fields

$$\mathbf{F}_1(\mathbf{x}) = \begin{bmatrix} -bx - y \\ x - \frac{d}{y} \\ f_{3,1}(\mathbf{x}) \end{bmatrix}, \quad \mathbf{F}_2(\mathbf{x}) = \begin{bmatrix} -bx - y \\ x - \frac{d}{y_{th}^2}y \\ f_{3,2}(\mathbf{x}) \end{bmatrix},\tag{3.2.12}$$

$$\mathbf{F}_3(\mathbf{x}) = \begin{bmatrix} 1 - bx - y \\ x - \frac{d}{y_{th}^2}y \\ f_{3,2}(\mathbf{x}) + k \end{bmatrix} \quad \text{and} \quad \mathbf{F}_4(\mathbf{x}) = \begin{bmatrix} 1 - bx - y \\ x - \frac{d}{y} \\ f_{3,1}(\mathbf{x}) + k \end{bmatrix},\tag{3.2.13}$$

where

$$f_{3,1}(\mathbf{x}) = (1 - kb)x + (\omega - k)y - \frac{d}{y} - \omega z - \omega y_r$$

and

$$f_{3,2}(\mathbf{x}) = (1 - kb)x + (\omega - k)y - \frac{d}{y_{th}^2}y - \omega z - \omega y_r.$$

It should be noted that $\mathbf{F}_1(\mathbf{x}) = \mathbf{F}_2(\mathbf{x})$ and $\mathbf{F}_3(\mathbf{x}) = \mathbf{F}_4(\mathbf{x})$ for all $\mathbf{x} \in \Sigma_2$, however, the first derivatives of $\mathbf{F}_1(\mathbf{x})$ and $\mathbf{F}_2(\mathbf{x})$, as well as $\mathbf{F}_3(\mathbf{x})$ and $\mathbf{F}_4(\mathbf{x})$, are not the same in Σ_2 . Thus, the switching boundary Σ_2 is a crossing switching boundary, that is, the system trajectories that reach Σ_2 , always cross it or are tangent to it. The following proposition predicts this.

Proposition 3.2.2. *There is no sliding motion at the switching boundary Σ_2 defined in (3.2.9).*

Proof. A straightforward calculus yields, $L_{\mathbf{F}_{1,2}(\mathbf{x})}h_2(\mathbf{x}) \cdot L_{\mathbf{F}_{3,4}(\mathbf{x})}h_2(\mathbf{x}) = (x - \xi(y))^2 \geq 0$, where ξ is the piecewise function defined as in (3.2.8). Therefore, Σ_2 is just a crossing boundary, containing a double tangency line at $x = \xi(y_{th})$ and $y = y_{th}$. \square

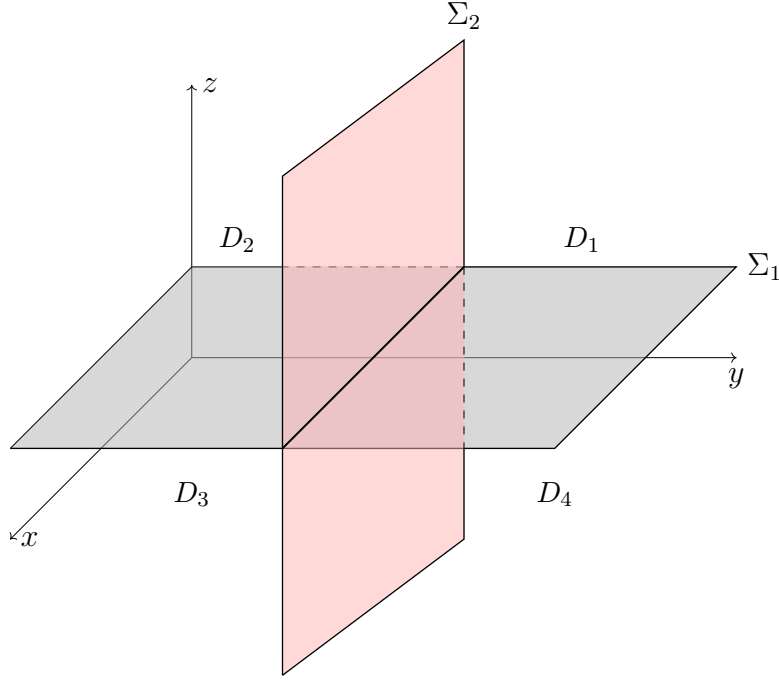


Figure 3.5: Switching boundaries defined in (3.2.9).

In order to analyze the dynamic behavior of system (3.2.11) on the switching boundary Σ_1 , we calculate the sliding and crossing regions according (1.2.7) taking into account the discontinuity of $\xi(y)$ at $y = y_{th}$ for which we divided the study in two cases as follows and they are depicted in Figure (3.6).

- (i) For $y \geq y_{th}$: the crossing and sliding regions are defined, respectively, by

$$\begin{aligned}\Sigma_{c_1} &= \{\mathbf{x} \in \Sigma_1 : y > 0, \quad \text{and} \quad x > \bar{\alpha}(y) \text{ or } x < \underline{\alpha}(y)\}, \\ \Sigma_{s_1} &= \{\mathbf{x} \in \Sigma_1 : y > 0, \quad \text{and} \quad \underline{\alpha}(y) < x < \bar{\alpha}(y)\},\end{aligned}$$

where

$$\bar{\alpha}(y) = \frac{(w - k)y^2 - wy_r y - d}{(bk - 1)y} \quad \text{and} \quad \underline{\alpha}(y) = \frac{(w - k)y^2 - (wy_r - k)y - d}{(bk - 1)y}.$$

- (ii) For $y < y_{th}$: the crossing and sliding regions are defined by

$$\begin{aligned}\Sigma_{c_2} &= \{\mathbf{x} \in \Sigma_1 : y > 0, \quad \text{and} \quad x > \bar{\beta}(y) \text{ or } x < \underline{\beta}(y)\}, \\ \Sigma_{s_2} &= \{\mathbf{x} \in \Sigma_1 : y > 0, \quad \text{and} \quad \underline{\beta}(y) < x < \bar{\beta}(y)\},\end{aligned}$$

where

$$\bar{\beta}(y) = \frac{(wy_{th}^2 - ky_{th}^2 - d)y + (k - wy_r)y_{th}^2}{(bk - 1)y_{th}^2} \quad \text{and} \quad \underline{\beta}(y) = \frac{(wy_{th}^2 - ky_{th}^2 - d)y - wy_r y_{th}^2}{(bk - 1)y_{th}^2}.$$

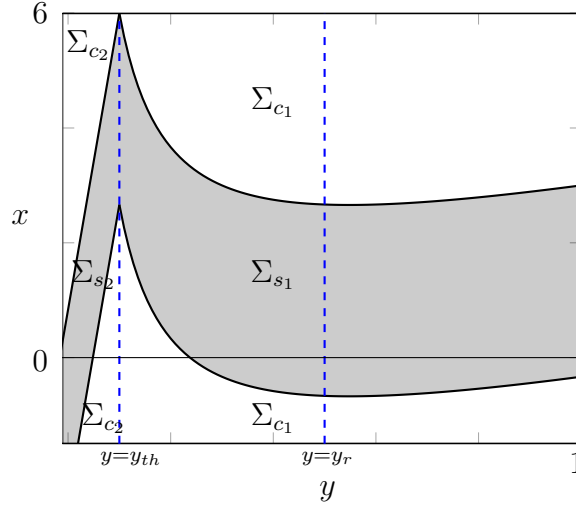


Figure 3.6: Sliding (gray region) and crossing regions (white region) in the (y, x) -plane for parameters $\omega = 1$, $b = 0.2$, $k = 2$, $y_{th} = 0.1$, $y_r = 0.5$ and $d = 0.3$.

3.2.2 Regular equilibria and stability

In what follows, we analyze the equilibria of the vector fields $\mathbf{F}_i(\mathbf{x})$, for $i = 1, 2, 3, 4$ and its stability considering only the dynamics with respect to the variables (x, y) , since that first and second components of the vector fields mentioned above are independent of the dynamic in their third component z , whose dynamic is stable since the associated eigenvalue is $-\omega < 0$. Thus, we just need to consider the reduced linearization Jacobian matrix given by

$$A = \begin{bmatrix} -b & -1 \\ 1 & -\xi'(y) \end{bmatrix}. \quad (3.2.14)$$

- (i) Vector field $\mathbf{F}_1(x, y, z)$ has no equilibrium for $d > 0$.
- (ii) Vector field $\mathbf{F}_2(x, y, z)$ has only one equilibrium point, given by $\bar{\mathbf{x}}_2 = (0, 0, -y_r)$, and it is virtual because $h_1(\bar{\mathbf{x}}_2) = -y_r < 0$. The stability in $\mathbf{F}_2(x, y, z)$ is equal to that of the vector field $\mathbf{F}_3(x, y, z)$ which we will see below.
- (iii) Vector field $\mathbf{F}_3(x, y, z)$ has an equilibrium point,

$$\bar{\mathbf{x}}_3 = \left(\frac{d}{bd + y_{th}^2}, \frac{y_{th}^2}{bd + y_{th}^2}, \frac{y_{th}^2}{bd + y_{th}^2} - y_r \right).$$

It is real for $d > \frac{(1-y_r)y_{th}^2}{by_r}$ ($h_1(\bar{\mathbf{x}}_3) < 0$) and $d > \frac{(1-y_{th})y_{th}}{b}$ ($h_2(\bar{\mathbf{x}}_3) < 0$), or equivalently $d > \max\left\{\frac{(1-y_{th})y_{th}}{b}, \frac{(1-y_r)y_{th}^2}{by_r}\right\} = \frac{(1-y_{th})y_{th}}{b}$ because $y_{th} < y_r$. Otherwise, it is virtual. Moreover this point is a boundary equilibrium for $d = \frac{(1-y_{th})y_{th}}{b}$ ($h_2(\bar{\mathbf{x}}_3) = 0$). The determinant and trace are given by

$$Det[A(\bar{\mathbf{x}}_3)] = \frac{bd + y_{th}^2}{y_{th}^2} \quad \text{and} \quad Tr[A(\bar{\mathbf{x}}_3)] = -\left(b + \frac{d}{y_{th}^2}\right).$$

This equilibrium is always stable because $d > 0$. Moreover, analyzing the discriminant $\Delta = Tr[A(\bar{\mathbf{x}}_3)]^2 - 4Det[A(\bar{\mathbf{x}}_3)]$ ($\Delta < 0$ or $\Delta > 0$) we have that $\bar{\mathbf{x}}_3$

is: (i) a virtual stable focus for $d \in (0, (2+b)y_{th}^2)$; (ii) a virtual stable node for $d \in \left((2+b)y_{th}^2, \frac{(1-y_{th})y_{th}}{b} \right)$; and (iii) a real stable node for $d > \frac{(1-y_{th})y_{th}}{b}$.

(iv) Vector field $\mathbf{F}_4(x, y, z)$ has two equilibrium points, namely

$$\bar{\mathbf{x}}_4^+ = \left(\frac{1+\gamma}{2b}, \frac{1-\gamma}{2}, \frac{1-2y_r-\gamma}{2} \right) \quad \text{and} \quad \bar{\mathbf{x}}_4^- = \left(\frac{1-\gamma}{2b}, \frac{1+\gamma}{2}, \frac{1-2y_r+\gamma}{2} \right),$$

with $\gamma = \sqrt{1-4bd}$ defined for $0 < d < 1/4b$. Equilibrium $\bar{\mathbf{x}}_4^+$ is real for $y_r > \frac{1-\gamma}{2}$ ($h_1(\bar{\mathbf{x}}_4^+) < 0$) and $y_{th} < \frac{1-\gamma}{2}$ ($h_2(\bar{\mathbf{x}}_4^+) > 0$). Otherwise it is virtual. It becomes a boundary equilibrium at Σ_1 for $y_r = \frac{1-\gamma}{2} > y_{th}$, or at Σ_2 for $y_{th} = \frac{1-\gamma}{2} < y_r$. Likewise, the point $\bar{\mathbf{x}}_4^-$ is real whenever $y_r > \frac{1+\gamma}{2}$ ($h_1(\bar{\mathbf{x}}_4^-) < 0$) and $y_{th} < \frac{1+\gamma}{2}$ ($h_2(\bar{\mathbf{x}}_4^-) > 0$). Otherwise it is virtual. It becomes a boundary equilibrium at Σ_1 for $y_r = \frac{1+\gamma}{2} > y_{th}$, or at Σ_2 for $y_{th} = \frac{1+\gamma}{2} < y_r$. The determinant and trace are given by

$$Det[A(\bar{\mathbf{x}}_4^\pm)] = \frac{4bd-1 \mp \gamma}{2bd} \quad \text{and} \quad Tr[A(\bar{\mathbf{x}}_4^\pm)] = -b + \frac{4d}{(1 \mp \gamma)^2}. \quad (3.2.15)$$

Equilibrium $\bar{\mathbf{x}}_4^+$ is a saddle point because $Det[A(\bar{\mathbf{x}}_4^+)] = \frac{4bd-1-\gamma}{2bd} < 0$ for all $0 < d < \frac{1}{4b}$. On the other hand, the equilibrium $\bar{\mathbf{x}}_4^-$ has $Det[A(\bar{\mathbf{x}}_4^-)] = \frac{4bd-1+\gamma}{2bd} > 0$ for all $0 < d < \frac{1}{4b}$. Moreover, $Tr[A(\bar{\mathbf{x}}_4^-)] = -b + \frac{4d}{(1+\gamma)^2} < 0$ whenever $0 < d < \frac{b}{(1+b^2)^2}$, thus $\bar{\mathbf{x}}_4^-$ is stable. Besides, for $\frac{b}{(1+b^2)^2} < d < \frac{1}{4b}$ we have $Tr[A(\bar{\mathbf{x}}_4^-)] = -b + \frac{4d}{(1+\gamma)^2} > 0$, this mean that $\bar{\mathbf{x}}_4^-$ is unstable.

Interesting phenomena, such as classical and discontinuous bifurcations, appear wrapping the equilibrium points of the vector fields \mathbf{F}_3 and \mathbf{F}_4 . In the following proposition, we can draw some conclusions from the previous stability analysis.

Proposition 3.2.3. *Consider the vector fields \mathbf{F}_3 and \mathbf{F}_4 defined in (3.2.13). The following statements hold.*

- (a) For $d = \frac{b}{(1+b^2)^2}$ a subcritical Hopf bifurcation occurs at $\bar{\mathbf{x}}_4^-$.
- (b) For $d = \frac{1}{4b}$ a saddle-node bifurcation occurs at $\bar{\mathbf{x}}_4^+ = \bar{\mathbf{x}}_4^- = (\frac{1}{2b}, \frac{1}{2}, \frac{1}{2} - y_r)$.
- (c) Assume $y_{th} < 1/2$. For $d = \frac{(1-y_{th})y_{th}}{b}$ a discontinuous saddle-node bifurcation occurs at $\bar{\mathbf{x}}_3 = \bar{\mathbf{x}}_4^+ = (\frac{1-y_{th}}{b}, y_{th}, y_{th} - y_r)$.

Proof. (a) From the second equation in (3.2.15) and using the trace of jacobian matrix (3.2.14) at $\bar{\mathbf{x}}_4^-$, we conclude the following holds for all $0 < b < 1$:

$$\begin{aligned} Det[A(\bar{\mathbf{x}}_4^-)]|_{d=\frac{b}{(1+b^2)^2}} &= (1+b^2)(1-b^2) > 0, \\ Tr[A(\bar{\mathbf{x}}_4^-)]|_{d=\frac{b}{(1+b^2)^2}} &= 0 \\ \frac{d}{dd}Tr[A(\bar{\mathbf{x}}_4^-)]|_{d=\frac{b}{(1+b^2)^2}} &= \frac{2(1+b^2)}{1-b^2} \neq 0. \end{aligned}$$

Thus, we show the necessary condition to obtain the Hopf bifurcation. The x and y components are decoupled from the z component, so consider the planar analytic system

$$\begin{aligned}\dot{x} &= -\frac{1}{1+b^2}(bx+y) + bxy - y^2, \\ \dot{y} &= \frac{1}{1+b^2}(x+by) + xy,\end{aligned}$$

obtained from a translation of (3.2.15) in such a way that $\bar{\mathbf{x}}_4^-$ is translated to the origin. Then, according to [54]-page 243, the *first Lyapunov coefficient* of the vector field \mathbf{F}_4 is given by

$$l_1^- = \frac{\pi b(1+b^2)^2(3-b^3)}{2\sqrt{2}(1-b^2)^{\frac{3}{2}}} > 0, \quad \forall 0 < b < 1.$$

Hence, we have an unstable limit cycle and so, this Hopf bifurcation is subcritical. It is important to note that at the bifurcation point the equilibrium $\bar{\mathbf{x}}_4^-$ is real if $y_r > \frac{1+\gamma}{2}$.

- (b) From stability analysis of \mathbf{F}_4 we obtained that the equilibria $\bar{\mathbf{x}}_4^+$ and $\bar{\mathbf{x}}_4^-$ are well defined for $0 < d < \frac{1}{4b}$ and collide with each other at $d = \frac{1}{4b}$, i.e., $\bar{\mathbf{x}}_4^+ = \bar{\mathbf{x}}_4^- = (\frac{1}{2b}, \frac{1}{2}, \frac{1}{2} - y_r)$, then both disappear for $d > \frac{1}{4b}$, where $\bar{\mathbf{x}}_4^+$ is saddle and $\bar{\mathbf{x}}_4^-$ is node near to the collision point. Therefore at $d = \frac{1}{4b}$ a saddle-node bifurcation occurs. It is worth mentioning that the equilibria involved are real for $y_r > 1/2$.
- (c) From stability analysis of \mathbf{F}_3 and \mathbf{F}_4 we obtained that the equilibria $\bar{\mathbf{x}}_3$ and $\bar{\mathbf{x}}_4^+$ are real for $d > \frac{(1-y_{th})y_{th}}{b}$, they collide for $d = \frac{(1-y_{th})y_{th}}{b}$, if $y_{th} < 1/2$, i.e., $\bar{\mathbf{x}}_3 = \bar{\mathbf{x}}_4^+ = (\frac{1-y_{th}}{b}, y_{th}, y_{th} - y_r)$ and then both equilibria disappear (become virtual) for $d < \frac{(1-y_{th})y_{th}}{b}$, where $\bar{\mathbf{x}}_3$ is a stable node and $\bar{\mathbf{x}}_4^+$ is a saddle near to the collision point. Therefore, for $d = \frac{(1-y_{th})y_{th}}{b}$ a discontinuous saddle-node bifurcation occurs. Notice that the bifurcation point is a nonsmooth-fold boundary equilibrium in Σ_2 , see Figure 3.7(b). □

The bifurcations presented in Proposition 3.2.3, will be observed in the numerical analysis carried out in Section 3.4.

3.2.3 Sliding vector field and pseudo-equilibria

The sliding vector field associated to the dynamical system (3.2.11) is calculated according to (1.2.12), and it is defined as

$$\mathbf{F}_s(x, y, z) = \begin{bmatrix} \frac{\omega(y_r - y) - x + \xi(y)}{k} \\ x - \xi(y) \\ 0 \end{bmatrix}, \quad (3.2.16)$$

where $(x, y, z) \in \Sigma_s \subset \Sigma_1$. Pseudo-equilibrium points of system (3.2.11) are obtained by solving the equation system $\mathbf{F}_s(x, y, 0) = 0$ taking into account $h_1(\mathbf{x}) = 0$ and the

discontinuity of $\xi(y)$ at $y = y_{th}$ ($h_2(\mathbf{x}) = 0$). So, we have a pseudo-equilibrium point that depends on the values of ξ , namely $\tilde{\mathbf{x}} = (\xi(y_r), y_r, 0)$. For $y_r \geq y_{th}$, then the pseudo-equilibrium has coordinates given by $\tilde{\mathbf{x}} = \left(\frac{d}{y_r}, y_r, 0\right)$. The reduced Jacobian matrix is given by

$$A(\tilde{\mathbf{x}}) = \begin{bmatrix} -\frac{1}{k} & -\frac{(\omega y_r^2 + d)}{k y_r^2} \\ 1 & \frac{d}{y_r^2} \end{bmatrix}.$$

Notice that $Det[A(\tilde{\mathbf{x}})] = \frac{\omega}{k} > 0$ and $Tr[A(\tilde{\mathbf{x}})] = \frac{kd - y_r^2}{k y_r^2} < 0$ if $d < \frac{y_r^2}{k}$, then $\tilde{\mathbf{x}}$ is stable, otherwise is unstable. Moreover, the pseudo-equilibrium is real (located in the sliding region) whenever $d < \frac{(1-y_r)y_r}{b}$.

Proposition 3.2.4. *Consider the vector field \mathbf{F}_s defined in (3.2.16). For $d = \frac{y_r^2}{k}$ a subcritical Hopf bifurcation occurs at $\tilde{\mathbf{x}}$.*

Proof. The proof is similar to Proposition 3.2.3(a) with the *first Lyapunov coefficient* of the vector field \mathbf{F}_s , which can be calculated, and it is given by

$$l_1^s = \frac{3\pi k^2}{4\sqrt{k\omega}(1+k\omega)y_r^2} > 0.$$

□

This phenomenon will be observed in the numerical analysis carried out in section 3.4.

3.2.4 Two local DIBs of equilibrium collision with borders

In the system (3.2.11), two types of equilibrium collision with the boundaries Σ_1 and Σ_2 can occur. The boundary equilibrium bifurcations (BEBs) (see [19]) are typical of PWS discontinuous systems, occurring by varying the parameter bifurcation d (chosen as the parameter bifurcation BEB) involving the equilibria of the vector fields \mathbf{F}_4 and \mathbf{F}_s , occurring in Σ_1 , studied in the next section. Another bifurcation is called discontinuous saddle-node (DSN) involving the equilibria of the vector fields \mathbf{F}_3 and \mathbf{F}_4 , occurring in Σ_2 (see Proposition 3.2.3), defined as a non-smooth analogue of the saddle-node bifurcation (see [22]).

Figure 3.7 shows the rise and disappearance of equilibria of the system (3.2.11) when varying the value of bifurcation parameter d for fixed $\omega = 1$, $b = 0.2$, $k = 2$, $y_{th} = 0.1$ and $y_r = 0.5$. In Figure 3.7(a) with $d = 0.3$, we illustrate the interaction between nullclines (black lines) given by $n_1 : x = \frac{1-y}{b}$ ($u = 1$) and $n_2 : x = -\frac{y}{b}$ ($u = 0$) and the CPL piecewise function (3.2.8) (red curve); notice that a virtual equilibrium point $\bar{\mathbf{x}}_2$ and $\bar{\mathbf{x}}_4^-$ of the vector field \mathbf{F}_2 and \mathbf{F}_4 , respectively; and the pseudo-equilibrium $\tilde{\mathbf{x}}$, appears.

In Figure 3.7(b) with $d = 0.45$ it can be seen that the nullcline n_1 touches the discontinuity point of the CPL piecewise function and a DSN occurs. As d increases until it reaches 1, in Figure 3.7(c), we can note the rise of the equilibria $\bar{\mathbf{x}}_3$ and $\bar{\mathbf{x}}_4^+$.

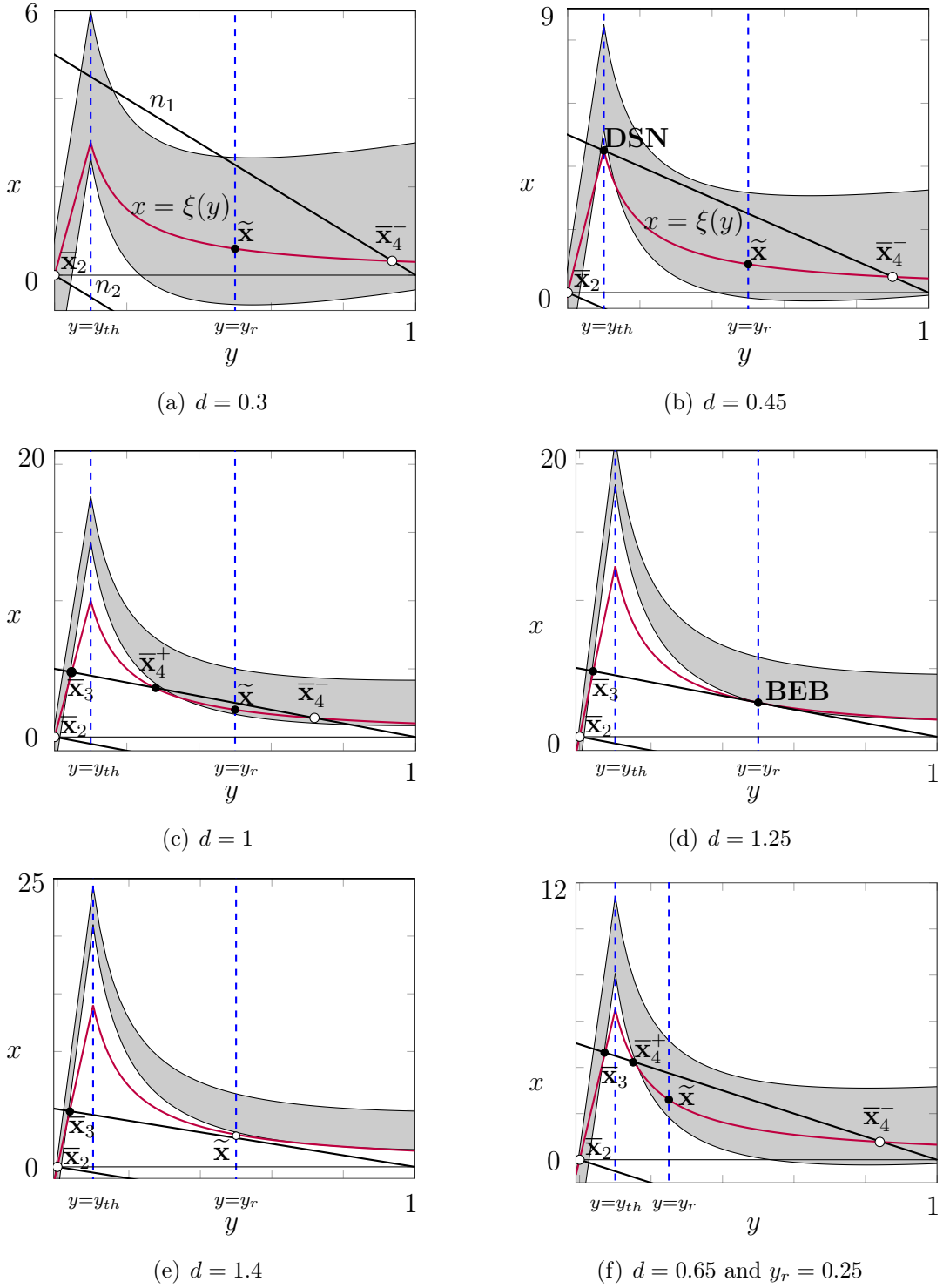


Figure 3.7: Equilibria of system (3.2.11) when varying the value of bifurcation parameter d for $w = 1$, $b = 0.2$, $k = 2$, $y_{th} = 0.1$, showing the collision between regular and pseudo-equilibrium points on the (y, x) -plane. Figures (a) to (e) $y_r = 0.5$ and figure (f) $y_r = 0.25$

Figure 3.7(d) shows the simultaneous collision of both equilibria \bar{x}_4^+ and \bar{x}_4^- with the pseudo-equilibrium \tilde{x} , which occurs for $d = 1.25$ (Here, a SN and a *degenerate* BEB)

occur simultaneously). In other words, at this point, it happens a typical two-parameter bifurcation of a Filippov system on a codimension-two point where a curve of BEB changes from persistence to nonsmooth-fold type, see [59]. The nonsmooth and persistence cases will be studied in detail in Section 3.3. From this point onwards, the pseudo-equilibrium comes out of the sliding region (gray region) and falls into the crossing region (white region) where it becomes virtual as observed in Figure 3.7(e) with $d = 1.4$. Finally, Figure 3.7(f) illustrates the behavior of the equilibrium of the normalized system (3.2.7) for other values in the bifurcation parameters; in this case for $d = 0.65$ and $y_r = 0.25$.

3.3 Boundary equilibrium bifurcations

A boundary equilibrium bifurcation (BEB) occurs when an equilibrium collides with a discontinuity surface in a **DPWS** system of ordinary differential equations due to the variation of one or more parameters. Such type of bifurcations have been identified in mathematical models of a wide variety of physical systems involving abrupt events, such as control systems with switching elements, and ecological systems; see e.g., [20, 58]. Various invariant sets (such as limit cycles) can be created in BEBs. But if we look only at equilibria, then there are two generic scenarios. These are distinguished by the relative coexistence of the regular equilibrium and the pseudo-equilibrium undergoing the BEB. When the regular equilibrium transitions to a pseudo-equilibrium (on the discontinuity surface) occurs the *persistence scenario*. In this case, if the regular equilibrium is real (resp. virtual), then the pseudo-equilibrium is virtual (resp. real). On the other hand, if the regular equilibrium collides and annihilates with a coexisting pseudo-equilibrium the *nonsmooth fold scenario* occurs. In this case, if the regular equilibrium is real (resp. virtual), then so is the pseudo-equilibrium; see [20] and references therein.

Some results on BEBs are presented in [20] for a particular class of **3D-DPWS** systems of the form

$$\dot{\mathbf{x}} = \begin{cases} \mathbf{F}^-(\mathbf{x}) = P\mathbf{x} + \mathbf{n}^-, & \text{if } h(\mathbf{x}) = z < 0 \\ \mathbf{F}^+(\mathbf{x}) = P\mathbf{x} + \mathbf{n}^+, & \text{if } h(\mathbf{x}) = z > 0 \end{cases}, \quad (3.3.1)$$

with $P = (p_{ij})_3$ for $i, j \in \{1, 2, 3\}$, and $\mathbf{n}^\pm = (n_1^\pm, n_2^\pm, n_3^\pm)$. In addition, the following assumptions are made: (i) $p_{31} \neq 0$ and/or $p_{32} \neq 0$, and $n_3^- - n_3^+ > 0$; (ii) there are (generally) two cusp points \mathbf{x}_c^\pm , one for each vector field $\mathbf{F}^\pm(\mathbf{x})$; (iii) $L_{\mathbf{F}^\pm}^3 h(\mathbf{x}_c^\pm)$ is not identically zero. The following result was essentially shown in [20].

Theorem 3.3.1. *Assume $a_{23} \neq 0$ and $\nu \neq \mu$, where*

$$a_{23} = \frac{8\text{Det}[P]}{(n_3^- - n_3^+)^3}, \quad \mu = -\frac{8\text{Det}[R^+]}{(n_3^- - n_3^+)^3}, \quad \nu = -\frac{8\text{Det}[R^-]}{(n_3^- - n_3^+)^3}, \quad R^\pm = \begin{bmatrix} p_{11} & p_{12} & n_1^\pm \\ p_{21} & p_{22} & n_2^\pm \\ p_{31} & p_{32} & n_3^\pm \end{bmatrix}.$$

Then, the system (3.3.1) has two regular equilibria and one pseudo-equilibrium point, given in canonical coordinates by

$$\bar{\mathbf{x}}^- = \left(-1, 0, \frac{\nu}{a_{23}}\right), \quad \bar{\mathbf{x}}^+ = \left(1, 0, \frac{\mu}{a_{23}}\right), \quad \tilde{\mathbf{x}} = \left(\frac{\nu + \mu}{\nu - \mu}, 0, 0\right),$$

and a BEB occurs for $\nu = 0$ if $\mu \neq 0$ or for $\mu = 0$ if $\nu \neq 0$. In addition, the following statements hold.

- (a) The BEB at $\mu = 0$ corresponds to persistence scenario if $a_{23}\nu > 0$, and to nonsmooth fold if $a_{23}\nu < 0$.
- (b) The BEB at $\nu = 0$ corresponds to persistence scenario if $a_{23}\mu < 0$, and to nonsmooth fold if $a_{23}\mu > 0$.

Now we are going to show the occurrence of BEBs in system (3.2.11). We chose the parameter d as the BEB bifurcation parameter. Taking $z = 0$ and solving the equations $\mathbf{F}_i(x, y, 0, d) = \mathbf{0}$, for $i = 1, 2, 3, 4$ respect to (x, y, z, d) , we get

$$(\bar{\mathbf{x}}_{b_1}, d_{B_1}) = \left(-\frac{y_r}{b}, y_r, 0, -\frac{y_r^2}{b} \right), \quad (3.3.2)$$

$$(\bar{\mathbf{x}}_{b_2}, d_{B_2}) = \left(-\frac{y_r}{b}, y_r, 0, -\frac{y_{th}^2}{b} \right), \quad (3.3.3)$$

$$(\bar{\mathbf{x}}_{b_3}, d_{B_3}) = \left(\frac{1-y_r}{b}, y_r, 0, \frac{(1-y_r)y_{th}^2}{by_r} \right), \quad (3.3.4)$$

$$(\bar{\mathbf{x}}_{b_4}, d_{B_4}) = \left(\frac{1-y_r}{b}, y_r, 0, \frac{(1-y_r)y_r}{b} \right), \quad (3.3.5)$$

where $\bar{\mathbf{x}}_{b_i}$ ($i = 1, 2, 3, 4$) denote the boundary equilibrium related to the vector field defined at (3.2.11), and appearing for the critical value $d = d_{B_i}$ ($i=1,2,3,4$) of the load parameter.

Once we assume $y_r > y_{th}$, the boundary equilibria $\bar{\mathbf{x}}_{b_2}$ and $\bar{\mathbf{x}}_{b_3}$ are always virtual, that is, the BEBs at these boundary equilibria are not observed. On the other hand, the boundary equilibria $\bar{\mathbf{x}}_{b_1}$ and $\bar{\mathbf{x}}_{b_4}$ are always real, and the BEBs at these boundaries equilibria are observed. However, as we are assuming that $d > 0$, the boundary equilibrium $\bar{\mathbf{x}}_{b_1}$ is left out of our study. In what follows, we study the BEBs that occur at the point $\bar{\mathbf{x}}_{b_4}$.

Lemma 3.3.2. *System (3.2.11) undergoes a Boundary Equilibrium Bifurcation for $d = \frac{(1-y_r)y_r}{b}$ if $y_r \neq \frac{1}{2}$. In addition, this BEB corresponds to persistence scenario if $y_r > \frac{1}{2}$, and to nonsmooth fold if $y_r < \frac{1}{2}$.*

Proof. A piecewise-linear version of (3.2.11) for $y > y_{th}$, at the boundary equilibrium point $(\bar{\mathbf{x}}_{b_4}, d_{B_4})$, is obtained and represented by

$$\dot{\mathbf{x}} = \begin{cases} P\mathbf{x} + \mathbf{n}^-, & \text{if } z < 0 \\ P\mathbf{x} + \mathbf{n}^+, & \text{if } z > 0 \end{cases}, \quad (3.3.6)$$

with

$$P = \begin{bmatrix} -b & -1 & 0 \\ 1 & d_{B_4}/y_r^2 & 0 \\ 1-bk & d_{B_4}/y_r^2 + \omega - k & -\omega \end{bmatrix} \quad (3.3.7)$$

$$\mathbf{n}^- = \begin{bmatrix} 1 \\ -(d+d_{B_4})/y_r \\ -(d+d_{B_4})/y_r - \omega y_r + k \end{bmatrix}, \quad \mathbf{n}^+ = \begin{bmatrix} 0 \\ -(d+d_{B_4})/y_r \\ -(d+d_{B_4})/y_r - \omega y_r \end{bmatrix}, \quad (3.3.8)$$

where $d_{B_4} = \frac{(1-y_r)y_r}{b}$ is the critical value for the BEB.

Following [20], first we check the hypotheses to obtain a canonical form. So, we assume in system (3.2.11) that $p_{31} = 1 - bk \neq 0$ and $n_3^- - n_3^+ = k > 0$. Moreover the parameters (y_r, k, b, ω) are easily selected so that

$$\begin{aligned} \text{Det}[Q] &= -\left(\frac{d_{B1,4}}{y_r}\right)^4 bk - \left(\frac{d_{B1,4}}{y_r}\right)^2 f(k, b, \omega) - g(k, b, \omega) \neq 0, \\ L_{\mathbf{F}^\pm}^3 h(\mathbf{x}_c^\pm) &= \text{Det}[R^\pm] \quad \text{not identically zero,} \end{aligned}$$

being

$$Q = \begin{bmatrix} \nabla h(\mathbf{x}_c^\pm) \\ \nabla L_{\mathbf{F}^\pm} h(\mathbf{x}_c^\pm) \\ \nabla L_{\mathbf{F}^\pm}^2 h(\mathbf{x}_c^\pm) \end{bmatrix},$$

$f(k, b, \omega) = \omega - k - b(1 - k(b + \omega - k))$ and $g(k, b, \omega) = 1 + (\omega - k)^2 + b^2 k \omega - b(k + \omega)$.

Next, we calculate the critical parameters a_{23} , ν and μ for our system using (3.3.6)-(3.3.8), namely

$$a_{23}(d) = \frac{8\omega b(d + d_{B1})}{k^3 y_r^2}, \quad \nu(d) = \frac{8\omega b(d - d_{B4})}{k^3 y_r}, \quad \mu(d) = \frac{8\omega b(d - d_{B1})}{k^3 y_r}.$$

Note that $\nu = \mu - \frac{8\omega}{k^3} < \mu$.

Regarding the vector field \mathbf{F}_4 , we get

$$\nu(d_{B4}) = 0, \quad a_{23}(d_{B4})\mu(d_{B4}) = \frac{64\omega^2(1 - 2y_r)}{k^6} \neq 0 \quad \text{if } y_r \neq 1/2.$$

If $y_r > 1/2$ then a *persistence* BEB is observed at the boundary equilibrium point $\bar{\mathbf{x}}_{b4}$, but if $y_r < 1/2$ then a *nonsmooth fold* BEB is observed. \square

3.4 Two-parameter bifurcation analysis

In this section, a two-parameter bifurcation study (codimension-two analysis) is presented. The two parameters are the power load (parameter d) and the voltage reference (y_r). They were chosen due to their relevance in the operation of the power distribution system. Bifurcation sets in $(y_r; d)$ -plane with the main local and global bifurcations are shown in Figure 3.8(a)-(d). In this analysis, we only consider the right side of the vertical line $y_r = y_{th}$, because we assumed $y_r > y_{th}$. The black parabolic curve indicates the occurrence of BEBs. In the complete parabolic curve of $d_B = d_{B4} = \frac{(1-y_r)y_r}{b}$, the left branch refers to the *nonsmooth fold* BEB_{NF} involving the equilibria $\bar{\mathbf{x}}_{4,+}$ and $\tilde{\mathbf{x}}$, of the vector fields \mathbf{F}_4 and \mathbf{F}_s , respectively. On the same curve, the right branch refers to the *persistence* BEB_P involving the equilibria $\bar{\mathbf{x}}_4^-$ and $\tilde{\mathbf{x}}$, of the vector fields \mathbf{F}_4 and \mathbf{F}_s , respectively.

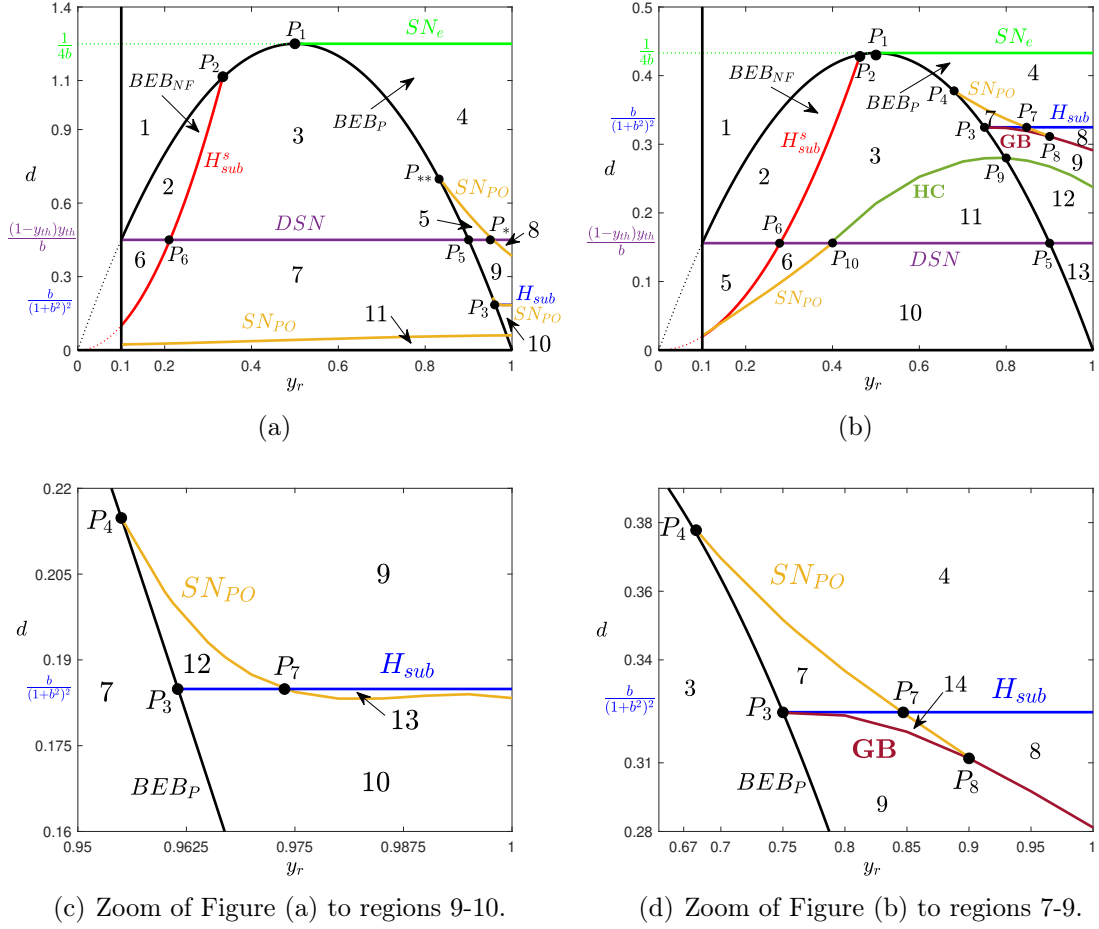


Figure 3.8: Bifurcation set in (y_r, d) -plane showing the main local and global bifurcation curves. a) (y_r, d) -plane assuming $b = 0.2$, $k = 0.1$ and $\omega = 1$. b) (y_r, d) -plane assuming $b = \sqrt{1/3}$, $k = 0.5$, $\omega = 1$.

The vector fields \mathbf{F}_4 and \mathbf{F}_s exhibit some classical bifurcations. The green line in Figure 3.8(a)-(b) refers to a *saddle-node bifurcation* (SN_e) at $d = 1/4b$ (see Proposition 3.2.3) defined for $0.5 < y_r < 1$. The blue straight line segment refers to *subcritical Hopf bifurcation* (H_{sub}) at $d = b/(1+b^2)^2$ (see a Proposition 3.2.3) of the equilibrium \bar{x}_4 defined for $0.96 < y_r < 1$. The red parabolic curve segment in $0.1 < y_r < 0.334$ indicates a *subcritical Hopf bifurcation* (H^s_{sub}) at $d = y_r^2/k$ of the pseudo-equilibrium \tilde{x} (see a Proposition 3.2.4); and the violet line refers to a *discontinuous saddle-node* (DSN) at $d = \frac{(1-y_{th})y_{th}}{b}$ (see Proposition 3.2.3). Table 3.2 shows the characteristics of the equilibria of system (3.2.11) for each region enumerated in Figure 3.8(a), and studied in the previous sections.

Regions	\bar{x}_3	\bar{x}_4^+	\bar{x}_4^-	\tilde{x}
1	real stable	virtual	virtual	virtual
2	real stable	real saddle	virtual	real unstable
3	real stable	real saddle	virtual	real stable
4	real stable	real saddle	real stable	virtual
5	real stable	real saddle	real unstable	virtual
6	virtual	virtual	virtual	real stable
7	virtual	virtual	virtual	real stable
8	virtual	virtual	real unstable	virtual
9	virtual	virtual	real unstable	virtual
10	virtual	virtual	real stable	virtual
11	virtual	virtual	virtual	real stable
12	virtual	virtual	real unstable	virtual
13	virtual	virtual	real stable	virtual

Table 3.2: Classification of Equilibria and Pseudo-equilibria according to figure 3.8(a).

Figure 3.8(b) shows two important *global bifurcations*: a *Homoclinic bifurcation* (HC) and a *Grazing-sliding bifurcation* (GS) represented by dark green curve and a maroon curve, respectively. Another important phenomenon occurs when two limit cycles collapse, one stable and the other unstable, which is called a *saddle-node bifurcation of periodic orbits* (SN_{PO}) represented by orange curves. These bifurcations are determined numerically as it will be seen in the next subsection.

The points $\{P_i\}$ in Figure 3.8 indicate the two-codimension bifurcations where two or more bifurcations occur simultaneously, but not necessarily involve the same equilibrium point. Such points in Figures 3.8(a)-(d) are: $P_1(1/2, 1/(4b))$, when the Saddle-node bifurcation (SN_e) occurs simultaneously to BEB_P ; $P_2(k/(b+k), k/(b+k)^2)$, when the subcritical Hopf bifurcation (H_{sub}^s) occurs together to BEB_{NF} ; $P_3(1/(1+b^2), b/(1+b^2)^2)$, when the subcritical Hopf bifurcation (H_{sub}) occurs at the same time to BEB_P ; P_4 , when the BEB_P occurs concomitantly to SN_{PO} ; $P_5((1 + \sqrt{1 - 4(1 - y_{th})y_{th}})/2, (1 - y_{th})y_{th}/b)$, when the DSN occurs together to BEB_P ; $P_6(\frac{(1-y_{th})y_{th}}{b}, \sqrt{\frac{k(1-y_{th})y_{th}}{b}})$, when the DSN occurs concurrently to H_{sub}^s ; and P_7 , when the subcritical Hopf bifurcation H_{sub} occurs at the same time to SN_{PO} . Bifurcation points that occur only for bifurcation set in Figures 3.8(a) are: P_* , when the DSN occurs simultaneously to SN_{PO} ; and at P_{**} a BEB_P occurs together to SN_{PO} . Bifurcation points that occur only for bifurcation set in Figures 3.8(b) are: At P_8 a Grazing sliding bifurcation (GS) occurs concurrently to SN_{PO} ; P_9 , when the homoclinic connection (HC) occurs concomitantly to BEB_P ; and P_{10} when the DSN occurs at the same time to SN_{PO} and an HC.

3.4.1 Limit cycle bifurcations

In this subsection we present some results of the numerical analysis of the existence of limit cycles and bifurcations, considering the bifurcation diagrams shown in Figure 3.9-3.14, which were used to obtain the curves of the bifurcation set diagrams shown in Figure 3.8.

For the sake of brevity we adopt in Figure 3.9-3.14 the following notation: (i) solid line

branches indicate stable invariant sets (equilibria or limit cycle), and dashed line branches indicate unstable ones; (ii) black line branches represent the amplitude of limit cycles; (iii) red line branch represents the coordinates of $\tilde{\mathbf{x}}$; (iv) blue and green line branches represent the coordinates of the equilibria $\bar{\mathbf{x}}_4^+$ and $\bar{\mathbf{x}}_4^-$, respectively; (v) violet line branch stands for the coordinates of the equilibrium $\bar{\mathbf{x}}_3$; (vi) dotted line branches stand for the virtual equilibria, while solid and dashed branches represent the real equilibria.

Figures 3.9(a)-(d) show the bifurcations diagram of system (3.2.11) with respect to variation in the bifurcation parameter d assuming $y_r = 0.25$. A saddle-node bifurcation occurs at $d = 1.25$ (point A) when the equilibria of \mathbf{F}_4 collapses. A saddle-node bifurcation of periodic orbits indicated by C and C' , occurs at $d = 0.029$ when two limit cycles collapse, one stable and one unstable with a smaller amplitude. Note that when increasing a constant power load d , the amplitude of the limit cycle decreases until it disappears in the subcritical Hopf bifurcation at $d = 0.62$ (point H), so the pseudo equilibria become unstable; and soon it collides with equilibrium $\bar{\mathbf{x}}_4^+$ at $d = 0.9375$ (point D) and set off virtual. As the power load increases further, the stable limit cycle disappears (collapses) when a saddle-node discontinuous (DSN) rises for $d = 0.45$ (point B). At this same point a collision between $\bar{\mathbf{x}}_3$ and $\bar{\mathbf{x}}_4^+$ occurs and becomes real from a DSN bifurcation. Note that between D and B the equilibrium $\bar{\mathbf{x}}_4^+$ is real unstable; outside this interval it is virtual and $\bar{\mathbf{x}}_4^-$ is also virtual.

Figure 3.10(a)-(d) show the bifurcations diagram with $y_r = 0.5$. In this case, a pseudo-equilibrium point collapsed with the saddle-node bifurcation in the degenerate boundary equilibrium point (A) at $d = 1.25$, thereafter it becomes virtual. Other bifurcations happen when the amplitude of the limit cycle increases as it varies, starting in the subcritical Hopf bifurcation at point A and disappearing (with maximum amplitude) on a saddle-node discontinuous at $d = 0.44995$ (point B). Notice that the change from the unstable to stable limit cycle occurs at $d = 0.04270$ (points C and C'). Between A and B the equilibrium $\bar{\mathbf{x}}_4^+$ is real; outside this interval it is virtual and $\bar{\mathbf{x}}_4^-$ is also virtual.

Figure 3.11 (a)-(d) show the bifurcations diagram with $y_r = 0.75$. A saddle-node bifurcation occurs at $d = 1.25$ (point A) when the equilibria of \mathbf{F}_4 collapses. In this case, a pseudo-equilibrium point collides with an equilibrium $\bar{\mathbf{x}}_4^-$ at a boundary equilibrium point in (D) at $d = 0.93$, after this, a pseudo-equilibrium becomes virtual. A discontinuous saddle-node bifurcation happens at $d = 0.449$ (point B); the change from the unstable to stable limit cycle occurs at $d = 0.051$ (points C and C'). Notice that between A and B , the equilibrium $\bar{\mathbf{x}}_4^+$ is real; outside this it is virtual; and between A and D the $\bar{\mathbf{x}}_4^-$ is real, outside this is virtual.

Figure 3.12(a)-(d) shows the bifurcations diagram with $y_r = 0.93$. Discontinuous saddle-node bifurcation occurs at $d = 1.25$ (point A) when the equilibria of \mathbf{F}_4 collapses. In this case, a pseudo-equilibrium point collapses with the equilibrium $\bar{\mathbf{x}}_4^-$ at a boundary equilibrium point in D at $d = 0.93$ after this becomes virtual. A saddle-node bifurcation of periodic orbits indicated by C and C' , occurs at $d = 0.4901$ when two limit cycles collapse, one stable and one unstable. The stable limit cycle disappears (collapses) when a discontinuous saddle-node bifurcation (DSN) arises for $d = 0.449$ at point B . The unstable limit cycle disappears when it collides with another stable limit cycle having a sliding segment in another SN_{PO} bifurcation in E and E' at $d = 0.0645$. Note that between A and B the equilibrium $\bar{\mathbf{x}}_4^+$ is real; outside this interval it is virtual; and between A and D the equilibrium $\bar{\mathbf{x}}_4^-$ is real, outside this interval is virtual.

Figure 3.13(a)-(d) shows the bifurcations diagram with $y_r = 0.99$. A saddle-node bifurcation occurs at $d = 1.25$ (point A) when the equilibria of \mathbf{F}_4 collapses. In this case, a pseudo-equilibrium point collapses with the equilibrium \bar{x}_4^- at a boundary equilibrium point in D at ($d=0.0495$) after this becomes virtual. A saddle-node bifurcation of periodic orbits indicated by C and C' , occurs at $d = 0.05889$ when two limit cycles collapse, one stable and one unstable. The stable limit cycle disappears (collapses) when a discontinuous saddle-node bifurcation (DSN) arises for $d = 0.449$ at point B . The unstable limit cycle disappears when it collides with another stable limit cycle having a sliding segment in another SN_{PO} bifurcation in E and E' at $d = 0.3928$. Another SN_{PO} occurs at point F (point $d = 0.18479$), from which bifurcates an unstable (smooth) limit cycle and a stable (non-smooth) limit cycle with a sliding segment. The unstable (smooth) limit cycle disappears in subcritical Hopf bifurcations at G ($d = 0.1849$). In this last situation, the coexistence of 4 limit cycles is observed, which is the maximum number of limit cycles found for system (3.2.11). Note that between A and B the equilibrium \bar{x}_4^+ is real unstable; outside this interval it is virtual; between A and G the equilibrium \bar{x}_4^- is unstable real and between G and D is real stable, outside this interval is virtual. Figure 3.15 shows a case with 3 limit cycles, from the simulation of the system in state space. Table 3.3 shows the maximum number of limit cycles in each region of Figure 3.8(a), and in Table 3.4 for the Figure 3.8(b).

Figure 3.14(a)-(d) shows the bifurcations diagram considering d as the bifurcation parameter for $b = \sqrt{\frac{1}{3}}$, $k = 0.5$, $\omega = 1$, $y_{th} = 0.1$ and $y_r = 0.937$, in this case a pseudo-equilibrium point collapses with the equilibrium \bar{x}_4^+ at a boundary equilibrium point in D at $d = 0.10224$, thereafter it becomes virtual. A saddle-node bifurcation occurs at $d = 1.25$ (point A) and a discontinuous saddle-node bifurcation happens at $d = 0.15588$ (point B). We observe the occurrence of a subcritical Hopf bifurcation in G at $d = 0.3247$ and the emergence of an unstable limit cycle (saddle) when decreasing the parameter d . This cycle is entirely contained in the region D_4 of the system state space, defined in (3.2.10) until it touches the switching boundary Σ_1 , and so a Grazing-sliding bifurcation occurs (P) at $d = 0.3047$. Then it becomes a cycle with a sliding part and persists until it disappears after the homoclinic connection in O at $d = 0.2558$.

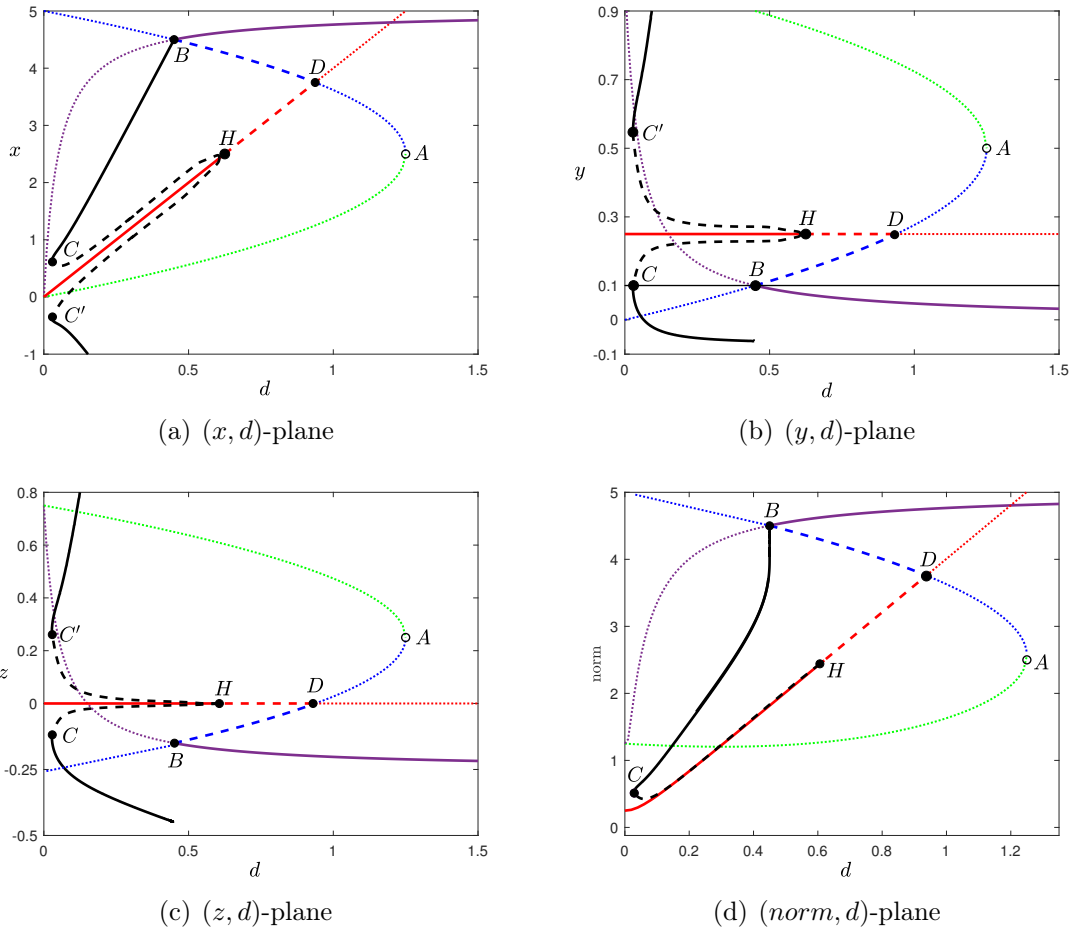


Figure 3.9: Bifurcation diagrams of system (3.2.11) considering d as the bifurcation parameter for $b = 0.2$, $k = 0.1$, $\omega = 1$, $y_{th} = 0.1$ and $y_r = 0.25$. Black curves stand for the limit cycle, red line denotes the pseudo-equilibria, blue and green line represent the equilibrium \bar{x}_4^+ and the equilibrium \bar{x}_4^- , respectively; the violet line stands for the equilibrium \bar{x}_3 . Dashed curve indicates the unstable equilibrium/limit cycle and the solid line indicates the stable equilibrium/limit cycle, and dotted curves mean the virtual equilibrium.

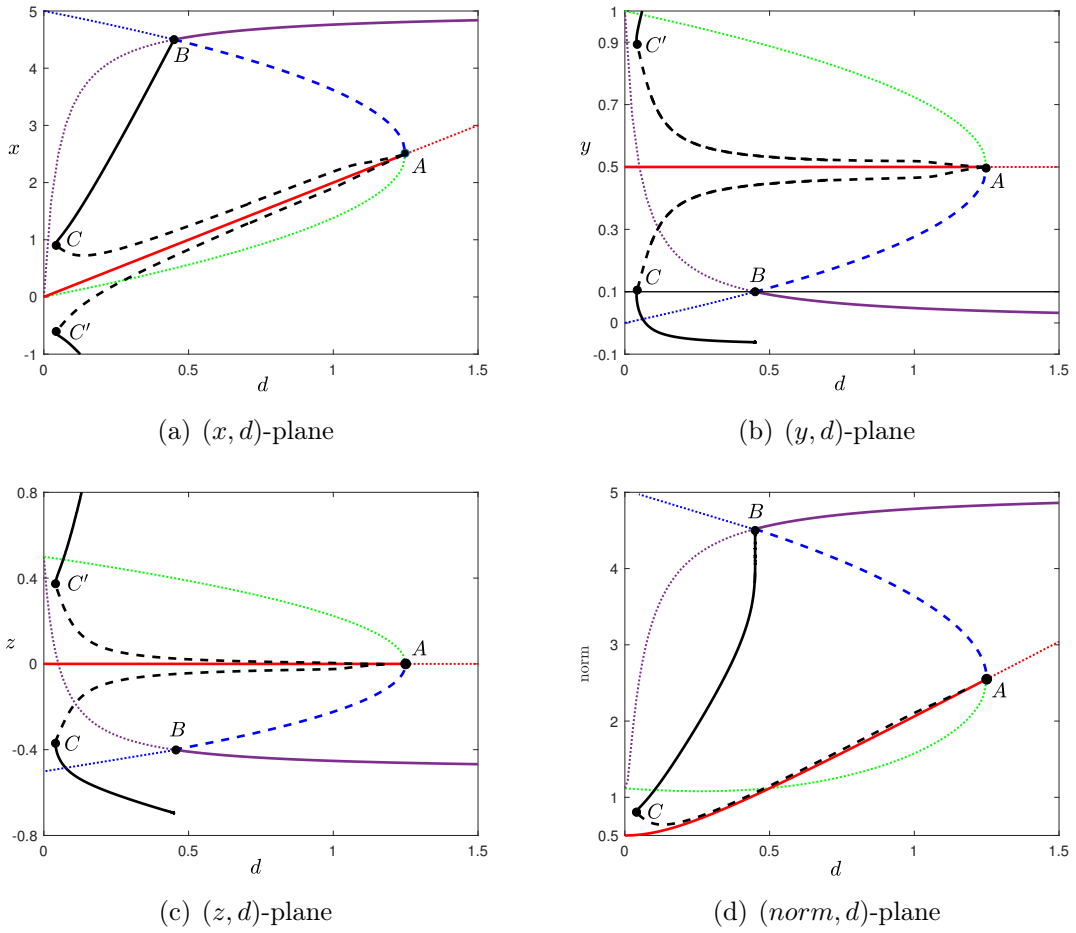


Figure 3.10: Bifurcation diagrams of system (3.2.11) considering d as the bifurcation parameter for $b = 0.2$, $k = 0.1$, $\omega = 1$, $y_{th} = 0.1$ and $y_r = 0.5$. Black curves stand for the limit cycle, red line denotes the pseudo-equilibria, blue and green line represent the equilibrium \bar{x}_4^+ and the equilibrium \bar{x}_4^- , respectively; the violet line stands for the equilibrium \bar{x}_3 . Dashed curve indicates the unstable equilibrium/limit cycle and the solid line indicates the stable equilibrium/limit cycle; and dotted curves mean the virtual equilibrium.

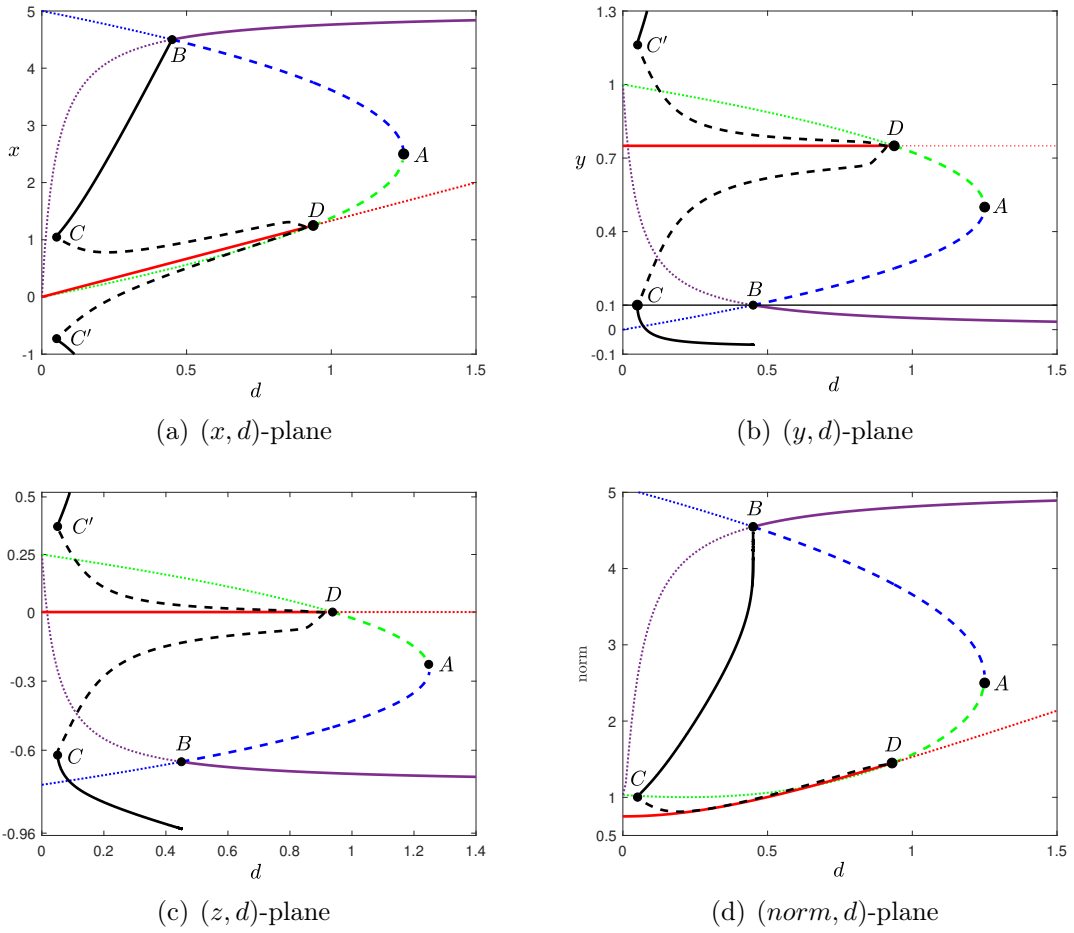


Figure 3.11: Bifurcation diagrams of system (3.2.11) considering d as the bifurcation parameter for $b = 0.2$, $k = 0.1$, $\omega = 1$, $y_{th} = 0.1$ and $y_r = 0.75$. Black curves stand for the limit cycle, red line denotes the pseudo-equilibria, blue and green line represent the equilibrium \bar{x}_4^+ and the equilibrium \bar{x}_4^- , respectively; the violet line stands for the equilibrium \bar{x}_3 . Dashed curve indicates the unstable equilibrium/limit cycle and the solid line indicates the stable equilibrium/limit cycle; and dotted curves mean the virtual equilibrium.

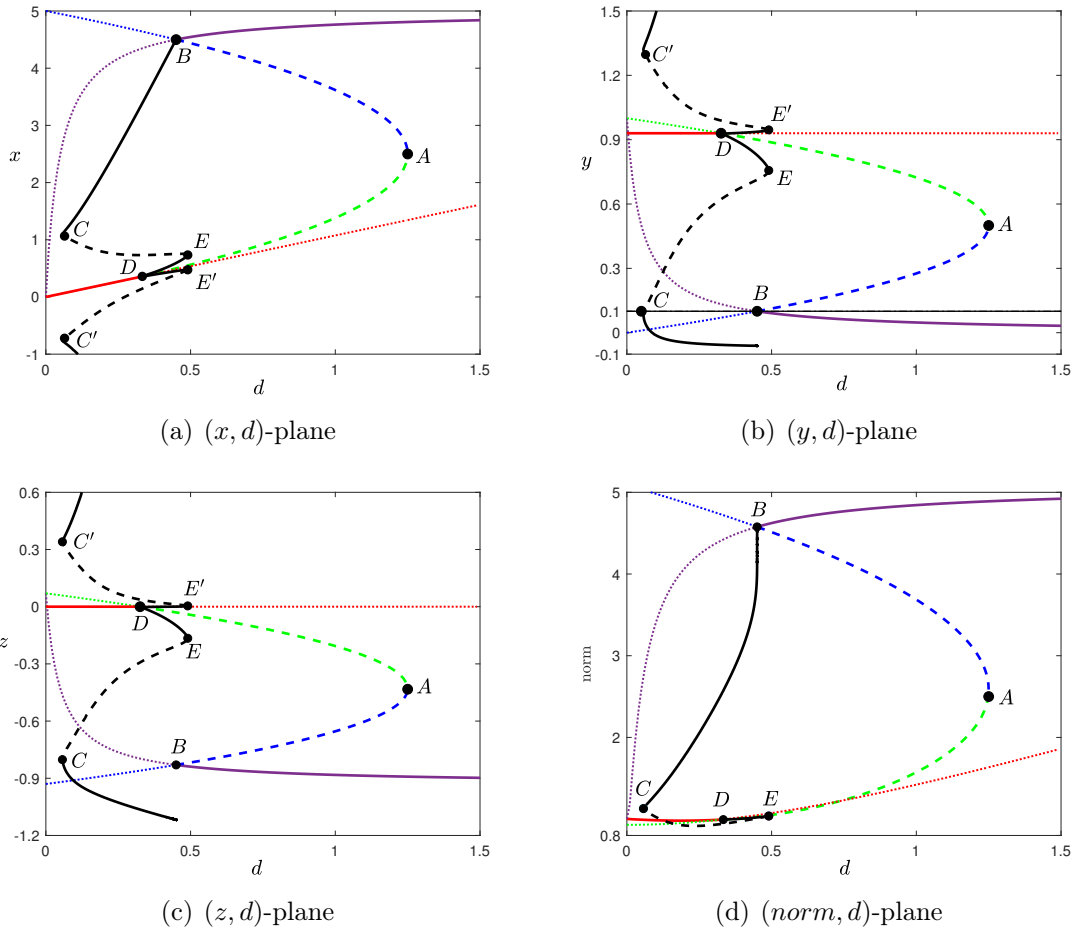


Figure 3.12: Bifurcation diagrams of system (3.2.11) considering d as the bifurcation parameter for $b = 0.2$, $k = 0.1$, $\omega = 1$, $y_{th} = 0.1$ and $y_r = 0.93$. Black curves stand for the limit cycle, red line denotes the pseudo-equilibria, blue and green line represent the equilibrium \bar{x}_4^+ and the equilibrium \bar{x}_4^- , respectively; the violet line stands for the equilibrium \bar{x}_3 . Dashed curve indicates the unstable equilibrium/limit cycle and the solid line indicates the stable equilibrium/limit cycle; and dotted curves mean the virtual equilibrium.

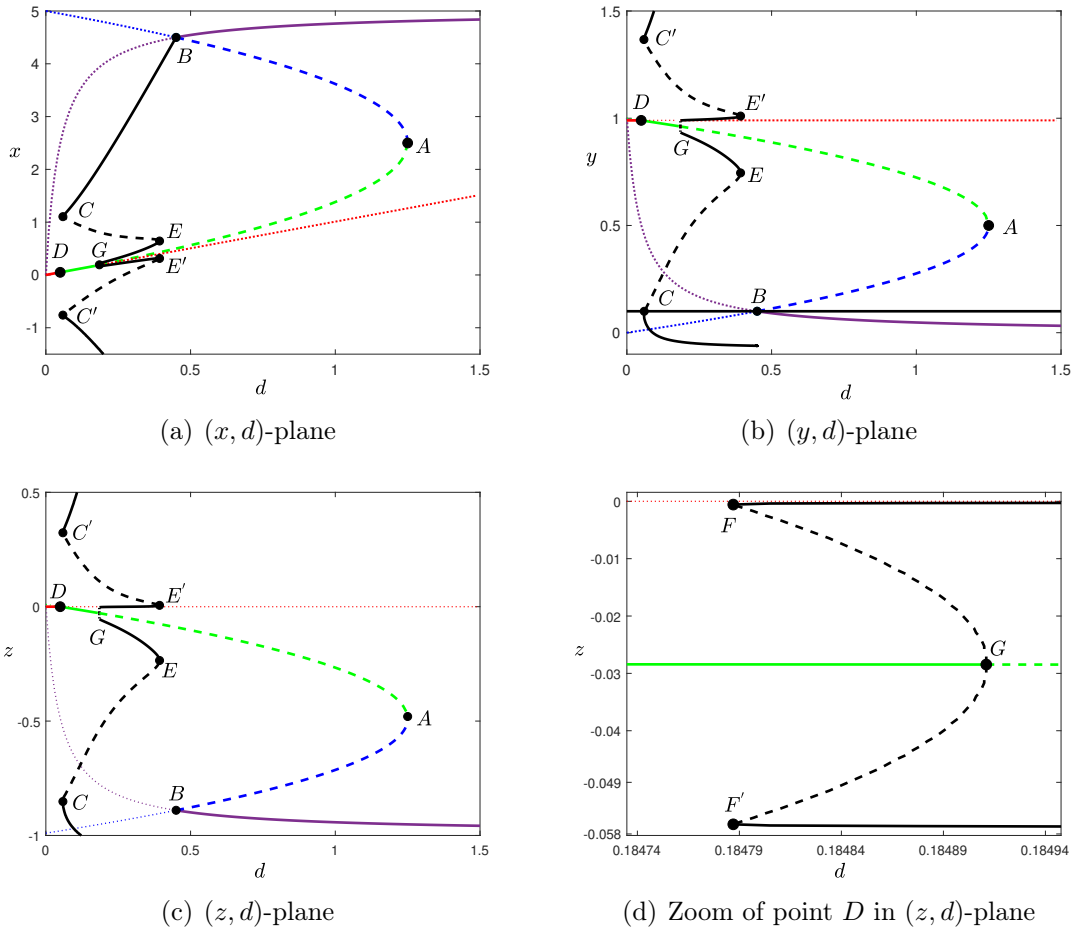


Figure 3.13: Bifurcation diagrams of system (3.2.11) considering d as the bifurcation parameter for $b = 0.2$, $k = 0.1$, $\omega = 1$, $y_{th} = 0.1$ and $y_r = 0.99$. Black curves stand for the limit cycle, red line denotes the pseudo-equilibria, blue and green line represent the equilibrium \bar{x}_4^+ and the equilibrium \bar{x}_4^- , respectively; the violet line stands for the equilibrium \bar{x}_3 . Dashed curve indicates the unstable equilibrium/limit cycle and the solid line indicates the stable equilibrium/limit cycle; and dotted curves mean the virtual equilibrium.

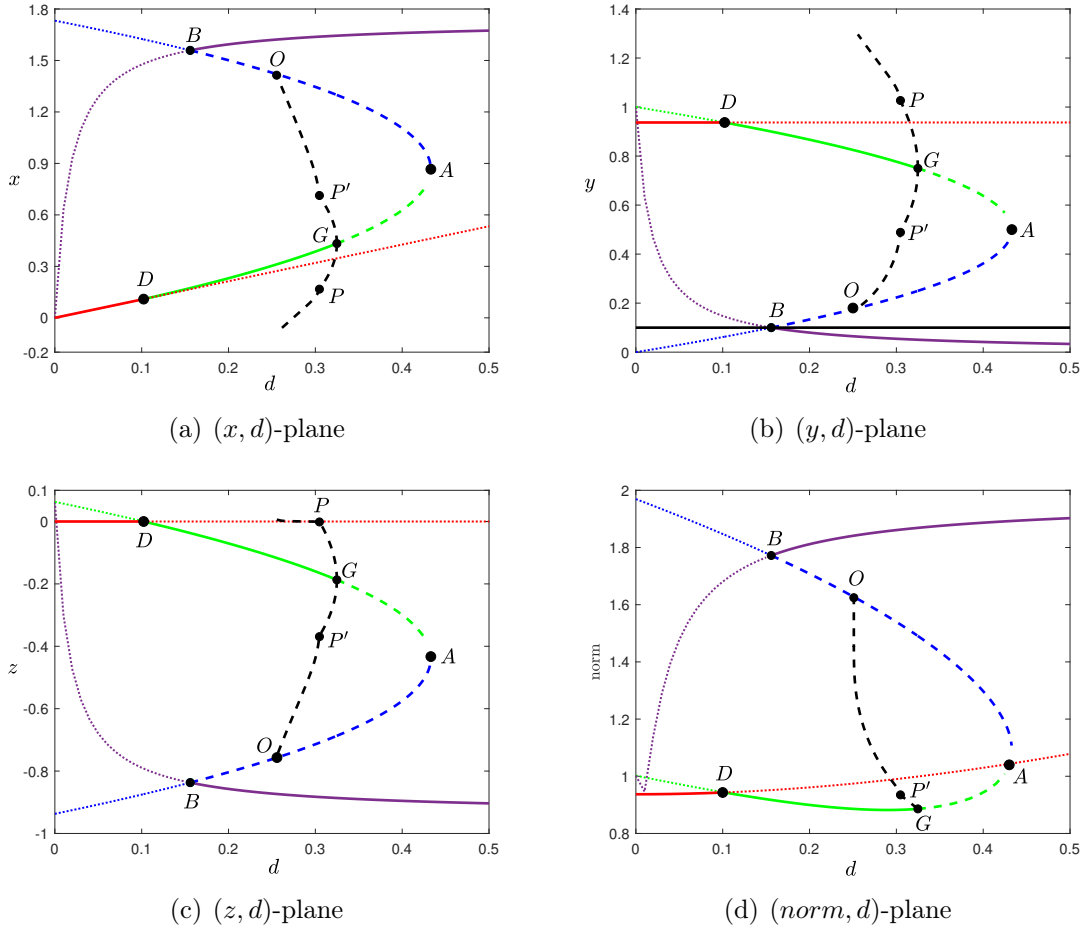


Figure 3.14: Bifurcation diagrams of system (3.2.11) considering d as the bifurcation parameter for $b = \sqrt{\frac{1}{3}}$, $k = 0.5$, $\omega = 1$, $y_{th} = 0.1$ and $y_r = 0.937$. Black curves stand for the limit cycle, red line denotes the pseudo-equilibria, blue and green line represent the equilibrium \bar{x}_4^+ and the equilibrium \bar{x}_4^- , respectively; the violet line stands for the equilibrium \bar{x}_3 . Dashed curve indicates the unstable equilibrium/limit cycle and the solid line indicates the stable equilibrium/limit cycle; and dotted curves mean the virtual equilibrium.

Regions	1	2	3	4	5	6	7	8	9	10	11	12	13
Stable limit cycle	0	0	0	0	1	1	1	1	2	1	0	0	2
Unstable limit cycle	0	0	1	0	1	0	1	0	1	0	0	1	2

Table 3.3: Number and stability of coexisting limit cycles from the bifurcation set of Figure 3.8(a).

Regions	1	2	3	4	5	6	7	8	9	10	11	12	13	14
Stable limit cycle	0	0	0	0	1	1	1	0	0	0	0	0	0	1
Unstable limit cycle	0	0	1	0	0	1	1	1	1	0	0	0	0	2

Table 3.4: Number and stability of coexisting limit cycles from the bifurcation set of Figure 3.8(b).

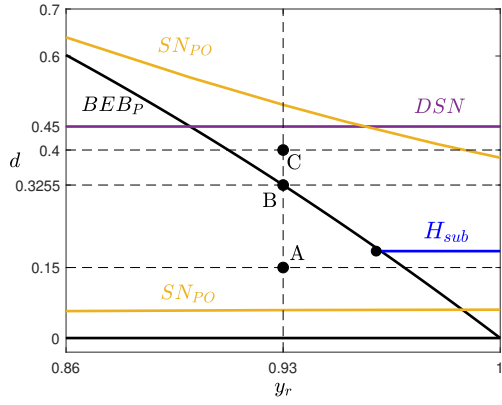
Boundary focus collision

If we take (y_r, d) in the parabola segment with extremes at P_{**} (resp. P_4) and P_3 , shown in Figure 3.8(a) (resp. 3.8(b)), then a persistence BEB involving the unstable focus equilibrium $\bar{\mathbf{x}}_4^-$ and the stable pseudo-node \tilde{x} , is observed in system (3.2.11). This dynamic scenario is simulated and shown in Figure 3.15(b)-(d), where the points of focus equilibrium, pseudo-node and boundary equilibrium are represented by green, red and black dots, respectively. A stable limit cycle with a sliding part rises in the state space for $d > d_{B_4} = 0.4$.

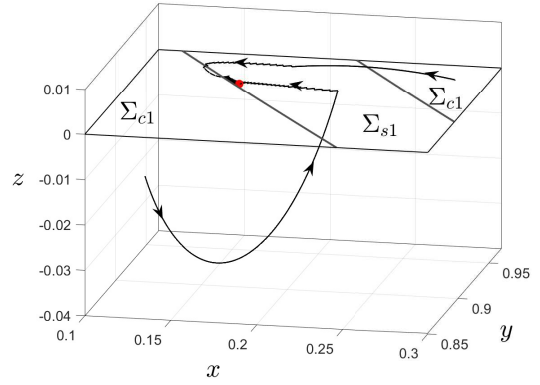
This kind of BEB is known as Boundary Focus Bifurcation (BFB), from which it was proved the existence of five generic critical cases; see [19]. In planar Filippov systems, such a BEB involves a regular focus equilibrium, a pseudo-equilibrium, and a fold singularity. In the case where the regular equilibrium is an unstable focus, the pseudo-equilibrium is stable and we have a persistence BEB, such a bifurcation produces a stable limit cycle that is composed of two orbit segments, one defined by the sliding vector field and the other by vector field below (or above) the switching boundary. In addition, this limit cycle is present in the state space when the focus is a real equilibrium close to the switching boundary and the pseudo-equilibrium is virtual and the fold singularity is visible.

Naturally, the scenario described in the previous paragraph also occurs in 3D systems, as we have observed from system (3.2.11). As in the two-dimensional case, a stable limit cycle with sliding segment arises from a boundary equilibrium of dynamic unstable focus for \mathbf{F}_4 and stable node for \mathbf{F}_s . But, unlike the planar case, here the tangential singularity involved is of the cusp type and divided the tangency line into visible and invisible folds. In addition, this limit cycle is present in the state space when the focus is a real equilibrium close to the Σ_1 , the pseudo-equilibrium is virtual and the cusp singularity is "visible" (that is, $L_{\mathbf{F}_4}^3 h(\mathbf{x}_c^-) < 0$ at the cusp point; see [20]).

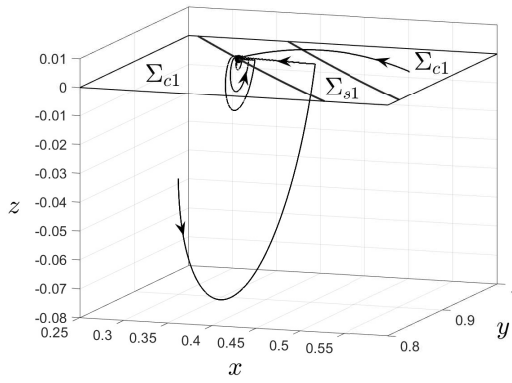
Beside the stable limit cycle with the sliding part mentioned above, there are also two more crossing limit cycles, one stable (blue cycle) and the other unstable (black cycle) as shown in Figure 3.15(e)-(f).



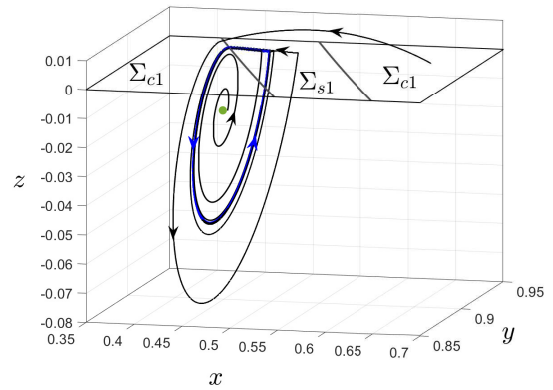
(a)



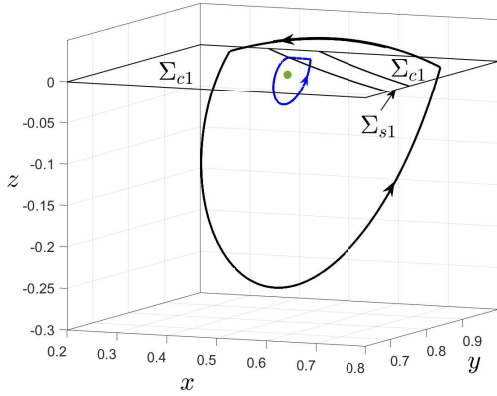
(b) $d = 0.15 < d_{B_4}$



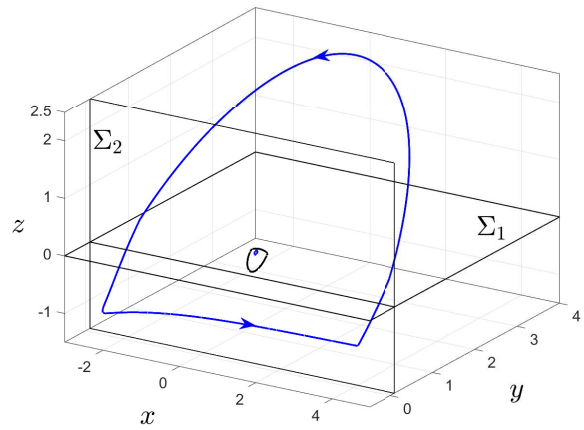
(c) $d = 0.3255 = d_{B_4}$



(d) $d = 0.4 > d_{B_4}$



(e) $d = 0.4$



(f) $d = 0.4$

Figure 3.15: Simulation results of system (3.2.11) with parameters $b = 0.2$, $\omega = 1$, $k = 0.1$ and $y_r = 0.93$ showing the stable limit cycle in blue color and the unstable limit cycle in black color; the points of focus equilibrium, pseudo-node and boundary equilibrium are represent by green, red and black dots, respectively.

Grazing-sliding Bifurcation

Consider in system (3.2.11) that $b = \sqrt{1/3}$, $\omega = 1$, $k = 0.5$, $y_r = 0.937$ and $d = 0.305$. In this case, there is an unstable limit cycle around the real focus equilibrium of the vector field \mathbf{F}_4 , which is tangent to the switching boundary Σ_1 , see Figure 3.16(a) (violet cycle). For a small perturbation in the parameter d (for $d < 0.305$) this limit cycle persists, but has a sliding segment thereafter, as shown in Figure 3.16(b) (maroon cycle). Then we have a *Grazing-sliding* bifurcation occurring in system (3.2.11) (see Figure 3.16(a)). More specifically, this type of bifurcation appears when a periodic orbit touches the surface where the system is discontinuous (switching boundary) (see [37, 60]). This result is expected according to the bifurcation diagrams in Figure 3.14.

A Homoclinic connection bifurcation occurs when the unstable limit cycle with sliding segment collides with the saddle equilibrium of the vector field \mathbf{F}_4 ; see Figure 3.16(b) (maroon cycle). This phenomenon is expected according to the bifurcation diagram shown in Figure 3.14(c). Notice that near the homoclinic connection is the stable node equilibrium of the vector field \mathbf{F}_3 . There is a combination of system parameters (point P_{10} in Figure 3.8(b)) such that the homoclinic connection is formed in a (nonsmooth) saddle-node equilibrium, which appears at the switching boundary Σ_2 when the regular equilibria node and saddle, of the vector fields \mathbf{F}_3 and \mathbf{F}_4 respectively, collide.

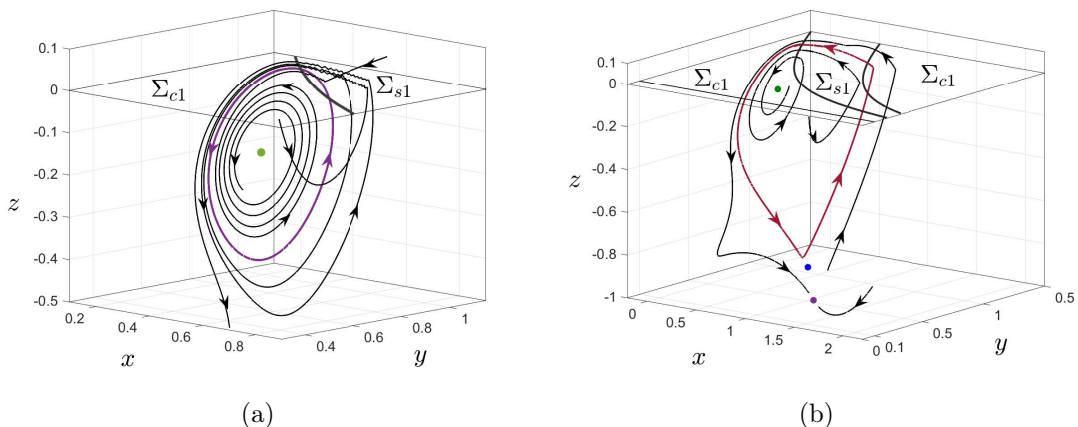


Figure 3.16: Simulation results of system (3.2.11) with parameters $b = \sqrt{1/3}$, $\omega = 1$, $k = 0.5$, $y_r = 0.937$ and $d = 0.305$ showing the Grazing-sliding bifurcation (see violet cycle) and the Homoclinic connection bifurcation (see maroon cycle).

3.5 Conclusion

This chapter addressed the nonlinear analysis of **DPWS** dynamical systems with two transverse switching boundaries through a real case study: a cascade of two buck converters connected to a common bus in a DC microgrid. A bifurcation approach is proposed in order to study local and global phenomena of a power electronic circuit feeding a piecewise constant power load and controlled by means of a sliding mode control law. In the interconnected power converters structure, the two boundaries were defined by (i) the SMC law of the first buck converter and (ii) a piecewise constant

power load modelling the second buck converter. The nonlinear behavior of this system was analyzed and some results on bifurcations induced by two transversal switching boundaries, obtained from a two-parameter analysis, were presented. Typical bifurcations of **DPWS** systems were detected in the system under study, such as the BEB, BFB, DSN and GS bifurcations. In addition, from the study carried out, we have predicted the coexistence of at least 4 limit cycles. Other bifurcations of equilibrium and limit cycles (Hopf, SN_e , SN_{PO} , HC) were also found in this case study.

The nonlinear analysis performed is very useful to determine the safe parameter region which guarantees robust stability at the desired operating point for the system, under changes considered in the parameters of load power and control reference voltage. This information can be summarized in bifurcation diagrams and bifurcation sets leading to practical rules for choosing the control parameters in order to achieve a suitable SMC design.

Chapter 4

Global stability of a Lotka-Volterra piecewise-smooth system with harvesting actions and two predators competing for one prey

In this chapter, we will study the global dynamics of a three-dimensional Lotka-Volterra system described by two predator species competing for one prey and with human harvesting action on the predator species. The harvesting action is introduced by means of two switching control actions defined on the predator species. A well-known result in the study of ecosystem modeling is that there are two states of coexistence of one of the predatory species with the prey species assuming that the principle of competitive exclusion or coexistence of competing species is fulfilled. In this sense, the three species cannot coexist in this class of system. In this chapter, it is proved that there is a global stable equilibrium point where the three species can coexist due to the proposed harvesting action.

4.1 Introduction

According to the theory of evolution, competition within a species and between species plays a fundamental role in natural selection. However, it is not always a simple phenomenon and can occur indirectly, affecting the structure of the ecosystems. In general, it is an important issue in nature and society since competition is related to the concept of selection that is required to obtain or facilitate success in certain environments. Therefore, the study of global dynamics on the competitive resource model is important to understand the behavior and survival mechanism of the fittest (natural selection). In addition, the analytical and numerical study of these models becomes very important in different lines of research, see [66, 69, 70, 71, 85].

The study of the dynamics of predator-prey systems was originated in the works of Lotka [68] and Volterra [67] who considered a model for one predator and one single prey in an uniform environment. They also argued that the coexistence of two or more predators competing for fewer prey resources is unfeasible, which is called *the principle of competitive exclusion*. Recently, the control strategy for predator-prey models has

generated much interest in the mathematical society [86], since to understand its dynamics it is important to use the qualitative analysis techniques related to Filippov non-smooth systems, which are part of **DPWS** systems. The stability of equilibria of the system, the existence of pseudo-equilibria of the sliding mode dynamics, different kinds of bifurcations, global stability, etc, are in constant study and some of them are also investigated using numerical analysis; see [87, 91, 90, 89, 88, 92].

We will study the dynamics of a 3-dimensional predator prey Lotka-Volterra system, which describes two predators competing for food or sharing one resource. The two predatory species are supposed to compete in a purely exploitative way without interference between rivals, the growth rate of the prey species is logistic or linear in the absence of predation, and the functional response of the predator is linear. Thus, the model given by a system of ordinary differential equations of the form

$$\begin{aligned}\frac{dS(t)}{dt} &= \left(r_3 - \frac{1}{K}S(t) - b_1x_1(t) - b_2x_2(t) \right) S(t), \\ \frac{dx_1(t)}{dt} &= (a_1S(t) - r_1)x_1(t) - u_1x_1(t), \\ \frac{dx_2(t)}{dt} &= (a_2S(t) - r_2)x_2(t) - u_2x_2(t),\end{aligned}\tag{4.1.1}$$

where $x_i(t)$ for $i = 1, 2$ stand for the population density of the i -th predator at time t , $S(t)$ represents the population density of the prey at time t , $r_3 > 0$ is the intrinsic rate of growth of the prey, $K > 0$ is the carrying capacity of the prey, which describes the richness of resources for prey.

Notice that, if $K = \infty$, then the prey can increase unlimited, which implies that the growth rate of the prey species is linear in the absence of predation; $b_i > 0$ is the effect of the i -th predation on the prey, $r_i > 0$ is the natural death rate of the i -th predator in the absence of prey, a_i is the efficiency and propagation rate of the i -th predator in the presence of prey. Notice that $x_i(t) \geq 0$ and $S(t) \geq 0$. Thus, system (4.1.1) is considered only in the non-negative octant \mathbb{R}_+^3 . The control variables $u_{1,2}$ stand for a proportional removal of the predator population given by

$$u_1 = k_1\phi_1(\rho_1) \quad \text{and} \quad u_2 = k_2\phi_2(\rho_2),$$

where $k_{1,2}$ are the control effort parameters to be designed and $\phi_{1,2}(\rho_{1,2})$ are defined as,

$$\phi_1(\rho_1) = \begin{cases} 1, & \text{if } \rho_1 > 0, \\ 0, & \text{if } \rho_1 < 0, \end{cases} \quad \text{and} \quad \phi_2(\rho_2) = \begin{cases} 1, & \text{if } \rho_2 > 0, \\ 0, & \text{if } \rho_2 < 0, \end{cases}\tag{4.1.2}$$

with $\rho_1 = x_1(t) - x_{r1}(t)$ and $\rho_2 = x_2(t) - x_{r2}(t)$ representing the variables that define the threshold, which is dependent on the system states, with x_{r1} and x_{r2} denote the reference parameters for predatory species.

It is worth mentioning that the model (4.1.1) without control was studied by Llibre and Xiao in [84], where results of the global dynamics of the system are presented.

System (4.1.1) under the proposed control strategy is represented by a piecewise smooth system with two switching boundaries that cross perpendicularly between them and has a sliding motion that is described in this work following Filippov's convention. The main result of this work is the proof of global stability of system (4.1.1) with two switching boundaries under the action of control (4.1.2). From this study, we have

explicitly determined the conditions on the system parameters so that the coexistence equilibrium (which is the reference pseudo-equilibrium of the system) of the predators is globally stable, see Theorem 4.4.1. As far as we know, there is no work in the literature that deals with the global stability of system (4.1.1) with harvesting actions defined by a sliding mode control strategy. Other contributions are: (i) the identification of a special boundary equilibrium bifurcations that occurs in sliding vector fields, called boundary pseudo-equilibrium bifurcation (BPEB), see Theorems 4.3.2 and 4.3.4; (ii) the description of the sliding dynamics on each switching boundary, even at the intersection between them, see sections 4.3.1-4.3.2.

This chapter is organized as follows. Section 4.2 presents a detailed analysis of the dynamics of the system. Conditions of global stability for the coexistence of the predators are given in Section 4.4. The main conclusions are presented in Section 4.5.

4.2 A two-predator one-prey system under harvesting actions

The system (4.1.1) is normalized by applying the change of variables and time, defined by

$$S = \frac{r_3}{\sqrt{a_1 a_2}} x, \quad x_1 = \frac{r_3}{b_1} y, \quad x_2 = \frac{r_3}{b_2} z, \quad t = \frac{1}{r_3} \tau. \quad (4.2.1)$$

Then, we obtain the simplified system

$$\begin{aligned} \dot{x} &= (1 - \beta x - y - z)x, \\ \dot{y} &= \left(\alpha x - \frac{r_1}{r_3} \right) y - \frac{u_1}{r_3} y, \\ \dot{z} &= \left(\frac{x}{\alpha} - \frac{r_2}{r_3} \right) z - \frac{u_2}{r_3} z, \end{aligned} \quad (4.2.2)$$

where x is the prey normalized variable, y and z are the predator normalized variables, $\alpha = \sqrt{\frac{a_1}{a_2}}$ and $\beta = \frac{1}{K\sqrt{a_1 a_2}}$ are normalized parameters. The control variables are rewritten as

$$u_1 = \frac{k_1}{2} (1 + \text{Sign}[h_1]), \quad \text{and} \quad u_2 = \frac{k_2}{2} (1 + \text{Sign}[h_2]),$$

being $h_1(\mathbf{x}) = y - y_r$ and $h_2(\mathbf{x}) = z - z_r$ the normalized switching functions, and $y_r = \frac{b_1}{r_3} x_{r1}$ and $z_r = \frac{b_2}{r_3} x_{r2}$ are the normalized reference parameters.

We denote the state variables by $\mathbf{x} = (x, y, z) \in \mathcal{D}$, where

$$\mathcal{D} = \{\mathbf{x} \in \mathbb{R}^3 : x \geq 0, \quad y \geq 0 \quad \text{and} \quad z \geq 0\}.$$

We consider $\mathcal{D}^* = \{\mathbf{x} \in \mathbb{R}^3 : x > 0, \quad y > 0 \quad \text{and} \quad z > 0\}$.

The system state space is divided into four different regions, given by

$$\begin{aligned}\mathcal{R}_{++} &= \{\mathbf{x} \in \mathcal{D} : h_1(\mathbf{x}) > 0 \text{ and } h_2(\mathbf{x}) > 0\}, \\ \mathcal{R}_{-+} &= \{\mathbf{x} \in \mathcal{D} : h_1(\mathbf{x}) < 0 \text{ and } h_2(\mathbf{x}) > 0\}, \\ \mathcal{R}_{--} &= \{\mathbf{x} \in \mathcal{D} : h_1(\mathbf{x}) < 0 \text{ and } h_2(\mathbf{x}) < 0\}, \\ \mathcal{R}_{+-} &= \{\mathbf{x} \in \mathcal{D} : h_1(\mathbf{x}) > 0 \text{ and } h_2(\mathbf{x}) < 0\},\end{aligned}$$

separated by two transverse switching boundaries, namely

$$\begin{aligned}\Sigma_1 &= \{\mathbf{x} \in \mathcal{D} : h_1(\mathbf{x}) = y - y_r = 0\}, \\ \Sigma_2 &= \{\mathbf{x} \in \mathcal{D} : h_2(\mathbf{x}) = z - z_r = 0\}.\end{aligned}$$

System (4.2.2) is then represented as a discontinuous piecewise smooth system of the form

$$\dot{\mathbf{x}} = \begin{cases} \mathbf{F}_{++}(\mathbf{x}), & \text{if } \mathbf{x} \in \mathcal{R}_{++}, \\ \mathbf{F}_{-+}(\mathbf{x}), & \text{if } \mathbf{x} \in \mathcal{R}_{-+}, \\ \mathbf{F}_{--}(\mathbf{x}), & \text{if } \mathbf{x} \in \mathcal{R}_{--}, \\ \mathbf{F}_{+-}(\mathbf{x}), & \text{if } \mathbf{x} \in \mathcal{R}_{+-}, \end{cases} \quad (4.2.3)$$

composed of the vector fields

$$\mathbf{F}_{ij}(\mathbf{x}) = \begin{bmatrix} (1 - \beta x - y - z)x \\ \alpha(x - \mu_1^i)y \\ \frac{1}{\alpha}(x - \mu_2^j)z \end{bmatrix}, \quad (4.2.4)$$

for $i = +, -$ and $j = +, -$, where μ_1^i and μ_2^j are normalized parameters defined by

$$\mu_1^+ = \frac{r_1 + k_1}{r_3 \alpha}, \quad \mu_2^+ = \frac{\alpha(r_2 + k_2)}{r_3}, \quad \mu_1^- = \frac{r_1}{r_3 \alpha}, \quad \mu_2^- = \alpha \frac{r_2}{r_3}. \quad (4.2.5)$$

Notice that $0 < \mu_l^- < \mu_l^+$ for $l = 1, 2$ since $k_{1,2} > 0$.

4.2.1 Dynamics of vector field \mathbf{F}_{ij}

System (4.2.3) has an equilibrium at the origin $\mathbf{0} = (0, 0, 0)$ and another equilibrium at the point $\mathbf{e} = (1/\beta, 0, 0)$ for all the values of the parameters. In addition, they are equilibria of both the vector fields \mathbf{F}_{++} , \mathbf{F}_{-+} , \mathbf{F}_{--} and \mathbf{F}_{+-} , but they are admissible only for \mathbf{F}_{--} . If $\mu_1^i \neq \mu_2^j$ then there are two more equilibria for each vector field \mathbf{F}_{ij} , located at the points

$$\mathbf{e}_1^i = (\mu_1^i, 1 - \beta\mu_1^i, 0) \quad \text{and} \quad \mathbf{e}_2^j = (\mu_2^j, 0, 1 - \beta\mu_2^j).$$

The point \mathbf{e}_1^- (resp. \mathbf{e}_1^+) is an equilibrium for the vector fields \mathbf{F}_{--} and \mathbf{F}_{-+} (resp. \mathbf{F}_{+-} and \mathbf{F}_{++}), but it is admissible only for \mathbf{F}_{--} (resp. \mathbf{F}_{+-}) and if $y_r > 1 - \beta\mu_1^- > 0$ (resp. $0 < y_r < 1 - \beta\mu_1^+$). The point \mathbf{e}_2^- (resp. \mathbf{e}_2^+) is an equilibrium for the vector fields \mathbf{F}_{--} and \mathbf{F}_{+-} (resp. \mathbf{F}_{-+} and \mathbf{F}_{++}), but it is admissible only for \mathbf{F}_{--} (resp. \mathbf{F}_{-+}) and if $z_r > 1 - \beta\mu_2^- > 0$ (resp. $0 < z_r < 1 - \beta\mu_2^+$). If $\mu_1^i = \mu_2^j = \mu^{ij} < 1/\beta$ then there are infinitely many equilibria of \mathbf{F}_{ij} located at the line segment $L^{ij} = \{(\mu^{ij}, 1 - \beta\mu^{ij} - z, z) : 0 \leq z \leq 1 - \beta\mu^{ij}\}$. Predators can coexist in the latter case, but this is a structurally unstable scenario as it is not preserved after a small variation in parameter μ_1^i or μ_2^j .

In what follows we consider only the cases of our interest, which are those that have equilibria \mathbf{e}_1^i and \mathbf{e}_2^j with coordinates in \mathcal{D} .

Proposition 4.2.1. *Assume in system (4.2.3) that $\mu_1^i \neq \mu_2^j$ and $\mu_{1,2}^+ < \frac{1}{\beta}$. The following statements hold on the equilibria of \mathbf{F}_{ij} .*

- (i) *The trivial equilibrium $\mathbf{0}$ is a saddle with a 2-dimensional stable manifold and a 1-dimensional unstable manifold.*
- (ii) *The equilibrium \mathbf{e} is a saddle with a 1-dimensional stable manifold and a 2-dimensional unstable manifold.*
- (iii) *The equilibrium \mathbf{e}_1^i is asymptotically stable if $\mu_1^i < \mu_2^j$, with local dynamics of focus (resp. node) for $\mu_1^i < \frac{1}{\beta} \frac{4\alpha}{\beta+4\alpha}$ (resp. \geq). If $\mu_1^i > \mu_2^j$ then it is a saddle-focus (resp. saddle) with a 2-dimensional stable manifold and a 1-dimensional unstable manifold for $\mu_1^i < \frac{1}{\beta} \frac{4\alpha}{\beta+4\alpha}$ (resp. \geq).*
- (iv) *The equilibrium \mathbf{e}_2^j is asymptotically stable if $\mu_1^i > \mu_2^j$, with local dynamics of focus (resp. node) if $\mu_2^j < \frac{1}{\beta} \frac{4}{\beta\alpha+4}$ (resp. \geq). If $\mu_1^i < \mu_2^j$ then it is a saddle-focus (resp. saddle) with a 2-dimensional stable manifold and a 1-dimensional unstable manifold for $\mu_2^j < \frac{1}{\beta} \frac{4}{\beta\alpha+4}$ (resp. \geq).*

Proof. The (i)-(iv) statements are easily proven from the eigenvalues of the Jacobian matrix given by: (i) $\lambda_1^{ij} = 1$, $\lambda_2^{ij} = -\alpha\mu_1^i$, $\lambda_3^{ij} = -\frac{1}{\alpha}\mu_2^j$ for the equilibrium $\mathbf{0}$; (ii) $\lambda_4^{ij} = -1$, $\lambda_5^{ij} = \alpha\left(\frac{1}{\beta} - \mu_1^i\right)$, $\lambda_6^{ij} = \frac{1}{\alpha}\left(\frac{1}{\beta} - \mu_2^j\right)$ for the equilibrium \mathbf{e} ; (iii) $\lambda_7^{ij} = \frac{1}{\alpha}(\mu_1^i - \mu_2^j)$, $\lambda_{8,9}^{ij} = -\frac{\beta\mu_1^i}{2}\left(1 \pm \sqrt{1 - \frac{4\alpha}{\mu_1^i\beta}\left(\frac{1}{\beta} - \mu_1^i\right)}\right)$ for equilibrium \mathbf{e}_1^i ; and (iv) $\lambda_{10}^{ij} = -\alpha(\mu_1^i - \mu_2^j)$, $\lambda_{11,12}^{ij} = -\frac{\beta\mu_2^j}{2}\left(1 \pm \sqrt{1 - \frac{4}{\alpha\mu_2^j\beta}\left(\frac{1}{\beta} - \mu_2^j\right)}\right)$ for the equilibrium \mathbf{e}_2^j . \square

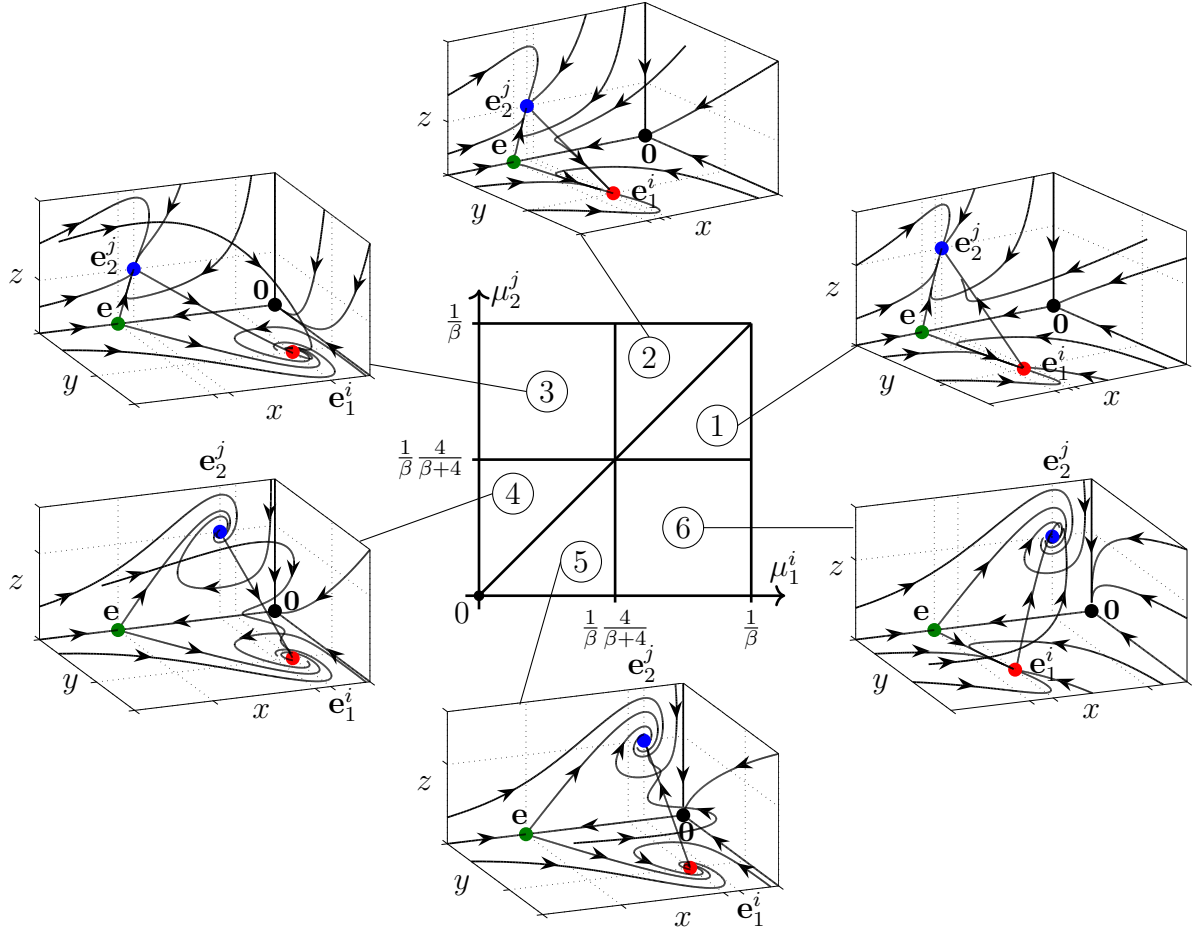


Figure 4.1: Phase portraits of the vector field \mathbf{F}_{ij} in \mathcal{D} from the choice of (μ_1^i, μ_2^j) , assuming $\mu_1^i \neq \mu_2^j$, $\mu_1^i < 1/\beta$, $\mu_2^j < 1/\beta$ and $\alpha = 1$. The green, blue and red dot represent the equilibrium points \mathbf{e} , \mathbf{e}_2^j and \mathbf{e}_1^i , respectively

It is well known in the literature that the Lotka-Volterra system (4.1.1) has a globally asymptotically stable equilibrium point if $\frac{r_1}{a_1} \neq \frac{r_2}{a_2}$, see for instance [66, 84] (that implies $\mu_1^i \neq \mu_2^j$ in the normalized system (4.2.3)); and [86, 93] with harvesting action on predator and prey species. In this case, if we assume the field \mathbf{F}_{ij} defined in the whole \mathcal{D} , then that vector field has a globally stable equilibrium. Whenever $\mu_1^i < \mu_2^j < 1/\beta$ the globally asymptotically stable equilibrium of \mathbf{F}_{ij} is the point \mathbf{e}_1^i , but if $\mu_2^j < \mu_1^i < 1/\beta$ then \mathbf{e}_2^j takes place. Such property is observed in the phase portraits of the vector field \mathbf{F}_{ij} in \mathcal{D} , obtained from the choice of μ_1^i and μ_2^j in the (μ_1^i, μ_2^j) -plane of parameters, as shown in Figure 4.1. Notice that k_1 and k_2 parameters are defined by (4.2.5) and both are also positive as previously defined in the text.

4.2.2 Configuration on $\Sigma = \Sigma_1 \cup \Sigma_2$

To study the contact of vector fields with the switching boundaries we use the Lie derivatives: $L_{\mathbf{F}_{ij}} h_k = \nabla h_k^T \cdot \mathbf{F}_{ij}$ and $L_{\mathbf{F}_{ij}}^q h_k = \nabla L_{\mathbf{F}_{ij}}^{q-1} h_k^T \cdot \mathbf{F}_{ij}$, for $k = 1, 2$ and $q = 2, 3$.

The flux of \mathbf{F}_{ij} is tangent to the switching boundary Σ_1 at the points $(x, y, z) \in \Sigma_1$

such that $L_{\mathbf{F}_{ij}}h_1(x, y_r, z) = \alpha y_r(x - \mu_1^i) = 0$, and it is tangent to Σ_2 at the points $(x, y, z) \in \Sigma_2$ such that $L_{\mathbf{F}_{ij}}h_2(x, y, z_r) = z_r(x - \mu_2^j)/\alpha = 0$. Then, we define two sets of tangential points for each vector field \mathbf{F}_{ij} , namely

$$T_1^i = \{(x, y, z) \in \Sigma_1 : x = \mu_1^i, y = y_r\} \quad \text{and} \quad T_2^j = \{(x, y, z) \in \Sigma_2 : x = \mu_2^j, z = z_r\}, \quad (4.2.6)$$

for $i, j \in \{+, -\}$. Note that T_1^+ is the tangency line for \mathbf{F}_{++} and \mathbf{F}_{+-} , and that T_1^- is the tangency line for \mathbf{F}_{-+} and \mathbf{F}_{--} . Similarly, T_2^+ is the tangency line for \mathbf{F}_{++} and \mathbf{F}_{-+} , and T_2^- is the tangency line for \mathbf{F}_{--} and \mathbf{F}_{+-} . In addition, the tangency lines T_1^+ and T_1^- are parallel straight lines in Σ_1 , while T_2^+ and T_2^- are parallel straight lines in Σ_2 .

In T_1^i and in T_2^j it may appear a cusp point with coordinates given by

$$\mathbf{q}_1^i = (\mu_1^i, y_r, 1 - \beta\mu_1^i - y_r) \quad \text{and} \quad \mathbf{q}_2^j = (\mu_2^j, 1 - \beta\mu_2^j - z_r, z_r),$$

respectively. Note that \mathbf{q}_1^i and \mathbf{q}_2^j have positive coordinates only if $y_r < 1 - \beta\mu_1^i$ and $z_r < 1 - \beta\mu_2^j$, respectively.

- (i) We say that \mathbf{q}_1^+ is a real cusp point for \mathbf{F}_{++} if $y_r + z_r < 1 - \beta\mu_1^+$, or for \mathbf{F}_{+-} if $y_r + z_r > 1 - \beta\mu_1^+$. If $y_r + z_r = 1 - \beta\mu_1^+$ then $\mathbf{q}_1^+ \in \Sigma_1 \cap \Sigma_2$ and it is a boundary cusp point.
- (ii) We say that \mathbf{q}_1^- is a real cusp point for \mathbf{F}_{-+} if $y_r + z_r < 1 - \beta\mu_1^-$, or for \mathbf{F}_{--} if $y_r + z_r > 1 - \beta\mu_1^-$. If $y_r + z_r = 1 - \beta\mu_1^-$ then $\mathbf{q}_1^- \in \Sigma_1 \cap \Sigma_2$ and it is a boundary cusp point.
- (iii) We say that \mathbf{q}_2^+ is a real cusp point for \mathbf{F}_{++} if $y_r + z_r < 1 - \beta\mu_2^+$, or for \mathbf{F}_{-+} if $y_r + z_r > 1 - \beta\mu_2^+$. If $y_r + z_r = 1 - \beta\mu_2^+$ then $\mathbf{q}_2^+ \in \Sigma_1 \cap \Sigma_2$ and it is a boundary cusp point.
- (iv) We say that \mathbf{q}_2^- is a real cusp point for \mathbf{F}_{+-} if $y_r + z_r < 1 - \beta\mu_2^-$, or for \mathbf{F}_{--} if $y_r + z_r > 1 - \beta\mu_2^-$. If $y_r + z_r = 1 - \beta\mu_2^-$ then $\mathbf{q}_2^- \in \Sigma_1 \cap \Sigma_2$ and it is a boundary cusp point.

Other points of T_1^i and in T_2^j are classified as visible or invisible fold.

Proposition 4.2.2. *Let T_1^i and T_2^j be the tangency lines of system (4.2.3), and assume $\mu_1^i \neq \mu_2^j$, $\bar{z}^i = 1 - \beta\mu_1^i - y_r \neq 0$ and $\bar{y}^j = 1 - \beta\mu_2^j - z_r \neq 0$, for $i, j \in \{+, -\}$.*

(i) *Tangential singularities in Σ_1 :*

- (a1) $(x, y, z) \in T_1^+$ is a visible fold point for all $z < \bar{z}^+$, an invisible fold point for all $z > \bar{z}^+$, and at $z = \bar{z}^+$ it is a cusp point.
- (b1) $(x, y, z) \in T_1^-$ is a visible fold point for all $z > \bar{z}^-$, an invisible fold point for all $z < \bar{z}^-$, and at $z = \bar{z}^-$ it is a cusp point.

(ii) *Tangential singularities in Σ_2 :*

- (a2) $(x, y, z) \in T_2^+$ is a visible fold point for all $y < \bar{y}^+$, an invisible fold point for all $y > \bar{y}^+$, and at $y = \bar{y}^+$ it is a cusp point.
- (b2) $(x, y, z) \in T_2^-$ is a visible fold point for all $y > \bar{y}^-$, an invisible fold point for all $y < \bar{y}^-$, and at $y = \bar{y}^-$ it is a cusp point.

Proof. (i) Computing the second and third Lie derivatives at the tangency lines T_1^i and at the cusp point \mathbf{q}_1^i , respectively, we get

$$\begin{aligned} L_{\mathbf{F}_{ij}}^2 h_1(\mu_1^i, y_r, z) &= \alpha y_r \mu_1^i (\bar{z}^i - z), \\ L_{\mathbf{F}_{ij}}^3 h_1(\mathbf{q}_1^i) &= -y_r \mu_1^i \bar{z}^i (\mu_1^i - \mu_2^j). \end{aligned}$$

(a1) Notice that, $L_{\mathbf{F}_{ij}}^2 h_1(\mu_1^+, y_r, z) \neq 0$ if $z \neq \bar{z}^+$, therefore, $(x, y, z) \in T_1^+$ is a visible fold for $z < \bar{z}^+$, and for $z > \bar{z}^+$ then $(x, y, z) \in T_1^+$ is a invisible fold. Now, if $z = \bar{z}^+$ then we have $L_{\mathbf{F}_{ij}}^2 h_1(\mu_1^+, y_r, z) = 0$ and $L_{\mathbf{F}_{ij}}^3 h_1(\mathbf{q}_1^+) \neq 0$, i.e., the point \mathbf{q}_1^+ is a cusp point.

(b1) Analogously, $(x, y, z) \in T_1^-$ is a visible fold point for all $z > \bar{z}^-$, an invisible fold point for all $z < \bar{z}^-$, and at $z = \bar{z}^-$ the point \mathbf{q}_1^- it is a cusp point.

(ii) Computing the second and third Lie derivatives at the tangency lines T_2^j and at the cusp point \mathbf{q}_2^j , respectively, we get

$$\begin{aligned} L_{\mathbf{F}_{ij}}^2 h_2(\mu_2^j, y, z_r) &= \frac{z_r \mu_2^j}{\alpha} (\bar{y}^j - y), \\ L_{\mathbf{F}_{ij}}^3 h_2(\mathbf{q}_2^j) &= z_r \mu_2^j \bar{y}^j (\mu_1^i - \mu_2^j). \end{aligned}$$

(a2) Notice that, $L_{\mathbf{F}_{ij}}^2 h_2(\mu_2^+, y_r, z) \neq 0$ if $y \neq \bar{y}^+$, therefore, $(x, y, z) \in T_2^+$ is a visible fold for $y < \bar{y}^+$, and for $y > \bar{y}^+$ then $(x, y, z) \in T_2^+$ is a invisible fold. Now, if $y = \bar{y}^+$ then we have $L_{\mathbf{F}_{ij}}^2 h_2(\mu_2^+, y_r, z) = 0$ and $L_{\mathbf{F}_{ij}}^3 h_2(\mathbf{q}_2^+) \neq 0$, i.e., the point \mathbf{q}_2^+ is a cusp point.

(b2) Likewise, $(x, y, z) \in T_2^-$ is a visible fold point for all $y > \bar{y}^-$, an invisible fold point for all $y < \bar{y}^-$, and at $y = \bar{y}^-$ the point \mathbf{q}_2^- it is a cusp point. □

Between the parallel tangency lines T_1^- and T_1^+ contained in Σ_1 , there is the attractive sliding region

$$\Sigma_1^{\text{as}} = \{(x, y, z) \in \Sigma_1 : \mu_1^- < x < \mu_1^+, z = y_r\}, \quad (4.2.7)$$

and on the outside there are the crossing regions

$$\Sigma_1^{\text{c}^+} = \{(x, y, z) \in \Sigma_1 : x > \mu_1^+, z = y_r\} \quad \text{and} \quad \Sigma_1^{\text{c}^-} = \{(x, y, z) \in \Sigma_1 : x < \mu_1^-, z = y_r\}.$$

The same configuration appears in Σ_2 , with the attractive sliding region

$$\Sigma_2^{\text{as}} = \{(x, y, z) \in \Sigma_2 : \mu_2^- < x < \mu_2^+, y = z_r\}, \quad (4.2.8)$$

and the crossing regions

$$\Sigma_2^{\text{c}^+} = \{(x, y, z) \in \Sigma_2 : x > \mu_2^+, y = z_r\} \quad \text{and} \quad \Sigma_2^{\text{c}^-} = \{(x, y, z) \in \Sigma_2 : x < \mu_2^-, y = z_r\}.$$

With that we have completed the set $\Sigma = \Sigma_1 \cup \Sigma_2$. Figure 4.2 shows a particular situation that occurs when $y_r > 1 - \beta \mu_1^-$, $z_r > 1 - \beta \mu_2^-$, $\mu_1^- < \mu_2^-$ and $\mu_1^+ > \mu_2^+$. In this case, the cusp points \mathbf{q}_1^i and \mathbf{q}_2^j have negative coordinates and, thus, the tangency lines T_1^+ and T_2^+ consist only of invisible fold points, while the tangency lines T_1^- and T_2^- consist only of visible fold points. Moreover, there is an intersection between the attractive sliding sets, given by $\Sigma_1^{\text{as}} \cap \Sigma_2^{\text{as}} = \{(x, y_r, z_r) : \mu_2^- < x < \mu_2^+\}$.

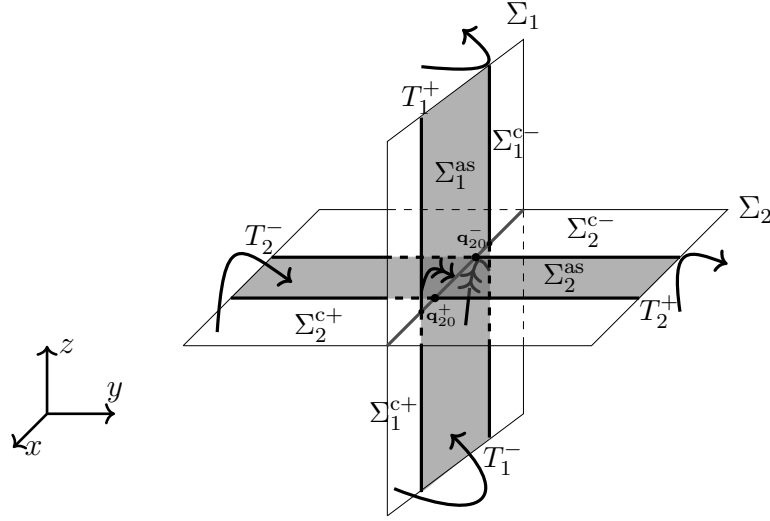


Figure 4.2: Configuration on $\Sigma = \Sigma_1 \cup \Sigma_2$ assuming $y_r > 1 - \beta\mu_1^-$, $z_r > 1 - \beta\mu_2^-$, $\mu_1^- < \mu_2^-$, $\mu_1^+ > \mu_2^+$, where $\mathbf{q}_{20}^+ = (\mu_2^+, y_r, z_r) \in T_2^+ \cap \Sigma_1$ and $\mathbf{q}_{20}^- = (\mu_2^-, y_r, z_r) \in T_2^- \cap \Sigma_1$ are fold points of the sliding vector field in Σ_1^{as} with its switching boundary $\Sigma_1 \cap \Sigma_2$.

4.3 Sliding vector fields and pseudo-equilibria

4.3.1 Sliding dynamics on Σ_1 and bifurcations

System (4.2.3) has sliding orbits on the switching boundary Σ_1 that are restricted to the attractive sliding region $\Sigma_1^{as} \subset \Sigma_1$, being extended to their borders given by the parallel tangency lines $T_1^- \subset \Sigma_1$ and $T_1^+ \subset \Sigma_1$. The sliding vector field $\mathbf{F}_{s1} : S_1 \rightarrow \mathcal{D}$ that governs the dynamics of the sliding motion in $S_1 = T_1^- \cup \Sigma_1^{as} \cup T_1^+$ is given by

$$\mathbf{F}_{s1}(x, y, z) = \begin{cases} \mathbf{F}_{s1}^-(x, y, z) & \text{if } h_2(x, y, z) < 0, \\ \mathbf{F}_{s1}^+(x, y, z) & \text{if } h_2(x, y, z) > 0, \end{cases} \quad (4.3.1)$$

where

$$\mathbf{F}_{s1}^j(x, y, z) = \begin{bmatrix} (1 - \beta x - y - z)x \\ 0 \\ \frac{1}{\alpha}(x - \mu_2^j)z \end{bmatrix}, \quad (4.3.2)$$

for $j = +, -$, and defined for $y = y_r$, $\mu_1^- \leq x \leq \mu_1^+$ and $z \geq 0$. This vector field is piecewise smooth and has the switching line $S_1^0 = \{(x, y_r, z_r) : \mu_1^- \leq x \leq \mu_1^+\}$ that divides the state space S_1 into two zones: $S_1^- = \{(x, y_r, z) : \mu_1^- \leq x \leq \mu_1^+, 0 \leq z < z_r\}$ and $S_1^+ = \{(x, y_r, z) : \mu_1^- \leq x \leq \mu_1^+, z > z_r\}$.

The regular equilibria of \mathbf{F}_{s1} , which are pseudo-equilibria for the system (4.2.3), are located at the points: $\mathbf{p}_{10} = (0, y_r, 0) \notin S_1$,

$$\mathbf{p}_{11} = \left(\frac{1 - y_r}{\beta}, y_r, 0 \right) \quad \text{and} \quad \mathbf{p}_{12}^j = (\mu_2^j, y_r, 1 - \beta\mu_2^j - y_r). \quad (4.3.3)$$

Note that \mathbf{p}_{10} is always a virtual equilibrium for both \mathbf{F}_{s1}^- and \mathbf{F}_{s1}^+ , thus being excluded of the stability analysis that follows. Point $\mathbf{p}_{11} \in S_1^-$ is a virtual equilibrium for \mathbf{F}_{s1}^+ and real

for $\mathbf{F}_{s_1}^-$ if $y_r \in (1 - \beta\mu_1^+, 1 - \beta\mu_1^-)$. But if $\mathbf{p}_{11} \notin S_1^-$, that is, if $y_r \notin [1 - \beta\mu_1^+, 1 - \beta\mu_1^-]$, then it is virtual for both $\mathbf{F}_{s_1}^+$ and $\mathbf{F}_{s_1}^-$. Moreover, it becomes a boundary equilibrium such that $\mathbf{p}_{11} = \mathbf{e}_1^- \in T_1^-$ if $y_r = 1 - \beta\mu_1^-$ or $\mathbf{p}_{11} = \mathbf{e}_1^+ \in T_1^+$ if $y_r = 1 - \beta\mu_1^+$. Point $\mathbf{p}_{12}^- \in S_1^-$ is a real equilibrium of $\mathbf{F}_{s_1}^-$ whenever $y_r \leq 1 - \beta\mu_2^- < y_r + z_r$ and $\mu_2^- \in (\mu_1^-, \mu_1^+)$, being that $\mathbf{p}_{12}^- = \mathbf{p}_{11}$ when $y_r = 1 - \beta\mu_2^-$. If $y_r + z_r = 1 - \beta\mu_2^-$ and $\mu_2^- \in (\mu_1^-, \mu_1^+)$ then it becomes a pseudo boundary equilibrium such that $\mathbf{p}_{12}^- = \mathbf{p} \in S_1^0$, where \mathbf{p} denotes the non-trivial pseudo-equilibrium of \mathbf{F}_{s_1} which will be introduced later. In other cases, that is, $\mathbf{p}_{12}^- \in S_1^+$ or $\mathbf{p}_{12}^- \notin S_1$, this equilibrium is virtual. Point $\mathbf{p}_{12}^+ \in S_1^+$ is a real equilibrium of $\mathbf{F}_{s_1}^+$ whenever $y_r + z_r < 1 - \beta\mu_2^+$ and $\mu_2^+ \in (\mu_1^-, \mu_1^+)$. If $y_r + z_r = 1 - \beta\mu_2^+$ and $\mu_2^+ \in (\mu_1^-, \mu_1^+)$ then it becomes a boundary equilibrium such that $\mathbf{p}_{12}^+ = \mathbf{p} \in S_1^0$. In other cases, that is, $\mathbf{p}_{12}^+ \in S_1^-$ or $\mathbf{p}_{12}^+ \notin S_1$, this equilibrium is virtual. Remember that we are assuming $\mu_1^+ \neq \mu_2^j$ for $i, j \in \{+, -\}$, then $\mathbf{p}_{12}^j \notin T_1^i$.

The following proposition presents the stability characteristics of these pseudo-equilibria.

Proposition 4.3.1. *Consider the pseudo-equilibrium points \mathbf{p}_{11} and \mathbf{p}_{12}^j , for $j = +, -$, of system (4.2.3). The following statements hold.*

- (i) \mathbf{p}_{11} is a stable pseudo-node if $y_r \in (1 - \beta\mu_2^-, 1)$, and a pseudo-saddle if $y_r > 1$ or $y_r < 1 - \beta\mu_2^-$.
- (ii) \mathbf{p}_{12}^j is a pseudo-saddle if $y_r > 1 - \beta\mu_2^j$, a stable pseudo-node if $y_r \in \left[1 - \beta\mu_2^j - \frac{\alpha\beta^2\mu_2^j}{4}, 1 - \beta\mu_2^j\right)$, and a stable pseudo-focus if $y_r < 1 - \beta\mu_2^j - \frac{\alpha\beta^2\mu_2^j}{4}$.

Proof. The sliding dynamics in S_1 is described by the vector field (4.3.1), which can be investigated by the two-dimensional system

$$\dot{x} = (1 - y_r - \beta x - z)x, \quad (4.3.4)$$

$$\dot{z} = \begin{cases} \frac{1}{\alpha}(x - \mu_2^-)z, & \text{if } z < z_r, \\ \frac{1}{\alpha}(x - \mu_2^+)z, & \text{if } z > z_r. \end{cases} \quad (4.3.5)$$

Jacobian matrix is

$$J_j(\bar{x}, \bar{z}) = \begin{pmatrix} -\beta\bar{x} & -\bar{x} \\ \bar{z}/\alpha & (\bar{x} - \mu_2^j)/\alpha \end{pmatrix},$$

where \bar{x} and \bar{z} denote the coordinates x and z of the equilibrium points \mathbf{p}_{11} and \mathbf{p}_{12}^j , with eigenvalues given by

$$L_{11} = \left\{ y_r - 1, \frac{1 - \beta\mu_2^- - y_r}{\alpha\beta} \right\} \quad \text{and} \quad L_{12}^j = \left\{ -\frac{\beta\mu_2^j}{2} \left(1 \pm \sqrt{1 - \frac{4}{\alpha\beta^2\mu_2^j}(1 - \beta\mu_2^j - y_r)} \right) \right\}$$

for \mathbf{p}_{11} and \mathbf{p}_{12}^j , respectively.

- (i) It is easy to see that the equilibrium point \mathbf{p}_{11} is a stable pseudo-node if $y_r \in (1 - \beta\mu_2^-, 1)$, since the eigenvalues in L_{11} are negative reals; and, it is a pseudo-saddle for $y_r > 1$ or $y_r < 1 - \beta\mu_2^-$ since the eigenvalues in L_{11} have opposite signs.
- (ii) It is easy to see that the equilibrium point \mathbf{p}_{12}^j is a pseudo-saddle if $y_r > 1 - \beta\mu_2^j$, since the eigenvalues in L_{12}^j have opposite signs; and, it is a stable pseudo-node

for $y_r \in \left[1 - \beta\mu_2^j - \frac{\alpha\beta^2\mu_2^j}{4}, 1 - \beta\mu_2^j\right)$ since the eigenvalues in L_{12}^j are negative reals; and, it is a stable pseudo-focus when $y_r < 1 - \beta\mu_2^j - \frac{\alpha\beta^2\mu_2^j}{4}$, since the eigenvalues in L_{12}^j are complex conjugate with a negative real part. \square

The vector field \mathbf{F}_{s1}^+ (resp. \mathbf{F}_{s1}^-) is tangent to the switching line $S_1^0 \subset \Sigma_1 \cap \Sigma_2$ at the point $\mathbf{q}_{20}^+ = (\mu_2^+, y_r, z_r) \in T_2^+ \cap \Sigma_1$ (resp. $\mathbf{q}_{20}^- = (\mu_2^-, y_r, z_r) \in T_2^- \cap \Sigma_1$), being this point classified as invisible fold if $y_r + z_r > 1 - \beta\mu_2^+$ (resp. $y_r + z_r < 1 - \beta\mu_2^-$) and visible fold if $y_r + z_r < 1 - \beta\mu_2^+$ (resp. $y_r + z_r > 1 - \beta\mu_2^-$). In the segment that joins the fold points \mathbf{q}_{20}^- and \mathbf{q}_{20}^+ , there is a new sliding motion, generated by the vector fields \mathbf{F}_{s1}^- and \mathbf{F}_{s1}^+ . If $\mu_2^j \in (\mu_1^-, \mu_1^+)$ then this sliding segment is all inside S_1^0 , as in the case shown in Figure 4.2. In general, the sliding segment is denoted by S and defined by

$$S = \Sigma_1^{\text{as}} \cap \Sigma_2^{\text{as}} = \{(x, y_r, z_r) : \max[\mu_1^-, \mu_2^-] < x < \min[\mu_1^+, \mu_2^+]\}. \quad (4.3.6)$$

These results are checked with the Lie derivatives: $L_{\mathbf{F}_{s1}^j} h_2(x, y_r, z_r) = \frac{z_r}{\alpha}(x - \mu_2^j)$ and $L_{\mathbf{F}_{s1}^j}^2 h_2(\mathbf{q}_{20}^j) = \frac{z_r \mu_2^j}{\alpha}(1 - \beta\mu_2^j - y_r - z_r)$.

The sliding dynamics in S has the equations

$$\begin{aligned} \dot{x} &= (1 - y_r - z_r - \beta x)x, \\ \dot{y} &= 0, \\ \dot{z} &= 0, \end{aligned} \quad (4.3.7)$$

with a stable non-trivial equilibrium at

$$\mathbf{p} = \left(\frac{1 - y_r - z_r}{\beta}, y_r, z_r \right). \quad (4.3.8)$$

The point \mathbf{p} is a pseudo-equilibrium of the sliding vector field \mathbf{F}_{s1} . In addition, it is real whenever

$$1 - \beta \min[\mu_1^+, \mu_2^+] < y_r + z_r < 1 - \beta \max[\mu_1^-, \mu_2^-]. \quad (4.3.9)$$

Considering only the switching boundary Σ_1 and the sliding motion occurring there, we get a two-dimensional **DPWS** system (4.3.4)-(4.3.5) with the switching boundary $S_1^0 \subset \Sigma_1$, which has three regular equilibria and one non-trivial pseudo-equilibrium. In this system (4.3.4)-(4.3.5) two *Persistence* bifurcations of boundary equilibria occur, which is one of the scenarios of the well-known *Boundary Equilibrium Bifurcation* (BEB), typical of **DPWS** systems, see for instance [20, 19]. However, such regular equilibria and pseudo-equilibrium of the two-dimensional **DPWS** system, are equivalent to the pseudo-equilibrium points \mathbf{p}_{11} , \mathbf{p}_{12}^+ , \mathbf{p}_{12}^- , and to the pseudo-equilibrium point \mathbf{p} . With that, the bifurcation point is a boundary pseudo-equilibrium of system (4.2.3) and, therefore, we renamed such a BEB as *Boundary Pseudo-Equilibrium Bifurcation* (BPEB). The following theorem predicts the unfolding scenarios of BPEBs in system (4.2.3), that occur in sliding dynamics restricted to Σ_1 .

Theorem 4.3.2. *Assume $\mu_2^j \in (\mu_1^-, \mu_1^+)$, $\mu_1^+ < 1/\beta$, $y_r < 1 - \beta\mu_2^+$ and $y_r + z_r \in (1 - \beta\mu_1^+, 1 - \beta\mu_1^-)$. System (4.2.3) undergoes a BPEB for $y_r + z_r = 1 - \beta\mu_2^+$ or for $y_r + z_r = 1 - \beta\mu_2^-$. Moreover, in both cases, the bifurcation is of the Persistence type and involves the pseudo-equilibria \mathbf{p} and \mathbf{p}_{12}^+ or \mathbf{p} and \mathbf{p}_{12}^- , as described below.*

- (a) If $y_r + z_r < 1 - \beta\mu_2^+$ then \mathbf{p} is virtual, \mathbf{p}_{12}^+ is real and \mathbf{p}_{12}^- is virtual.
- (b) If $y_r + z_r = 1 - \beta\mu_2^+$ then $\mathbf{p} = \mathbf{p}_{12}^+$ becomes a boundary pseudo-equilibrium, and \mathbf{p}_{12}^- remains virtual.
- (c) If $y_r + z_r \in (1 - \beta\mu_2^+, 1 - \beta\mu_2^-)$ then \mathbf{p} is real, \mathbf{p}_{12}^- and \mathbf{p}_{12}^+ are virtual.
- (d) If $y_r + z_r = 1 - \beta\mu_2^-$ then $\mathbf{p} = \mathbf{p}_{12}^-$ becomes a boundary pseudo-equilibrium, and \mathbf{p}_{12}^+ remains virtual.
- (e) If $y_r + z_r > 1 - \beta\mu_2^-$ then \mathbf{p} is virtual, \mathbf{p}_{12}^- is real and \mathbf{p}_{12}^+ is virtual.

Proof. (a) If $y_r + z_r < 1 - \beta\mu_2^+$ then by (4.3.9) we have that \mathbf{p} is virtual, since $\mathbf{p} \notin S_1^0$; and, by (4.3.3) we have that \mathbf{p}_{12}^+ is real and \mathbf{p}_{12}^- is virtual, since $\mathbf{p}_{12}^+ \in S_1^+$ and $\mathbf{p}_{12}^- \in S_1^+$.

(b) If $y_r + z_r = 1 - \beta\mu_2^+$ then by (4.3.9) we have that $\mathbf{p} = \mathbf{p}_{12}^+$ is a boundary pseudo-equilibrium, since $\mathbf{p}_{12}^+ \in S_1^0$; and, by (4.3.3) we have that \mathbf{p}_{12}^- is virtual since $\mathbf{p}_{12}^- \in S_1^+$.

(c) If $y_r + z_r \in (1 - \beta\mu_2^+, 1 - \beta\mu_2^-)$ then by (4.3.9) we have that \mathbf{p} is real since $\mathbf{p} \in S_1$; and, by (4.3.3) we have that \mathbf{p}_{12}^- and \mathbf{p}_{12}^+ are virtual, since $\mathbf{p}_{12}^- \in S_1^+$ and $\mathbf{p}_{12}^+ \in S_1^-$.

(d) If $y_r + z_r = 1 - \beta\mu_2^-$ then by (4.3.9) we have that $\mathbf{p} = \mathbf{p}_{12}^-$ is a boundary pseudo-equilibrium since $\mathbf{p}_{12}^- \in S_1^0$; and, by (4.3.3) we have that \mathbf{p}_{12}^+ is virtual since $\mathbf{p}_{12}^+ \in S_1^-$.

(e) If $y_r + z_r > 1 - \beta\mu_2^-$ then by (4.3.9) we have that \mathbf{p} is virtual since $\mathbf{p} \notin S_1^0$; and, by (4.3.3) we have that \mathbf{p}_{12}^- is real and \mathbf{p}_{12}^+ is virtual, since $\mathbf{p}_{12}^- \in S_1^-$ and $\mathbf{p}_{12}^+ \in S_1^-$. \square

A bifurcation set in the (y_r, z_r) -plane of parameters is shown in Figure 4.3(a), and in 4.3(b) there are shown some planar phase portraits of the sliding dynamics of system (4.2.3) restricted to $S_1 = T_1^- \cup \Sigma_1^{as} \cup T_1^+ \subset \Sigma_1$. We are considering the hypothesis of Theorem 4.3.2 and also $y_r < 1 - \beta\mu_2^j - \frac{\alpha\beta^2\mu_2^j}{4}$ from the Proposition 4.3.1, in order to obtain \mathbf{p}_{12}^j and \mathbf{p} inside Σ_1^{as} , and also to obtain a focus dynamics in (x, z) -plane for both the pseudo-equilibria \mathbf{p}_{12}^+ and \mathbf{p}_{12}^- . For any (y_r, z_r) in the regions 1, 2 or 3, on the left horizontal dashed line in red color, the statement (a), (c) or (e) of Theorem 4.3.2 occurs, respectively. These scenarios are structurally stable and the planar phase portrait for each case is shown in Figure 4.3(b). For any (y_r, z_r) at the border of regions 1 and 2 (solid red line) or at the border of regions 2 and 3 (solid blue line), the statement (b) or (d) of Theorem 4.3.2 occurs, respectively. In both cases, a Persistence bifurcation occurs at a boundary pseudo-focus. Looking at the planar sliding dynamics, we observe the presence of typical unfoldings from boundary-focus bifurcations of Planar Filippov systems, see [19].

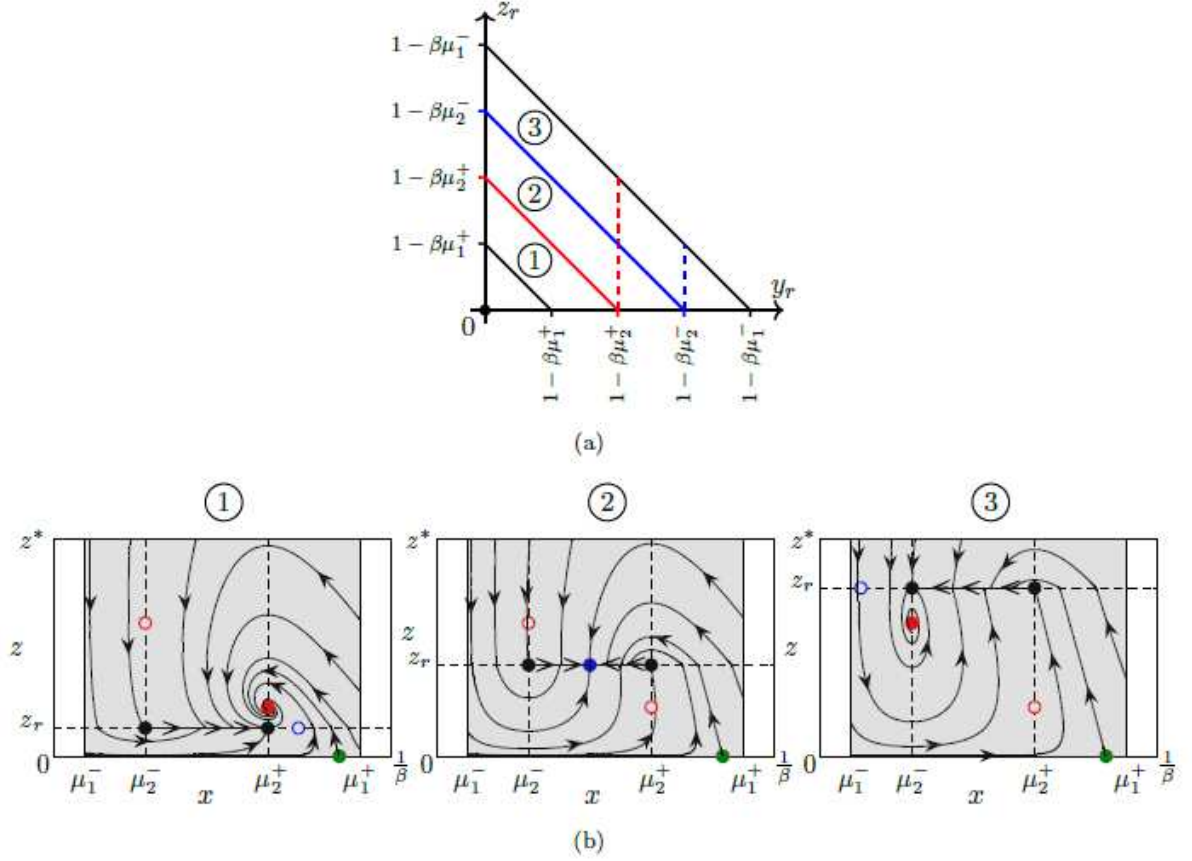


Figure 4.3: Sliding dynamics in Σ_1 . In (a) is shown a set of bifurcations in the (y_r, z_r) -plane of parameters assuming $\mu_2^\pm \in (\mu_1^-, \mu_1^+)$ and $\mu_1^+ < 1/\beta$, where the red and blue lines indicate the Persistence BPEB involving the boundary pseudo-equilibrium $\mathbf{p} = \mathbf{p}_{12}^+$ and $\mathbf{p} = \mathbf{p}_{12}^-$, respectively. For points (y_r, z_r) in the regions 1, 2 or 3, one of the pseudo-equilibria involved becomes real, and all of them, real and virtual, are located in Σ_1^{as} , being that \mathbf{p}_{12}^+ (resp. \mathbf{p}_{12}^-) have positive coordinates if on the left of the horizontal dashed line in red (resp. blue) color. In (b) there are shown some phase portraits of the sliding dynamics restricted to $S_1 = T_1^- \cup \Sigma_1^{as} \cup T_1^+ \subset \Sigma_1$, taking (y_r, z_r) in the regions 1 (left), 2 (center) and 3 (right) of the bifurcations set. The green dot represents the \mathbf{p}_{11} point, the red dots represent the \mathbf{p}_{12}^\pm points and the blue dot represents the \mathbf{p} point. They are virtual when represented by a small circle with an empty interior. The black dots represent the pseudo-folds \mathbf{q}_{20}^+ and \mathbf{q}_{20}^- . Consider $z^* = 1 - \beta\mu_2^-$.

4.3.2 Sliding dynamics on Σ_2 and bifurcations

We now consider the sliding orbits of system (4.2.3) restricted to attractive sliding region $\Sigma_2^{as} \subset \Sigma_2$, including its borders located at the parallel tangency lines $T_2^- \subset \Sigma_2$ and $T_2^+ \subset \Sigma_2$. The sliding vector field $\mathbf{F}_{s2} : S_2 \rightarrow \mathbb{R}^3$ that governs the dynamics of the sliding motion in $S_2 = T_2^- \cup \Sigma_2^{as} \cup T_2^+$ is given by

$$\mathbf{F}_{s2}(x, y, z) = \begin{cases} \mathbf{F}_{s2}^-(x, y, z) & \text{if } h_1(x, y, z) < 0, \\ \mathbf{F}_{s2}^+(x, y, z) & \text{if } h_1(x, y, z) > 0, \end{cases} \quad (4.3.10)$$

where

$$\mathbf{F}_{s2}^i(x, y, z) = \begin{bmatrix} (1 - \beta x - y - z)x \\ \alpha(x - \mu_1^i)y \\ 0 \end{bmatrix}, \quad (4.3.11)$$

for $i = +, -$, and defined for $z = z_r$, $\mu_2^- \leq x \leq \mu_2^+$ and $y \geq 0$. This vector field is piecewise smooth and has the switching line $S_2^0 = \{(x, y_r, z_r) : \mu_2^- \leq x \leq \mu_2^+\}$ that divides the state space S_2 into two zones: $S_2^- = \{(x, y, z_r) : \mu_2^- \leq x \leq \mu_2^+, 0 \leq y < y_r\}$ and $S_2^+ = \{(x, y, z_r) : \mu_2^- \leq x \leq \mu_2^+, y > y_r\}$.

Sliding dynamics on Σ_2 has the same characteristics as the sliding dynamics on Σ_1 described in the previous subsection. We then proceed in a similar way to the previous subsection. The regular equilibria of \mathbf{F}_{s2} , which are pseudo-equilibria for the system (4.2.3), are located at the points: $\mathbf{p}_{20} = (0, 0, z_r) \notin S_2$,

$$\mathbf{p}_{21} = \left(\frac{1 - z_r}{\beta}, 0, z_r \right) \quad \text{and} \quad \mathbf{p}_{22}^i = (\mu_1^i, 1 - \beta\mu_1^i - z_r, z_r) \quad (4.3.12)$$

Proposition 4.3.3. *Consider the pseudo-equilibrium points \mathbf{p}_{21} and \mathbf{p}_{22}^i , for $i = +, -$, of system (4.2.3). The following statements hold.*

- (i) \mathbf{p}_{21} is a stable pseudo-node if $z_r \in (1 - \beta\mu_1^-, 1)$, and a pseudo-saddle if $z_r > 1$ or $z_r < 1 - \beta\mu_1^-$.
- (ii) \mathbf{p}_{22}^i is a pseudo-saddle if $z_r > 1 - \beta\mu_1^i$, a stable pseudo-node if $z_r \in \left[1 - \beta\mu_1^i - \frac{\alpha\beta^2\mu_1^i}{4}, 1 - \beta\mu_1^i \right)$, and a stable pseudo-focus if $z_r < 1 - \beta\mu_1^i - \frac{\alpha\beta^2\mu_1^i}{4}$.

Proof. The sliding dynamics in S_2 is described by the two-dimensional PWS system

$$\dot{x} = (1 - z_r - \beta x - y)x, \quad (4.3.13)$$

$$\dot{y} = \begin{cases} \alpha(x - \mu_1^-)y, & \text{if } y < y_r, \\ \alpha(x - \mu_1^+)y, & \text{if } y > y_r. \end{cases} \quad (4.3.14)$$

Jacobian matrix is

$$J_i(\bar{x}, \bar{z}) = \begin{pmatrix} -\beta\bar{x} & -\bar{x} \\ \alpha\bar{y} & \alpha(\bar{x} - \mu_1^i) \end{pmatrix},$$

where \bar{x} and \bar{y} denote the coordinates x and y of the equilibrium points \mathbf{p}_{21} and \mathbf{p}_{22}^i , with eigenvalues given by

$$L_{21} = \left\{ z_r - 1, \frac{\alpha(1 - \beta\mu_1^- - z_r)}{\beta} \right\} \quad \text{and} \quad L_{22}^i = \left\{ -\frac{\beta\mu_1^i}{2} \left(1 \pm \sqrt{1 - \frac{4\alpha}{\beta^2\mu_1^i}(1 - \beta\mu_1^i z_r)} \right) \right\}$$

for \mathbf{p}_{21} and \mathbf{p}_{22}^i , respectively.

- (i) It is easy to see that the equilibrium point \mathbf{p}_{21} is a stable pseudo-node if $z_r \in (1 - \beta\mu_1^-, 1)$, since the eigenvalues in L_{21} are negative reals; and, it is a pseudo-saddle for $z_r > 1$ or $z_r < 1 - \beta\mu_1^-$ since the eigenvalues in L_{21} have opposite signs.
- (ii) It is easy to see that the equilibrium point \mathbf{p}_{22}^i is a pseudo-saddle if $z_r > 1 - \beta\mu_1^i$, since the eigenvalues in L_{22}^i have opposite signs; and, it is a stable pseudo-node for $z_r \in \left[1 - \beta\mu_1^i - \frac{\alpha\beta^2\mu_1^i}{4}, 1 - \beta\mu_1^i\right)$ since the eigenvalues in L_{22}^i are negative reals; and, it is a stable pseudo-focus when $z_r < 1 - \beta\mu_1^i - \frac{\alpha\beta^2\mu_1^i}{4}$, since the eigenvalues in L_{22}^i are complex conjugate with a negative real part.

□

The vector field $\mathbf{F}_{s_2}^+$ (resp. $\mathbf{F}_{s_2}^-$) is tangent to the switching line $S_2^0 \subset \Sigma_1 \cap \Sigma_2$ at the point $\mathbf{q}_{10}^+ = (\mu_1^+, y_r, z_r) \in T_1^+ \cap \Sigma_2$ (resp. $\mathbf{q}_{10}^- = (\mu_1^-, y_r, z_r) \in T_1^- \cap \Sigma_2$), being this point classified as invisible fold if $y_r + z_r > 1 - \beta\mu_1^+$ (resp. $y_r + z_r < 1 - \beta\mu_1^-$) and visible fold if $y_r + z_r < 1 - \beta\mu_1^+$ (resp. $y_r + z_r > 1 - \beta\mu_1^-$). In the segment that joins the fold points \mathbf{q}_{10}^- and \mathbf{q}_{10}^+ , there is a new sliding motion, this generated by the vector fields $\mathbf{F}_{s_2}^-$ and $\mathbf{F}_{s_2}^+$. If $\mu_1^i \in (\mu_2^-, \mu_2^+)$ then the sliding segment S , given in (4.3.6), is all inside S_2^0 . These results are checked with the Lie derivatives: $L_{\mathbf{F}_{s_2}^i} h_1(x, y_r, z_r) = y_r \alpha (x - \mu_1^i)$ and $L_{\mathbf{F}_{s_2}^i}^2 h_1(\mathbf{q}_{10}^i) = y_r \mu_1^i \alpha (1 - \beta\mu_1^i - y_r - z_r)$. The sliding dynamics of vector field (4.3.10) in S is described by the same equations for the sliding dynamics of vector field (4.3.1), given in (4.3.7) and analyzed in the previous subsection. So, the pseudo-equilibrium \mathbf{p} , given in (4.3.8), is also pseudo-equilibrium of the vector field (4.3.10). In addition, it is real whenever $y_r + z_r$ satisfies the condition given in (4.3.9).

Considering only the switching boundary Σ_2 and the sliding motion occurring there, we get a two-dimensional **DPWS** system with a switching line defined in $S_2 \subset \Sigma_2$, which has three regular equilibria and one non-trivial pseudo-equilibrium. In vector field (4.3.10) two *Persistence* bifurcations of boundary equilibria occur, involving the pseudo-equilibrium points \mathbf{p}_{21} , \mathbf{p}_{22}^+ , \mathbf{p}_{22}^- , and the pseudo-equilibrium point \mathbf{p} . With that, the bifurcation point is a boundary pseudo-equilibrium (BPEB) of system (4.2.3). The following theorem predicts the unfolding scenarios of BPEBs in system (4.2.3), that occur in sliding dynamics restricted to Σ_2 .

Theorem 4.3.4. *Assume $\mu_1^i \in (\mu_2^-, \mu_2^+)$, $\mu_2^+ < 1/\beta$, $z_r < 1 - \beta\mu_1^+$ and $y_r + z_r \in (1 - \beta\mu_2^+, 1 - \beta\mu_2^-)$. System (4.2.3) undergoes a Boundary Pseudo-Equilibrium Bifurcation for $y_r + z_r = 1 - \beta\mu_1^+$ or for $y_r + z_r = 1 - \beta\mu_1^-$. Moreover, in both cases the bifurcation is of the Persistence type and involves the pseudo-equilibria \mathbf{p} and \mathbf{p}_{22}^+ or \mathbf{p} and \mathbf{p}_{22}^- , as described below.*

- (a) *If $y_r + z_r < 1 - \beta\mu_1^+$ then \mathbf{p} is virtual, \mathbf{p}_{22}^+ is real and \mathbf{p}_{22}^- is virtual.*
- (b) *If $y_r + z_r = 1 - \beta\mu_1^+$ then $\mathbf{p} = \mathbf{p}_{22}^+$ becomes a boundary pseudo-equilibrium, and \mathbf{p}_{22}^- remains virtual.*
- (c) *If $y_r + z_r \in (1 - \beta\mu_1^+, 1 - \beta\mu_1^-)$ then \mathbf{p} is real, \mathbf{p}_{22}^- and \mathbf{p}_{22}^+ are virtual.*
- (d) *If $y_r + z_r = 1 - \beta\mu_1^-$ then $\mathbf{p} = \mathbf{p}_{22}^-$ becomes a boundary pseudo-equilibrium, and \mathbf{p}_{22}^+ remains virtual.*

(e) If $y_r + z_r > 1 - \beta\mu_1^-$ then \mathbf{p} is virtual, \mathbf{p}_{22}^- is real and \mathbf{p}_{22}^+ is virtual.

Proof. Analogously to Theorem 4.3.2, we have

- (a) If $y_r + z_r < 1 - \beta\mu_1^+$ then by (4.3.9) we have that \mathbf{p} is virtual, since $\mathbf{p}_3 \notin S_2^0$; and, by (4.3.12) we have that \mathbf{p}_{22}^+ is real and \mathbf{p}_{22}^- is virtual, since $\mathbf{p}_{22}^+ \in S_2^+$ and $\mathbf{p}_{22}^- \in S_2^+$.
- (b) If $y_r + z_r = 1 - \beta\mu_1^+$ then by (4.3.9) we have that $\mathbf{p} = \mathbf{p}_{22}^+$ is a boundary pseudo-equilibrium, since $\mathbf{p}_{22}^+ \in S_2^0$; and, by (4.3.12) we have that \mathbf{p}_{22}^- is virtual since $\mathbf{p}_{22}^- \in S_2^+$.
- (c) If $y_r + z_r \in (1 - \beta\mu_1^+, 1 - \beta\mu_1^-)$ then by (4.3.9) we have that \mathbf{p} is real since $\mathbf{p} \in S_2$; and, by (4.3.12) we have that \mathbf{p}_{22}^- and \mathbf{p}_{22}^+ are virtual, since $\mathbf{p}_{22}^- \in S_2^+$ and $\mathbf{p}_{22}^+ \in S_2^-$.
- (d) If $y_r + z_r = 1 - \beta\mu_1^-$ then by (4.3.9) we have that $\mathbf{p} = \mathbf{p}_{22}^-$ is a boundary pseudo-equilibrium since $\mathbf{p}_{22}^- \in S_2^0$; and, by (4.3.12) we have that \mathbf{p}_{22}^+ is virtual since $\mathbf{p}_{22}^+ \in S_2^-$.
- (e) If $y_r + z_r > 1 - \beta\mu_1^-$ then by (4.3.9) we have that \mathbf{p} is virtual since $\mathbf{p} \notin S_2^0$; and, by (4.3.12) we have that \mathbf{p}_{22}^- is real and \mathbf{p}_{22}^+ is virtual, since $\mathbf{p}_{22}^- \in S_2^-$ and $\mathbf{p}_{22}^+ \in S_2^-$.

□

Sliding dynamics on $\Sigma_1 \cap \Sigma_2$

By sections 4.3.1- 4.3.2, there is a sliding segment $S = \Sigma_1^{as} \cap \Sigma_2^{as}$ defined in (4.3.6), since

$$\begin{aligned} L_{\mathbf{F}_{s1}^+} h_2(x, y_r, z_r) &< 0 < L_{\mathbf{F}_{s1}^-} h_2(x, y_r, z_r), \\ L_{\mathbf{F}_{s2}^+} h_1(x, y_r, z_r) &< 0 < L_{\mathbf{F}_{s2}^-} h_1(x, y_r, z_r), \end{aligned}$$

where $L_{\mathbf{F}_{s1}^j} h_2(x, y_r, z_r) = \frac{z_r}{\alpha}(x - \mu_2^j)$ and $L_{\mathbf{F}_{s2}^i} h_1(x, y_r, z_r) = y_r \alpha(x - \mu_1^i)$. Then, we can define a sliding vector field in S as

$$\mathbf{F}_s(x, y, z) = \begin{bmatrix} (1 - \beta x - y - z)x \\ 0 \\ 0 \end{bmatrix}.$$

When the trajectories achieve the sliding boundary and the states are forced to follow a trajectory over the sliding segment S , then the dynamics described by \mathbf{F}_s at the intersection of the switching boundaries become unidimensional as follows:

$$\dot{x} = (1 - \beta x - y_r - z_r)x, \quad (4.3.15)$$

where $(x, y_r, z_r) \in S$. Notice that the first coordinate of \mathbf{p} defined in (4.3.8) is an equilibrium point for (4.3.15) that is real whenever condition (4.3.9) is satisfied, this mean that $\mathbf{p} \in S$, and it is stable since $\ddot{x}(\mathbf{p}) = y_r + z_r - 1 < -\beta \max[\mu_1^-, \mu_2^-] < 0$. Being that $S \subset \Sigma_1 \cap \Sigma_2$, we have that \mathbf{p} is the pseudo-equilibrium of the normalized system (4.2.3) in the sliding segment S . In summary, we have the following result.

Lemma 4.3.5. *Assuming the condition (4.3.9), system (4.2.3) has an unique real pseudo-equilibrium in the sliding segment $S \subset \Sigma_1 \cup \Sigma_2$, with coordinates denoted by \mathbf{p} , given in (4.3.8), and it is stable.*

4.4 Conditions of global stability for the coexistence of predators

In this section, the conditions for the global stability of the pseudo-equilibrium point \mathbf{p} where the three species can coexist are formulated. Such conditions are derived from the analysis of equilibria and stability carried out in the previous sections.

Theorem 4.4.1. *Assume the condition (4.3.9) holds and $\mu_{1,2}^- < \mu_{1,2}^+ < 1/\beta$. Then the pseudo-equilibrium $\mathbf{p} = (x_r, y_r, z_r)$, where $x_r = \frac{1-y_r-z_r}{\beta}$, is a globally stable point for system (4.2.3) in \mathcal{D}^* .*

Proof. The planes $x = 0$, $y = 0$ and $z = 0$, of two-dimensional coordinates in \mathbb{R}^3 , are invariant sets of system (4.2.3). Then a solution of (4.2.3) with a positive initial condition remains in the positive octant forever. In the study carried out in [84] it was proved that all solutions of system (4.1.1) with positive initial conditions are positive and bounded in forward time. So, the solutions of (4.2.3) for each vector field \mathbf{F}_{ij} are also positive and bounded in forward time.

By Lemma 4.3.5, taking any combination of parameters satisfying the condition (4.3.9) and $\mu_{1,2}^- < \mu_{1,2}^+ < 1/\beta$, then there is an unique real pseudo-equilibrium point and it is stable, being denoted by $\mathbf{p} = (x_r, y_r, z_r)$ (coordinates explained in (4.3.8)), with $x_r = \frac{1-y_r-z_r}{\beta}$, and located in the attractive sliding segment that appears at $\Sigma_1 \cap \Sigma_2$. Under such conditions and according to Section 4.2.1 and Proposition 4.2.1, the vector field \mathbf{F}_{--} has two real saddle equilibria (denoted by $\mathbf{0}$ and \mathbf{e}) and the vector field \mathbf{F}_{+-} or \mathbf{F}_{+} may have a real equilibrium (denoted by \mathbf{e}_2^+ or \mathbf{e}_1^+ , respectively), but it is also of the saddle type. These equilibrium points appear on the borders of \mathcal{D} . So, \mathbf{p} is the only attractor point for system (4.2.3). Furthermore, every future orbit starting in \mathcal{D}^* converges to \mathbf{p} , which can converge in finite time to a few system orbits (because \mathbf{p} is a pseudo-equilibrium).

To prove the global stability of \mathbf{p} we use the Lyapunov function

$$V(\mathbf{x}) = \frac{1}{\alpha} \left(y - y_r - y_r \ln \frac{y}{y_r} \right) + \alpha \left(z - z_r - z_r \ln \frac{z}{z_r} \right) + x - x_r - x_r \ln \frac{x}{x_r}, \quad (4.4.1)$$

such that $V(\mathbf{p}) = 0$ and $V(\mathbf{x}) > 0 \quad \forall \mathbf{x} \in \mathcal{D}^* \setminus \mathbf{p}$. From the derivative of $V(\mathbf{x})$ with respect to time we obtain

$$\frac{dV(\mathbf{x})^{ij}}{dt} = (x_r - \mu_1^i)y + (x_r - \mu_2^j)z - (x - \mu_1^i)y_r - (x - \mu_2^j)z_r + (1 - \beta x)(x - x_r), \quad \text{for } i, j \in \{+, -\}.$$

Note that $(x_r - \mu_1^i)y + (x_r - \mu_2^j)z \leq (x_r - \mu_1^i)y_r + (x_r - \mu_2^j)z_r$, i.e., $(x_r - \mu_1^i)(y - y_r) + (x_r - \mu_2^j)(z - z_r) \leq 0$, since: (i) if $i = -$, then $y \leq y_r$ and $x_r > \mu_1^-$; (ii) if $i = +$, then $y \geq y_r$ and $x_r < \mu_1^+$; (iii) if $j = -$, then $z \leq z_r$ and $x_r > \mu_2^-$; (iv) if $j = +$, then $z \geq z_r$ and $x_r < \mu_2^+$. So we concluded that

$$\begin{aligned} \frac{dV(\mathbf{x})^{ij}}{dt} &< (x_r - \mu_1^i)y_r + (x_r - \mu_2^j)z_r - (x - \mu_1^i)y_r - (x - \mu_2^j)z_r + (1 - \beta x)(x - x_r) \\ &= -\beta(x - x_r)^2, \end{aligned}$$

and $dV(\mathbf{x})^{ij}/dt < 0$ for all $\mathbf{x} \in \mathcal{D}^* \setminus \mathbf{p}$. Therefore, the pseudo-equilibrium \mathbf{p} is the global attractor of the system. \square

4.4.1 Simulation results

The simulations below show the interaction between one prey and two populations of predators under the proposed control. See Figures 4.4-4.5 where the blue point stands for the pseudo-equilibrium point \mathbf{p} (where the three species can coexist) and the trajectories are represented by black curves.

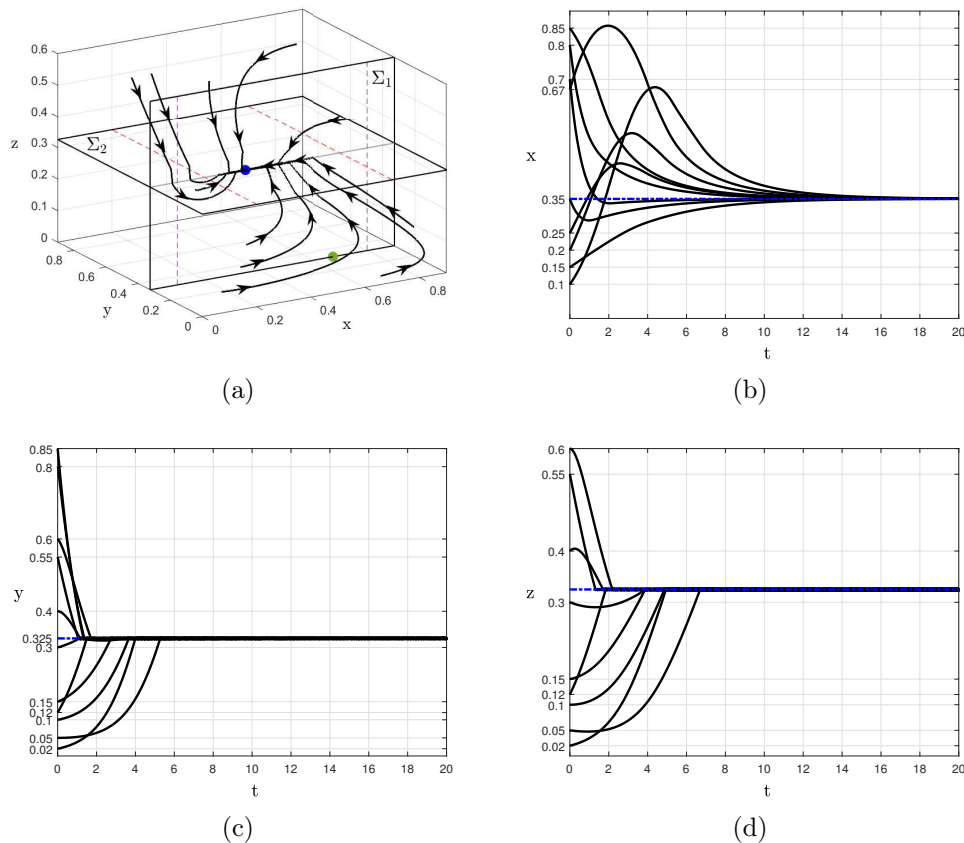


Figure 4.4: Figure (a) shows a phase portrait of the system with parameters $\mu_1^+ = 0.8$, $\mu_1^- = 0.1$, $\mu_2^+ = 0.7$, $\mu_2^- = 0.2$, $\beta = 1$, $\alpha = 1$, $y_r = z_r = 0.325$ for various initial conditions of the prey and predators populations. The green dot represents the point \mathbf{p}_{11} and the blue dot represents the pseudo-equilibrium point \mathbf{p} . Figures (b)-(d) exhibit the population dynamics for one prey and two predators over time for distinct initial conditions.

Figures 4.4(a)-4.5(a) show a phase portrait of system (4.2.3) assuming the hypothesis under system parameters of Theorem 4.4.1. It is observed how the trajectories of different initial conditions go to the pseudo-equilibrium point as expected.

Figures 4.4(b)-4.5(b) expose the prey population change through time (days), in the beginning, the number of prey increasing until a maximum of approximately 85% of its carrying capacity depending on its initial condition, and after that, the prey population decreases until it stabilizes at \mathbf{p} .

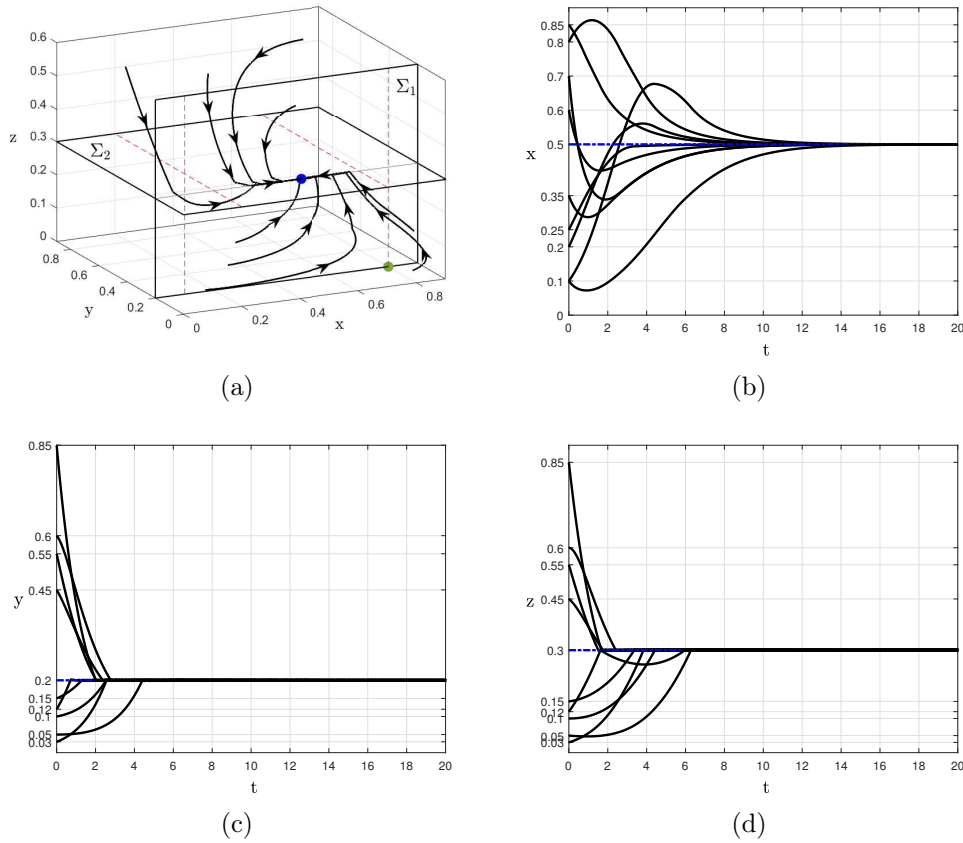


Figure 4.5: Figure (a) shows a phase portrait of the system with parameters $\mu_1^+ = 0.8$, $\mu_1^- = 0.1$, $\mu_2^+ = 0.7$, $\mu_2^- = 0.2$, $\beta = 1$, $\alpha = 1$, $y_r = 0.2$ and $z_r = 0.3$ ($y_r < z_r$) for various initial conditions of the prey and predators populations. The green dot represents the point \mathbf{p}_{11} and the blue dot represents the pseudo-equilibrium point \mathbf{p} . Figures (b)-(d) exhibit the population dynamics for one prey and two predators over time for distinct initial conditions.

Figures 4.4(c-d)-4.5(c-d) display the population size of each predator over time. We observe that, at first, the two predators thrive when prey is abundant, but after a few days, outnumber prey and their population diminishes until it stabilizes at \mathbf{p} .

For Figures 4.4-4.5 we choose the parameters $\mu_1^+ = 0.8$, $\mu_1^- = 0.1$, $\mu_2^+ = 0.7$, $\mu_2^- = 0.2$, $\beta = 1$, $\alpha = 1$, with the difference that in Figure 4.4 we take on $y_r = z_r = 0.325$, and in Figure 4.5 we have $y_r < z_r$ such that $y_r = 0.2$ and $z_r = 0.3$.

4.4.2 Harvesting control

In ecological systems, the control action can be associated with human interference in the natural environment, which can take the form of a harvesting policy [93]. There are basically two main reasons for obtaining control strategies for predator-prey systems. The first one is to allow sustainable exploitation of its resources. The other one is to restore ecological balance. These subjects have been treated by Cunha and Pagano [94] and Meza *et al.* [95]. Furthermore, it is important to remark that the implementation of a certain control signal u in the real predator-prey system might come across two major problems: (i) feedback control laws require the measurement of the population sizes of

both species at every instant of time. However, this might not always be possible in numerous predator-prey interactions found in nature; (ii) the second problem is that the control signals should model the human action on the ecosystem. Note that, in (4.2.2), the control signals u_1 and u_2 represent the instantaneous rates of change (with respect to t) of y and z respectively, that have to be applied into the system by human action. Hence, if the control signals exhibit elevated rates of signal variation and/or assume a different value at every instant of time, one can argue that human action cannot respond in that manner in many ecosystems found in nature. In order to tackle these problems, it is desirable to determine control signals that can be implemented by environmental agencies as management policies. Note that, the harvesting control does not impose any switching frequency limit because the switch rule is state-based instead of time-based. Consequently, the switching may evolve to unacceptable high frequencies. This behavior is treated in the literature as chattering (see more details in [93]). According to May and Beddington [96], a constant harvest quota is an idealized model of real management policies adopted by environmental agencies. Hence, in order to adequate human actions to the control signals, a control strategy that determines piecewise-constant control signals from periodic measurements of the prey and predator population sizes is proposed in [93].

4.5 Conclusion

This chapter addressed the study of the global dynamics of a Lotka-Volterra piecewise-smooth system with two predators competing for one prey where the resource for prey is limited (i.e., K is bounded). A control harvesting strategy defined by two switching boundaries that determine piecewise-constant control signals for the tracking problem of predator-prey systems was proposed since this type of signal is an idealized model of management policies adopted by environmental agencies. The reference trajectories of the two predator species are chosen to restore the original dynamics of a disturbed system and to guarantee the global stability of the pseudo-equilibrium point where the two predator species and one prey specie can coexist. In this sense, a proof of the global stability condition for the pseudo-equilibrium point was presented.

Chapter 5

Nonlinear analysis of DC power converters connected in parallel

In this chapter, we study a method of stability analysis of the nonlinear dynamics of a DC-DC buck converter controlled by a step-mode control law (SMC) connected to two power converters: a boost converter and a buck converter, both modeled by CPL by parts functions.

5.1 Introduction

Dc distribution systems are becoming increasingly common in industrial applications, most specifically the distributed power systems (DPSs) with multiple switching power converters, such as dc micro-grids, electric vehicles, aircraft, communication systems, and other applications which provide more efficient conversion of energy, to reduce cost, power quality, efficiency, and simpler power electronic interfaces and control.

Most research focuses on dc distributed power systems with a single DC bus. So, they may not be able to very succinctly assess the stability of multivoltage DC distributed power systems, since power sources and loads are connected with interfacing power converters via a DC bus, where each converter in the DC distribution system is expected to be well designed when operating as a standalone system by ensuring a sufficient phase margin at the cut-off frequency of the converter and the stability of the whole system. However, the stability assessment is valid only when the system is subject to small signal disturbance. In practice, the DC distribution system is often confronted by large disturbances, such as during start-up or abrupt load change. These factors may intensify through the interaction of the subsystems, resulting in undesirable consequences on the system's transient stability performance. Some analysis methods have been proposed, such as the phase-plane analysis which is suitable for numerical simulations (see [80]), and bifurcation analysis which can give boundaries of stable operation of the system for stability assessment (see [81, 82]).

In this work, the system under study can be considered as a piecewise smooth dynamical system in \mathbb{R}^3 (for short, 3D-PWS system) with three switching boundaries defined by (i) the SMC law designed to control the voltage output of the first buck converter; (ii) the voltage threshold at $v_{bus} = V_{th1}$ due to the non-smooth characteristic of the CPL of the buck converter; and (iii) the voltage threshold at $v_{bus} = V_{th2}$ due to the

non-smooth characteristic of the CPL of the boost converter. It is noteworthy that the sliding motion occurs only at the SMC-boundary and the vector field that governs this motion, calculated following Filippov's convention, is continuous but not differentiable at the intersection with the CPL-boundary, which involves us with the theory of **CPWS** systems and Filippov systems (**DPWS**) [1, 34, 8].

The main goal of this chapter is to analyze the stability of multivoltage-level dc distributed power system given by a DC-DC buck converter controlled by a sliding mode control (SMC) law connected to two power converters where one of them is a boost converter and another is a buck converter, both modeled by a CPL piecewise function. We also study local phenomena associated with bifurcations induced by the switching boundaries, as the Boundary Equilibrium Bifurcations (BEBs, [20, 19, 24, 23]) and Discontinuous Saddle-Node (DSN, [22]), which are part of the group of Discontinuous Induced Bifurcations (DIBs, [41, 43]). Classic bifurcations as the Hopf and Saddle-Node equilibria (see [49, 50]) are also investigated.

In the qualitative analysis performed we use standard tools for **DPWS** systems. Numerical continuation methods based on AUTO software are also employed to obtain bifurcation sets and bifurcation diagrams. The CPL equations used in this work are class \mathcal{C}^0 functions, that is, continuous but with discontinuous derivatives. As a significant part of this work involves the bifurcation analysis of dynamic systems, \mathcal{C}^∞ models are more suitable for performing numerical continuation calculations using computational packages such as XPP-AUTO (see [83]), which help us to better understand the dynamic behavior of this system and also to verify the analytical results.

Theoretical background for understanding the dynamics of Filippov systems and some preliminary results on **DPWS** systems relevant to our purposes can be found in [8, 42, 82].

The remainder of this chapter is organized as follows. The modeling of the DC-DC buck converter controlled by a sliding mode control (SMC) law connected to two power converters both modeled by CPL piecewise functions is developed in section 5.2, where we analyze the existence, local stability and bifurcations of regular equilibria and pseudo-equilibria. Due to the complexity of our model, we divided it into three case studies. In section 5.3 we study the first case where $V_{th1} = V_{th2}$. In section 5.4 we study the second case where $V_{th1} < V_{th2}$. In section 5.5 we study the third case where $V_{th1} > V_{th2}$. Finally, in section 5.6 we present a brief conclusion.

5.2 Model description

The behavior of a DC-DC buck converter controlled by a sliding mode control (SMC) law connected to two converters in parallel: a boost converter and a buck converter, both modeled by CPL piecewise functions; is given by

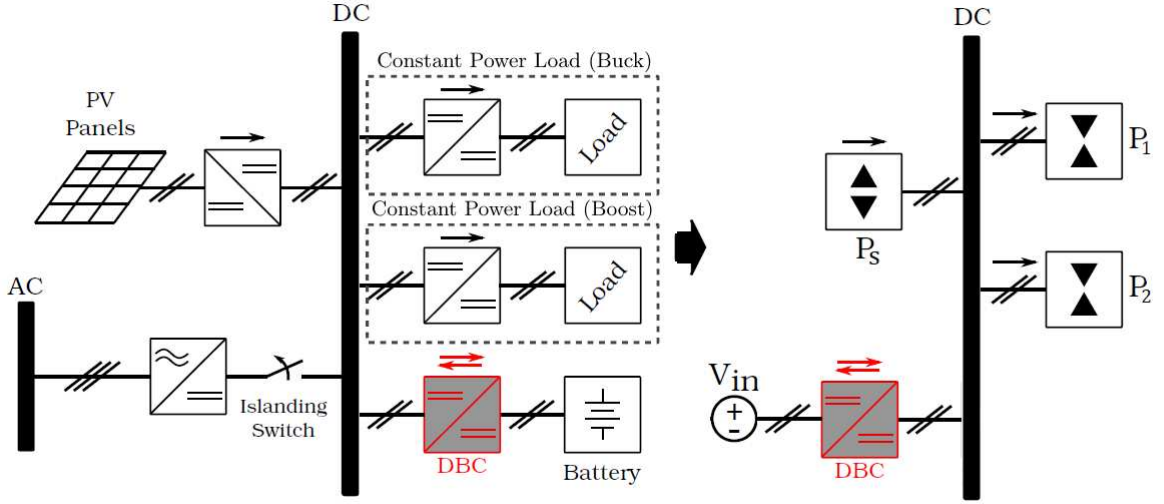


Figure 5.1: Block diagram of the studied DC microgrid. Simplified system diagram assuming that the loads are represented by CPLs and the PV source by a CPS. V_{in} is the battery voltage and DBC stands for the bidirectional power converter controlling the DC bus voltage.

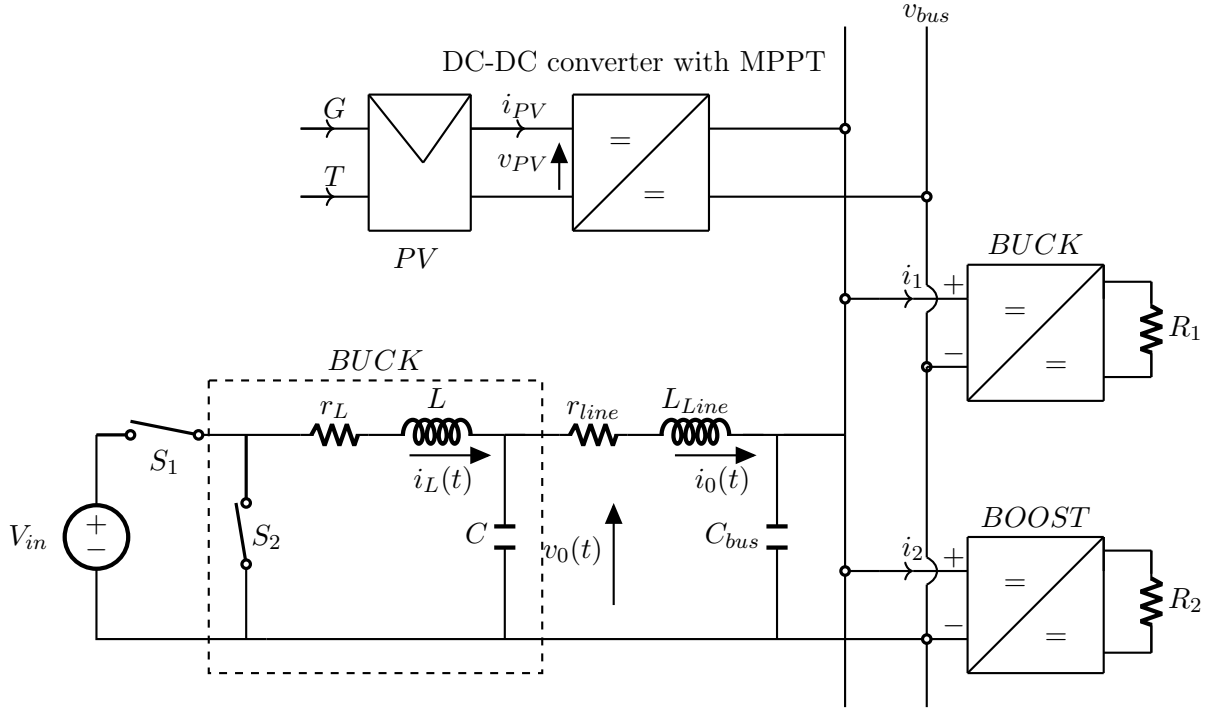
$$\begin{aligned}
L \frac{di_L}{dt} &= uV_{in} - r_L i_L - v_0, \\
C \frac{dv_0}{dt} &= i_L - i_0, \\
L_{line} \frac{di_0}{dt} &= v_0 - v_{bus} - i_0 r_{line}, \\
C_{bus} \frac{dv_{bus}}{dt} &= i_0 - (q_1 \xi_1(v_{bus}, V_{th1}) + q_2 \xi_2(v_{bus}, V_{th2})) + \frac{P_s}{v_0}, \\
\frac{dz_F}{dt} &= \omega_F (i_L - z_F),
\end{aligned} \tag{5.2.1}$$

where $q_i = \{0, 1\}$, with $i = 1, 2$. In system (5.2.1), $\xi_1(v_{bus}, V_{th1})$ is a CPL piecewise function of convorsor Buck defined by

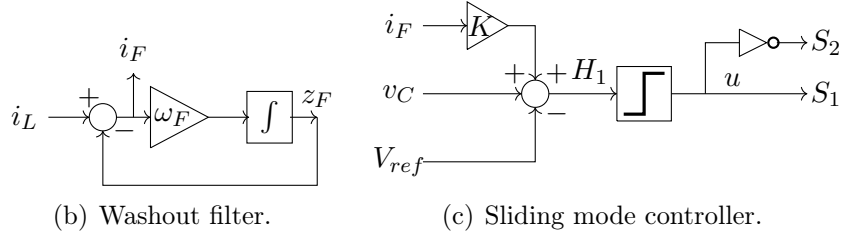
$$\xi_1(v_{bus}, V_{th1}) = \begin{cases} \frac{P_1}{v_{bus}}, & \text{if } v_{bus} \geq V_{th1}, \\ \frac{P_1 v_{bus}}{V_{th1}^2}, & \text{if } v_{bus} < V_{th1}, \end{cases}$$

and $\xi_2(v_{bus}, V_{th2})$ is a CPL piecewise function of convorsor Boost defined by

$$\xi_2(v_{bus}, V_{th2}) = \begin{cases} \frac{P_2}{v_{bus}}, & \text{if } v_{bus} \geq V_{th2}, \\ I_{th}, & \text{if } v_{bus} < V_{th2}, \end{cases}$$



(a) dc-dc buck converter connected to two load converters and a PV source converter.



(b) Washout filter.

(c) Sliding mode controller.

Figure 5.2: Basic topology of a dc-dc buck converter controlled by a sliding mode and washout filter control strategy, connected to two converters in parallel. The control function is defined as $u = \frac{1}{2}(1 - \text{sign}[H(i_L, v_C, z_F)])$. The filtered inductor current given by $i_F = i_L - z_F$ expresses the difference between the inductor current i_L and the filtered signal z_F .

where L , C , L_{line} , C_{bus} and r_{line} denotes the inductance of the capacitor, the voltage capacitor, the inductance of the bus, bus capacitor and the inductor resistance, respectively. Due to the complexity of the model in Figure 5.1, we will consider the battery as a constant value. The power consumed by the load (load parameter) is denoted by $P_{1,2} \in \mathbb{R}$ and $V_{th1,th2}$ are the voltage threshold. $i_L \in (-i_{max}, i_{max})$, for some $i_{max} > 0$, are the inductor current and $I_{th} = i_{max} = \frac{P_2}{V_{th2}}$. The output buck current is denoted by i_0 . Variable z_F denotes a filtered inductor current and $\omega_F \leq 1/\sqrt{LC}$ is the cut-off filter frequency. In Figure 5.2 the parameter G is the solar irradiation, T the temperature on the PV module of a DC-DC converter with maximum power point tracking (MPPT) and P_s represents a constant power source that is the PV+converter operating in MPPT

mode. The control law u is defined as

$$u = \frac{1}{2}(1 - \text{sign}[H_1(i_L, v_0, z_F)]), \quad (5.2.2)$$

where $u = 0$ means that switch S is off and $u = 1$ means that it is on. From this, the control surface is chosen as

$$H_1(i_L, v_0, z_F) = v_0 - v_0^* + K(i_L - z_F) = 0,$$

where $K > 0$ is the control parameter, which must be adjusted properly to ensure stability at least local stability of the desired operating point and $v_0 \approx v_0^* < V_{in}$ represents the reference voltage, that is, the desired voltage for the output value, with V_{in} denoting the source voltage.

It is a cumbersome problem to analyze all possible cases, therefore, in this chapter, we will focus our study analysis on the stability condition at the pseudo-equilibrium point of system (5.2.1) assuming $q_1 = q_2 = 1$, $L_{line} \cong 0$ and $r_{line} \cong 0$, consequently $v_0 = v_{bus}$. We define $C_e = C + C_{bus}$ as a capacitance equivalent to the voltage capacitor and the bus capacitor. The other cases remain open problems. Thus, the system of equations defined in (5.2.1) can be reduced to

$$\begin{aligned} L \frac{di_L}{dt} &= uV_{in} - r_L i_L - v_0, \\ C_e \frac{dv_0}{dt} &= i_L - (\xi_1(v_0, V_{th1}) + \xi_2(v_0, V_{th2})) + \frac{P_s}{v_0}, \\ \frac{dz_F}{dt} &= \omega_F(i_L - z_F), \end{aligned} \quad (5.2.3)$$

with

$$\xi_1(v_0, V_{th1}) = \begin{cases} \frac{P_1}{v_0}, & \text{if } v_0 \geq V_{th1}, \\ \frac{P_1 v_0}{V_{th1}^2}, & \text{if } v_0 < V_{th1}, \end{cases} \quad (5.2.4)$$

and

$$\xi_2(v_0, V_{th2}) = \begin{cases} \frac{P_2}{v_0}, & \text{if } v_0 \geq V_{th2}, \\ I_{th}, & \text{if } v_0 < V_{th2}. \end{cases}$$

System (5.2.3) is normalized by applying the change of variables and time given by Table 5.1 Then, we obtain the simplified system of the form

$$\begin{aligned} \dot{x} &= u - bx - y, \\ \dot{y} &= x - \xi_0(y) + \frac{d_3}{y}, \\ \dot{z} &= (1 - kb)x + (\omega - k)y - \xi_0(y) - \omega z - \omega y_r + ku + \frac{d_3}{y}, \end{aligned} \quad (5.2.5)$$

State and Time Variables	Parameters
$i_L = V_{in} \sqrt{\frac{C_e}{L}} x$	$v_r = V_{in} y_r$
$v_0 = V_{in} y$	$\omega_F = \frac{\omega}{\sqrt{LC_e}}$
$z_F = i_L + \frac{v_0 - v_r - V_{in} z}{K}$	$K = k \sqrt{\frac{L}{C_e}}$
$t = \sqrt{C_e L} \tau$	$P_1 = V_{in}^2 \sqrt{\frac{C_e}{L}} d_1$
	$P_2 = V_{in}^2 \sqrt{\frac{C_e}{L}} d_2$
	$P_s = V_{in}^2 \sqrt{\frac{C_e}{L}} d_3$
	$r_L = b \sqrt{\frac{L}{C_e}}$

Table 5.1: Normalized variable, parameters and time.

where $\xi_0(y) = \xi_1(y) + \xi_2(y)$, $\xi_1(y)$ is a normalized CPL piecewise function of the buck converter given by

$$\xi_1(y) = \begin{cases} \frac{d_1}{y}, & \text{if } y \geq y_{th1}, \\ \frac{d_1 y}{y_{th1}^2}, & \text{if } y < y_{th1}, \end{cases} \quad (5.2.6)$$

and $\xi_2(y)$ is a normalized CPL piecewise function of boost converter given by

$$\xi_2(y) = \begin{cases} \frac{d_2}{y}, & \text{if } y \geq y_{th2}, \\ \frac{d_2}{y_{th2}}, & \text{if } y < y_{th2}, \end{cases} \quad (5.2.7)$$

such that x , y and z are the normalized variables of the inductor current, capacitor voltage and filter, respectively, of the first buck converter. The normalized parameters $d_1 > 0$, $d_2 > 0$, $\omega \in (0, 1]$, $k > 0$, $b > 0$, y_{th1} , y_{th2} and y_r correspond to the CPL to buck converter, CPL to boost converter, inductor resistance, filter cut-off frequency, control parameter, inductor resistance, the voltage threshold of the capacitor voltage at CPL to the buck converter and CPL to the boost converter (respectively) and the reference voltage, respectively. We denoted $\mathbf{x} = (x, y, z) \in D$, where

$$D = \{\mathbf{x} \in \mathbb{R}^3 : x \in (-x_{max}, x_{max}), x_{max} > 0, y > 0, z \in \mathbb{R}\}.$$

From the normalized system (5.2.5), the control law given in equation (5.2.2), can be rewritten as $u = \frac{1}{2}[1 - \text{sign}(z)]$, so we redefine the planar switching surface as $h_1(\mathbf{x}) = z = 0$. In addition, there are two additional switching boundaries more, imposed by CPL of buck converter and boost converter, and given by $h_2(\mathbf{x}) = y - y_{th1} = 0$ and $h_3(\mathbf{x}) = y - y_{th2} = 0$, respectively. In this way, the switching boundaries are defined by

$$\begin{aligned} \Sigma_1 &= \{\mathbf{x} \in D : h_1(\mathbf{x}) = z = 0\}, \\ \Sigma_2 &= \{\mathbf{x} \in D : h_2(\mathbf{x}) = y - y_{th1} = 0\}, \\ \Sigma_3 &= \{\mathbf{x} \in D : h_3(\mathbf{x}) = y - y_{th2} = 0\}. \end{aligned} \quad (5.2.8)$$

We analyze the normalized system (5.2.5) in three cases, when $y_{th1} = y_{th2}$, $y_{th1} < y_{th2}$ and $y_{th1} > y_{th2}$.

5.3 Case study for $y_{th1} = y_{th2}$

Throughout this section we define $y_{th} = y_{th1} = y_{th2}$, $\Sigma_{\{2,3\}} = \Sigma_2 = \Sigma_3$ and $h_{\{2,3\}}(\mathbf{x}) = h_2(\mathbf{x}) = h_3(\mathbf{x})$, as shown in the Figure 5.3(a). Due to the switching boundaries defined in (5.2.8), the state space of the system is divided into four different regions, namely

$$\begin{aligned} D_1 &= \{\mathbf{x} \in D : h_1(\mathbf{x}) > 0 \text{ and } h(\mathbf{x}) > 0\}, \\ D_2 &= \{\mathbf{x} \in D : h_1(\mathbf{x}) > 0 \text{ and } h(\mathbf{x}) < 0\}, \\ D_3 &= \{\mathbf{x} \in D : h_1(\mathbf{x}) < 0 \text{ and } h(\mathbf{x}) < 0\}, \\ D_4 &= \{\mathbf{x} \in D : h_1(\mathbf{x}) < 0 \text{ and } h(\mathbf{x}) > 0\}. \end{aligned}$$

In each one of these regions there is a distinct vector field acting, then the system (5.2.5) is represented as a 3D-DPWS system of the form

$$\dot{\mathbf{x}} = \begin{cases} \mathbf{F}_1(\mathbf{x}), & \text{if } \mathbf{x} \in D_1, \\ \mathbf{F}_2(\mathbf{x}), & \text{if } \mathbf{x} \in D_2, \\ \mathbf{F}_3(\mathbf{x}), & \text{if } \mathbf{x} \in D_3, \\ \mathbf{F}_4(\mathbf{x}), & \text{if } \mathbf{x} \in D_4, \end{cases} \quad (5.3.1)$$

composed of the vector fields

$$\begin{aligned} \mathbf{F}_1(\mathbf{x}) &= \begin{bmatrix} -bx - y \\ x - \frac{d_1+d_2}{y} + \frac{d_3}{y} \\ f_{1,3} \end{bmatrix}, & \mathbf{F}_2(\mathbf{x}) &= \begin{bmatrix} -bx - y \\ x - \frac{d_1y+d_2y_{th}}{y_{th}^2} + \frac{d_3}{y} \\ f_{2,3} \end{bmatrix}, \\ \mathbf{F}_3(\mathbf{x}) &= \begin{bmatrix} 1 - bx - y \\ x - \frac{d_1y+d_2y_{th}}{y_{th}^2} + \frac{d_3}{y} \\ f_{2,3} + k \end{bmatrix} & \text{and } \mathbf{F}_4(\mathbf{x}) &= \begin{bmatrix} 1 - bx - y \\ x - \frac{d_1+d_2}{y} + \frac{d_3}{y} \\ f_{1,3} + k \end{bmatrix}, \end{aligned}$$

where

$$\begin{aligned} f_{1,3} &= (1 - kb)x + (\omega - k)y - \frac{d_1 + d_2}{y} - \omega z - \omega y_r + \frac{d_3}{y}, \\ f_{2,3} &= (1 - kb)x + (\omega - k)y - \frac{d_1y + d_2y_{th}}{y_{th}^2} - \omega z - \omega y_r + \frac{d_3}{y}. \end{aligned}$$

Proposition 5.3.1. *There is no sliding motion at the switching boundaries $\Sigma_{\{2,3\}}$ defined in (5.2.8).*

Proof. A straightforward calculus produces, $L_{\mathbf{F}_{1,3}(\mathbf{x})}h_{\{2,3\}}(\mathbf{x}) \cdot L_{\mathbf{F}_{2,4}(\mathbf{x})}h_{\{2,3\}}(\mathbf{x}) = (x - \xi_0(y) + \frac{d_3}{y})^2 \geq 0$, Therefore, $\Sigma_{\{2,3\}}$ is just a crossing boundary, containing a double tangency line at $x = \xi_0(y_{th}) - \frac{d_3}{y_{th}}$ and $y = y_{th}$, and $z \in \mathbb{R}$. \square

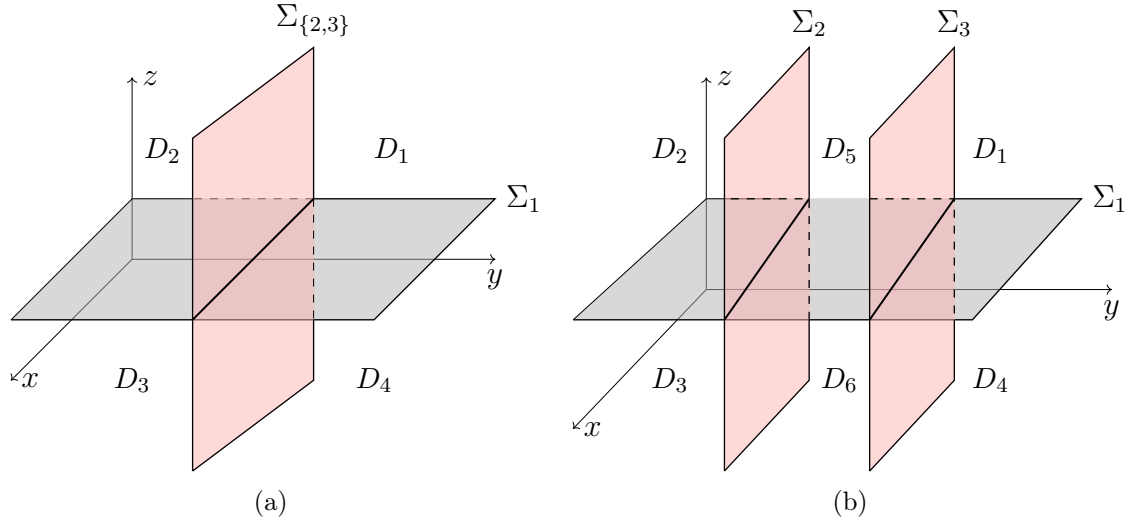


Figure 5.3: Show the switching boundaries defined in (5.2.8). Figure (a) shows the switching boundaries when $y_{th1} = y_{th2}$, defined by $\Sigma_{\{2,3\}}$. Figure (b) shows the switching boundaries when $y_{th1} \neq y_{th2}$.

In order to analyze the dynamic behavior of system (5.2.5) on the switching boundary Σ_1 , we calculate the sliding and crossing regions taking into account the discontinuity at $y = y_{th}$. For this we divided the study in cases as follows.

- (i) For $y \geq y_{th}$: the crossing and sliding regions are defined, respectively, by

$$\Sigma_{c_1} = \{\mathbf{x} \in \Sigma_1 : x > \bar{\alpha}(y) \text{ or } x > \underline{\alpha}(y)\}, \quad (5.3.2)$$

$$\Sigma_{s_1} = \{\mathbf{x} \in \Sigma_1 : \bar{\alpha}(y) < x < \underline{\alpha}(y)\}, \quad (5.3.3)$$

where

$$\bar{\alpha}(y) = \frac{1}{(1 - kb)y} (d_1 + d_2 - d_3 + (\omega(z - y) + ky)y + \omega y_r),$$

$$\underline{\alpha}(y) = \frac{1}{(1 - kb)y} (d_1 + d_2 - d_3 + (\omega(z - y) + k(y - 1))y + \omega y_r).$$

- (ii) For $y < y_{th}$: the crossing and sliding regions are defined by

$$\Sigma_{c_2} = \{\mathbf{x} \in \Sigma_1 : x > \bar{\beta}(y) \text{ or } x > \underline{\beta}(y)\}, \quad (5.3.4)$$

$$\Sigma_{s_2} = \{\mathbf{x} \in \Sigma_1 : \bar{\beta}(y) < x < \underline{\beta}(y)\}, \quad (5.3.5)$$

where

$$\bar{\beta}(y) = \frac{1}{(1 - kb)} \left(\frac{d_1 y + d_2 y_{th}}{y_{th}^2} - \frac{d_3}{y} + \omega(y_r - y) + ky + \omega z \right),$$

$$\underline{\beta}(y) = \frac{1}{(1 - kb)} \left(\frac{d_1 y + d_2 y_{th}}{y_{th}^2} - \frac{d_3}{y} + \omega(y_r - y) + k(y - 1) + \omega z \right).$$

5.3.1 Regular equilibria and stability

In what follows, we analyze the equilibria of the vector fields $\mathbf{F}_i(\mathbf{x})$, for $i = 1, 2, 3, 4$ and its stability considering only the dynamics with respect to the variables (x, y) , since that the first and second component of the vector fields mentioned above are independent of the dynamics in their third component z , whose dynamic is stable the associated eigenvalue is $-\omega < 0$. Thus, we just need to consider the reduced linearization Jacobian matrix given by

$$A = \begin{bmatrix} -b & -1 \\ 1 & -\left(\xi'_0(y) + \frac{d_3}{y^2}\right) \end{bmatrix}. \quad (5.3.6)$$

- (i) $\mathbf{F}_1(\mathbf{x})$ has no equilibrium point for $d_1 > 0$ and $d_2 > 0$.
(ii) $\mathbf{F}_2(\mathbf{x})$ has an equilibrium point, given by

$$\bar{\mathbf{x}}_2^\pm = \left(\frac{(d_2 \pm \gamma/\sqrt{b})y_{th}}{2(bd_1 + y_{th}^2)}, \frac{-bd_2y_{th} \mp y_{th}\gamma\sqrt{b}}{bd_1 + y_{th}^2}, \frac{-\left(2bd_1y_r + bd_2y_{th} + 2y_ry_{th}^2 \pm y_{th}\gamma\sqrt{b}\right)}{2(bd_1 + y_{th}^2)} \right).$$

where $\gamma = \sqrt{bd_2^2 + 4d_1d_3 + 4d_3y_{th}^2}$. Equilibrium $\bar{\mathbf{x}}_2^+$ is virtual because $h_1(\bar{\mathbf{x}}_2^+) < 0$. In other hand, $\bar{\mathbf{x}}_2^-$ is real for $y_r < \frac{(\gamma\sqrt{b}-bd_2)y_{th}}{2bd_1+2y_{th}^2}$ ($h_1(\bar{\mathbf{x}}_2^-) > 0$) and $d_3 < \frac{(bd_1+y_{th}^2+bd_2)^2-b^2d_2^2}{4bd_1+4by_{th}^2}$ ($h_{\{2,3\}}(\bar{\mathbf{x}}_2^-) < 0$). Moreover, this point is a boundary equilibrium point if

- $y_r = \frac{(\gamma\sqrt{b}-bd_2)y_{th}}{2bd_1+2y_{th}^2}$ ($h_1(\bar{\mathbf{x}}_2^-) = 0$) and $d_3 = \frac{(bd_1+y_{th}^2+bd_2)^2-b^2d_2^2}{4bd_1+4by_{th}^2}$ ($h_{\{2,3\}}(\bar{\mathbf{x}}_2^-) = 0$),
- $y_r = \frac{(\gamma\sqrt{b}-bd_2)y_{th}}{2bd_1+2y_{th}^2}$ ($h_1(\bar{\mathbf{x}}_2^-) = 0$) and $d_3 > \frac{(bd_1+y_{th}^2+bd_2)^2-b^2d_2^2}{4bd_1+4by_{th}^2}$ ($h_{\{2,3\}}(\bar{\mathbf{x}}_2^-) < 0$),
- $y_r > \frac{(\gamma\sqrt{b}-bd_2)y_{th}}{2bd_1+2y_{th}^2}$ ($h_1(\bar{\mathbf{x}}_2^-) > 0$) and $d_3 = \frac{(bd_1+y_{th}^2+bd_2)^2-b^2d_2^2}{4bd_1+4by_{th}^2}$ ($h_{\{2,3\}}(\bar{\mathbf{x}}_2^-) = 0$).

The determinant and trace are given by

$$\begin{aligned} Det[A(\bar{\mathbf{x}}_2^\pm)] &= \frac{bd_2^2 + 4bd_1d_3 + 4d_3y_{th}^2 \mp d_2\gamma\sqrt{b}}{2d_3y_{th}^2}, \\ Tr[A(\bar{\mathbf{x}}_2^\pm)] &= -b - \frac{d_1}{y_{th}^2} - \frac{4d_3(bd_1 + y_{th}^2)^2}{(bd_2y_{th} \pm y_{th}\gamma\sqrt{b})^2}. \end{aligned}$$

Equilibrium $\bar{\mathbf{x}}_2^-$ is stable because $Det[A(\bar{\mathbf{x}}_2^-)] > 0$ and $Tr[A(\bar{\mathbf{x}}_2^-)] < 0$ for $\frac{-bd_2^2}{4(bd_1+y_{th}^2)} < d_3 < \frac{-b^2d_2^2(d_1+by_{th}^2)}{(2bd_1+y_{th}^2+b^2y_{th}^2)^2}$.

- (iii) $\mathbf{F}_3(\mathbf{x})$ has an equilibrium point, given by

$$\bar{\mathbf{x}}_3^\pm = \left(\frac{1}{b} + \frac{bd_2y_{th} - y_{th}^2 \pm \beta}{2b(bd_1 + y_{th}^2)}, \frac{y_{th}^2 - bd_2y_{th} \mp \beta}{2(bd_1 + y_{th}^2)}, -y_r - \frac{bd_2 + y_{th} - y_{th}^2 \pm \beta}{2(bd_1 + y_{th}^2)} \right).$$

where $\beta = \sqrt{4bd_3y_{th}^2(bd_1 + y_{th}^2) + (y_{th}^2 - bd_2y_{th})^2}$. Equilibrium $\bar{\mathbf{x}}_3^+$ is real for $y_r > -\frac{bd_2+y_{th}-y_{th}^2+\beta}{2(bd_1+y_{th}^2)}$ ($h_1(\bar{\mathbf{x}}_3^+) < 0$) and $d_1+d_2-d_3 < \frac{(1-y_{th})y_{th}}{b}$ ($h_{\{2,3\}}(\bar{\mathbf{x}}_3^+) < 0$). Moreover, this point is a boundary equilibrium point if

- $y_r = -\frac{bd_2+y_{th}-y_{th}^2+\beta}{2(bd_1+y_{th}^2)} (h_1(\bar{\mathbf{x}}_3^+) = 0)$ and $d_1+d_2-d_3 = \frac{(1-y_{th})y_{th}}{b} (h_{\{2,3\}}(\bar{\mathbf{x}}_3^+) = 0)$,
- $y_r = -\frac{bd_2+y_{th}-y_{th}^2+\beta}{2(bd_1+y_{th}^2)} (h_1(\bar{\mathbf{x}}_3^+) = 0)$ and $d_1+d_2-d_3 < \frac{(1-y_{th})y_{th}}{b} (h_{\{2,3\}}(\bar{\mathbf{x}}_3^+) < 0)$,
- $y_r > -\frac{bd_2+y_{th}-y_{th}^2+\beta}{2(bd_1+y_{th}^2)} (h_1(\bar{\mathbf{x}}_3^+) < 0)$ and $d_1+d_2-d_3 = \frac{(1-y_{th})y_{th}}{b} (h_{\{2,3\}}(\bar{\mathbf{x}}_3^+) = 0)$.

In other hand, $\bar{\mathbf{x}}_3^-$ is real for $y_r > -\frac{bd_2+y_{th}-y_{th}^2-\beta}{2(bd_1+y_{th}^2)} (h_1(\bar{\mathbf{x}}_3^-) < 0)$ and $d_1+d_2-d_3 > \frac{(1-y_{th})y_{th}}{b} (h_{\{2,3\}}(\bar{\mathbf{x}}_3^-) < 0)$. Moreover, this point is a boundary equilibrium point if

- $y_r = -\frac{bd_2+y_{th}-y_{th}^2-\beta}{2(bd_1+y_{th}^2)} (h_1(\bar{\mathbf{x}}_3^-) = 0)$ and $d_1+d_2-d_3 = \frac{(1-y_{th})y_{th}}{b} (h_{\{2,3\}}(\bar{\mathbf{x}}_3^-) = 0)$,
- $y_r = -\frac{bd_2+y_{th}-y_{th}^2-\beta}{2(bd_1+y_{th}^2)} (h_1(\bar{\mathbf{x}}_3^-) = 0)$ and $d_1+d_2-d_3 > \frac{(1-y_{th})y_{th}}{b} (h_{\{2,3\}}(\bar{\mathbf{x}}_3^-) < 0)$,
- $y_r > -\frac{bd_2+y_{th}-y_{th}^2-\beta}{2(bd_1+y_{th}^2)} (h_1(\bar{\mathbf{x}}_3^-) < 0)$ and $d_1+d_2-d_3 = \frac{(1-y_{th})y_{th}}{b} (h_{\{2,3\}}(\bar{\mathbf{x}}_3^-) = 0)$.

The determinant and trace are given by

$$Det[A(\bar{\mathbf{x}}_3^\pm)] = \frac{-2(bd_2 - y_{th})(bd_1 + y_{th}^2)}{y_{th} \left(y_{th}^2 - bd_2 y_{th} \mp \sqrt{y_{th}^2 (b^2(d_2^2 + 4d_1d_3) + y_{th}^2 - 2by_{th}(d_2 - 2d_3y_{th}))} \right)},$$

$$Tr[A(\bar{\mathbf{x}}_3^\pm)] = -b - \frac{d_1}{y_{th}^2} + \frac{4d_3(bd_1 + y_{th}^2)^2}{\left(\pm bd_2 y_{th} \mp y_{th}^2 + \sqrt{y_{th}^2 (b^2(d_2^2 + 4d_1d_3) + y_{th}^2 - 2by_{th}(d_2 - 2d_3y_{th}))} \right)^2}.$$

Equilibrium $\bar{\mathbf{x}}_3^+$ is a stable point because $Det[A(\bar{\mathbf{x}}_3^+)] > 0$ and $Tr[A(\bar{\mathbf{x}}_3^+)] < 0$ for $d_1 < \frac{-y_{th}^2}{b}$ and $d_3 < \frac{(bd_2 - y_{th})^2(d_1 + by_{th}^2)}{(b^2 - 1)^2 y_{th}^4}$. In other hand, $\bar{\mathbf{x}}_3^-$ is a saddle point, since $Det[A(\bar{\mathbf{x}}_3^-)] < 0$ for all $0 < d_1 < \frac{-y_{th}}{b}$.

(iv) $\mathbf{F}_4(\mathbf{x})$ has an equilibrium point, given by

$$\bar{\mathbf{x}}_4^\pm = \left(\frac{1 \pm \gamma}{2b}, \frac{1 \mp \gamma}{2}, \frac{1 \mp \gamma - 2y_r}{2} \right),$$

with $\gamma = \sqrt{1 - 4b(d_1 + d_2 - d_3)}$. Equilibrium $\bar{\mathbf{x}}_4^+$ is real for $y_r > \frac{1-\gamma}{2} (h_1(\bar{\mathbf{x}}_4^+) < 0)$ and $y_{th} < \frac{1-\gamma}{2} (h(\bar{\mathbf{x}}_4^+) > 0)$. Otherwise, it is virtual. Moreover, $\bar{\mathbf{x}}_4^+$ becomes a boundary equilibrium point if

- $y_r = \frac{1-\gamma}{2} (h_1(\bar{\mathbf{x}}_4^+) = 0)$ and $y_{th} < \frac{1-\gamma}{2} (h(\bar{\mathbf{x}}_4^+) > 0)$,
- $y_r > \frac{1-\gamma}{2} (h_1(\bar{\mathbf{x}}_4^+) < 0)$ and $y_{th} = \frac{1-\gamma}{2} (h(\bar{\mathbf{x}}_4^+) = 0)$,
- $y_r = \frac{1-\gamma}{2} (h_1(\bar{\mathbf{x}}_4^+) = 0)$ or $y_{th} = \frac{1-\gamma}{2} (h(\bar{\mathbf{x}}_4^+) = 0)$.

Analogously, the equilibrium $\bar{\mathbf{x}}_4^-$ is real for $y_r > \frac{1+\gamma}{2} (h_1(\bar{\mathbf{x}}_4^-) < 0)$ and $y_{th} < \frac{1+\gamma}{2} (h(\bar{\mathbf{x}}_4^-) > 0)$. Furthermore, it becomes a boundary equilibrium point at if

- $y_r = \frac{1+\gamma}{2} (h_1(\bar{\mathbf{x}}_4^-) = 0)$ and $y_{th} < \frac{1+\gamma}{2} (h(\bar{\mathbf{x}}_4^-) > 0)$,

- $y_r > \frac{1+\gamma}{2}$ ($h_1(\bar{\mathbf{x}}_4^-) < 0$) and $y_{th} = \frac{1+\gamma}{2}$ ($h(\bar{\mathbf{x}}_4^-) = 0$),
- $y_r = \frac{1+\gamma}{2}$ ($h_1(\bar{\mathbf{x}}_4^-) = 0$) or $y_{th} = \frac{1+\gamma}{2}$ ($h(\bar{\mathbf{x}}_4^-) = 0$).

The determinant and trace are given by

$$Det[A(\bar{\mathbf{x}}_4^\pm)] = \frac{2 - 4b(d_1 + d_2 - d_3) \mp \gamma}{(\gamma \mp 1)^2} \quad \text{and} \quad Tr[A(\bar{\mathbf{x}}_4^\pm)] = -b + \frac{4b(d_1 + d_2 - d_3)}{(\gamma \mp 1)^2}.$$

Equilibrium $\bar{\mathbf{x}}_4^+$ is a stable point because $Det[A(\bar{\mathbf{x}}_4^+)] > 0$ and $Tr[A(\bar{\mathbf{x}}_4^+)] < 0$ for $\frac{1}{4b} < d_1 + d_2 - d_3 < \frac{b}{(1+b^2)^2}$. In other hand, $\bar{\mathbf{x}}_4^-$ is a saddle point, since $Det[A(\bar{\mathbf{x}}_4^-)] < 0$ for all $0 < d_1 + d_2 - d_3 < \frac{1}{4b}$.

5.3.2 Sliding vector field and pseudo-equilibria

Sliding vector field associated to the dynamical system (5.2.3) is defined as

$$\mathbf{F}_s(\mathbf{x}) = \begin{bmatrix} \frac{\omega(y_r - y) - x + \xi_0(y) + \omega z}{k} - \frac{d_3}{y} \\ x - \xi_0(y) + \frac{d_3}{y} \\ 0 \end{bmatrix}, \quad (5.3.7)$$

where $(x, y, z) \in \Sigma_s \subset \Sigma_1$. The pseudo equilibrium points are given by $\tilde{\mathbf{x}} = (\xi_0(y), y, 0)$ that depend of values of $\xi_0(y)$, i.e, the discontinuity at $y = y_{th}$. So, there are two pseudo-equilibrium,

$$\tilde{\mathbf{x}}_1 = \left(\frac{d_1 + d_2 - d_3}{y_r}, y_r, 0 \right) \quad \text{and} \quad \tilde{\mathbf{x}}_2 = \left(\frac{d_1 y_r + d_2 y_{th}}{y_{th}^2} - \frac{d_3}{y_r}, y_r, 0 \right),$$

for $y \geq y_{th}$ and $y < y_{th}$, respectively. By hypothesis $y_r > y_{th}$, then the pseudo-equilibrium $\tilde{\mathbf{x}}_2$ is always virtual, so the stability analysis will be just for the pseudo-equilibrium point $\tilde{\mathbf{x}}_1$.

Since the first and second components of $\mathbf{F}_s(\mathbf{x})$ mentioned above are decoupled from the third component, then we only need to consider the reduced Jacobian matrix given by

$$A = \begin{bmatrix} -\frac{1}{k} & -\frac{(\omega - \xi_0'(y))}{k} + \frac{d_3}{k y_r^2} \\ 1 & -\xi_0'(y) - \frac{d_3}{y_r^2} \end{bmatrix}.$$

Pseudo-equilibrium $\tilde{\mathbf{x}}_1$ is stable because $Det[A(\tilde{\mathbf{x}}_1)] = \frac{\omega}{k} > 0$ and $Tr[A(\tilde{\mathbf{x}}_1)] = \frac{k(d_1 + d_2 - d_3) - y_r^2}{k y_r^2} < 0$ for $0 < k < \frac{y_r^2}{d_1 + d_2 - d_3}$ with $d_1 + d_2 \neq d_3$, otherwise is unstable. Moreover, the pseudo-equilibrium $\tilde{\mathbf{x}}_1$ is real (located in the sliding region) whenever $d_1 + d_2 - d_3 < \frac{(1 - y_r) y_r}{b}$.

Proposition 5.3.2. *Consider the vector field \mathbf{F}_s defined in (5.3.7). For $d_1 + d_2 = \frac{y_r^2}{k} + d_3$ a subcritical Hopf bifurcation occurs at $\tilde{\mathbf{x}}_1$.*

Proof. From the determinant and trace at $\tilde{\mathbf{x}}_1$, we conclude the following

$$\begin{aligned}
\text{Det}[A(\tilde{\mathbf{x}}_1)]|_{d_1+d_2=\frac{y_r^2}{k}+d_3} &= \frac{\omega}{k} > 0, \\
\text{Tr}[A(\tilde{\mathbf{x}}_1)]|_{d_1+d_2=\frac{y_r^2}{k}+d_3} &= 0 \\
\frac{d}{d(d_1+d_2)}\text{Tr}[A(\tilde{\mathbf{x}}_1)]|_{d_1+d_2=\frac{y_r^2}{k}+d_3} &= \frac{1}{y_r^2} \neq 0.
\end{aligned}$$

Thus, we show the necessary condition to obtain Hopf bifurcation. Notice that, the x and y components are decoupled from z component in (5.3.7). Now, desingularizing the vector field $\mathbf{F}_s|_{\xi_0(y)=\frac{d_1+d_2}{y}}$ (see (5.3.7)) and considering $\mathbf{F}_{ds} = ky\mathbf{F}_s|_{\xi_0(y)=\frac{d_1+d_2}{y}}$, the differential equations that describe $\mathbf{F}_{ds}(x, y)$ are expressed as

$$\begin{aligned}
\dot{x} &= \omega(y_r - y)y - xy + d_1 + d_2 - d_3, \\
\dot{y} &= k(xy - (d_1 + d_2) + d_3),
\end{aligned} \tag{5.3.8}$$

then, translating the pseudo-equilibrium $\tilde{\mathbf{x}}_1$ to the origin in (5.3.8) with $d_1 + d_2 = \frac{y_r^2}{k} + d_3$, we get

$$\begin{aligned}
\dot{x} &= -\omega y^2 - xy - y_x r - \left(\frac{y_r^2}{k} + \omega y_r\right)y, \\
\dot{y} &= ky_r x + kxy + y_r y,
\end{aligned} \tag{5.3.9}$$

according to [19]-page 243, the *first Lyapunov coefficient* of the vector field \mathbf{F}_s can be calculated, and it is given by

$$l_1^s = \frac{3\pi k^2}{4\sqrt{k\omega}(1+k\omega)y_r^2} > 0.$$

Hence, we have an unstable limit cycle and so, this Hopf bifurcation is subcritical. \square

5.3.3 Boundary equilibrium bifurcation

Now we are going to show the occurrence of BEBs in system 5.3.1. By hypothesis $y_r > y_{th}$, in addition to that taking $z = 0$, $y = y_r$ and solving the equations $\mathbf{F}_i(x, y_r, 0, d) = \mathbf{0}$ with $d = d_1 + d_2 - d_3$, for $i = 1, 2, 3, 4$ respect to (x, y, z, d) , we get a boundary equilibrium

$$(\bar{\mathbf{x}}_{b_4}, d_{B_4}) = \left(\frac{1 - y_r}{b}, y_r, 0, \frac{(1 - y_r)y_r}{b} \right), \tag{5.3.10}$$

where $\bar{\mathbf{x}}_{b_4}$ denote the boundary equilibrium related to the vector field $\mathbf{F}_4(\mathbf{x})$ and appearing for the critical value $d_1 + d_2 - d_3 = d_{B_4}$ of the load parameter. Notice that, The boundary equilibrium related to the vector fields \mathbf{F}_i , for $i = 1, 2, 3$ are left out of our study, since by hypothesis $d_1 > 0$, $d_2 > 0$, $d_3 > 0$ and $y_r > y_{th}$. Therefore, the BEB occurs just at the point $\bar{\mathbf{x}}_{b_4}$.

In Figure 5.5 a two-parameter bifurcation study is presented. The power load parameter (d_1) and the control parameter (k). The black line indicates the occurrence of BEB_{NF} involving the equilibria $\bar{\mathbf{x}}_4^+$ and $\tilde{\mathbf{x}}_1$, of the vector fields \mathbf{F}_4 and \mathbf{F}_s , respectively. The green line refers to a saddle-node bifurcation (SN_e) at $d_1 = d_3 - d_2 + 1/4b$. The blue

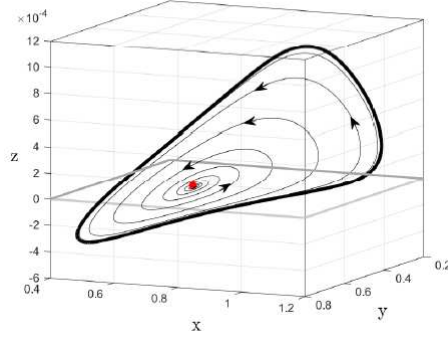


Figure 5.4: Simulation results of system (5.3.1) with parameters $b = 0.006742$, $k = 0.6742$, $d_2 = d_3 = 0.02575$, $y_{th1} = 0.0416667$, $y_{th2} = 0.0833333$ and $y_r = 0.5$ showing the unstable limit cycle in black color; the point of pseudo equilibrium is represented by red.

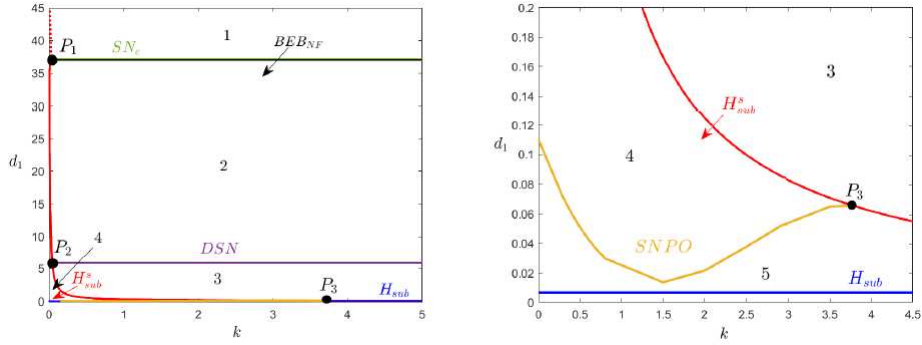


Figure 5.5: Bifurcation set in (k, d_1) -plane showing the main local bifurcations assuming $b = 0.006742$, $k = 0.6742$, $d_2 = d_3 = 0.02575$, $y_{th1} = 0.0416667$, $y_{th2} = 0.0833333$, $\omega = 0.461288$ and $y_r = 0.5$.

straight line segment refers to subcritical Hopf bifurcation (H_{sub}) at $d_1 = d_3 - d_2 + b/(1+b^2)^2$ of the equilibrium \bar{x}_4^- . The red parabolic curve segment indicates a subcritical Hopf bifurcation (H_{sub}^s) at $d_1 = d_3 - d_2 + y_r^2/k$ of the pseudo-equilibrium \tilde{x}_1 and the purple line refers to a discontinuous saddle-node (DSN) at $d_1 = d_3 - d_2 + (1 - y_{th1})y_{th1}/b$. The point P_i with $i = 1, 2$ indicates the codimension-two bifurcations occur simultaneously, but not necessarily involving the same equilibrium point. In P_1 the subcritical Hopf bifurcation (H_{sub}^s) occurs together to BEB_{NF} and, in P_2 the DSN occurs concomitantly to H_{sub}^s .

5.4 Case study for $y_{th1} < y_{th2}$

Due to the switching boundaries defined in (5.2.8) and assuming that $y_{th1} < y_{th2}$, as shown in the Figure 5.3(b). Observe that in this case the state space of the system is divided into six different regions, namely

$$\begin{aligned}
D_1 &= \{\mathbf{x} \in D : h_1(\mathbf{x}) > 0, h_2(\mathbf{x}) > 0 \text{ and } h_3(\mathbf{x}) > 0\}, \\
D_2 &= \{\mathbf{x} \in D : h_1(\mathbf{x}) > 0, h_2(\mathbf{x}) < 0 \text{ and } h_3(\mathbf{x}) < 0\}, \\
D_3 &= \{\mathbf{x} \in D : h_1(\mathbf{x}) < 0, h_2(\mathbf{x}) < 0 \text{ and } h_3(\mathbf{x}) < 0\}, \\
D_4 &= \{\mathbf{x} \in D : h_1(\mathbf{x}) < 0, h_2(\mathbf{x}) > 0 \text{ and } h_3(\mathbf{x}) > 0\}, \\
D_5 &= \{\mathbf{x} \in D : h_1(\mathbf{x}) > 0, h_2(\mathbf{x}) > 0 \text{ and } h_3(\mathbf{x}) < 0\}, \\
D_6 &= \{\mathbf{x} \in D : h_1(\mathbf{x}) < 0, h_2(\mathbf{x}) > 0 \text{ and } h_3(\mathbf{x}) < 0\},
\end{aligned}$$

such that $\mathbf{x} = (x, y, z) \in D$. In each one of these regions there is a distinct vector field acting, then the system (5.2.5) is represented as a 3D-DPWS system of the form

$$\dot{\mathbf{x}} = \begin{cases} \mathbf{F}_1(\mathbf{x}), & \text{if } \mathbf{x} \in D_1, \\ \mathbf{F}_2(\mathbf{x}), & \text{if } \mathbf{x} \in D_2, \\ \mathbf{F}_3(\mathbf{x}), & \text{if } \mathbf{x} \in D_3, \\ \mathbf{F}_4(\mathbf{x}), & \text{if } \mathbf{x} \in D_4, \\ \mathbf{F}_5(\mathbf{x}), & \text{if } \mathbf{x} \in D_5, \\ \mathbf{F}_6(\mathbf{x}), & \text{if } \mathbf{x} \in D_6, \end{cases} \quad (5.4.1)$$

composed by the vector fields

$$\begin{aligned}
\mathbf{F}_1(\mathbf{x}) &= \begin{bmatrix} -bx - y \\ x - \frac{d_1+d_2}{y} + \frac{d_3}{y} \\ f_{1,3} \end{bmatrix}, & \mathbf{F}_2(\mathbf{x}) &= \begin{bmatrix} -bx - y \\ x - \frac{d_1y}{y_{th1}^2} - \frac{d_2}{y_{th2}} + \frac{d_3}{y} \\ f_{2,3} \end{bmatrix}, \\
\mathbf{F}_3(\mathbf{x}) &= \begin{bmatrix} 1 - bx - y \\ x - \frac{d_1y}{y_{th1}^2} - \frac{d_2}{y_{th2}} + \frac{d_3}{y} \\ f_{2,3} + k \end{bmatrix} & \mathbf{F}_4(\mathbf{x}) &= \begin{bmatrix} 1 - bx - y \\ x - \frac{d_1+d_2}{y} + \frac{d_3}{y} \\ f_{1,3} + k \end{bmatrix}, \\
\mathbf{F}_5(\mathbf{x}) &= \begin{bmatrix} -bx - y \\ x - \frac{d_2}{y_{th2}} - \frac{d_1}{y} + \frac{d_3}{y} \\ f_{3,3} \end{bmatrix} & \text{and } \mathbf{F}_6(\mathbf{x}) &= \begin{bmatrix} 1 - bx - y \\ x - \frac{d_2}{y_{th2}} - \frac{d_1}{y} + \frac{d_3}{y} \\ f_{3,3} + k \end{bmatrix},
\end{aligned}$$

where

$$\begin{aligned}
f_{1,3} &= (1 - kb)x + (\omega - k)y - \frac{d_1 + d_2}{y} + \frac{d_3}{y} - \omega z - \omega y_r, \\
f_{2,3} &= (1 - kb)x + (\omega - k)y - \frac{d_1y}{y_{th1}^2} - \frac{d_2}{y_{th2}} + \frac{d_3}{y} - \omega z - \omega y_r, \\
f_{3,3} &= (1 - kb)x + (\omega - k)y - \frac{d_2}{y_{th2}} - \frac{d_1}{y} + \frac{d_3}{y} - \omega z - \omega y_r.
\end{aligned}$$

Proposition 5.4.1. *There are no sliding motion at the switching boundaries Σ_2 and Σ_3 defined in (5.2.8).*

Proof. A straightforward calculus produces, $L_{\mathbf{F}_{2,3}(\mathbf{x})}h_2(\mathbf{x}) \cdot L_{\mathbf{F}_{5,6}(\mathbf{x})}h_2(\mathbf{x}) = (x - \xi_0(y) + \frac{d_3}{y})^2 \geq 0$ and $L_{\mathbf{F}_{1,4}(\mathbf{x})}h_3(\mathbf{x}) \cdot L_{\mathbf{F}_{5,6}(\mathbf{x})}h_3(\mathbf{x}) = (x - \xi_0(y) + \frac{d_3}{y})^2 \geq 0$. Therefore, Σ_2 and Σ_3 is just a crossing boundary. Containing a double tangency line at $x = \xi_0(y_{th}) - \frac{d_3}{y_{th}}$ and $y = y_{th}$, and $z \in \mathbb{R}$. \square

In order to analyze the dynamic behavior of system (5.2.5) on the switching boundary Σ_1 , we calculate the sliding and crossing regions taking into account the discontinuity at $y = y_{th1}$ and $y = y_{th2}$, for this we divided the study in cases as follows.

- (i) For $y \geq y_{th2}$, the crossing and sliding regions are defined by Σ_{c_1} and Σ_{s_1} as defined in (5.3.2) and (5.3.3), respectively.
- (ii) For $y_{th1} \leq y < y_{th2}$, the crossing and sliding regions are defined as follows

$$\Sigma_{c_3} = \{ \mathbf{x} \in \Sigma_1 : x > \bar{\rho}(y) \text{ or } x > \underline{\rho}(y) \}, \quad (5.4.2)$$

$$\Sigma_{s_3} = \{ \mathbf{x} \in \Sigma_1 : \bar{\rho}(y) < x < \underline{\rho}(y) \}, \quad (5.4.3)$$

where

$$\bar{\rho}(y) = \frac{1}{(1 - kb)} \left(\frac{d_1}{y} + \frac{d_2}{y_{th2}} - \frac{d_3}{y} + ky + \omega(y_r - y)y + \omega z \right),$$

$$\underline{\rho}(y) = \frac{1}{(1 - kb)} \left(\frac{d_1}{y} + \frac{d_2}{y_{th2}} - \frac{d_3}{y} + k(y - 1)y + \omega(y_r - y) + \omega z \right).$$

- (iii) For $y < y_{th1}$, the crossing and sliding regions are defined as follows

$$\Sigma_{c_4} = \{ \mathbf{x} \in \Sigma_1 : x > \bar{\varpi}(y) \text{ or } x > \underline{\varpi}(y) \}, \quad (5.4.4)$$

$$\Sigma_{s_4} = \{ \mathbf{x} \in \Sigma_1 : \bar{\varpi}(y) < x < \underline{\varpi}(y) \}, \quad (5.4.5)$$

where

$$\bar{\varpi}(y) = \frac{1}{(1 - kb)} \left(\frac{d_1 y}{y_{th1}^2} + \frac{d_2}{y_{th2}} - \frac{d_3}{y} + ky + \omega(y_r - y) + \omega z \right),$$

$$\underline{\varpi}(y) = \frac{1}{(1 - kb)} \left(\frac{d_1 y}{y_{th1}^2} + \frac{d_2}{y_{th2}} - \frac{d_3}{y} + k(y - 1)y + \omega(y_r - y) + \omega z \right).$$

5.4.1 Regular equilibria and stability

As we mentioned in Subsection 5.3.1, the first and second component of the vector fields $\mathbf{F}_i(\mathbf{x})$ ($i = 1, 2, 3, 4, 5, 6$) are independent of the dynamic in their third component z , whose dynamic is stable the associated eigenvalue is $-\omega < 0$. Thus, we just need to consider the reduced linearization Jacobian matrix as defined in (5.3.6). Then, we will analyze the equilibria of the vector fields $\mathbf{F}_i(\mathbf{x})$ for $i = 1, 2, 3, 4, 5, 6$ and its stabilities considering only the dynamics with respect to the variables (x, y) .

- (i) $\mathbf{F}_1(\mathbf{x})$ has no equilibrium point for $d_1 > 0$ and $d_2 > 0$.
- (ii) $\mathbf{F}_2(\mathbf{x})$ has an equilibrium point, given by

$$\bar{\mathbf{x}}_2^\pm = \left(\frac{d_2 y_{th1}^2 \pm y_{th1} \rho / \sqrt{b}}{2(bd_1 + y_{th1}^2) y_{th2}}, \frac{-bd_2 y_{th1}^2 \mp y_{th1} \rho \sqrt{b}}{2(bd_1 + y_{th1}^2) y_{th2}}, \frac{-bd_2 y_{th1}^2 - 2bd_1 y_r y_{th2} - 2y_r y_{th1}^2 y_{th2} \mp y_{th1} \rho}{2(bd_1 + y_{th1}^2) y_{th2}} \right),$$

where $\rho = \sqrt{bd_2^2 y_{th1}^2 + 4d_3(bd_1 + y_{th1}^2)y_{th2}^2}$. Equilibrium $\bar{\mathbf{x}}_2^+$ is virtual because $h_1(\bar{\mathbf{x}}_2^+) < 0$. Equilibrium $\bar{\mathbf{x}}_2^-$ is real for $y_r < \frac{y_{th1}\rho - bd_2 y_{th1}}{2(bd_1 + y_{th1}^2)y_{th2}}$ ($h_1(\bar{\mathbf{x}}_2^-) > 0$), $d_3 < d_1 + \frac{y_{th1}(bd_2 + y_{th1}y_{th2})}{by_{th2}}$ ($h_2(\bar{\mathbf{x}}_2^-) < 0$) and $d_3 < d_2 + \frac{y_{th2}^2(bd_1 + y_{th1}^2)}{by_{th1}^2}$ ($h_3(\bar{\mathbf{x}}_2^-) < 0$). Otherwise, it is virtual. Moreover, $\bar{\mathbf{x}}_2^-$ becomes a boundary equilibrium point if

- $y_r = \frac{y_{th1}\rho - bd_2 y_{th1}}{2(bd_1 + y_{th1}^2)y_{th2}}$ ($h_1(\bar{\mathbf{x}}_2^-) = 0$), $d_3 < d_1 + \frac{y_{th1}(bd_2 + y_{th1}y_{th2})}{by_{th2}}$ ($h_2(\bar{\mathbf{x}}_2^-) < 0$) and $d_3 < d_2 + \frac{y_{th2}^2(bd_1 + y_{th1}^2)}{by_{th1}^2}$ ($h_3(\bar{\mathbf{x}}_2^-) < 0$),
- $y_r < \frac{y_{th1}\rho - bd_2 y_{th1}}{2(bd_1 + y_{th1}^2)y_{th2}}$ ($h_1(\bar{\mathbf{x}}_2^-) > 0$), $d_3 = d_1 + \frac{y_{th1}(bd_2 + y_{th1}y_{th2})}{by_{th2}}$ ($h_2(\bar{\mathbf{x}}_2^-) = 0$) and $d_3 < d_2 + \frac{y_{th2}^2(bd_1 + y_{th1}^2)}{by_{th1}^2}$ ($h_3(\bar{\mathbf{x}}_2^-) < 0$),
- $y_r < \frac{y_{th1}\rho - bd_2 y_{th1}}{2(bd_1 + y_{th1}^2)y_{th2}}$ ($h_1(\bar{\mathbf{x}}_2^-) > 0$), $d_3 < d_1 + \frac{y_{th1}(bd_2 + y_{th1}y_{th2})}{by_{th2}}$ ($h_2(\bar{\mathbf{x}}_2^-) < 0$) and $d_3 = d_2 + \frac{y_{th2}^2(bd_1 + y_{th1}^2)}{by_{th1}^2}$ ($h_3(\bar{\mathbf{x}}_2^-) = 0$).

The determinant and trace are given by

$$Det[A(\bar{\mathbf{x}}_2^-)] = \frac{2(bd_1 + y_{th1}^2)(bd_2^2 y_{th1}^2 + 4d_3(bd_1 + y_{th1}^2)y_{th2}^2 - d_2 y_{th1} \rho \sqrt{b})}{y_{th1}^2(\rho \sqrt{b} - d_2 y_{th1} \sqrt{b})^2},$$

$$Tr[A(\bar{\mathbf{x}}_2^-)] = -b - \frac{d_1}{y_{th1}^2} - \frac{4d_3(bd_1 + y_{th1}^2)^2 y_{th2}^2}{(bd_2 y_{th1}^2 - y_{th1} \rho \sqrt{b})^2}.$$

Equilibrium $\bar{\mathbf{x}}_2^-$ is stable because $Det[A(\bar{\mathbf{x}}_2^-)] > 0$ and $Tr[A(\bar{\mathbf{x}}_2^-)] < 0$ for $d_3 > 0$.

(iii) $\mathbf{F}_3(\mathbf{x})$ has an equilibrium point, given by

$$\bar{\mathbf{x}}_3^\pm = \left(\frac{2bd_1 y_{th2} + y_{th1}^2(bd_2 + y_{th2}) \pm \xi}{2b(bd_1 + y_{th1}^2)y_{th2}}, \frac{-y_{th1}^2(bd_2 - y_{th2}) \mp \xi}{2(bd_1 + y_{th1}^2)y_{th2}}, \frac{-2bd_1 y_r y_{th2} - y_{th1}^2(bd_2 + (2y_r - 1)y_{th2}) \mp \xi}{2(bd_1 + y_{th1}^2)y_{th2}} \right),$$

where $\xi = \sqrt{4bd_3 y_{th1}^2(bd_1 + y_{th1}^2)y_{th2}^2 + y_{th1}^4(y_{th2} - bd_2)^2}$. Equilibrium $\bar{\mathbf{x}}_3^+$ is real for $y_r > \frac{(y_{th1}^2 - bd_2 y_{th2})y_{th2} - \xi}{2(bd_1 + y_{th1}^2)y_{th2}}$ ($h_1(\bar{\mathbf{x}}_3^+) < 0$), $d_3 > d_1 + \frac{y_{th1}^2}{b} + \frac{d_2 y_{th1}}{y_{th2}} - \frac{y_{th1}}{b}$ ($h_2(\bar{\mathbf{x}}_3^+) < 0$) and $d_3 > \frac{y_{th2}^2 + y_{th1}^2(bd_2 - y_{th2})}{by_{th1}^2(bd_1 + y_{th1}^2)}$ ($h_3(\bar{\mathbf{x}}_3^+) < 0$). Otherwise, it is virtual. Moreover, $\bar{\mathbf{x}}_2^-$ becomes a boundary equilibrium point if

- $y_r = \frac{(y_{th1}^2 - bd_2 y_{th2})y_{th2} - \xi}{2(bd_1 + y_{th1}^2)y_{th2}}$ ($h_1(\bar{\mathbf{x}}_3^+) = 0$), $d_3 > d_1 + \frac{y_{th1}^2}{b} + \frac{d_2 y_{th1}}{y_{th2}} - \frac{y_{th1}}{b}$ ($h_2(\bar{\mathbf{x}}_3^+) < 0$) and $d_3 > \frac{y_{th2}^2 + y_{th1}^2(bd_2 - y_{th2})}{by_{th1}^2(bd_1 + y_{th1}^2)}$ ($h_3(\bar{\mathbf{x}}_3^+) < 0$),
- $y_r > \frac{(y_{th1}^2 - bd_2 y_{th2})y_{th2} - \xi}{2(bd_1 + y_{th1}^2)y_{th2}}$ ($h_1(\bar{\mathbf{x}}_3^+) < 0$), $d_3 = d_1 + \frac{y_{th1}^2}{b} + \frac{d_2 y_{th1}}{y_{th2}} - \frac{y_{th1}}{b}$ ($h_2(\bar{\mathbf{x}}_3^+) = 0$) and $d_3 > \frac{y_{th2}^2 + y_{th1}^2(bd_2 - y_{th2})}{by_{th1}^2(bd_1 + y_{th1}^2)}$ ($h_3(\bar{\mathbf{x}}_3^+) < 0$),
- $y_r > \frac{(y_{th1}^2 - bd_2 y_{th2})y_{th2} - \xi}{2(bd_1 + y_{th1}^2)y_{th2}}$ ($h_1(\bar{\mathbf{x}}_3^+) < 0$), $d_3 > d_1 + \frac{y_{th1}^2}{b} + \frac{d_2 y_{th1}}{y_{th2}} - \frac{y_{th1}}{b}$ ($h_2(\bar{\mathbf{x}}_3^+) < 0$) and $d_3 = \frac{y_{th2}^2 + y_{th1}^2(bd_2 - y_{th2})}{by_{th1}^2(bd_1 + y_{th1}^2)}$ ($h_3(\bar{\mathbf{x}}_3^+) = 0$),

- $y_r = \frac{(y_{th1}^2 - bd_2 y_{th2}) y_{th2} - \xi}{2(bd_1 + y_{th1}^2) y_{th2}}$ ($h_1(\bar{\mathbf{x}}_3^+) = 0$), $d_3 = d_1 + \frac{y_{th1}^2}{b} + \frac{d_2 y_{th1}}{y_{th2}} - \frac{y_{th1}}{b}$ ($h_2(\bar{\mathbf{x}}_3^+) = 0$)
and $d_3 > \frac{y_{th2}^2 + y_{th1}^2 (bd_2 - y_{th2})}{by_{th1}^2 (bd_1 + y_{th1}^2)}$ ($h_3(\bar{\mathbf{x}}_3^+) < 0$),
- $y_r = \frac{(y_{th1}^2 - bd_2 y_{th2}) y_{th2} - \xi}{2(bd_1 + y_{th1}^2) y_{th2}}$ ($h_1(\bar{\mathbf{x}}_3^+) = 0$), $d_3 > d_1 + \frac{y_{th1}^2}{b} + \frac{d_2 y_{th1}}{y_{th2}} - \frac{y_{th1}}{b}$ ($h_2(\bar{\mathbf{x}}_3^+) < 0$)
and $d_3 = \frac{y_{th2}^2 + y_{th1}^2 (bd_2 - y_{th2})}{by_{th1}^2 (bd_1 + y_{th1}^2)}$ ($h_3(\bar{\mathbf{x}}_3^+) = 0$).

Equilibrium $\bar{\mathbf{x}}_3^-$ is real for $y_r > \frac{(y_{th1}^2 - bd_2 y_{th2}) y_{th2} + \xi}{2(bd_1 + y_{th1}^2) y_{th2}}$ ($h_1(\bar{\mathbf{x}}_3^-) < 0$), $d_3 < \frac{(bd_1 + y_{th1}^2) y_{th2} + (bd_2 - y_{th2}) y_{th1}}{by_{th2}}$ ($h_2(\bar{\mathbf{x}}_3^-) < 0$) and $d_3 < \frac{(bd_1 + y_{th1}^2) y_{th2}^2 + (bd_2 - y_{th2}) y_{th1}^2}{by_{th1}^2}$ ($h_3(\bar{\mathbf{x}}_3^-) < 0$). Otherwise, it is virtual. Furthermore, it becomes a boundary equilibrium point if

- $y_r = \frac{(y_{th1}^2 - bd_2 y_{th2}) y_{th2} + \xi}{2(bd_1 + y_{th1}^2) y_{th2}}$ ($h_1(\bar{\mathbf{x}}_3^-) < 0$), $d_3 < \frac{(bd_1 + y_{th1}^2) y_{th2} + (bd_2 - y_{th2}) y_{th1}}{by_{th2}}$ ($h_2(\bar{\mathbf{x}}_3^-) < 0$) and $d_3 < \frac{(bd_1 + y_{th1}^2) y_{th2}^2 + (bd_2 - y_{th2}) y_{th1}^2}{by_{th1}^2}$ ($h_3(\bar{\mathbf{x}}_3^-) < 0$),
- $y_r > \frac{(y_{th1}^2 - bd_2 y_{th2}) y_{th2} + \xi}{2(bd_1 + y_{th1}^2) y_{th2}}$ ($h_1(\bar{\mathbf{x}}_3^-) < 0$), $d_3 = \frac{(bd_1 + y_{th1}^2) y_{th2} + (bd_2 - y_{th2}) y_{th1}}{by_{th2}}$ ($h_2(\bar{\mathbf{x}}_3^-) = 0$) and $d_3 < \frac{(bd_1 + y_{th1}^2) y_{th2}^2 + (bd_2 - y_{th2}) y_{th1}^2}{by_{th1}^2}$ ($h_3(\bar{\mathbf{x}}_3^-) < 0$),
- $y_r > \frac{(y_{th1}^2 - bd_2 y_{th2}) y_{th2} + \xi}{2(bd_1 + y_{th1}^2) y_{th2}}$ ($h_1(\bar{\mathbf{x}}_3^-) < 0$), $d_3 < \frac{(bd_1 + y_{th1}^2) y_{th2} + (bd_2 - y_{th2}) y_{th1}}{by_{th2}}$ ($h_2(\bar{\mathbf{x}}_3^-) < 0$) and $d_3 = \frac{(bd_1 + y_{th1}^2) y_{th2}^2 + (bd_2 - y_{th2}) y_{th1}^2}{by_{th1}^2}$ ($h_3(\bar{\mathbf{x}}_3^-) = 0$),
- $y_r = \frac{(y_{th1}^2 - bd_2 y_{th2}) y_{th2} + \xi}{2(bd_1 + y_{th1}^2) y_{th2}}$ ($h_1(\bar{\mathbf{x}}_3^-) = 0$), $d_3 = \frac{(bd_1 + y_{th1}^2) y_{th2} + (bd_2 - y_{th2}) y_{th1}}{by_{th2}}$ ($h_2(\bar{\mathbf{x}}_3^-) = 0$) and $d_3 < \frac{(bd_1 + y_{th1}^2) y_{th2}^2 + (bd_2 - y_{th2}) y_{th1}^2}{by_{th1}^2}$ ($h_3(\bar{\mathbf{x}}_3^-) < 0$),
- $y_r = \frac{(y_{th1}^2 - bd_2 y_{th2}) y_{th2} + \xi}{2(bd_1 + y_{th1}^2) y_{th2}}$ ($h_1(\bar{\mathbf{x}}_3^-) = 0$), $d_3 < \frac{(bd_1 + y_{th1}^2) y_{th2} + (bd_2 - y_{th2}) y_{th1}}{by_{th2}}$ ($h_2(\bar{\mathbf{x}}_3^-) < 0$) and $d_3 = \frac{(bd_1 + y_{th1}^2) y_{th2}^2 + (bd_2 - y_{th2}) y_{th1}^2}{by_{th1}^2}$ ($h_3(\bar{\mathbf{x}}_3^-) = 0$).

The determinant and trace are given by

$$Det[A(\bar{\mathbf{x}}_3^\pm)] = \frac{4b^2 d_1 d_3 y_{th2}^2 \mp bd_2 \xi - y_{th2} \xi + y_{th1}^2 (b^2 d_2^2 + y_{th2}^2 + 2by_{th2} (2d_3 y_{th2} - d_2))}{2bd_3 y_{th1}^2 y_{th2}^2},$$

$$Tr[A(\bar{\mathbf{x}}_3^\pm)] = -b - \frac{d_1}{y_{th1}^2} - \frac{4d_3 (bd_1 + y_{th1}^2)^2 y_{th2}^2}{(\pm bd_2 y_{th1}^2 \mp y_{th1}^2 y_{th2} + \xi)^2}.$$

Equilibrium $\bar{\mathbf{x}}_3^\pm$ is stable because $Det[A(\bar{\mathbf{x}}_3^\pm)] > 0$ and $Tr[A(\bar{\mathbf{x}}_3^\pm)] < 0$ for $d_3 > \frac{-y_{th1}^2 (y_{th2} - bd_2)^2}{4b(bd_1 + y_{th1}^2) y_{th2}^2}$.

(iv) $\mathbf{F}_4(\mathbf{x})$ has an equilibrium point, given by

$$\bar{\mathbf{x}}_4^\pm = \left(\frac{1 \pm \gamma}{2b}, \frac{1 \mp \gamma}{2}, \frac{1 \mp \gamma - 2y_r}{2} \right),$$

with $\gamma = \sqrt{1 - 4b(d_1 + d_2 - d_3)}$. Equilibrium $\bar{\mathbf{x}}_4^+$ is real for $y_r > \frac{1-\gamma}{2}$ ($h_1(\bar{\mathbf{x}}_4^+) < 0$), $y_{th1} < \frac{1-\gamma}{2}$ ($h_2(\bar{\mathbf{x}}_4^+) > 0$) and $y_{th2} < \frac{1-\gamma}{2}$ ($h_3(\bar{\mathbf{x}}_4^+) > 0$). Otherwise, it is virtual. Moreover, becomes a boundary equilibrium point if

- $y_r = \frac{1-\gamma}{2} (h_1(\bar{\mathbf{x}}_4^+) = 0)$, $y_{th1} = \frac{1-\gamma}{2} (h_2(\bar{\mathbf{x}}_4^+) = 0)$ and $y_{th2} < \frac{1-\gamma}{2} (h_3(\bar{\mathbf{x}}_4^+) > 0)$, respectively,
- $y_r = \frac{1-\gamma}{2} (h_1(\bar{\mathbf{x}}_4^+) = 0)$, $y_{th1} < \frac{1-\gamma}{2} (h_2(\bar{\mathbf{x}}_4^+) > 0)$ and $y_{th2} = \frac{1-\gamma}{2} (h_3(\bar{\mathbf{x}}_4^+) = 0)$,
- $y_r = \frac{1-\gamma}{2} (h_1(\bar{\mathbf{x}}_4^+) = 0)$, $y_{th1} < \frac{1-\gamma}{2} (h_2(\bar{\mathbf{x}}_4^+) > 0)$ and $y_{th2} < \frac{1-\gamma}{2} (h_3(\bar{\mathbf{x}}_4^+) > 0)$,
- $y_r > \frac{1-\gamma}{2} (h_1(\bar{\mathbf{x}}_4^+) < 0)$, $y_{th1} = \frac{1-\gamma}{2} (h_2(\bar{\mathbf{x}}_4^+) = 0)$ and $y_{th2} < \frac{1-\gamma}{2} (h_3(\bar{\mathbf{x}}_4^+) > 0)$,
- $y_r > \frac{1-\gamma}{2} (h_1(\bar{\mathbf{x}}_4^+) < 0)$, $y_{th1} < \frac{1-\gamma}{2} (h_2(\bar{\mathbf{x}}_4^+) > 0)$ and $y_{th2} = \frac{1-\gamma}{2} (h_3(\bar{\mathbf{x}}_4^+) = 0)$.

Analogously, the equilibrium $\bar{\mathbf{x}}_4^-$ is real for $y_r > \frac{1+\gamma}{2} (h_1(\bar{\mathbf{x}}_4^-) < 0)$, $y_{th1} < \frac{1+\gamma}{2} (h_2(\bar{\mathbf{x}}_4^-) > 0)$ and $y_{th2} < \frac{1+\gamma}{2} (h_3(\bar{\mathbf{x}}_4^-) > 0)$. Otherwise, it is virtual. Furthermore, it becomes a boundary equilibrium point if

- $y_r = \frac{1-\gamma}{2} (h_1(\bar{\mathbf{x}}_4^-) = 0)$, $y_{th1} = \frac{1-\gamma}{2} (h_2(\bar{\mathbf{x}}_4^-) = 0)$ and $y_{th2} < \frac{1-\gamma}{2} (h_3(\bar{\mathbf{x}}_4^-) > 0)$,
- $y_r = \frac{1-\gamma}{2} (h_1(\bar{\mathbf{x}}_4^-) = 0)$, $y_{th1} < \frac{1-\gamma}{2} (h_2(\bar{\mathbf{x}}_4^-) > 0)$ and $y_{th2} = \frac{1-\gamma}{2} (h_3(\bar{\mathbf{x}}_4^-) = 0)$,
- $y_r = \frac{1-\gamma}{2} (h_1(\bar{\mathbf{x}}_4^-) = 0)$, $y_{th1} < \frac{1-\gamma}{2} (h_2(\bar{\mathbf{x}}_4^-) > 0)$ and $y_{th2} < \frac{1-\gamma}{2} (h_3(\bar{\mathbf{x}}_4^-) > 0)$,
- $y_r > \frac{1-\gamma}{2} (h_1(\bar{\mathbf{x}}_4^-) < 0)$, $y_{th1} = \frac{1-\gamma}{2} (h_2(\bar{\mathbf{x}}_4^-) = 0)$ and $y_{th2} < \frac{1-\gamma}{2} (h_3(\bar{\mathbf{x}}_4^-) > 0)$,
- $y_r > \frac{1-\gamma}{2} (h_1(\bar{\mathbf{x}}_4^-) < 0)$, $y_{th1} < \frac{1-\gamma}{2} (h_2(\bar{\mathbf{x}}_4^-) > 0)$ and $y_{th2} = \frac{1-\gamma}{2} (h_3(\bar{\mathbf{x}}_4^-) = 0)$.

The determinant and trace are given by

$$Det[A(\bar{\mathbf{x}}_4^\pm)] = \frac{2 - 4b(d_1 + d_2 - d_3) \mp \gamma}{(\gamma \mp 1)^2} \quad \text{and} \quad Tr[A(\bar{\mathbf{x}}_4^\pm)] = -b + \frac{4b(d_1 + d_2 - d_3)}{(\gamma \mp 1)^2}.$$

Equilibrium $\bar{\mathbf{x}}_4^+$ is a stable point because $Det[A(\bar{\mathbf{x}}_4^+)] > 0$ and $Tr[A(\bar{\mathbf{x}}_4^+)] < 0$ for $\frac{1}{4b} < d_1 + d_2 - d_3 < \frac{b}{(1+b^2)^2}$. In other hand, $\bar{\mathbf{x}}_4^-$ is a saddle point, since $Det[A(\bar{\mathbf{x}}_4^-)] < 0$ for all $0 < d_1 + d_2 - d_3 < \frac{1}{4b}$.

(v) $\mathbf{F}_5(\mathbf{x})$ has an equilibrium point, given by

$$\bar{\mathbf{x}}_5^\pm = \left(\frac{d_2 \pm \zeta/\sqrt{b}}{2y_{th2}}, \frac{-bd_2 \mp \zeta\sqrt{b}}{2y_{th2}}, \frac{-bd_2 - 2y_r y_{th2} \mp \zeta\sqrt{b}}{2y_{th2}} \right),$$

where $\zeta = \sqrt{bd_2^2 + 4(d_3 - d_1)y_{th2}^2}$. Equilibrium $\bar{\mathbf{x}}_5^+$ is virtual, because $h_1(\bar{\mathbf{x}}_5^+) < 0$. Equilibrium $\bar{\mathbf{x}}_5^-$ is real for $y_r < \frac{\xi\sqrt{b}-bd_2}{2y_{th2}} (h_1(\bar{\mathbf{x}}_5^-) > 0)$, $y_{th1} < \frac{\xi\sqrt{b}-bd_2}{2y_{th2}} (h_2(\bar{\mathbf{x}}_5^-) > 0)$ and $d_3 - d_1 - d_2 > \frac{y_{th2}^2}{b} (h_3(\bar{\mathbf{x}}_5^-) < 0)$. Otherwise, it is virtual. Moreover, it becomes a boundary equilibrium point if

- $y_r = \frac{\xi\sqrt{b}-bd_2}{2y_{th2}} (h_1(\bar{\mathbf{x}}_5^-) = 0)$, $y_{th1} < \frac{\xi\sqrt{b}-bd_2}{2y_{th2}} (h_2(\bar{\mathbf{x}}_5^-) > 0)$ and $d_3 - d_1 - d_2 > \frac{y_{th2}^2}{b} (h_3(\bar{\mathbf{x}}_5^-) < 0)$,
- $y_r < \frac{\xi\sqrt{b}-bd_2}{2y_{th2}} (h_1(\bar{\mathbf{x}}_5^-) > 0)$, $y_{th1} = \frac{\xi\sqrt{b}-bd_2}{2y_{th2}} (h_2(\bar{\mathbf{x}}_5^-) = 0)$ and $d_3 - d_1 - d_2 > \frac{y_{th2}^2}{b} (h_3(\bar{\mathbf{x}}_5^-) < 0)$,
- $y_r < \frac{\xi\sqrt{b}-bd_2}{2y_{th2}} (h_1(\bar{\mathbf{x}}_5^-) > 0)$, $y_{th1} < \frac{\xi\sqrt{b}-bd_2}{2y_{th2}} (h_2(\bar{\mathbf{x}}_5^-) > 0)$ and $d_3 - d_1 - d_2 = \frac{y_{th2}^2}{b} (h_3(\bar{\mathbf{x}}_5^-) = 0)$,

- $y_r = \frac{\xi\sqrt{b}-bd_2}{2y_{th2}} (h_1(\bar{\mathbf{x}}_5^-) = 0)$, $y_{th1} = \frac{\xi\sqrt{b}-bd_2}{2y_{th2}} (h_2(\bar{\mathbf{x}}_5^-) = 0)$ and $d_3 - d_1 - d_2 > \frac{y_{th2}^2}{b}$ ($h_3(\bar{\mathbf{x}}_5^-) < 0$),
- $y_r = \frac{\xi\sqrt{b}-bd_2}{2y_{th2}} (h_1(\bar{\mathbf{x}}_5^-) = 0)$, $y_{th1} < \frac{\xi\sqrt{b}-bd_2}{2y_{th2}} (h_2(\bar{\mathbf{x}}_5^-) > 0)$ and $d_3 - d_1 - d_2 = \frac{y_{th2}^2}{b}$ ($h_3(\bar{\mathbf{x}}_5^-) = 0$).

The determinant and trace are given by

$$\begin{aligned} Det[A(\bar{\mathbf{x}}_5^-)] &= \frac{2bd_2^2 + 8(d_3 - d_1)y_{th2}^2 - 2d_2\zeta\sqrt{b}}{(\zeta - d_2\sqrt{b})^2}, \\ Tr[A(\bar{\mathbf{x}}_5^-)] &= -b + \frac{4(d_1 - d_3)y_{th2}^2}{(bd_2 - \zeta\sqrt{b})^2} \end{aligned}$$

Equilibrium $\bar{\mathbf{x}}_5^-$ is stable because $Det[A(\bar{\mathbf{x}}_5^-)] > 0$ and $Tr[A(\bar{\mathbf{x}}_5^-)] < 0$ for $\frac{4d_1y_{th2}^2 - bd_2^2}{4y_{th2}^2} < d_3 < d_1 - \frac{b^3d_2^2}{(1+b^2)^2y_{th2}^2}$.

(vi) $\mathbf{F}_6(\mathbf{x})$ has an equilibrium point, given by

$$\bar{\mathbf{x}}_6^\pm = \left(\frac{bd_2 + y_{th2} \pm \eta}{2by_{th2}}, \frac{-bd_2 + y_{th2} \mp \eta}{2y_{th2}}, \frac{y_{th2} - bd_2 - 2y_r y_{th2} \mp \eta}{2y_{th2}} \right),$$

where $\eta = \sqrt{4b(d_3 - d_1)y_{th2}^2 + (y_{th2} - bd_2)^2}$. Equilibrium $\bar{\mathbf{x}}_6^+$ is real for $y_r > \frac{y_{th2} - bd_2 - \eta}{2y_{th2}} (h_1(\bar{\mathbf{x}}_6^+) < 0)$, $y_{th1} < \frac{y_{th2} - bd_2 - \eta}{2y_{th2}} (h_2(\bar{\mathbf{x}}_6^+) > 0)$ and $d_3 > d_1 + d_2 + \frac{(y_{th2} - 1)y_{th2}}{b}$ ($h_3(\bar{\mathbf{x}}_6^+) < 0$). Otherwise it is virtual. Moreover, it becomes a boundary equilibrium point if

- $y_r = \frac{y_{th2} - bd_2 - \eta}{2y_{th2}} (h_1(\bar{\mathbf{x}}_6^+) = 0)$, $y_{th1} < \frac{y_{th2} - bd_2 - \eta}{2y_{th2}} (h_2(\bar{\mathbf{x}}_6^+) > 0)$ and $d_3 > d_1 + d_2 + \frac{(y_{th2} - 1)y_{th2}}{b}$ ($h_3(\bar{\mathbf{x}}_6^+) < 0$),
- $y_r > \frac{y_{th2} - bd_2 - \eta}{2y_{th2}} (h_1(\bar{\mathbf{x}}_6^+) < 0)$, $y_{th1} = \frac{y_{th2} - bd_2 - \eta}{2y_{th2}} (h_2(\bar{\mathbf{x}}_6^+) = 0)$ and $d_3 > d_1 + d_2 + \frac{(y_{th2} - 1)y_{th2}}{b}$ ($h_3(\bar{\mathbf{x}}_6^+) < 0$),
- $y_r > \frac{y_{th2} - bd_2 - \eta}{2y_{th2}} (h_1(\bar{\mathbf{x}}_6^+) < 0)$, $y_{th1} < \frac{y_{th2} - bd_2 - \eta}{2y_{th2}} (h_2(\bar{\mathbf{x}}_6^+) > 0)$ and $d_3 = d_1 + d_2 + \frac{(y_{th2} - 1)y_{th2}}{b}$ ($h_3(\bar{\mathbf{x}}_6^+) = 0$),
- $y_r = \frac{y_{th2} - bd_2 - \eta}{2y_{th2}} (h_1(\bar{\mathbf{x}}_6^+) = 0)$, $y_{th1} = \frac{y_{th2} - bd_2 - \eta}{2y_{th2}} (h_2(\bar{\mathbf{x}}_6^+) = 0)$ and $d_3 > d_1 + d_2 + \frac{(y_{th2} - 1)y_{th2}}{b}$ ($h_3(\bar{\mathbf{x}}_6^+) < 0$),
- $y_r = \frac{y_{th2} - bd_2 - \eta}{2y_{th2}} (h_1(\bar{\mathbf{x}}_6^+) = 0)$, $y_{th1} < \frac{y_{th2} - bd_2 - \eta}{2y_{th2}} (h_2(\bar{\mathbf{x}}_6^+) > 0)$ and $d_3 = d_1 + d_2 + \frac{(y_{th2} - 1)y_{th2}}{b}$ ($h_3(\bar{\mathbf{x}}_6^+) = 0$).

Equilibrium $\bar{\mathbf{x}}_6^-$ is real for $y_r > \frac{y_{th2} - bd_2 + \eta}{2y_{th2}} (h_1(\bar{\mathbf{x}}_6^-) < 0)$, $y_{th1} < \frac{y_{th2} - bd_2 + \eta}{2y_{th2}} (h_2(\bar{\mathbf{x}}_6^-) > 0)$ and $d_3 < d_1 + d_2 + \frac{(y_{th2} - 1)y_{th2}}{b}$ ($h_3(\bar{\mathbf{x}}_6^-) < 0$). Otherwise, it is virtual. Furthermore, it becomes a boundary equilibrium point if

- $y_r = \frac{y_{th2} - bd_2 + \eta}{2y_{th2}} (h_1(\bar{\mathbf{x}}_6^-) = 0)$, $y_{th1} < \frac{y_{th2} - bd_2 + \eta}{2y_{th2}} (h_2(\bar{\mathbf{x}}_6^-) > 0)$ and $d_3 < d_1 + d_2 + \frac{(y_{th2} - 1)y_{th2}}{b}$ ($h_3(\bar{\mathbf{x}}_6^-) < 0$),

- $y_r > \frac{y_{th2}-bd_2+\eta}{2y_{th2}}$ ($h_1(\bar{\mathbf{x}}_6^-) < 0$), $y_{th1} = \frac{y_{th2}-bd_2\eta}{2y_{th2}}$ ($h_2(\bar{\mathbf{x}}_6^-) = 0$) and $d_3 < d_1 + d_2 + \frac{(y_{th2}-1)y_{th2}}{b}$ ($h_3(\bar{\mathbf{x}}_6^-) < 0$),
- $y_r > \frac{y_{th2}-bd_2+\eta}{2y_{th2}}$ ($h_1(\bar{\mathbf{x}}_6^-) < 0$), $y_{th1} < \frac{y_{th2}-bd_2\eta}{2y_{th2}}$ ($h_2(\bar{\mathbf{x}}_6^-) > 0$) and $d_3 = d_1 + d_2 + \frac{(y_{th2}-1)y_{th2}}{b}$ ($h_3(\bar{\mathbf{x}}_6^-) = 0$),
- $y_r = \frac{y_{th2}-bd_2+\eta}{2y_{th2}}$ ($h_1(\bar{\mathbf{x}}_6^-) = 0$), $y_{th1} = \frac{y_{th2}-bd_2\eta}{2y_{th2}}$ ($h_2(\bar{\mathbf{x}}_6^-) = 0$) and $d_3 < d_1 + d_2 + \frac{(y_{th2}-1)y_{th2}}{b}$ ($h_3(\bar{\mathbf{x}}_6^-) < 0$),
- $y_r = \frac{y_{th2}-bd_2+\eta}{2y_{th2}}$ ($h_1(\bar{\mathbf{x}}_6^-) = 0$), $y_{th1} < \frac{y_{th2}-bd_2\eta}{2y_{th2}}$ ($h_2(\bar{\mathbf{x}}_6^-) > 0$) and $d_3 = d_1 + d_2 + \frac{(y_{th2}-1)y_{th2}}{b}$ ($h_3(\bar{\mathbf{x}}_6^-) = 0$).

The determinant and trace are given by

$$\begin{aligned} Det[A(\bar{\mathbf{x}}_6^\pm)] &= \frac{2\eta}{\pm bd_2 \mp y_{th2} + \eta}, \\ Tr[A(\bar{\mathbf{x}}_6^\pm)] &= -b + \frac{4(d_1 - d_3)y_{th2}^2}{(\pm bd_2 \mp y_{th2} + \eta)^2}. \end{aligned}$$

Equilibrium $\bar{\mathbf{x}}_6^\pm$ are stables because $Det[A(\bar{\mathbf{x}}_6^\pm)] > 0$ and $Tr[A(\bar{\mathbf{x}}_6^\pm)] < 0$ for $d_3 \in (-\infty, d_1 - \frac{1}{4by_{th2}^2}(y_{th2}^2 - bd_2)^2) \cup (d_1, +\infty)$ and $d_3 \in (d_1 - \frac{b(bd_2 - y_{th2})^2}{(1+b^2)^2 y_{th2}^2}, d_1)$, respectively.

5.4.2 Sliding vector field and pseudo-equilibria

Sliding vector field associated of the dynamical system (5.2.3) is defined by (5.3.7), where $(x, y, z) \in \Sigma_s \subset \Sigma_1$. The pseudo equilibrium point is given by $\tilde{\mathbf{x}} = (\xi_0(y), y, 0)$ that depend of values of $\xi_0(y)$, i.e, the discontinuity at $y = y_{th1}$ and $y = y_{th2}$. So, there are three pseudo-equilibrium points namely,

$$\begin{aligned} \tilde{\mathbf{x}}_1 &= \left(\frac{d_1 + d_2 - d_3}{y_r}, y_r, 0 \right), \\ \tilde{\mathbf{x}}_2 &= \left(\frac{d_1 y_r}{y_{th1}^2} + \frac{d_2}{y_{th2}} - \frac{d_3}{y_r}, y_r, 0 \right), \\ \tilde{\mathbf{x}}_3 &= \left(\frac{d_2}{y_{th2}} + \frac{d_1}{y_r} - \frac{d_3}{y_r}, y_r, 0 \right), \end{aligned}$$

for $y \geq y_{th2}$, $y < y_{th1}$ and $y_{th1} \leq y < y_{th2}$, respectively. By hypothesis, $y_r > y_{th2} > y_{th1}$, then the pseudo-equilibria $\tilde{\mathbf{x}}_2$ and $\tilde{\mathbf{x}}_3$ are always virtual, so the stability analysis will be only for the pseudo-equilibrium point $\tilde{\mathbf{x}}_1$ as studied in the Subsection 5.3.2.

5.5 Case study for $y_{th1} > y_{th2}$

Due to the switching boundaries defined in (5.2.8) and assuming that $y_{th1} > y_{th2}$. Observe that in this case the state space of the system is divided into six different regions, namely

$$\begin{aligned}
D_1 &= \{\mathbf{x} \in D : h_1(\mathbf{x}) > 0, h_2(\mathbf{x}) > 0 \text{ and } h_3(\mathbf{x}) > 0\}, \\
D_2 &= \{\mathbf{x} \in D : h_1(\mathbf{x}) > 0, h_2(\mathbf{x}) < 0 \text{ and } h_3(\mathbf{x}) < 0\}, \\
D_3 &= \{\mathbf{x} \in D : h_1(\mathbf{x}) < 0, h_2(\mathbf{x}) < 0 \text{ and } h_3(\mathbf{x}) < 0\}, \\
D_4 &= \{\mathbf{x} \in D : h_1(\mathbf{x}) < 0, h_2(\mathbf{x}) > 0 \text{ and } h_3(\mathbf{x}) > 0\}, \\
D_5 &= \{\mathbf{x} \in D : h_1(\mathbf{x}) > 0, h_2(\mathbf{x}) < 0 \text{ and } h_3(\mathbf{x}) > 0\}, \\
D_6 &= \{\mathbf{x} \in D : h_1(\mathbf{x}) < 0, h_2(\mathbf{x}) < 0 \text{ and } h_3(\mathbf{x}) > 0\}.
\end{aligned}$$

In each one of these regions there is a distinct vector field acting, then the system (5.2.5) is represented as a 3D-DPWS system of the form

$$\dot{\mathbf{x}} = \begin{cases} \mathbf{F}_1(\mathbf{x}), & \text{if } \mathbf{x} \in D_1, \\ \mathbf{F}_2(\mathbf{x}), & \text{if } \mathbf{x} \in D_2, \\ \mathbf{F}_3(\mathbf{x}), & \text{if } \mathbf{x} \in D_3, \\ \mathbf{F}_4(\mathbf{x}), & \text{if } \mathbf{x} \in D_4, \\ \mathbf{F}_5(\mathbf{x}), & \text{if } \mathbf{x} \in D_5, \\ \mathbf{F}_6(\mathbf{x}), & \text{if } \mathbf{x} \in D_6, \end{cases} \quad (5.5.1)$$

composed by the vector fields

$$\begin{aligned}
\mathbf{F}_1(\mathbf{x}) &= \begin{bmatrix} -bx - y \\ x - \frac{d_1+d_2}{y} + \frac{d_3}{y} \\ f_{1,3} \end{bmatrix}, & \mathbf{F}_2(\mathbf{x}) &= \begin{bmatrix} -bx - y \\ x - \frac{d_1y}{y_{th1}^2} - \frac{d_2}{y_{th2}} + \frac{d_3}{y} \\ f_{2,3} \end{bmatrix}, \\
\mathbf{F}_3(\mathbf{x}) &= \begin{bmatrix} 1 - bx - y \\ x - \frac{d_1y}{y_{th1}^2} - \frac{d_2}{y_{th2}} + \frac{d_3}{y} \\ f_{2,3} + k \end{bmatrix}, & \mathbf{F}_4(\mathbf{x}) &= \begin{bmatrix} 1 - bx - y \\ x - \frac{d_1+d_2}{y} + \frac{d_3}{y} \\ f_{1,3} + k \end{bmatrix}, \\
\mathbf{F}_5(\mathbf{x}) &= \begin{bmatrix} -bx - y \\ x - \frac{d_1y}{y_{th1}^2} - \frac{d_2}{y} + \frac{d_3}{y} \\ f_{3,3} \end{bmatrix} & \text{and } \mathbf{F}_6(\mathbf{x}) &= \begin{bmatrix} 1 - bx - y \\ x - \frac{d_1y}{y_{th1}^2} - \frac{d_2}{y} + \frac{d_3}{y} \\ f_{3,3} + k \end{bmatrix},
\end{aligned}$$

where

$$\begin{aligned}
f_{1,3} &= (1 - kb)x + (\omega - k)y - \frac{d_1 + d_2}{y} + \frac{d_3}{y} - \omega z - \omega y_r, \\
f_{2,3} &= (1 - kb)x + (\omega - k)y - \frac{d_1y}{y_{th1}^2} + \frac{d_3}{y} - \frac{d_2}{y_{th2}} - \omega z - \omega y_r, \\
f_{3,3} &= (1 - kb)x + (\omega - k)y - \frac{d_1y}{y_{th1}^2} + \frac{d_3}{y} - \frac{d_2}{y} - \omega z - \omega y_r.
\end{aligned}$$

Proposition 5.5.1. *There are no sliding motion at the switching boundaries Σ_2 and Σ_3 defined in (5.2.8).*

Proof. A straightforward calculus produces, $L_{\mathbf{F}_{2,3}(\mathbf{x})}h_2(\mathbf{x}) \cdot L_{\mathbf{F}_{5,6}(\mathbf{x})}h_2(\mathbf{x}) = (x - \xi_0(y) + \frac{d_3}{y})^2 \geq 0$ and $L_{\mathbf{F}_{1,4}(\mathbf{x})}h_3(\mathbf{x}) \cdot L_{\mathbf{F}_{5,6}(\mathbf{x})}h_3(\mathbf{x}) = (x - \xi_0(y) + \frac{d_3}{y})^2 \geq 0$. Therefore, Σ_2 and Σ_3 is just a crossing boundary. Containing a double tangency line at $x = \xi_0(y_{th}) - \frac{d_3}{y_{th}}$ and $y = y_{th}$, and $z \in \mathbb{R}$. \square

In order to analyze the dynamic behavior of system (5.2.5) on the switching boundary Σ_1 , we calculate the sliding and crossing regions taking into account the discontinuity at $y = y_{th1}$ and $y = y_{th2}$, for this we divided the study in cases as follows.

- (i) For $y \geq y_{th1}$, the crossing and sliding regions are defined by Σ_{c_1} and Σ_{s_1} as defined in (5.3.2) and (5.3.3), respectively.
- (ii) For $y_{th2} \leq y \leq y_{th1}$, the crossing and sliding regions are defined as follows

$$\Sigma_{c_5} = \{\mathbf{x} \in \Sigma_1 : x > \bar{\varkappa}(y) \text{ or } x > \underline{\varkappa}(y)\}, \quad (5.5.2)$$

$$\Sigma_{s_5} = \{\mathbf{x} \in \Sigma_1 : \bar{\varkappa}(y) < x < \underline{\varkappa}(y)\}, \quad (5.5.3)$$

where

$$\begin{aligned} \bar{\varkappa}(y) &= \frac{1}{(1-kb)} \left(\frac{d_1 y}{y_{th1}^2} + \frac{d_2}{y} - \frac{d_3}{y} + ky + \omega(y_r - y) + \omega z \right), \\ \underline{\varkappa}(y) &= \frac{1}{(1-kb)} \left(\frac{d_1 y}{y_{th1}^2} + \frac{d_2}{y} - \frac{d_3}{y} + k(y-1) + \omega(y_r - y) + \omega z \right). \end{aligned}$$

- (iii) For $y < y_{th2}$, the crossing and sliding regions are defined by Σ_{c_4} and Σ_{s_4} as defined in (5.4.4) and (5.4.5), respectively.

5.5.1 Regular equilibria and stability

As mentioned in Subsection 5.3.1, the first and second components of the vector fields $\mathbf{F}_i(\mathbf{x})$ ($i = 1, 2, 3, 4, 5, 6$) are independent of the dynamic in their third component z , whose dynamic is stable the associated eigenvalue is $-\omega < 0$. Thus, we just need to consider the reduced linearization Jacobian matrix as defined in (5.3.6). In this case, the regular equilibria and stabilities in the vector fields $\mathbf{F}_i(\mathbf{x})$ with $i = 1, 2, 3, 4$ are equal to Section 5.4, when $y_{th1} < y_{th2}$. Then, we will analyze the equilibria of the vector fields $\mathbf{F}_i(\mathbf{x})$ for $i = 5, 6$ and its stabilities.

- (i) $\mathbf{F}_5(\mathbf{x})$ has an equilibrium point, given by

$$\bar{\mathbf{x}}_5^\pm = \left(\pm \frac{\nu}{b\sqrt{bd_1 + y_{th1}^2}}, \mp \frac{\nu}{\sqrt{bd_1 + y_{th1}^2}}, -y_r \mp \frac{\nu}{\sqrt{bd_1 + y_{th1}^2}} \right),$$

where, $\nu = \sqrt{b(d_3 - d_2)y_{th1}^2}$. Equilibrium $\bar{\mathbf{x}}_5^+$ is virtual, because $h_1(\bar{\mathbf{x}}_5^+) < 0$. Equilibrium $\bar{\mathbf{x}}_5^-$ is real for $y_r < \frac{\nu}{\sqrt{bd_1 + y_{th1}^2}}$ ($h_1(\bar{\mathbf{x}}_5^-) > 0$), $d_3 - d_1 - d_2 < \frac{y_{th1}^2}{b}$ ($h_2(\bar{\mathbf{x}}_5^-) < 0$) and $d_3 < d_2 + \frac{(bd_1 + y_{th1}^2)y_{th2}^2}{y_{th1}^2}$ ($h_3(\bar{\mathbf{x}}_5^-) > 0$). Moreover, it becomes a boundary equilibrium point if

- $y_r = \frac{\nu}{\sqrt{bd_1 + y_{th1}^2}}$ ($h_1(\bar{\mathbf{x}}_5^-) = 0$), $d_3 - d_1 - d_2 < \frac{y_{th1}^2}{b}$ ($h_2(\bar{\mathbf{x}}_5^-) < 0$) and $d_3 < d_2 + \frac{(bd_1 + y_{th1}^2)y_{th2}^2}{y_{th1}^2}$ ($h_3(\bar{\mathbf{x}}_5^-) > 0$),
- $y_r < \frac{\nu}{\sqrt{bd_1 + y_{th1}^2}}$ ($h_1(\bar{\mathbf{x}}_5^-) > 0$), $d_3 - d_1 - d_2 = \frac{y_{th1}^2}{b}$ ($h_2(\bar{\mathbf{x}}_5^-) = 0$) and $d_3 < d_2 + \frac{(bd_1 + y_{th1}^2)y_{th2}^2}{y_{th1}^2}$ ($h_3(\bar{\mathbf{x}}_5^-) > 0$),

- $y_r < \frac{\nu}{\sqrt{bd_1+y_{th1}^2}}$ ($h_1(\bar{\mathbf{x}}_5^-) > 0$), $d_3 - d_1 - d_2 < \frac{y_{th1}^2}{b}$ ($h_2(\bar{\mathbf{x}}_5^-) < 0$) and $d_3 = d_2 + \frac{(bd_1+y_{th1}^2)y_{th2}^2}{y_{th1}^2}$ ($h_3(\bar{\mathbf{x}}_5^-) = 0$),
- $y_r = \frac{\nu}{\sqrt{bd_1+y_{th1}^2}}$ ($h_1(\bar{\mathbf{x}}_5^-) = 0$), $d_3 - d_1 - d_2 = \frac{y_{th1}^2}{b}$ ($h_2(\bar{\mathbf{x}}_5^-) = 0$) and $d_3 < d_2 + \frac{(bd_1+y_{th1}^2)y_{th2}^2}{y_{th1}^2}$ ($h_3(\bar{\mathbf{x}}_5^-) > 0$),
- $y_r = \frac{\nu}{\sqrt{bd_1+y_{th1}^2}}$ ($h_1(\bar{\mathbf{x}}_5^-) = 0$), $d_3 - d_1 - d_2 < \frac{y_{th1}^2}{b}$ ($h_2(\bar{\mathbf{x}}_5^-) < 0$) and $d_3 = d_2 + \frac{(bd_1+y_{th1}^2)y_{th2}^2}{y_{th1}^2}$ ($h_3(\bar{\mathbf{x}}_5^-) = 0$).

The determinant and trace are given by

$$Det[A(\bar{\mathbf{x}}_5^-)] = 2 + \frac{2bd_1}{y_{th1}^2} \quad \text{and} \quad Tr[A(\bar{\mathbf{x}}_5^-)] = -b - \frac{1}{b} - \frac{2d_1}{y_{th1}^2}.$$

Equilibrium $\bar{\mathbf{x}}_5^-$ are stables because $Det[A(\bar{\mathbf{x}}_5^-)] > 0$ and $Tr[A(\bar{\mathbf{x}}_5^-)] < 0$ for all $d_1 > 0$.

(ii) $\mathbf{F}_6(\mathbf{x})$ has an equilibrium point, given by

$$\bar{\mathbf{x}}_6^\pm = \left(\frac{2bd_1 + y_{th1}^2 \pm y_{th1}\delta}{2b(bd_1 + y_{th1}^2)}, \frac{y_{th1}^2 \mp y_{th1}\delta}{2(bd_1 + y_{th1}^2)}, \frac{y_{th1}^2 - 2y_r(bd_1 + y_{th1}^2) \mp y_{th1}\delta}{2(bd_1 + y_{th1}^2)} \right),$$

where $\delta = \sqrt{y_{th1}^2 - 4b(d_2 - d_3)(bd_1 + y_{th1}^2)}$. Equilibrium $\bar{\mathbf{x}}_6^+$ is real for $y_r > \frac{(y_{th1}-\delta)y_{th1}}{2(bd_1+y_{th1}^2)}$ ($h_1(\bar{\mathbf{x}}_6^+) < 0$), $d_3 - d_1 - d_2 > \frac{(y_{th1}-1)y_{th1}}{b}$ ($h_2(\bar{\mathbf{x}}_6^+) < 0$) and $d_3 - d_2 < \frac{(bd_1y_{th2}+y_{th1}^2y_{th2}-y_{th1}^2)y_{th2}}{by_{th1}^2}$ ($h_3(\bar{\mathbf{x}}_6^+) > 0$). Moreover, it becomes a boundary equilibrium point if

- $y_r = \frac{(y_{th1}-\delta)y_{th1}}{2(bd_1+y_{th1}^2)}$ ($h_1(\bar{\mathbf{x}}_6^+) = 0$), $d_3 - d_1 - d_2 > \frac{(y_{th1}-1)y_{th1}}{b}$ ($h_2(\bar{\mathbf{x}}_6^+) < 0$) and $d_3 - d_2 < \frac{(bd_1y_{th2}+y_{th1}^2y_{th2}-y_{th1}^2)y_{th2}}{by_{th1}^2}$ ($h_3(\bar{\mathbf{x}}_6^+) > 0$),
- $y_r > \frac{(y_{th1}-\delta)y_{th1}}{2(bd_1+y_{th1}^2)}$ ($h_1(\bar{\mathbf{x}}_6^+) < 0$), $d_3 - d_1 - d_2 = \frac{(y_{th1}-1)y_{th1}}{b}$ ($h_2(\bar{\mathbf{x}}_6^+) = 0$) and $d_3 - d_2 < \frac{(bd_1y_{th2}+y_{th1}^2y_{th2}-y_{th1}^2)y_{th2}}{by_{th1}^2}$ ($h_3(\bar{\mathbf{x}}_6^+) > 0$),
- $y_r > \frac{(y_{th1}-\delta)y_{th1}}{2(bd_1+y_{th1}^2)}$ ($h_1(\bar{\mathbf{x}}_6^+) < 0$), $d_3 - d_1 - d_2 > \frac{(y_{th1}-1)y_{th1}}{b}$ ($h_2(\bar{\mathbf{x}}_6^+) < 0$) and $d_3 - d_2 = \frac{(bd_1y_{th2}+y_{th1}^2y_{th2}-y_{th1}^2)y_{th2}}{by_{th1}^2}$ ($h_3(\bar{\mathbf{x}}_6^+) = 0$),
- $y_r = \frac{(y_{th1}-\delta)y_{th1}}{2(bd_1+y_{th1}^2)}$ ($h_1(\bar{\mathbf{x}}_6^+) = 0$), $d_3 - d_1 - d_2 = \frac{(y_{th1}-1)y_{th1}}{b}$ ($h_2(\bar{\mathbf{x}}_6^+) = 0$) and $d_3 - d_2 < \frac{(bd_1y_{th2}+y_{th1}^2y_{th2}-y_{th1}^2)y_{th2}}{by_{th1}^2}$ ($h_3(\bar{\mathbf{x}}_6^+) > 0$),
- $y_r = \frac{(y_{th1}-\delta)y_{th1}}{2(bd_1+y_{th1}^2)}$ ($h_1(\bar{\mathbf{x}}_6^+) = 0$), $d_3 - d_1 - d_2 > \frac{(y_{th1}-1)y_{th1}}{b}$ ($h_2(\bar{\mathbf{x}}_6^+) < 0$) and $d_3 - d_2 = \frac{(bd_1y_{th2}+y_{th1}^2y_{th2}-y_{th1}^2)y_{th2}}{by_{th1}^2}$ ($h_3(\bar{\mathbf{x}}_6^+) = 0$).

On the other hand, $\bar{\mathbf{x}}_6^-$ is real for $y_r > \frac{(y_{th1}-\delta)y_{th1}}{2(bd_1+y_{th1}^2)}$ ($h_1(\bar{\mathbf{x}}_6^-) < 0$), $d_3 - d_1 - d_2 < \frac{(y_{th1}-1)y_{th1}}{b}$ ($h_2(\bar{\mathbf{x}}_6^-) < 0$) and $d_3 - d_2 > \frac{(bd_1y_{th2}+y_{th1}^2y_{th2}-y_{th1}^2)y_{th2}}{by_{th1}^2}$ ($h_3(\bar{\mathbf{x}}_6^-) > 0$), otherwise it is virtual. Moreover, it becomes a boundary equilibrium point if

- $y_r = \frac{(y_{th1}-\delta)y_{th1}}{2(bd_1+y_{th1}^2)}$ ($h_1(\bar{\mathbf{x}}_6^-) = 0$), $d_3 - d_1 - d_2 < \frac{(y_{th1}-1)y_{th1}}{b}$ ($h_2(\bar{\mathbf{x}}_6^-) < 0$) and $d_3 - d_2 > \frac{(bd_1y_{th2}+y_{th1}^2y_{th2}-y_{th1}^2)y_{th2}}{by_{th1}^2}$ ($h_3(\bar{\mathbf{x}}_6^-) > 0$),
- $y_r > \frac{(y_{th1}-\delta)y_{th1}}{2(bd_1+y_{th1}^2)}$ ($h_1(\bar{\mathbf{x}}_6^-) < 0$), $d_3 - d_1 - d_2 = \frac{(y_{th1}-1)y_{th1}}{b}$ ($h_2(\bar{\mathbf{x}}_6^-) = 0$) and $d_3 - d_2 > \frac{(bd_1y_{th2}+y_{th1}^2y_{th2}-y_{th1}^2)y_{th2}}{by_{th1}^2}$ ($h_3(\bar{\mathbf{x}}_6^-) > 0$),
- $y_r > \frac{(y_{th1}-\delta)y_{th1}}{2(bd_1+y_{th1}^2)}$ ($h_1(\bar{\mathbf{x}}_6^-) < 0$), $d_3 - d_1 - d_2 < \frac{(y_{th1}-1)y_{th1}}{b}$ ($h_2(\bar{\mathbf{x}}_6^-) < 0$) and $d_3 - d_2 = \frac{(bd_1y_{th2}+y_{th1}^2y_{th2}-y_{th1}^2)y_{th2}}{by_{th1}^2}$ ($h_3(\bar{\mathbf{x}}_6^-) = 0$),
- $y_r = \frac{(y_{th1}-\delta)y_{th1}}{2(bd_1+y_{th1}^2)}$ ($h_1(\bar{\mathbf{x}}_6^-) = 0$), $d_3 - d_1 - d_2 = \frac{(y_{th1}-1)y_{th1}}{b}$ ($h_2(\bar{\mathbf{x}}_6^-) = 0$) and $d_3 - d_2 > \frac{(bd_1y_{th2}+y_{th1}^2y_{th2}-y_{th1}^2)y_{th2}}{by_{th1}^2}$ ($h_3(\bar{\mathbf{x}}_6^-) > 0$),
- $y_r = \frac{(y_{th1}-\delta)y_{th1}}{2(bd_1+y_{th1}^2)}$ ($h_1(\bar{\mathbf{x}}_6^-) = 0$), $d_3 - d_1 - d_2 < \frac{(y_{th1}-1)y_{th1}}{b}$ ($h_2(\bar{\mathbf{x}}_6^-) < 0$) and $d_3 - d_2 = \frac{(bd_1y_{th2}+y_{th1}^2y_{th2}-y_{th1}^2)y_{th2}}{by_{th1}^2}$ ($h_3(\bar{\mathbf{x}}_6^-) = 0$).

The determinant and trace are given by

$$Det[A(\bar{\mathbf{x}}_6^\pm)] = 2 - \frac{1}{2b(d_2 - d_3)} + \frac{b(d_1 + d_2)}{y_{th1}^2} \mp \frac{y_{th1}\delta}{2b(d_2 - d_3)y_{th1}^2}$$

$$Tr[A(\bar{\mathbf{x}}_6^\pm)] = -b - \frac{d_2}{y_{th1}^2} + \frac{4(d_2 - d_3)(bd_1 + y_{th1}^2)^2}{(y_{th1}^2 \mp y_{th1}\delta)^2}.$$

Equilibrium $\bar{\mathbf{x}}_6^+$ is a stable point because $Det[A(\bar{\mathbf{x}}_6^+)] > 0$ and $Tr[A(\bar{\mathbf{x}}_6^+)] < 0$ for $d_3 \in (d_2 - \frac{y_{th1}^2}{4b(bd_1+y_{th1}^2)}, d_2)$

5.5.2 Sliding vector field and pseudo-equilibria

Sliding vector field associated to the dynamical system (5.2.3) is defined by (5.3.7), where $(x, y, x) \in \Sigma_s \subset \Sigma_1$. The pseudo equilibrium point is given by $\tilde{\mathbf{x}} = (\xi_0(y), y, 0)$ that depend of values of $\xi_0(y)$, i.e, the discontinuity at $y = y_{th1}$ and $y = y_{th2}$. In this case, there are three pseudo-equilibrium points namely,

$$\tilde{\mathbf{x}}_1 = \left(\frac{d_1 + d_2 - d_3}{y_r}, y_r, 0 \right),$$

$$\tilde{\mathbf{x}}_2 = \left(\frac{d_1 y_r}{y_{th1}^2} + \frac{d_2}{y_{th2}} - \frac{d_3}{y_r}, y_r, 0 \right),$$

$$\tilde{\mathbf{x}}_3 = \left(\frac{d_1 y_r^2 + d_2 y_{th1}^2}{y_r} - \frac{d_3}{y_r}, y_r, 0 \right),$$

for $y \geq y_{th1}$, $y < y_{th2}$ and $y_{th2} \leq y < y_{th1}$, respectively. By hypothesis $y_r > y_{th1} > y_{th2}$, then the pseudo-equilibria $\tilde{\mathbf{x}}_2$ and $\tilde{\mathbf{x}}_3$ are always virtual, so the stability analysis will be only for the pseudo-equilibrium point $\tilde{\mathbf{x}}_1$ as studied in the Subsection 5.3.2.

5.6 Conclusion

This chapter discussed the nonlinear dynamics of a dc-dc buck converter controlled by a sliding mode control (SMC) law connected to two power converters where one of them is a boost converter and the other is a buck converter, both modeled by a CPL piecewise function. The main goal was to guarantee system stability by balancing the power of sources and loads through a storage element for this the nonlinear effects of the two constant power loads and of a sliding mode controller.

Chapter 6

Final Remarks

In this Thesis, we reviewed some concepts and definitions of the **DPWS** systems theory, giving tools for the analysis of the dynamic behavior of these systems and we lay the foundations for the development of the work. The main contributions of this thesis work are contained in chapters 2, 3, 4 and 5; which resulted in three published articles and one article that is still in development:

- *Multiple boundaries sliding mode control applied to capacitor voltage-balancing systems*, Communications in Nonlinear Science and Numerical Simulation (2020), DOI:10.1016/j.cnsns.2020.105430;
- *Bifurcation analysis of 3D-PWS systems with two transversal switching boundaries: A case study in power electronics*, Physica D Nonlinear Phenomena (2022), DOI:10.1016/j.physd.2022.133505;
- *Global stability of a Lotka-Volterra piecewise-smooth system with harvesting actions and two predators competing for one prey*, Journal of Mathematical Analysis and Applications (2023), DOI:10.1016/j.jmaa.2023.126998;
- *Nonlinear analysis of DC power converters connected in parallel* (in progress).

The main results and contributions of this Thesis are summarized below:

In Chapter 2, a new active capacitor voltage balancing method for MMCs was studied in depth based on a sliding mode control with multiple switching boundaries. The main contribution in this part was to show analytically the local stability of the voltage balanced system for an arbitrary number of submodules (see Theorem 2.2.1 in Section 2.2). Other important results are:

- the description of the global dynamics of systems with two SM, modeled by **2D-DPWS** systems with two perpendicular switching straight lines, see Section 2.3;
- the description of the global sliding dynamics of systems with two SM, considering the presence of inductors in the circuit, being modeled by **3D-DPWS** systems with two perpendicular switching planes, see Section 2.4;
- the characterization of the sliding vector field at the intersection of the two perpendicular switching planes, for the setting of the previous item;

- the identification and classification of typical singularities for the system class under study;
- numerical simulations of the studied systems are provided which help us to better understand the dynamic behavior of these systems, in addition to checking the analytical results.

In Chapter 3, local and global phenomena of power electronic circuits feeding a piecewise constant power load controlled by a sliding-mode control law were studied. These electronic circuits were modeled as a dynamic **3D-DPWS** system with two transverse switching boundaries, with only sliding on one of them and only crossing on the other. Among the most important result, we highlight:

- The non-linear behavior of this system was analyzed and some results were presented on bifurcations induced by the two transverse switched boundaries, such as BEB, BFB, DSN and GB;
- We had predicted numerically the coexistence of at least 4 limit cycles, in addition, we found other bifurcations of equilibrium and limit cycles, such as Hopf, SNe, SNPO and HC bifurcations. These results are very useful to determine the safe parameter region which guarantees robust stability at the desired operating point for the system, in order to achieve a suitable SMC design.
- Numerical simulations are also provided to obtain bifurcation sets and bifurcation diagrams.

In Chapter 4, we study the global dynamics of a piecewise smooth Lotka-Volterra system with two predators competing for prey where prey resources are limited. In this study, the control harvesting strategy was defined by two switching thresholds that determine piecewise constant control signals for the tracking problem of predator-prey systems. The main contribution in this chapter was the proof of the global stability condition for the pseudo-equilibrium point, which is where two predator species and one prey species can coexist. Other contributions:

- the identification of a special boundary equilibrium bifurcation that occurs in sliding vector fields called *boundary pseudo-equilibrium bifurcation* (BPEB);
- the description of the sliding dynamics on each switching boundary, even at the intersection between them.

In Chapter 5, a qualitative analysis of the stability of DC power converters connected in parallel was carried out. This system was composed of a bidirectional DC-DC buck converter controlled by a sliding mode control law (SMC) and connected to two power converters, where one of them is a boost converter and the other is a buck converter, both represented by two CPL functions by parts. A photovoltaic (PV + MPPT converter) source modeled as a CPS was also included in the microgrid to make a more generic analysis. Local phenomena associated with bifurcations induced by switching boundaries as Boundary Equilibrium Bifurcations (BEBs) and Discontinuous Saddle-Node (DSN),

which are part of the class of Discontinuous Induced Bifurcations (DIBs), were also studied. Furthermore, the well-known Hopf and Saddle-Node of equilibrium points bifurcation were also studied. Numerical continuation methods using AUTO software were employed to obtain bifurcation sets and bifurcation diagrams.

Finally, we can conclude that although this Thesis provides a minor contribution to the theoretical aspects of DPWS systems with multiple boundaries, the cases studied in chapters 2, 3, 4 and 5 contribute to unravel the dynamic richness of this class of systems, providing some insights to deal with this class of systems in engineering applications.

Bibliography

- [1] A. F. Filippov. *Differential Equations with Discontinuous Righthand Sides*. *Kluwer Academic Publishers*, Dordrecht, 1988.
- [2] A. M. Y. M. Ghias, J. Pou, V. G. Agelidis and M. Ciobotaru. Optimal switching transition-based voltage balancing method for flying capacitor multilevel converters. *IEEE Trans. on Power Electronics*, 30 (4) (2015) 1804–1817. doi:10.1109/TPEL.2014.2323084
- [3] L. Luo, Y. Zhang, L. Jia, N. Yang, L. Yang and H. Zhang. Capacitor static voltage balance based on auxiliary-power supply pulse width control for MMC. *IET Power Electronics*, 11 (2018) 1796–1803. doi:10.1049/iet-pel.2017.0672
- [4] L. Luo, Y. Zhang, L. Jia and N. Yang. A novel method based on self-power supply control for balancing capacitor static voltage in MMC. *IEEE Transactions on Power Electronics*, 33 (2018) 1038–1049. doi:10.1109/TPEL.2017.2679130
- [5] A. Lesnicar and R. Marquardt. An innovative modular multilevel converter topology suitable for a wide power range. *Proc. 2003 IEEE Bologna PowerTech Conf.*, (2003) 6–11. doi:10.1109/PTC.2003.1304403
- [6] S. Debnath, J. Qin and M. Saeedifard. Control and stability analysis of modular multilevel converter under low-frequency operation. *IEEE Trans. on Ind. Electronics*, 62 (9) (2015) 5329–5339. doi:10.1109/TIE.2015.2414908
- [7] L. H. T. Schmidt, G. J. M. D. Sousa, M. L. Heldwein and D. J. Pagano. Passive Capacitor Voltage Balancing in Modular Multilevel Converter During its Precharge: Analysis and Design. *15th Brazilian Power Electronics Conference and 5th IEEE Southern Power Electronics Conference*, (2019) 323–328. doi:10.1109/COBEP/SPEC44138.2019.9065701
- [8] M. Di Bernardo, C. J. Budd, A. R. Champneys and P. Kowalczyk. *Piecewise-Smooth Dynamical Systems: Theory and Applications*. *Appl. Math. Sci. Springer-Verlag*, Vol. 163, 2008. doi:10.1007/978-1-84628-708-4
- [9] L. Dieci and L. Lopez, Sliding motion in Filippov differential systems: Theoretical results and a computational approach. *SIAM J. Numerical Analysis*, 47 (2009) 2023–2051. doi:10.1137/080724599
- [10] L. Dieci, C. Elia and L. Lopez. A Filippov sliding vector field on an attracting co-dimension 2 discontinuity surface, and a limited loss-of-attractivity analysis. *J. Differential Equations*, 254 (2013) 1800–1832. doi:10.1016/j.jde.2012.11.007

- [11] J. Alexander and T. Seidman. Sliding modes in intersecting switching surfaces, I: Blending. *Houston J. Math.*, 24 (1998) 545–569.
- [12] J. Alexander and T. Seidman. Sliding modes in intersecting switching surfaces, II: hysteresis. *Houston J. Math.*, 25 (1999) 185–211.
- [13] M. R. Jeffrey, G. Kafanas and D. J. W. Simpson. Jitter in piecewise-smooth dynamical systems with intersecting discontinuity surfaces. *International Journal of Bifurcation and Chaos*, 28 (6) (2018) 1830020. doi:10.1142/S0218127418300203
- [14] V. I. Utkin. Sliding modes and their application in variable structure systems. *MiR*, 1978.
- [15] V. I. Utkin, J. Guldner and J. Shi. Sliding Mode Control in Electro-Mechanical Systems. *Automation and Control Engineering*, CRC Press, 2009. doi:10.1080/10241230306724.
- [16] C. Bonet, T. M. Seara, E. Fossas and M. R. Jeffrey. A unified approach to explain contrary effects of hysteresis and smoothing in nonsmooth systems. *Communications in Nonlinear Science and Numerical Simulation*, 50 (2017) 142 – 168. doi:10.1016/j.cnsns.2017.02.014.
- [17] C. Wang, J. Tang and J. Ma. Minireview on signal exchange between nonlinear circuits and neurons via field coupling. *Eur. Phys. J. Spec. Top.*, 228 (2019) 1907–1924. doi:10.1140/epjst/e2019-800193-8.
- [18] M. R. Jeffrey. Dynamics at a switching intersection: Hierarchy, isonomy, and multiple sliding. *SIAM J. Appl. Dyn. Syst.*, 13 (3) (2014) 1082–1105. doi:10.1137/13093368X.
- [19] Y. A. Kuznetsov, S. Rinaldi and A. Gragnani. One-parameter bifurcations in planar Filippov systems. *International Journal of Bifurcation and Chaos*, 13 (8) (2003) 2157–2188. doi:10.1142/S0218127403007874.
- [20] R. Cristiano and D. J. Pagano, Two-parameter boundary equilibrium bifurcations in 3D-Filippov systems. *J. Nonlinear Sci.*, 29 (2019) 2845–2875. doi:10.1007/s00332-019-09560-5.
- [21] M. A. Teixeira. Stability conditions for discontinuous vector fields. *Journal of Differential Equations*, 88 (1990) 15–29. doi:10.1016/0022-0396(90)90106-Y.
- [22] D. J. W. Simpson. Bifurcations in Piecewise-Smooth Continuous Systems. *World Scientific Series on Nonlinear Science Series A*, 70 (2010). doi:10.1142/7612.
- [23] D. J. W. Simpson. A general framework for boundary equilibrium bifurcations of Filippov systems. *Chaos: An Interdisciplinary Journal of Nonlinear Science*, 28 (2018) 103114. doi:10.1063/1.5037947.
- [24] D. J. Pagano, E. Ponce and F. Torres. On Double Boundary Equilibrium Bifurcations in Piecewise Smooth Planar Systems. *Qualitative Theory of Dynamical Systems*, 10 (2) (2011) 277–301. doi:10.1007/s12346-011-0050-0.

- [25] P. A. Glendinning. Classification of boundary equilibrium bifurcations in planar Filippov systems. *Chaos: An Interdisciplinary Journal of Nonlinear Science*, 26 (1) (2016) 013108. doi:10.1063/1.4940017.
- [26] P. A. Glendinning and M. R. Jeffrey. Grazing-sliding bifurcations, border collision maps and the curse of dimensionality for piecewise smooth bifurcation theory. *Nonlinearity*, 28 (1) (2015) 263. doi:10.1088/0951-7715/28/1/263.
- [27] M. di Bernardo, P. Kowalczyk and A. Nordmark. Bifurcations of dynamical systems with sliding: derivation of normal-form mappings. *Physica D: Nonlinear Phenomena*, 170 (3) (2002) 175–205. doi:10.1016/S0167-2789(02)00547-X.
- [28] P. Glendinning, P. Kowalczyk and A. Nordmark. Attractors near grazing–sliding bifurcations. *Nonlinearity*, 25 (2012) 1867–1885. doi:10.1088/0951-7715/25/6/1867.
- [29] L. Benadero, R. Cristiano, D. J. Pagano and E. Ponce. Nonlinear Analysis of Interconnected Power Converters: A Case Study. *IEEE Journal on Emerging and Selected Topics in Circuits and Systems*, 5 (3) (2015) 326–335. doi:10.1109/JETCAS.2015.2462017.
- [30] A. P. N. Tahim, D. J. Pagano, E. Lenz and V. Stramosk. Modeling and Stability Analysis of Islanded DC Microgrids Under Droop Control. *IEEE Transactions on Power Electronics* 30 (8) (2015) 4597–4607. doi:10.1109/TPEL.2014.2360171.
- [31] A. P. N. Tahim, D. J. Pagano, M. L. Heldwein and E. Ponce. Control of interconnected power electronic converters in dc distribution systems. *XI Brazilian Power Electronics Conference*, (2011) 269–274. doi:10.1109/COBEP.2011.6085269.
- [32] D. C. Hamill, J. H. B. Deane and D. J. Jefferies. Modeling of chaotic DC-DC converters by iterated nonlinear mappings. *IEEE Transactions on Power Electronics*, 7 (1) (1992) 25–36. doi:10.1109/63.124574.
- [33] J. H. B. Deane and D. C. Hamill. Analysis, simulation and experimental study of chaos in the buck converter. *21st Annual IEEE Conference on Power Electronics Specialists*, 7 (1) (1990) 491–498. doi:10.1109/PESC.1990.131228.
- [34] M. R. Jeffrey. Hidden Dynamics: The Mathematics of Switches, Decisions and Other Discontinuous Behaviour. *Springer*, (2019). doi:10.1007/978-3-030-02107-8.
- [35] J. Llibre, E. Ponce and C. Valls. Two Limit Cycles in Liénard Piecewise Linear Differential Systems. *Journal of Nonlinear Science*, 28 (2019) 1499–1522. doi:10.1007/s00332-018-9523-5.
- [36] E. Freire, E. Ponce, J. Ros, E. Vela and A. Amador. Hopf bifurcation at infinity in 3D symmetric piecewise linear systems. Application to a Bonhoeffer–van der Pol oscillator. *Nonlinear Analysis: Real World Applications*, 54 (2020) 1468–1218. doi:doi.org/10.1016/j.nonrwa.2020.103112.
- [37] D. Simpson. Grazing-Sliding Bifurcations Creating Infinitely Many Attractors. *International Journal of Bifurcation and Chaos*, 27 (2017) 1–15. doi:10.1142/S0218127417300427.

- [38] P. Glendinning, P. Kowalczyk and A. B. Nordmark. Multiple attractors in grazing-sliding bifurcations in Filippov-type flows. *IMA Journal of Applied Mathematics*, 81 (2016) 711–722. doi:10.1093/imamat/hxw014.
- [39] A. B. Nordmark. Non-periodic motion caused by grazing incidence in an impact oscillator. *Journal of Sound and Vibration*, 145 (1991) 279–297. doi:doi.org/10.1016/0022-460X(91)90592-8.
- [40] L. Dieci. Sliding motion on the intersection of two manifolds: Spirally attractive case. *Communications in Nonlinear Science and Numerical Simulation*, 26 (2015) 65–74. doi:10.1016/j.cnsns.2015.02.002.
- [41] M. Di Bernardo and S. J. Hogan. Discontinuity-induced bifurcations of piecewise smooth dynamical systems. *Philosophical Transactions of the Royal Society of London A: Mathematical, Physical and Engineering Sciences*, 368 (2010) 4915–4935. doi:10.1016/j.cnsns.2015.02.002.
- [42] R. Cristiano, D. J. Pagano and M. M. Henao. Multiple boundaries sliding mode control applied to capacitor voltage-balancing systems. *Commun Nonlinear Sci Numer Simulat.*, 91 (2020). doi:10.1016/j.cnsns.2020.105430.
- [43] M. Di Bernardo, A. Nordmark and G. Olivar. Discontinuity-induced bifurcations of equilibria in piecewise-smooth and impacting dynamical systems. *Physica D: Nonlinear Phenomena*, 237 (2008) 119–136. doi:10.1016/j.cnsns.2020.105430.
- [44] D. J. W. Simpson. DHopf-like boundary equilibrium bifurcations involving two foci in Filippov systems. *Journal of Differential Equations*, 267 (2019) 6133–6151. doi:doi.org/10.1016/j.jde.2019.06.016.
- [45] S. Fernández-García, A. Teruel and V. Carmona. Saddle-node of limit cycles in planar piecewise linear systems and applications. *Discrete and Continuous Dynamical Systems*, 39 (2019) 5275–5299. doi:10.3934/dcds.2019215.
- [46] E. Freire, E. Ponce and F. Torres. A general mechanism to generate three limit cycles in planar Filippov systems with two zones. *Nonlinear Dynamics*, 78 (2014) 251–263. doi:10.1007/s11071-014-1437-7.
- [47] B. Xu, F. Yang, Y. Tang and Mu Lin. Homoclinic Bifurcations in Planar Piecewise-Linear Systems. *Discrete Dynamics in Nature and Society*, (2013) 732321. doi:10.1007/s11071-014-1437-7.
- [48] B. R. de Freitas, J. Llibre and J. C. Medrado. Limit cycles of continuous and discontinuous piecewise-linear differential systems in \mathbb{R}^3 . *Journal of Computational and Applied Mathematics*, 338 (2018) 311–323. doi:10.1016/j.cam.2018.01.028.
- [49] Yu. A. Kuznetsov. Elements of Applied Bifurcation Theory. *Springer-Verlag, New York*, 112 (2004). doi:10.1007/978-1-4757-3978-7.
- [50] L. M. Perko. Differential Equations and Dynamical Systems. *Texts in Applied Mathematics, Springer-Verlag, New York*, 7 (1991). doi:10.1007/978-1-4613-0003-8.

- [51] A. P. N. Tahim, D. J. Pagano and E. Ponce. Nonlinear Control of Boost Bidirectional Converters in Stand-alone dc Microgrids. *51st IEEE Conference on Decision and Control - CDC, Maui, Hawaii, USA*, (2012). doi:10.3182/20130904-3-FR-2041.00121.
- [52] D. J. Pagano and E. Ponce. On The Robustness of the DC-DC Boost Converter Under Washout SMC. *Power Electronics Conference, Brazil, 2009*, (2009) 110–115. doi:10.1109/COBEP.2009.5347639.
- [53] H. C. Lee and E. H. Abed. Washout filter in the bifurcation control of high alpha flight dynamics. *Proc. of the American Control Conference, Boston*, 1 (1991) 206–211. doi:10.23919/ACC.1991.4791359.
- [54] A. A. Andronov, E. A. Leontovich, I. I. Gordon and A. G. Maier. Theory of Bifurcations of Dynamical Systems on a Plane. *Israel Program for Scientific Translations, Jerusalem*, (1971).
- [55] J. P. Palis and W. De Melo. Geometric Theory of Dynamical Systems: An Introduction. *Springer-Verlag, New York*, (1982).
- [56] J. Guckenheimer and P. Holmes. Nonlinear Oscillations, Dynamical Systems, and Bifurcations of Vector Fields. *Springer-Verlag, New York*, (1983).
- [57] P. Hartman. Ordinary Differential Equations. *John Wiley & Sons, Inc., New York*, (1964).
- [58] V. Křivan. On the Gause predator-prey model with a refuge: A fresh look at the history. *J. Theor. Biol.*, 274 (2011) 67–73. doi:10.1016/201101016.
- [59] F. Dercole, F. D. Rossa, A. Colombo and Y. A. Kuznetsov. Two Degenerate Boundary Equilibrium Bifurcations in Planar Filippov Systems. *SIAM Journal on Applied Dynamical Systems*, 10 (2011) 1525–1553. doi:10.1137/100812549.
- [60] A. Nordmark and P. Kowalczyk. A codimension-two scenario of sliding solutions in grazing–sliding bifurcations. *Nonlinearity*, 19 (2005) 1–26. doi:10.1088/0951-7715/19/1/001.
- [61] R. Cristiano, D. J. Pagano, L. Benadero and E. Ponce. Bifurcation analysis of a DC-DC bidirectional power converter operating with constant power load. *International Journal of Bifurcation and Chaos*, 26 (4) (2016) 1630010 (18 pages). doi:10.1142/S021812741630010X.
- [62] E. Ponce and D. J. Pagano. Sliding dynamics bifurcations in the control of boost converters. *In Preprints of the 18th IFAC World Congress, Milano, Italy*, (2011) 13293–13298. doi:10.3182/20110828-6-IT-1002.02603.
- [63] A. Jacquemard, M. A. Teixeira and D. J. Tonon. Piecewise smooth reversible dynamical systems at a two-fold singularity. *International Journal of Bifurcation and Chaos*, 22(8):1250192 (2012) 13 pages. doi:10.1142/S0218127412501921.

- [64] R. I. Leine and H. Nijmeijer. Dynamics and Bifurcations of Non-Smooth Mechanical Systems. *Springer-Verlag Berlin Heidelberg*, 18 (2004). doi:10.1007/978-3-540-44398-8.
- [65] J. Llibre and D. Xiao. Global dynamics of a Lotka-Volterra model with two predators competing for one prey. *SIAM J. Appl. Math.*, 74(2) (2014) 434–453. doi:10.1137/130923907.
- [66] A. Korobeinikov and G. C. Wake. Global properties of the three-dimensional predator-prey Lotka-Volterra systems. *Journal of Applied Mathematics and Decision Sciences*, 3(2) (1999) 155–162. doi:10.1155/s1173912699000085.
- [67] V. Volterra. Variazioni e fluttuazione del numero di individui in specie animali conviventi. *Mem. Accad. Lincei*, 2 (1926) 31–113.
- [68] A. J. Lotka. Elements of Physical Biology. *Williams and Wilkins, Baltimore, MD*, (1925).
- [69] G. J. Butler and P. Waltman. Bifurcation from a limit cycle in a two predator-one prey ecosystem modeled on a chemostat. *J. Math. Biol.*, 12 (1981), 295–449.
- [70] F. Brauer and C. Castillo-Chavez. Mathematical Models in Population Biology and Epidemiology. *Springer-Verlag, Heidelberg*, (2000). doi:10.1007/978-1-4614-1686-9.
- [71] E. Chauvet, J. E. Pullet, J. P. Previte and Z. Walls. A Lotka-Volterra three-species food chain. *Math. Mag.*, 75 (2002), 243–255. doi:10.2307/3219158.
- [72] S. H. Piltz, M. A. Porter and P. K. Maini. Prey Switching with a Linear Preference Trade-Off. *SIAM J. Applied Dynamical Systems*, 13(2), (2014), 658–682. doi:10.1137/130910920.
- [73] J. A. Massotti. Equilibria bifurcations in VSS: characterization and classification. M.Sc. in Electrical Engineering. *Federal University of Santa Catarina*. Brazil, (2005).
- [74] H. B. Silveira. A control strategy for Predator-Prey Systems using Piecewise-Constant Signals. M.Sc. in Electrical Engineering. *Federal University of Santa Catarina*. Brazil, (2004).
- [75] F. B. Cunha. Analysis and control of VSS. M.Sc. in Electrical Engineering. *Federal University of Santa Catarina*. Brazil, (2002).
- [76] L. H. T. Schmidt. Analysis and Design of Passive Capacitor Voltage-Balancing in Modular Multilevel Converter During Pre-charge Operation. Msc. in Automation and Systems Engineering. *Federal University of Santa Catarina*. Brazil, (2020).
- [77] R. Cristiano. Bifurcations in DPWS Dynamical Systems with Applications in Power Electronics. M.Sc. in Automation and Systems Engineering. *Federal University of Santa Catarina, Brazil*. Outubro, (2013).

- [78] R. Cristiano. Bifurcation Analysis in Discontinuous Piecewise-Smooth Systems: Applications in Power Electronics. Doctoral Thesis in Automation and Systems Engineering. *Federal University of Santa Catarina* Brazil, (2018).
- [79] V. Stramoski. Nonlinear control of power electronic converters interconnected in DC microgrids. M.Sc. in Automation and Systems Engineering. *Federal University of Santa Catarina*. Brazil, (2014).
- [80] F. Zhang and Y. Yan. Start-Up Process and Step Response of a DC-DC Converter Loaded by Constant Power Loads. *IEEE Transactions on Industrial Electronics*, 58(1), (2011), 298-304. doi:10.1109/TIE.2010.2045316.
- [81] R. Cristiano and D. Pagano. Bifurcation Analysis of a DC-DC Bidirectional Power Converter Operating with Constant Power Loads. *International Journal of Bifurcation and Chaos*, 26, (2016), 1630010. doi:10.1142/S021812741630010X.
- [82] M. M. Henao, R. Cristiano and D. J. Pagano. Bifurcation analysis of 3D-PWS systems with two transversal switching boundaries: A case study in power electronics. *Physica D: Nonlinear Phenomena*, 442, (2022), 133505. doi:10.1016/j.physd.2022.133505.
- [83] B. Ermentrout. Simulating, Analyzing, and Animating Dynamical Systems: A Guide to XPPAUT for Researchers and Students. *Society for Industrial and Applied Mathematics-SIAM*, (2002). doi:10.1115/1.1579454.
- [84] J. Llibre and D. Xiao. Global Dynamics of a Lotka-Volterra Model with Two Predators Competing for One Prey. *SIAM Journal on Applied Mathematics*, 74(2), (2014), 434-453. doi:10.1137/130923907.
- [85] M. Kot. Elements of Mathematical Ecology. *Cambridge University Press*, (2000). doi:10.1017/CB09780511608520.
- [86] N. Cao, Y. Zhang and X. Liu. Dynamics and Bifurcations in Filippov Type of Competitive and Symbiosis Systems. *International Journal of Bifurcation and Chaos*, 32(13), (2022), 2250190. doi:10.1142/S0218127422501905.
- [87] D. Greenhalgh, Q.J.A. Khan and J. S. Pettigrew. An eco-epidemiological predator-prey model where predators distinguish between susceptible and infected prey. *Mathematical Methods in the Applied Sciences*, 40, (2016), 146-166. doi:10.1002/mma.3974.
- [88] Y. Wang and H. Wu. Global dynamics of Lotka-Volterra equations characterizing multiple predators competing for one prey. *Journal of Mathematical Analysis and Applications*, 491(1), (2020), 124293. doi:10.1016/j.jmaa.2020.124293.
- [89] S. A. A. Hamdallah, A. A. Arafa, S. Tang and Y. Xu. Complex dynamics of a Filippov three-species food chain model. *International Journal of Bifurcation and Chaos*, 31, (2021), 2150074. doi:10.1142/S0218127421500747.
- [90] W. Qin, X. Tan, M. Tosato and X. Liu. Threshold control strategy for a non-smooth Filippov ecosystem with group defense. *Applied Mathematics and Computation*, 362, (2019), 124532. doi:10.1016/j.amc.2019.06.046.

- [91] W. Li, L. Huang and J. Wang. Global asymptotical stability and sliding bifurcation analysis of a general Filippov-type predator-prey model with a refuge. *Applied Mathematics and Computation*, 405, (2021), 126263. doi:10.1016/j.amc.2021.126263.
- [92] X. Zhang and S. Tang. Existence of multiple sliding segments and bifurcation analysis of Filippov prey-predator model. *Applied Mathematics and Computation*, 239, (2014), 265-284. doi:10.1016/j.amc.2014.04.098.
- [93] H. B. Silveira and D. J. Pagano. Piecewise-constant control signal for predator-prey systems: Application to ecological recovery. *IFAC Proceedings*, 38(1), (2005), 79-84. doi:10.3182/20050703-6-CZ-1902.02184.
- [94] F.B. Cunha and D. J. Pagano. Bifurcation analysis of the Lotka-Volterra model subject to variable structure control. *IFAC Proceedings*, 35(1), (2002), 101-106. doi:10.3182/20020721-6-ES-1901.01407.
- [95] M. E. M. Meza, A. Bhaya and E. Kaszkurewicz. Control of one and two species predator-prey models using continuous robust threshold policies. *IFAC Proceedings*, 35(1), (2002), 107-112. doi:10.3182/20020721-6-ES-1901.01408.
- [96] R. M. May and J. R. Beddington. Maximum sustainable yield in systems subject to harvesting at more than one trophic level. *Math. Biosci.*, 51(4), (1980), 261-281. doi:10.1016/0025-5564(80)90103-0.
- [97] C. A. Buzzi, P. R. da Silva and M. A. Teixeira. Slow-fast systems on algebraic varieties bordering piecewise-smooth dynamical systems. *Bulletin des Sciences Mathématiques*, 136(4), (2012), 444-462. doi:10.1016/j.bulsci.2011.06.001.
- [98] M.A. Teixeira and P.R. da Silva. Regularization and singular perturbation techniques for non-smooth systems. *Physica D: Nonlinear Phenomena*, 241(22), (2012), 1948-1955. doi:10.1016/j.physd.2011.06.022.
- [99] D. Panazzolo and P.R. da Silva. Regularization of discontinuous foliations: Blowing up and sliding conditions via Fenichel theory. *Journal of Differential Equations*, 263, (2017), 8362-8390. doi:10.1016/j.jde.2017.08.042.
- [100] M. R. Jeffrey, T. I. Seidman, M. A. Teixeira and V. I. Utkin. Into higher dimensions for nonsmooth dynamical systems. *Physica D: Nonlinear Phenomena*, 434, (2022), 133222. doi:10.1016/j.physd.2022.133222.
- [101] S. Wiggins. Introduction to Applied Nonlinear Dynamical Systems and Chaos. *Springer New York*, 2 (2003). doi:10.1007/0-387-21749-5_10.
- [102] M. S. P. Eastham. The asymptotic solution of linear differential systems, applications of the Levinson theorem. *Clarendon Press, Oxford*, (1989).